Centre for Sustainable Energy Technologies

Faculty of Science and Engineering

EVALUATION OF URBAN HEAT ISLAND SITUATION IN DEVELOPED CITIES OF ZHEJIANG PROVINCE

Tianfeng SHEN

Thesis submitted to the University of Nottingham for the degree of Doctor of Philosophy

October 2015

ABSTRACT

The rapid and unsustainable urbanization process causes a serious existing thermal environmental problem that aggravates climatic change and generates a higher temperature in urban area than in rural area. Based on literature review, this is the first research that uses field measurement methodology to investigate the urban heat island (UHI) effect in Hangzhou and Ningbo cities of Zhejiang Province. This study aims to investigate reciprocal interaction of UHI effect with urban building energy based on the air temperature and relative humidity measurement in research area.

There are three main factors including vegetation cover, urban building configuration and surface material properties, and human activities, contributing to the UHI development. Through using ENVI-met simulation, the study has investigated how the West Lake and the Xixi Wetland ecological areas in the city act as passive thermal comfort systems in improving the outdoor built environment and mitigating UHI effect. However, according to the observation, the UHI effect in Hangzhou is still more intense than that in Ningbo. The monthly average UHII values in Hangzhou ranged between 1℃ and 4℃, whilst the highest monthly average UHII in Ningbo is only as high as 1.5℃.

Additionally, the study has evaluated that the UHI effect is most pronounce in winter

days, because there is serious air pollution, high concentration of Particulate Matter (PM) and low wind speed in winter days in China. The result has also proved that the night time UHI effect is significantly more intense than the day time UHI effect. It has been validated in the study that UHI effect can be mitigated by three effective strategies, such as the application of cool materials on urban surfaces, modifying urban geometry to improve wind flow and expanding green space in urban areas.

Owing to the hourly air temperature and relative humidity collected from strategically selected sites around the city, modified TMY weather dataset has been established. The research employed a case study of China Telecom Business Office Building in Hangzhou to evaluate the impact of UHI on urban building energy consumption. It implies that there is about 20% cooling demand underestimated in the hot months and about 25% heating demand overestimated in the cold months for the office building located in the urban city of Hangzhou, if the building is designed based on currently available weather dataset without considering UHI effect.

Based on the application of artificial neural network (ANN) and genetic programming (GP) techniques, the research has provided algorithms to link factors such as “Distance from City Centre”, “Surrounding Albedo”, “Land Use of the Area (residential, commercial, industrial, recreational etc.)”, “Sky View Factor” to predict the UHI intensity for any site compared to a reference site.

PUBLICATION

The published papers as results of this PhD project are listed as below:

L Bourikas, T Shen, PAB James, DHC Chow, MF Jentsch, J Darkwa, AS Bahaj (2013) *"Addressing the Challenge of Interpreting Microclimatic Weather Data Collected from Urban Sites."* Journal of Power and Energy Engineering vol 1 pp 7-15

T. Shen; D. H. C. Chow; J. Darkwa (2013) "*Simulating the influence of microclimatic design on mitigating the Urban Heat Island effect in the Hangzhou Metropolitan Area of China"* International Journal of Low-Carbon Technologies 2013; doi: 10.1093/ijlct/ctt050

T. Shen; DHC. Chow; J. Darkwa (2013) *"Strategies and Approaches of Mitigating Urban Heat Island to Develop Low Carbon Cities in Zhejiang Province"* 2nd Low Carbon Earth Summit (19-21 October 2012, Guangzhou Baiyun International Convention Center, Guangzhou, China)

T. Shen; DHC. Chow; J. Darkwa (2013) *"A review on the research of Urban Heat Island: The case study of Hangzhou and Ningbo, China"* 2nd Low Carbon Earth Summit (19-21 October 2012, Guangzhou Baiyun International Convention Center, Guangzhou, China)

T. Shen, DHC. Chow, T. Cui, J. Darkwa (2013) *"Generating a modified weather data file for urban building design and sustainable urban planning accounting for the Urban Heat Island (UHI) effect"* 12th International Conference on Sustainable Energy Technologies (26th-29th August, 2013, The Hong Kong Polytechnic University, HK)

T. Shen, DHC. Chow, J. Darkwa, R. Yao (2014) *"Impact of Urban Heat Island on Building Cooling Energy Consumption in Hangzhou"* 13th International Conference on Sustainable Energy Technologies (25th-28th August, 2014, Geneva)

ACKNOWLEDGMENT

This research was undertaken in the Centre for Sustainable Energy Technologies (CSET) at the University of Nottingham Ningbo China. I would like to thank all staff members of CSET, May Liu, Fred Guan and Kate Yuan. Special thanks are due to my colleagues, Dr. Kokogiannakis Georgios, Yeboah Siegfried, Dr. Tongyu Zhou, Dengfeng Du, Kaining Fang, Jingjing Shao, Yilin LI, Weiguang Su, Decruz Aloysius and Yan Qu for their care and support.

I would express my deepest gratitude to my supervisors, Dr. David Chow and Prof. Jo Darkwa. Their constant encouragement, guidance and support from the initial to the final level enabled me to develop an understanding of this research project. Essential support of this research was also provided by Hangzhou Street Lighting Administration Bureau and Ningbo Street Lighting Administration Bureau.

This thesis would never become a reality without the patience and support of my wife Yiqian, my daughter Pengyu and my parents. They have kept me full of joy and smiles during my PhD study years.

TABLE OF CONTENT

LIST OF FIGURES

LIST OF TABLES

NOMENCLATURE

A……………………………………………………………………….Area (m^2)

C_p………………………………………………Specific heat capacity ($kJkg^{-1}\ m^{-3}$)

e_a…………………………………………………………….………….. Air vapour pressure (Pa)

e_s……………………………………………..……….. Surface vapour pressure (Pa)

K…………………………………………………………...……..Karman's constant

L……………………………………………..Radiance values ($Wm^{-2}sr^{-1}\mu m^{-1}$)

Pa…………………………..…………………………Atmospheric pressure (kPa)

Q^*…………………………………………….……..Net all-wave radiation (W/m^2)

Q_E ………………………………………Turbulent heat fluxes for latent heat (W/m^2)

Q_F…………………………………...…………Anthropogenic heat flux (W/m^2)

Q_H……………………...………..Turbulent heat fluxes for sensible heat (W/m^2)

Q_I…………………………………...………….. Incident solar radiation (W/m^2)

Q_L……………………………..………………..Net long-wave radiation (W/m^2)

$Q_{L\downarrow}$………………………………….……….Downward long-wave radiation (W/m^2)

$Q_{L\uparrow}$…………………………...…………Upward long-wave radiation (W/m^2)

Q_R…………………………………...………Reflected solar radiation (W/m^2)

r_a…………………………………………...…Air resistance coefficient (s/m)

RH……………………………………………………….....Relative humidity (%)

r_s…………………………………….……...…Surface resistance coefficient (s/m)

T………………………………………………………………Temperature (°C)

T_a……………………………..……………………..…Air temperature (°C)

T_R………………………………..……………………Surface temperature (°C)

$\overline{u_z}$…………………….……………….. Horizontal wind speed at height z (m/s)

υ…..Wind speed (m/s)

V………………………..……………………………………Volume (m^3)

z_0……………………………………...…... Aerodynamic roughness length (m)

ΔQ_A……………………………………………………Net local advection (W/m^2)

ΔQ_S…………………………………….………….Net storage heat flux (W/m^2)

ΔT_{u-r}…………………...... Temperature difference between urban and rural area (℃)

Greek letters

α………………………………………….……….…………….Reflectance (%)

α_m…………………………………………………………….. Fractional change (%)

ε……………………………………………..Wavelength – average emissivity (%)

σ………………………………………………………Stefan-Boltzmann constant

ρ……………………………………….……………….…….Density (kg/m^3)

φ_H………………………………………………….Stability correction parameter (%)

Θ…..…………………………………………….. Volumetric soil water content (kg/m^3)

θ_s……………………….....………Volumetric soil water content at saturation (kg/m^3)

Subscripts

C……………………………………………………………………...Commercial

E……………………………………………………………………Educational

ER……………………………………………………………..Ecological Reserve

F………………………….……………………………………….Farmland

I…………………………………………………………………….Industrial

PG……………………………………………………………………Public Green

R……………………………………………………………………..Residential

SU-A………………………………………………………..Special use-Airport

TMY……………………………………...………..Test Meteorological Year

TRY…………………………………………………………..Test Reference Year

UHI…………………………………………………………Urban Heat Island

UHII……………………………………………………Urban Heat Island Intensity

YRD…………………………………………………………Yangtze River Delta

CHAPTER 1: INTRODUCTION

1.1 Research problem statement

Urbanisation is inevitable as China continues to develop economically. The urban population of China stood at 50.6% in 2011, with a projected annual growth rate of 2.85% from 2010 to 2015[1]. The percentage of urban population in China are low in comparison to countries in developed world (for example: USA: 82% in 2010, UK: 80% in 2010, Japan: 91.3% in 2011) [1], but are expected to increase significantly during the 12th Five-Year Plan period (2011-2015) as the government puts in more effort to increase urbanisation. Since the big metropolitan cities in China already get extremely crowded, one of the key aspects of future urbanisation is the increase in scale of size and developments of some of the middle-ranking towns close to the big metropolitan cities.

This will undoubtedly result in even more overall economic benefits but at the same time, urbanisation can also bring unwelcome aspects to the lives of citizens, especially if it is not planned properly in the first instance. One of the accompanying aspects of urbanisation is the increase of temperatures at city centres. This is known as Urban Heat Island (UHI) effect. UHI has significantly adverse impacts on urban building energy consumptions and outdoor air quality.

Amongst other things, the thermal performance of buildings is highly affected by UHI. In the building design process, various options are tested in computational simulations to predict buildings' heating and cooling requirements for the site they are located. As well as the building design and thermal properties of materials proposed, one of the most crucial aspects of running these simulations is the hourly weather data file for the city or location of the building. Usually, in order to estimate the yearly energy load from heating and cooling, Typical Meteorological Year (TMY) or Test Reference Year (TRY) is used. These are synthetic weather years, "stitching" together the most average months from a period of 20 or 30 years, linking various weather parameters, and give an average year for the location for that period. In order to work out sizes of mechanical plants, Design Summer Years or Design Winter Years are recommended [2].

Currently, weather files used for building simulations in China are generated by Climatic Data Centre of China Meteorological Administration and Tsinghua University. The source data is from the official meteorological dataset collected by the Climatic Data Centre that belongs to the National Meteorological Information Centre of China Meteorological Administration. There are two types of official meteorological dataset, one is the ground climatic dataset of China and the other is the weather radiation dataset of China [3]. 270 national weather stations across the country are selected from national ground climatic observation network to cover different regions of China. Fig. 1.1 shows the countrywide distribution of all selected 270 national weather stations in China [3].

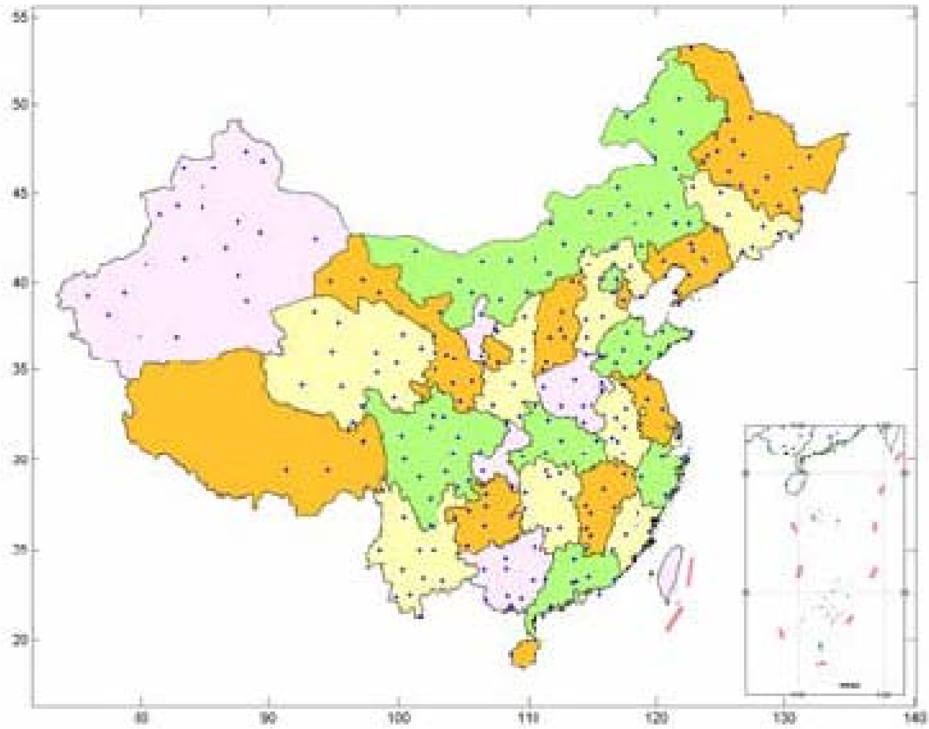

Fig. 1.1: Countrywide distribution of national weather station [3]

The elements of ground climatic data, such as ambient dry-bulb temperature, wet-bulb temperature, relative humidity, surface temperature, wind speed, wind direction, local atmospheric pressure, solar radiations and other meteorological parameters are all involved in the selected dataset. The time span of the selected ground climatic data is from 1971 to 2003 [4]. Regulation on the Protection of Meteorological Facilities and Meteorological Observation Environment that was adopted at the 214th executive meeting of the State Council on August 22, 2012 stipulates that the heights of all the buildings within the distance of 1000m from the national weather station should be less than the 10% of the distance from the building to the station [5].

There is therefore the need for updating the data, but even with updating, there remains a fundamental problem with using these files for estimating the performance of buildings which need evaluating. Most of the raw weather data file used to compile such weather files are obtained from weather stations, usually located in rural areas some distance away from city centres. However, most buildings are built in urban areas, and with UHI effect, the difference in temperatures between urban areas and rural areas can be great. Thus, using weather files generated from data from airfield sites could result in an under-estimation of cooling load and also possibly an over-estimation of heating load for the buildings.

In this regard the research was focused on investigating different factors that contributed to UHI and correlating them into reference weather data of the city. The research was also proposed to link factors such as “Distance from City Centre”, “Surrounding Albedo”, “Land Use of the Area (residential, commercial, industrial, recreational etc.)”, “Sky View Factor” to predict the UHI intensity for any site compared to a reference site. This provided a more appropriate set of weather data for sites where buildings are built for different days of the year. This provided better estimation of heating and cooling load for buildings, and ultimately provided better solutions for evaluating the performance of buildings. As a part of this investigation, it was also possible to provide useful finding for implementing feasible features to mitigate the effects of UHI. This could prove to be particularly useful especially for future urban planning of growing cities in China.

1.2 Aim and objectives of the research

UHI is being intensively studied currently, because of its seriously adverse environmental and economic impacts on urban society. There is a fundamental premise of this study that not merely energy performance of urban buildings is influenced by UHI effect, but UHI effect is formed and influenced by urban buildings as well. Therefore, this study was aimed to investigate the reciprocal interaction of UHI effect with urban building energy. In order to integrate UHI effect and urban building energy, the following research objectives were established:

1. To identify the most significant causes that contribute to UHI formation.
2. Through real data collection and mathematical analysis, to establish the relationship of UHI intensity with factors such as “Distance from City Centre”, “Surrounding Albedo”, “Land Use of the Area (residential, commercial, industrial, recreational etc.)”, “Sky View Factor (SVF)” for different months of the year and different times of the day.
3. To explore potential strategies to mitigate UHI effect
4. To generate algorithms linking the currently available Typical Meteorological Year (TMY) Weather Data from the calculated UHI intensities to modified TMY Weather Data.
5. To simulate possible changes in heating and cooling energy for urban buildings due to UHI effect.

1.3 Research area

In view of the huge size of China and limited time factor, the data collection exercise was carried out in two cities, i.e. Hangzhou and Ningbo both located in Zhejiang province, being one of the fastest developing provinces in the country. For instance in 2013 the average urbanisation rate of Zhejiang province was about 59.3% which is 8% higher than the national level [6]. As the capital of Zhejiang province, Hangzhou recorded the highest urbanisation rate of 73.5% in 2013 and Ningbo as the second biggest city achieved an urbanisation rate of 69% [6]. Although the land area of Hangzhou and Ningbo are not largest in Zhejiang Province, their Gross Domestic Products (GDP) values are highest (Hangzhou: 621.3 billion Chinese Yuan in 2012; Ningbo: RMB 395.1 billion Chinese Yuan in 2012) [6].

According to Zhejiang meteorological statistics for the period 1981 to 2010, Hangzhou experienced average 27.2 days per year when average temperatures were higher than 35℃ [6]. Since 2003, this value has increased to more than 35 days per year, which makes Hangzhou becomes the second hottest city in China [7]. As a coastal city, the summer overheating situation of Ningbo is better than Hangzhou, but there is also an evident air temperature rise in Ningbo. Particularly, the number of days of average temperature higher than 35℃ in Ningbo was below 10 days per year in the 1960s, while the number increased to 22 days in the 1990s and 45 days in 2007 [8].

Furthermore, both Hangzhou and Ningbo urban areas have large space of natural ecological resources, such as West Lake and Xixi Wetland in Hangzhou and the confluence of three rivers (Fenghua river, Yao river and Yong river) in Ningbo. The research surmised these spaces in urban areas probably could remedy their UHI effect significantly. It is significant to investigate the possible remedy with these urban natural ecological spaces for UHI situation.

Hence, Hangzhou and Ningbo are recognised as the most developed cities in Zhejiang province and were selected as the research area in this study. Over the next decade the borders of the urban agglomeration are expected to expand further and these two cities will attract more people from the countryside. The expansion of city borders and the changes in land use as well building density usually have a prominent, and often ominous, effect on the air temperature development within the urban canopy layer.

1.4 Structure of the thesis

This thesis is based on the following structure:

Chapter 1 introduces the research conducted in the project and highlights the research problem, aim, objectives and the research area.

Chapter 2 is literature review regarding the introduction of UHI and urban energy balance. This chapter also reviews literature by summarising the current situation of UHI in Hangzhou and Ningbo cities. Two main research methodologies, including observational approaches and computer simulation approaches, are discussed in this chapter. The chapter highlights some adverse impacts of UHI as well.

Chapter 3 presents a case study to simulate UHI situation in Hangzhou by using ENVI-met programme. This chapter compares the consequences of different development scenarios about Xixi Wetland and West Lake on Hangzhou urban micro-climate. In addition to that, this chapter also mainly evaluates the impact of wind speed on mitigating UHI.

Chapter 4 introduces the main research methodology of field measurement that is applied to investigate UHI situations in this research. This chapter also identifies some challenges occurring during the observation and provides strategies to solve these challenges.

Chapter 5 analyses the data information collected from field measurement. This chapter highlights the UHI situations in Hangzhou and Ningbo. The effects of urban design factors and other meteorological parameters on UHI development are discussed in this chapter as well. This chapter also explains how three main factors contribute to UHI formation and how UHI can be mitigated effectively.

Chapter 6 presents the impact of UHI on urban building energy consumption. Existing available typical meteorological year (TMY) weather dataset is modified by considering local UHI effect in this chapter. This chapter also evaluates the energy performance of an example urban office building with UHI effect by using Energy-plus software.

Chapter 7 proposes applying two statistical models of artificial neural network (ANN) and genetic programming (GP) to predict UHI effect.

Chapter 8 presents the main conclusions of this thesis with suggestions for future work.

CHAPTER 2: LITERATURE REVIEW

2.1 Introduction

A number of notable efforts have been contributed to investigating the UHI situation in the world. This chapter starts the literature review with definition of UHI and urban energy balance, followed by the UHI situations in Hangzhou and Ningbo cities. It further gives a comprehensive review of different approaches applied in studying UHI effect. Finally, it also covers a basic review regarding the adverse impacts of UHI.

2.2 Urban heat island (UHI)

The excessive and unplanned growth of urbanization of human civilization has caused undesired side effects around the world, like Urban Heat Island (UHI) effect. According to Luke Howard, urban heat island is a metropolitan area that is significantly warmer than its surrounding rural areas [9]. It hypothesizes that the air temperature difference (ΔT_{u-r}) between urban area and rural area must increase from the edge of the city toward its centre [10]. This temperature difference between urban and surrounding rural area is also defined as Urban Heat Island Intensity (UHII). UHII is an indicator of evaluating the severity of UHI of an area [11, 12]. Heat island effect is commonly associated with cities, as their surfaces are characterised by low sky view factor, low albedo, high impermeability and high thermal energy storage capacity [13].

2.2.1 The factors that contribute to UHI formation

Rizwan, Dennis and Liu demonstrated that UHI is the mutual response of many factors which could broadly be categorized as controllable and uncontrollable factors in Fig. 2.1 [14]. Controllable factors can be further categorized as sky view factor (SVF), green area, building material, air pollutants and anthropogenic heat sources. Wind speed, cloud cover, season and such temporary effect variables are determined as uncontrollable factors.

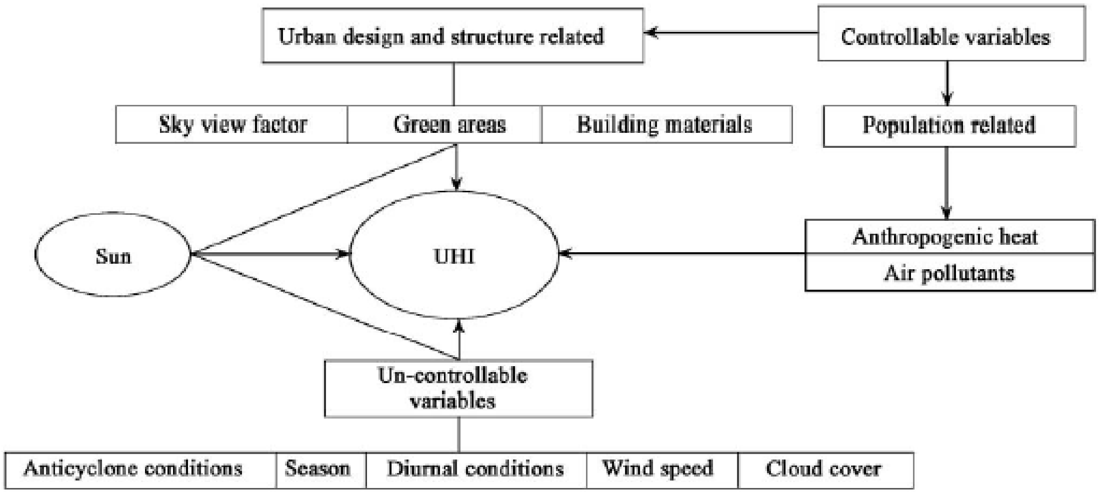

Fig. 2.1: Factors that contribute to UHI formation [14]

2.3 Urban energy balance

In order to study the contribution of different urban factors to the development of the UHI, it is indispensable to study the sensitivity of energetic balance with respect to thermal or geometric characteristics of the urban surface. Knowledge of the surface energy balance is considered fundamental to an understanding of the boundary layer meteorology and climatology of any sites. The heat generated within and stored by the city can be presented with the urban energy balance, which takes all the exchanges of energy into account (Fig. 2.2).

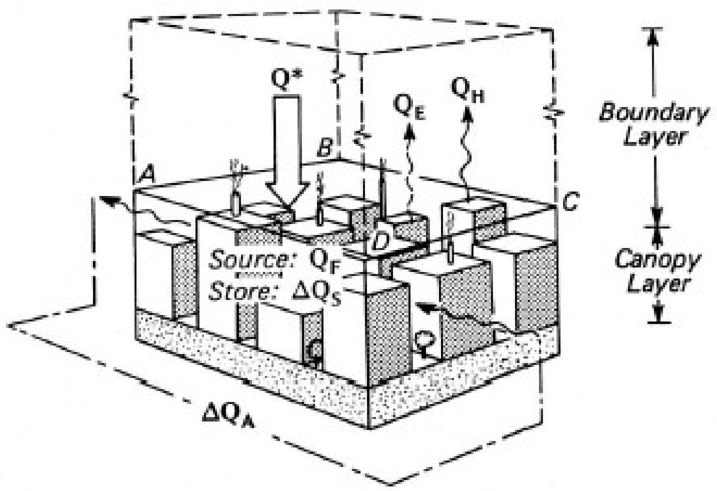

Fig. 2.2: Schematic of the volumetric averaging approach to urban energy balance [15]

The energy balance equation of any site was first proposed by Oke in 1977, as expressed below [16],

$$Q^* + Q_F = Q_H + Q_E + \Delta Q_S + \Delta Q_A \tag{2.1}$$

where, Q^* is net all-wave radiation at the top; Q_F is anthropogenic heat flux; Q_H and Q_E are respectively turbulent heat fluxes for sensible and latent heat; ΔQ_S is the net storage heat flux which includes soil heat flux and also the heating and cooling of the complete urban fabric and ΔQ_A is net local advection (the heat advection through the sides of the control volume).

Fig. 2.3 shows example energy balances for a typical natural landscape in rural area and an urban place in Houston [17]. The main differences regarding the energy balance in urban and rural areas are involving reflected solar radiation, outgoing infrared heat, latent heat release, sensible heat release, storage heat energy and anthropogenic heat.

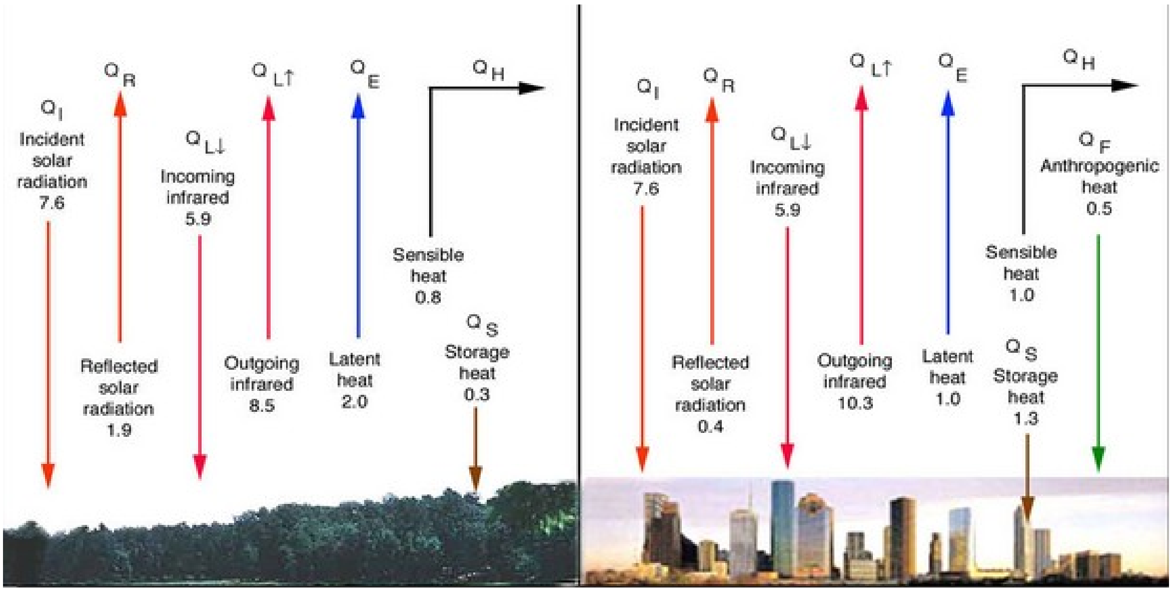

Fig. 2.3: Typical daily summer energy balances in rural and urban places in Houston (unit: kWh/m^2/day) [17]

2.3.1 Radiant heat

Net all wave radiation, Q* represents the short-wave and long-wave radiation received by the surface. The incident solar radiation, Q_I and downward long-wave radiation, $Q_{L\downarrow}$ are almost same for both rural and urban locations because the same sun shines on both environments with equal intensity. But rural space with a higher albedo value (reflectance, α) than urban area, reflects more solar radiation, Q_R. The upward long-wave radiation, $Q_{L\uparrow}$ from both rural and urban environments depends on the average effective temperature of the respective surfaces. The urban area with higher surface temperature will emit more long-wave radiation to the atmosphere. Thus, the net all wave radiation, Q* includes the short-wave radiant energy from sun and the long-wave radiation energy between the surface and the atmosphere (net infra-red energy, Q_L), can be presented by the following equation:

$$Q^* = (Q_I - Q_R) + Q_L = (1-\alpha) \times Q_I + (Q_{L\downarrow} - Q_{L\uparrow}) \tag{2.2}$$

The net infra-red energy, Q_L can be expressed, using Stefan's equation[18], as

$$Q_L = Q_{L\downarrow} - Q_{L\uparrow} = Q_{L\downarrow} - \{\varepsilon\sigma T_1^4 + (1-\varepsilon)Q_{L\downarrow}\} = \varepsilon(Q_{L\downarrow} - \sigma T_1^4) \tag{2.3}$$

Where ε is the wavelength – average emissivity of the surface, and the Stefan-Boltzmann constant $\sigma = 5.67 \times 10^{-8} \mathrm{Wm^{-2}K^{-4}}$.

Studies indicated that air emissivity, ε is strongly coupled to air vapour pressure (e_a) and air temperature (T_a) near the surface [19]:

$$\varepsilon = 1.24(e_a/T_a)^{1/7} \tag{2.4}$$

Air emissivity, ε can also be approximated by the empirical formula of Swinbank, because air vapour pressure also has strong correlation with air temperature, as follows [20]:

$$\varepsilon = 0.92 \times 10^{-5} T_a^2 \tag{2.5}$$

2.3.2 Anthropogenic heat

Anthropogenic heat, Q_F including cooling and heating buildings, industry, transportation and lighting, can affect the near-surface air temperature and potentially contribute to create the UHI effect. In a temperate city, anthropogenic heat flux may be a negligible component in summer, yet a significant component of the urban energy balance in winter. The value of anthropogenic heat is impossible to estimate over short time intervals, since it varies diurnally and with respect to ambient temperature in winter [21]. Usually, anthropogenic heat flux can be estimated to be a constant over a long period time. For example, in most major US cities, anthropogenic heat ranges between 20 and 40Wm^{-2} in summer and between 70 and 210 Wm^{-2} in winter [22]. Tab. 2.1 lists the annual average estimated anthropogenic heat flux, Q_F in selected cities [23].

Tab. 2.1: The annual average anthropogenic heating for selected city cores [23]

City	$\mathbf{Q_F}$ $(\mathbf{Wm^{-2}})$
Chicago	53
Cincinnati	26
Los Angeles	21
Fairbanks	19
St. Louis	16
Manhattan, NY City	117-159
Moscow	127
Montreal	99
Budapest	43
Osaka	26
Vancouver	19
West Berlin	21

2.3.3 Sensible heat flux

The sensible heat is carried from warm surfaces to the cooler air above by turbulent eddies and the reverse transport occurs when the air is warmer than the surface [24]. Urban areas generally have a larger sensible heat flux than rural surroundings and can maintain a positive sensible heat flux throughout the night [25]. The sensible heat flux from the street canyon into the boundary layer is increased by the increased surface area, but is decreased by the buildings reducing the local flow speeds.

The sensible heat flux, Q_H, over the surface area strongly depends on surface-air temperature difference and air resistance to heat transfer and can be calculated as below [26]:

$$Q_H = \rho C_p (T_R - T_a)/r_a \tag{2.6}$$

where ρ ($1.205 \mathrm{kg\,m^{-3}}$ at $20°\mathrm{C}$) is the air density, C_p ($1005 \mathrm{Jkg^{-1}\,m^{-3}}$) is the specific heat of the air at constant pressure, r_a (s/m) is the air resistance coefficient to heat transfer, T_R is the temperature at surface level and T_a is the temperature at atmospheric level.

The air resistance r_a is related to wind speed whose function is given as [27]:

$$r_a = \frac{\ln\left(\frac{z}{z_0}\right) - \varphi_H}{k\overline{u_z}} \tag{2.7}$$

Where k (0.4) is Karman's constant, $\overline{u_z}$ is horizontal wind speed at height z (m/s), z_0 is aerodynamic roughness length and φ_H is the stability correction parameter. φ_H can be negligible under the assumption of neutral stability.

2.3.4 Latent heat flux

The energy required for evaporation is generally termed as the latent heat flux, Q_E, which is typically smaller in urban areas than the rural surroundings, because there are less water space, green space and soil surface in urban areas.

The latent heat flux, Q_E, is given as [26]:

$$Q_E = 0.622L(e_a - e_s)/[P_a(r_a + r_s)] \tag{2.8}$$

where L ($2.45 \times 10^6 \mathrm{J\,kg^{-1}}$) is the latent heat of vaporization, e_a and e_s are the air and surface vapour pressures respectively, P_a (101.325 kPa) is the atmospheric pressure, r_s is the surface resistance (s m^{-1}), given empirically as [27]:

$$r_s = 100 \times (0.413\,\theta_s/\theta)^{1.5} \tag{2.9}$$

where θ is the volumetric soil water content (kg m^{-3}) and θ_s is the volumetric soil water content at saturation (kg m^{-3}).

2.3.5 Net storage heat flux

The net storage heat flux, ΔQ_S, is the net exchange of energy by sensible and latent heat changes in the urban canopy air layer, including the ground, vegetation and buildings [25]. It has been confirmed that the net storage heat flux depends on the urban structure, the thermal properties (thermal conductivity and heat capacity) of the urban materials, and the sun-surface-atmosphere coupling. The more intensive effect of nocturnal urban heat island is mainly caused by the nocturnal heat release from urban fabric, due to the difference in these characteristics between rural and urban spaces.

There are four common methods that could be used to predict the net storage heat flux.

a) Energy balance residual method

According to the energy balance, the net storage heat flux (ΔQ_S) can be determined as the residual from direct observations of the net all-wave radiation (Q^*), anthropogenic heat (Q_F), sensible (Q_H) and latent heat (Q_H) fluxes, as follows [28]:

$$\Delta Q_S = Q^* + Q_F - (Q_H + Q_E) \tag{2.10}$$

Where net advection term, ΔQ_A is ignored in the formula.

The primary drawback of RES is the accumulation in the net storage heat flux of measurement errors of each heat flux term in the energy balance, and error of having neglected any unmeasured terms, like the advection heat flux.

b) Objective hysteresis model

The objective hysteresis model (OHM) was proposed by Grimmond et al. in 1991 to calculate the storage heat flux as a function of net all-wave radiation and the surface properties of the site [29]. This method describes the observed nonlinear (hysteresis) relation between radiative forcing and heat storage changes for urban areas according to

$$\Delta Q_S = \sum_{i=1}^{n}(f_i a_{1i})\, Q^* + \sum_{i=1}^{n}(f_i a_{2i})\frac{\partial Q^*}{\partial t} + \sum_{i=1}^{n}(f_i a_{3i}) \tag{2.11}$$

where i is one of n surface types of varying fraction (f), such as roofs, walls, lawns, or roads. The time derivate of net radiation is approximated as $0.5(Q^*_{t+1} - Q^*_{t-1})$, with t = 1 h, and the coefficients of a area empirically derived from independent studies relating ΔQ_S to Q^* over specific urban surface types.

c) Town energy balance

The Town Energy Balance (TEB) model was primarily developed to simulate the energy and water exchanges between the city and the atmosphere [30]. It can also simulate the radiative, thermal, moisture and wind effects produced by the presence of buildings and streets based on local canyon geometry. The model can take conductions in roofs, roads and walls separately into account in TEB.

d) Thermal mass scheme

Another method to estimate the net storage heat flux is derived from basic concepts of heat conduction and volumetric heat storage in a material. The "struktur" model of Peikorz estimated the storage heat flux from the sum of the heat content changes of all components of the urban system [31]. So based on the "struktur" model, a thermal mass scheme (TMS) is constructed whereby exterior and interior surface temperature changes and information on the thermal properties and constriction area combined to estimate the net storage heat flux [28],

$$\Delta Q_S = \sum_{i=1}^{n} \Delta Q_{Si} = \sum_{i=1}^{n} \frac{1}{A_i} \int C_i \frac{\Delta T}{\Delta t} dV_i \tag{2.12}$$

where the index I identifies n surface types within the urban volume, Ai is the surface area of component I within the system, C_i is the heat capacity of material I, $\frac{\Delta T}{\Delta t}$ is the volumetric change in temperature over a given time period, and dVi is the element volume.

2.3.6 Net advection heat flux

The net advection heat flux, ΔQ_A is the net energy transferred to or from the system through advection under the form of sensible or latent heat. This term is commonly negligible in the urban energy balance, because urban areas are surrounded by buildings with an almost uniform density, but the net advection heat flux may be imported in the boundaries between the urban and the rural environment [28]. The net advection heat flux for the Marseille site was estimated by using a network of temperature and humidity sensors in a previous research [32].

2.4 The situation of UHI effect in the world

Due to the adverse environmental and economic impacts of UHI, the research regarding UHI situations at different types of cities located in different climate zones was being intensively studied.

The presence of UHI effect is quite clear in tropic area. For example, although there was no distinct borderline between urban and rural areas in Singapore, the maximum temperature difference of 4.01℃ between well planted area and CBD area [33]. The research also proved that green areas in cities can be considered as potential measure in mitigating UHI effect [33]. In the kind of hot humid climate, like Hong Kong, mitigating summer time nocturnal UHI effect is especially crucial to reduce the space-conditioning cost [34]. Schwarz, Lautenbach and Seppelt had a remote sensing-based surface UHI study whose dataset covered a total of 263 European cities on subtropics temperate and boreal continent [35]. Most UHI studies focus on its negative effect during summer, nevertheless, UHI effect is desirable during cold days. In London where the maximum UHI intensity in the order of 9.0℃ is observed in core area during winter, it is indispensable to devise meaningful strategies to mitigate the UHI during summer and retain its positive effects during winter. For instance, it is certified that the impact of surface albedo on lowering winter UHI is not as significant as summer [36].

2.5 The situation of UHI effect in Zhejiang Province

A constant increase in temperature has been recorded by researchers. There was a research project carried out a comprehensive ecological analysis of Chinese urban thermo-effect at 89 major Chinese cities in the past 50 years. The result indicated that the respective maximum urban thermo-effects in the 2000s and in the 1990s compared to that in the 1950s are 1.97K and 1.50K, respectively [37].

The Yangtze River Delta (YRD) as one of most developed dynamic, densely populated and concentrated urbanization area situated on the eastern seaboard of China is composed of Shanghai, southern Jiangsu and northern Zhejiang, as Fig. 2.4 shows [38]. Among the Yangtze River Delta area, Zhejiang Province is selected as the research area.

Following the success of Shanghai Pudong's development, the Zhejiang Province has come to realize the importance of having large city hubs for economic development. Zhejiang exhibited the highest average annual per capita growth in China between 1978 and 1995 [39]. Rapid urbanization process contributes to the situation of UHI and urban climate change in Zhejiang Province, especially Hangzhou and Ningbo certainly.

Fig. 2.4: Geographic location of the YRD [38]

2.5.1 The situation of UHI effect in Hangzhou

Hangzhou, the capital of Zhejiang Province, lies 180km southwest of Shanghai. Hangzhou with a total area of 16,596km^2 forms part of Yangtze River Delta region which is one of most developed dynamic, densely populated and concentrated urbanization area situated on the eastern seaboard of China, as Fig. 2.5 shows [40]. In 2011, the population of the Hangzhou Municipality was 8.7 million, of which approximately 5.38 million was in the administratively defined urban core[41]. Hangzhou focused on strengthening its central position through developing its technological innovations, distribution of commodities and tourism. The GDP of Hangzhou reached 11.3 billion USD in 2011, a rise of 10.1% over the previous year [41]. The city has enjoyed a double-digit GDP growth rate for 21 years in a row. Rapid urbanization process contributes to the formation of UHI and urban climate change in Hangzhou. The past 20 years has witnessed a significant rising of the average temperature in Hangzhou city. Since 2003, up to 40-50 days of continuous high temperature appeared in the summer of Hangzhou, which made it become the second hottest city in summer of China [7].

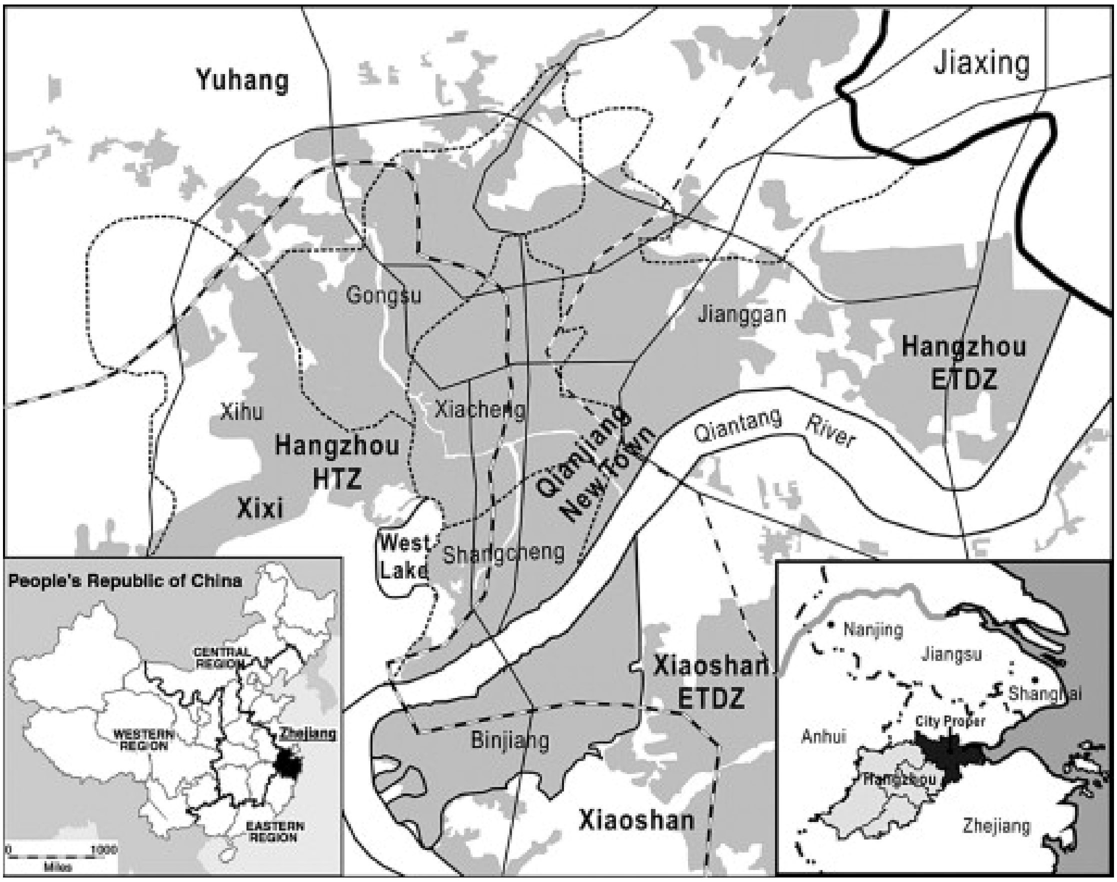

Fig. 2.5: Geographic location of Hangzhou [40]

Figure 2.6 displays the land surface temperature of Hangzhou which was measured by satellite-based thermal infrared remote sensing technology in 1991, 2000 and 2007. The obvious UHI situation in Hangzhou can be discovered even in 1991 and the situation was being more intense since 1991. According to the prior research measurement, it was found that the difference between highest surface temperature and lowest surface temperature occurred in Hangzhou was as high as 15℃ [42].

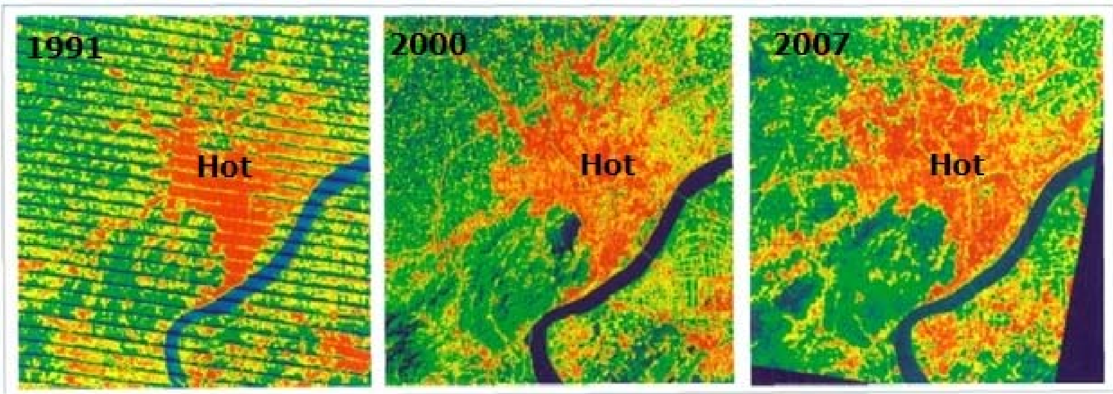

Fig. 2.6: Land surface temperature of Hangzhou in 1991, 2000 and 2007 [42]

2.5.2 The situation of UHI effect in Ningbo

In terms of Ningbo, as a major deep-water port for foreign trade, Ningbo has become an import industrial and economic centre in Zhejiang Province. Ningbo with a total land area of 9695km^2 is located in the middle of the eastern seaboard of mainland China, to the south of the Yangtze River Delta (see Fig. 2.7). Three major rivers flow through the plains of Ningbo: Yao River, Fenghua River and Yong River. In 2005, the total population of Ningbo was 5.57 million, of whom 1.83 million resided in urban areas

[43]. According to the statistics of the sixth national census, permanent residents of Ningbo have amounted to 7.61 million in 2011 [44]. Ningbo Municipal Statistics Bureau also figured out that the total GDP of this city reached 94.8 billion US dollars and per capita GDP has exceeded 12,300 US dollars in 2011 [45].

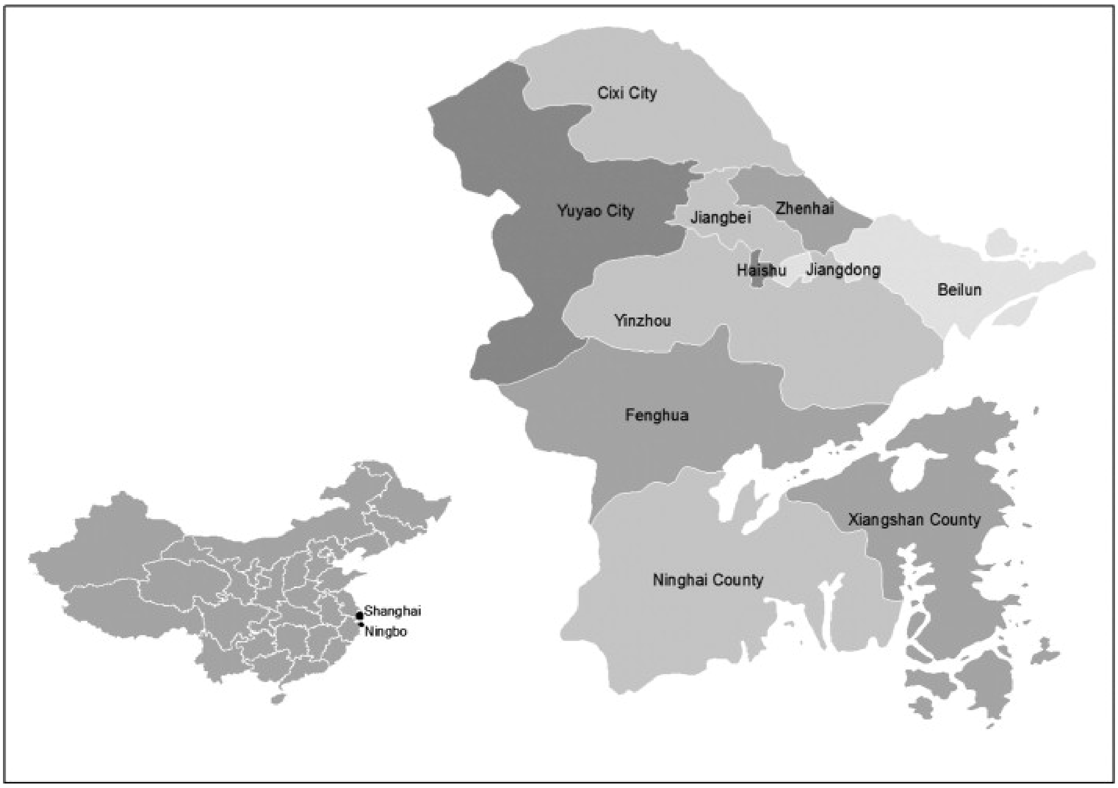

Fig. 2.7: Geographic location of Ningbo [46]

There is a weather station built up in 1961 at Ningbo Lishe International Airport which is about 6km away from Ningbo city centre. The temperature difference between this weather station and the city centre is used to predict the UHI intensity. According to the weather data recording from Ningbo Meteorology Bureau, it could be discovered from Fig. 2.8 that the average temperature at the city centre was even lower than in rural area from 1960s to 1970s. However, afterwards, the temperature difference between urban area and rural area was increasing by a rate of 0.13°C/55 years from 1961 to 2005, as the air temperature in urban area increases much faster than rural area. At the end of 2005, the temperature of city centre was 0.72°C higher than rural area [47].

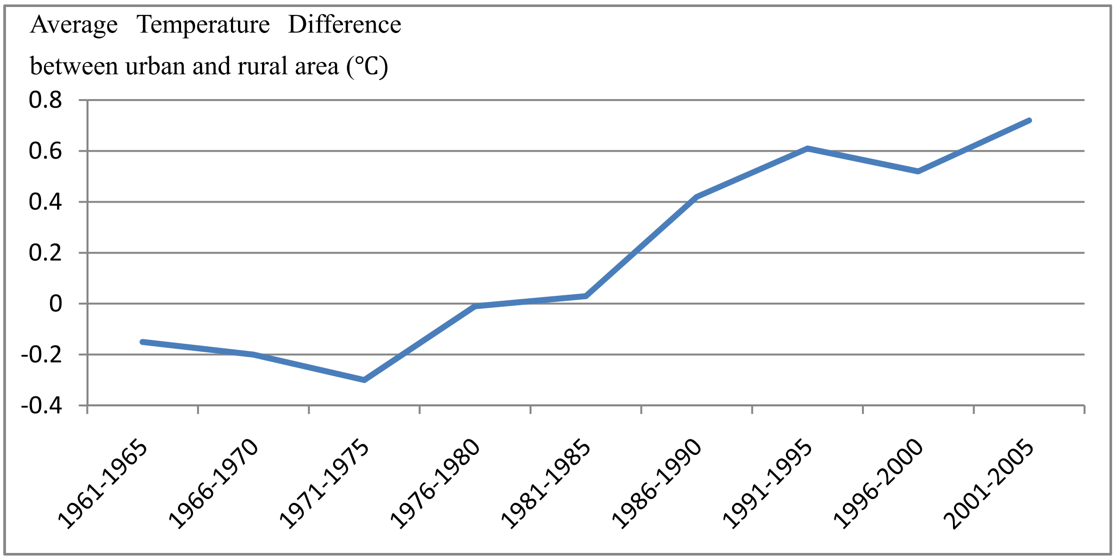

Fig. 2.8: Temperature difference between urban and rural area from 1961 to 2005 [47]

2.6 Approaches to study UHI

Observational approaches and simulation approaches are two popularised ways which have been applied by previous researchers in investigating UHI.

2.6.1 Observational approaches

A usual way to examine the UHI phenomenon is through setting sensors to measure ambient air temperature in a certain research urban area for a period of time. The UHI intensity is deduced through the comparison between the air temperature measured at urban area and that measured at rural area. Field measurement was first used by Howard to investigate UHI of London in 1818 [48]. In order to investigate the UHI situation in Athens, there were 23 experimental stations installed in the Athens urban and suburban regions to observe hourly ambient air temperature and humidity from 1997 to 1998 [49]. In terms of new case study of London, the locations of new measurements are shown in Fig. 2.9 and the reference location is London Heathrow Airport [50]. These measurement locations were decided only under consideration of distance from city centre, but comparing to the field measurement applied in this research, locations were strategically decided based on land-uses, SVF, distance and albedo of spaces.

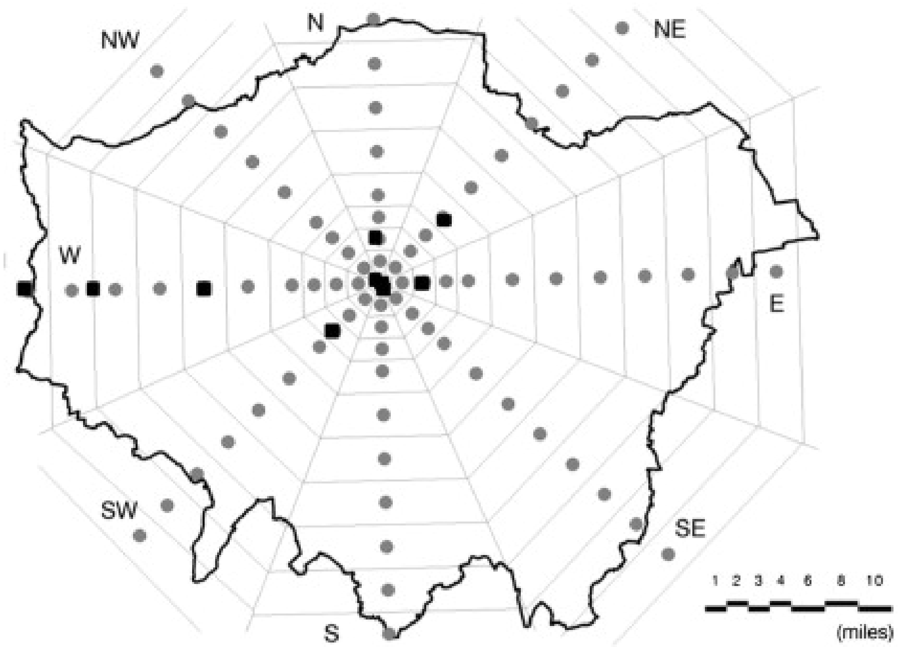

Fig. 2.9: The fixed temperature stations along the eight transects of the Greater London Area [50]

Another different way applied to observe UHI effect is via automobiles. In 1950 Sundborg's remarkable study of the local climate of Uppsala first used a thermometer attached to a car to provide a spatial picture of the urban heat island [51]. Fig. 2.10 shows the instrument mounted on the automobile roof.

Fig. 2.10: The instrument mounted on the automobile [51]

Saitoh and Shimada previously conducted field observation tests via automobiles for the ambient temperature in Sendai City in 1990 [52]. Afterward, in the research of Tokyo UHI, they also used three automobiles equipped with measuring devices to collect ambient temperature in the Tokyo metropolitan area on the day of 14 March 1992 [53]. As Fig. 2.11 displays, the total number of observation points is 359. Although the researchers thought that the ambient temperature varied slightly during the measurement period, these data were not collected simultaneously, unlike the method of field measurement. Hence, the measurement via automobile devices has been gradually abandoned in current research of UHI study.

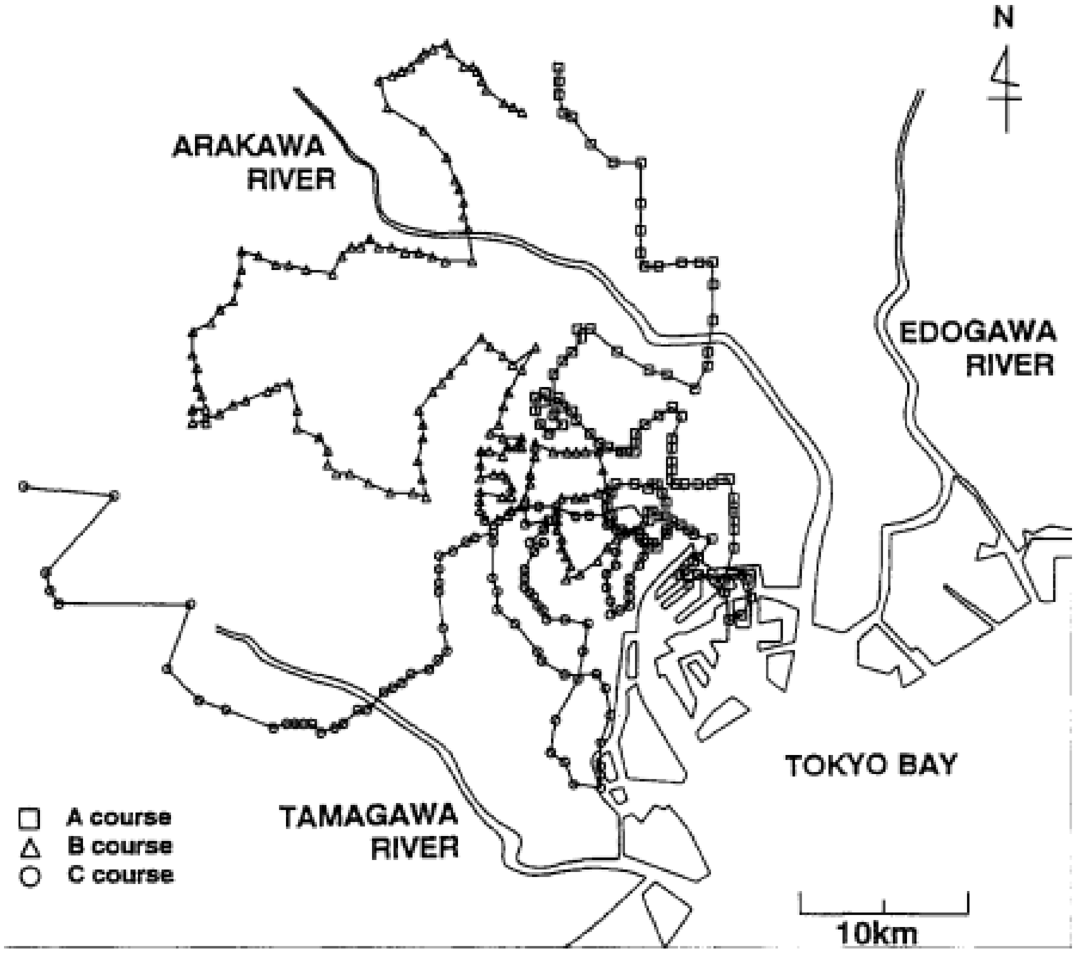

Fig. 2.11: Observation points and highway locations [53]

Although field measurement is an independent approach to measure air temperature, it has some limitations. The development and installation of measurement devices around a city are generally expensive and time-consuming task. For a long time of measurement, it is also difficult to filter the effect of unpredictable errors and the insecurity issues. The other weak point of field measurement is data analysis after collecting data. It is because limited stationary network or mobile stations can be sited and only a limited kind of parameters can be measured simultaneously.

Currently, due to the development of space technology and larger scale of UHI measurement required, airborne or satellite remote sensing techniques are applied as an alternative method [54]. The definition of urban remote sensing is study of urban environments from a distance- via measurements of emitted or reflected electromagnetic energy [55]. Generally, there are three methods have been developed to estimate land-surface temperature from space: the single infrared channel method, the spilt window method and a new day-night MODIS land-surface temperature method [56]. The relationship between UHI and land use changes in the region of Pearl River Delta in Guangzhou Province was investigated. In that study, Landsat TM and ETM+ images from 1990 to 2000 were selected to retrieve the brightness temperatures and land use types, as Fig. 2.12 shows [57].

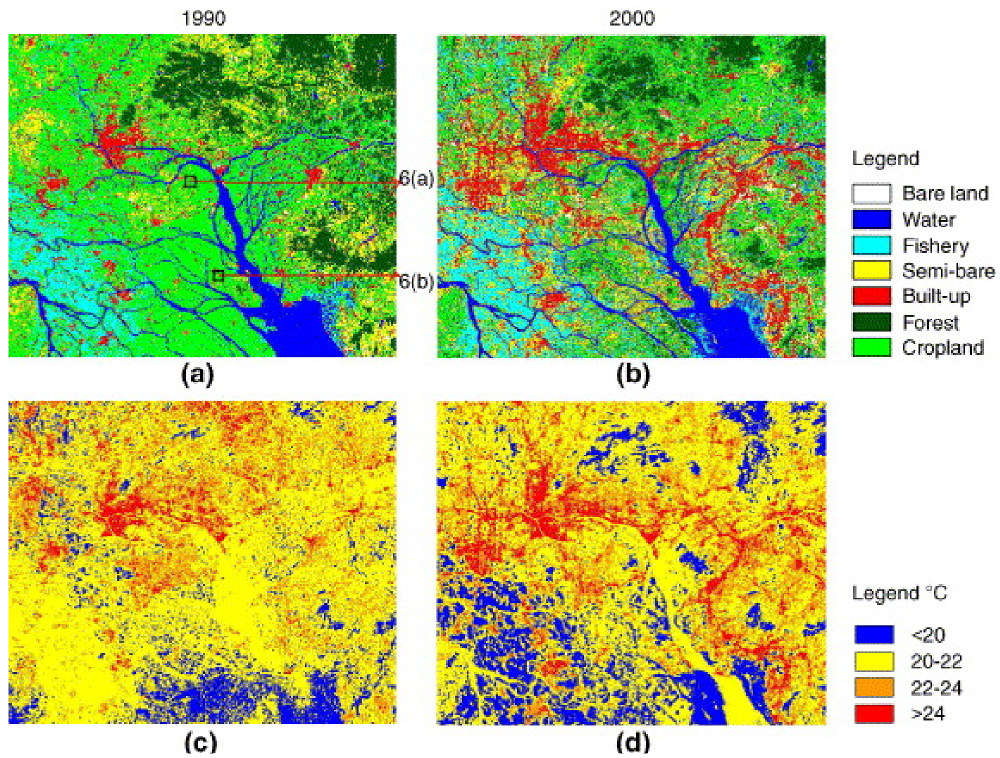

Fig. 2.12: Land use pattern and temperature distribution in the PRD region in 1990 and 2000 [57]

The resultant temperature measured by thermal remote sensing technologies contains the effects of surface moisture, surface emissivity, surface albedo, the irradiative input at the surface and the effects of the near surface atmosphere. Despite this, remote sensing is a very expensive approach and there is invariably a probability of cloudy sky when the satellite images capture the UHI over a land. The measured surface temperature can be significantly different from the ambient air temperature measured through field measurement in which turbulence and velocity activities have impact on the ambient air temperature [58].

2.6.2 Simulation Approaches

Computational simulation or mathematical model is also an effective strategy to assist the research regarding urban climate. Two kinds of models are normally applied in the UHI literature: the meso-scale meteorological model and the micro-scale model, by solving the governing equations of fluid in the urban area [59]. So far, soft computing software, such as Computational Fluid Dynamics (CFD) [60] and ENVI-met [61] have been widely used in the climate modelling.

2.6.2.1 Computational Fluid Dynamics (CFD)

In the summer of 2002, a simulation model in terms of Kyoto city was developed through CFD to simulate unsteady state heat conduction of grounds and building walls, radiation heat exchange between them and airflow. It was approved that the model could predict the real thermal environment of the Kyoto urban area, such as air temperature, humidity, wind velocity and boundary layer heat flux [62]. A canyon air temperature (CAT) model in Adelaide, Australia was also produced by CFD to test field data measured in a monitoring programme from 2000 to 2001. The predicted air temperature was correlated well with measured data over extended periods after the iterative calibration of model [63].

CFD is commonly applied to model urban environment, because CFD can simultaneously solve the governing equations of fluid inside the urban area: conservation of mass, potential temperature and momentum. The main difficulty that need to be overcome is the description of boundary conditions that in a complex urban setting are usually not defined with sufficient accuracy [63].

2.6.2.2 ENVI-met

Computer simulation using ENVI-met was the method that provided enough control on certain variables while providing enough flexibility to change others. ENVI-met, developed by Dr. Michael Bruse, is based on several principles of fluid dynamics, thermo-dynamics and atmospheric physics [64]. It has the ability to calculate the microclimatic dynamics of complex urban structures, flow between buildings and heat exchange processes between the various surfaces. The basic data structure of

ENVI-met is represented in Fig.2.13.

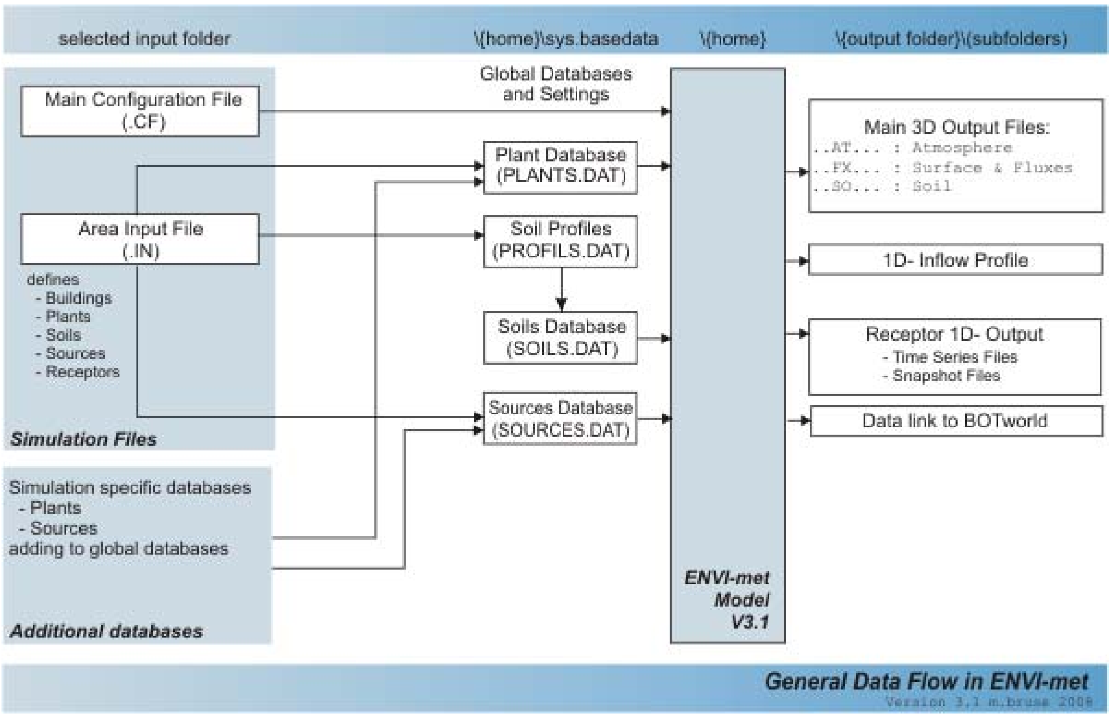

Fig. 2.13: Basic data structure of ENVI-met [64]

ENVI-met is also quite recommended by some researchers in urban climatology, building design and planning research, such as Fahmy and Sharples for studying green structures [65] and Okeil for airflow behaviour simulation [66]. In order to substantiate field measurement findings, Thapar and Yannas used the software to measure temperature variations and wind speed around specific urban forms [67]. Hedquist et al. used ENVI-met along with field measurements and CFD software and reported accurate results in terms of temperature variations in high density areas [68].

2.7 Adverse impacts of UHI

The adverse impacts of UHI include the deterioration of living environment, increase in building energy consumption [69], elevated emission of air pollutants [70] and greenhouse gases and even an increase in mortality rates [71]. Additionally, Lin et al. found that the UHI effect also has a significant impact on land sea circulation [72]. It could enhance the sea breeze in the daytime and weaken the land breeze during the night time, which is adverse to air pollution diffusion and impact the air quality during night time.

2.8 Concluding remark

This chapter has presented the comprehensive reviews about the significant subjects related to this research. The first issue that has been addressed is the background information of UHI effect. The UHI effect can be defined as a metropolitan area which is warmer than its surrounding regions. Controllable factors, including sky view factor (SVF), green area, building material, air pollutants and anthropogenic heat sources, and uncontrollable factors, such as wind speed, cloud cover, season and other temporary effect variables, all contribute to the UHI formation. Unlike uncontrollable factors, controllable factors are mainly determined by human activities.

In theory, investigating the sensitivity of energetic balance with respect to thermal or geometric characteristics of the urban surface is regarded as an effective way to understand the UHI development. The generation of energy balance equation is based on six types of heat energy, involving radiant heat, anthropogenic heat, latent heat, sensible heat, net storage heat and net advection heat.

The literature reviews have indicated that most metropolitan areas over the world are suffering from UHI situation. Hangzhou and Ningbo, as two most developed cities of Zhejiang province in China, whose UHI situations are becoming more serious with their rapid urbanisation development.

This review has also addressed that observational approach and simulation approached have been widely used in studying UHI so far. Each methodology has its own limitations and strengths. Both two types of approaches were therefore applied and complemented each other to study UHI in this research.

Through the numerous investigation of UHI effect, the adverse impacts of UHI have been noticed, such as the deterioration of living environment, increase in building energy consumption, elevated emission of air pollutants and greenhouse gases and even an increase in mortality rates.

CHAPTER 3: SIMULATION WORK OF UHI

3.1 Introduction

Urban expansion can reduce natural underlying surfaces and also weaken the curb of natural ecology on the heat island. Before executing the real field measurement, this research first applied simulation approach to investigate the UHI effect. Based on the adaptive use of ENVI-met (with LEONARDO programme), the study selected Hangzhou as a case study to indentify how natural ecological resources, such as water space and wetland, playing positive roles to improving outdoor built environment and remedying UHI intensity. This study compared the consequences of different development scenarios referring to Xixi Wetland and West Lake on Hangzhou urban climate. Moreover, the study also evaluated the impact of wind speed and direction on mitigating UHI.

In order to understand and solve problems in complex environmental settings effectively, environmental modelling has been used more frequently in scientific research area. For this case study, the ENVI-met climate model (Version 3.1 Beta 5) developed by the Research Group Climatology at Ruhr-University Bochum in Germany for the microclimate modelling was selected to simulate urban climate parameters, such as air temperature, relative humidity and wind velocity [64]. Mirzaei and Haghighat [73] commented that there are several limitations referring to the field measurement approach to UHI research. These include expensive costs and time-consuming of taking field measurements; making it difficult to achieve an overall picture of UHI pattern and obtaining consistent results. Therefore, this initial study was conducted using the three-dimensional numerical model ENVI-met, which is mainly applied to simulate the surface–plant–air interactions in the urban environment. ENVI-met is based on several principles of fluid dynamics, thermo-dynamics and atmospheric physics and has been widely applied in urban climatology, building design and planning research. The quantitative evaluation has shown that the ENVI-met model is capable of predicting the thermal behaviour of different ground surfaces with good accuracy [65, 74, 75].

3.2 Running case study

West Lake is a famous tourist lake, located west of the city centre of Hangzhou, with latitude of $30°15'$N and longitude of $120°10'$E. West Lake is a small shallow lake with an average depth of only 1.56 m, and its area is 5.66 km^2 [76]. Xixi National Wetland Park is also located in the west part of Hangzhou, only 6 km from the city centre and 5 km from the West Lake. Historically, Xixi Wetland covered an area of 60 km^2 and currently, the overall area of the protected Xixi Wetland is 11.5 km^2 because of human activities. West Lake and Xixi Wetland are both rare urban ecological resources in Hangzhou. They serve similar functions and complement each other in improving the urban environment. The effects of the West Lake and Xixi Wetland on the urban microclimate in Hangzhou city were investigated in this research. Fig. 3.1 shows the general layout of Hangzhou city and locations of West Lake and Xixi Wetland.

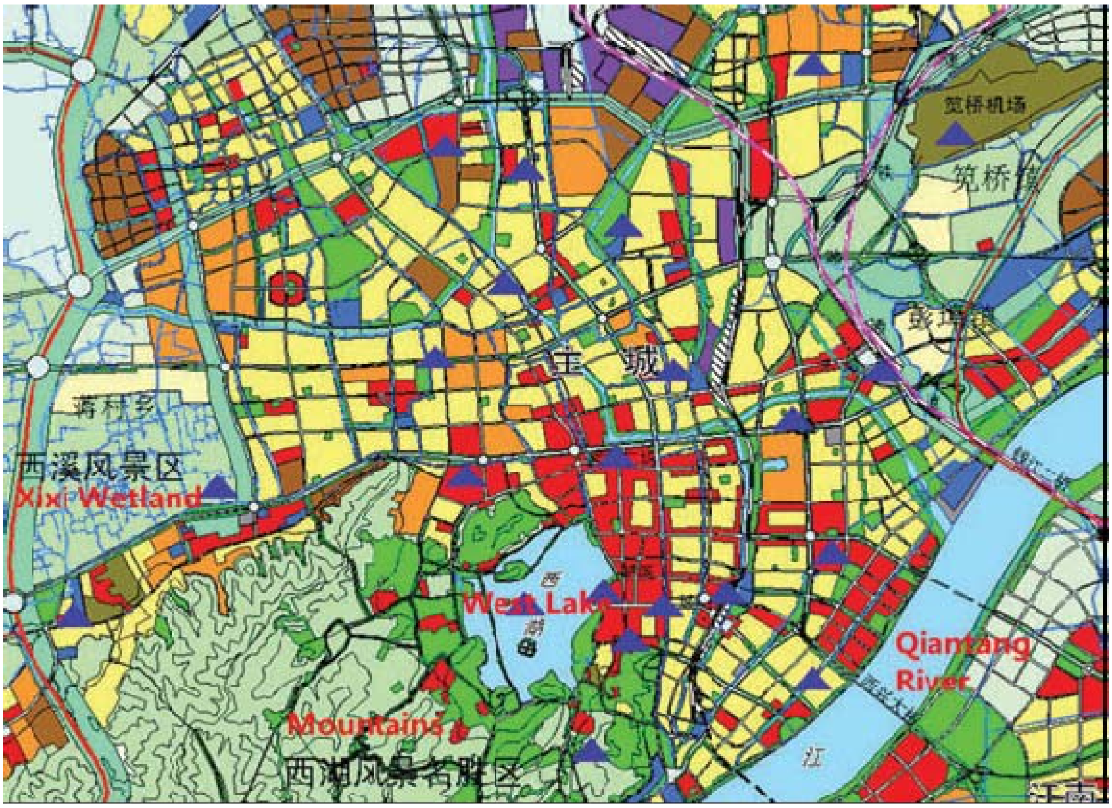

Fig. 3.1: The General Layout of Hangzhou City [77]

The programme simulated the model for a 24-h period, with updating surface data every 60s, starting from 12:00, 23 June 2011, designated as the start of summer. The settings to run the simulation are listed in Tab. 3.1. The thermal properties of the building system are defined by the indoor temperature and the heat transmission through the walls and roofs. In addition, the mean albedo of walls and roofs were set as below. The most paramount part of simulation conditions are the environmental parameters, such as initial outdoor temperature, wind speed and relative humidity. The case study assumes that there is no dynamic change of these environmental parameters during the running period. Besides, for each type of building facade is assumed to be parameterised with a single mean thermal property. A user-specified area input file defining the three-dimensional geometry of the study area is required for the simulation. The file would include geo-coded building dimensions (e.g. width and height), soil (e.g. type and texture), surface (e.g. concrete or water) and vegetation types. However, since ENVI-met is limited to simulate at micro-scale, the whole area of Hangzhou is perhaps too large for it to model completely. Thus, the model used in this study focuses on an area of Hangzhou around the West Lake and Xixi Wetland.

Tab. 3.1: Selected input parameters for ENVI-met base simulation

Category	**User input during simulation**
Test date	23 June 2011
Test period	24hours
Wind speed in 10m above ground	2m/s
Wind direction (0=N; 90=E; 180=S; 270=W)	135
Mean roughness length of study area	0.2
Specific humidity in 2500m	9g water/kg dry air
Relative humidity in 2m	40%
Initial atmospheric temperature	308K
Fraction of low clouds (x/8)	2
Fraction of medium clouds (x/8)	4
Fraction of high clouds (x/8)	2
Soil inputs	
Initial soil temperature at upper layer (1-20cm)	313K
Initial soil temperature at middle layer (20-50cm)	315K
Initial soil temperature at lower layer (below 50cm)	317K
Moisture content upper layer	40%
Moisture content middle layer	45%
Moisture content lower layer	50%
Building inputs	
Building interior temperature	298K
Mean heat transmission of walls	1.94W/m^{2}K
Mean heat transmission of roofs	6 W/m^{2}K
Mean wall albedo	0.2
Mean roof albedo	0.3

3.3 Results

The results referring to temperature, relative humidity and wind speed were obtained from the simulation with ENVI-met programme. The urban air temperature performances based on different development scenarios were compared in this part as well.

3.3.1 Air temperature distribution

According to the input conditions listed in Tab. 3.1, Fig. 3.2 reveals an obvious heat island in Hangzhou urban area. The maximum UHI intensity in Hangzhou city centre is up to 4.0-4.5℃ and gradually weakened from the urban core area to the urban boundary areas. It can also be noticed that the densely concentrated buildings gather more heat and cause the more intense of UHI effect. Air temperatures are relatively lower in areas concentrated with vegetation and water surfaces, such as the Xixi Wetland, West Lake and Qiantang River. Moreover, wind flow can spread the cold air in these areas, producing cooling effect on their surroundings.

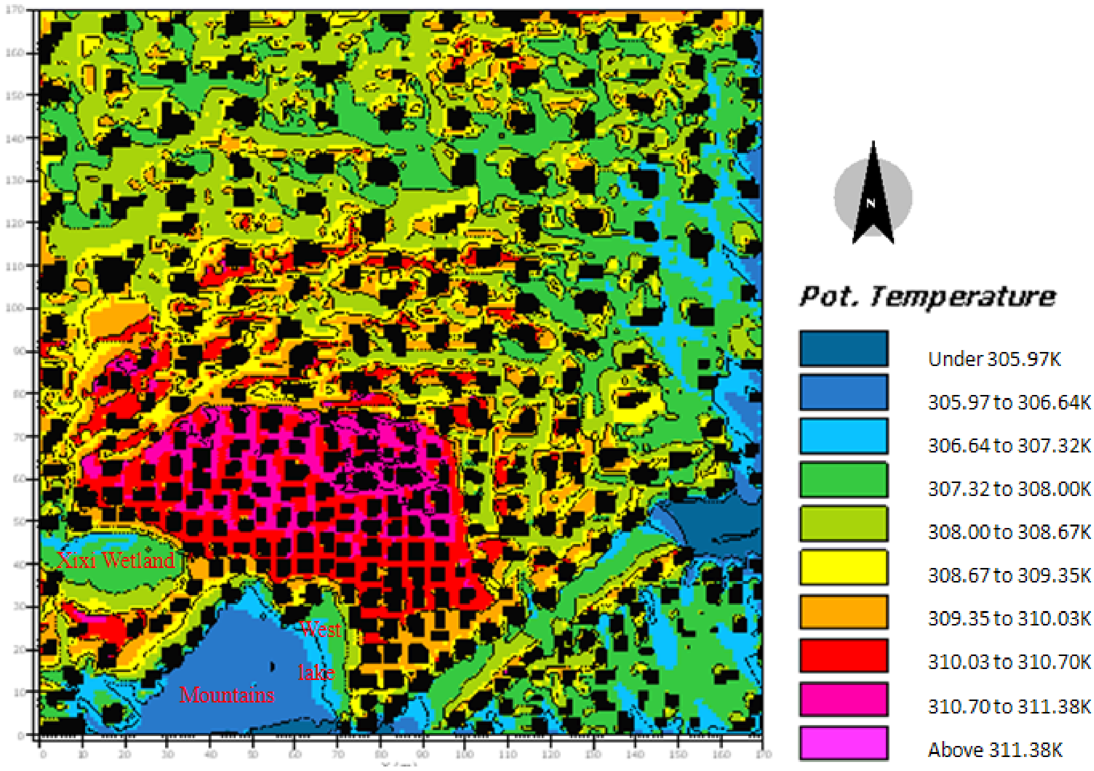

Fig. 3.2: Simulated temperature distribution in Hangzhou city centre at 13:00 23rd June 2011.

3.3.2 Relative humidity distribution

Fig. 3.3 shows the relative humidity distribution in Hangzhou city centre. There is a phenomenon that the relative humidity in urban area is 20% lower than boundary areas, which is normally called the Urban Dry Island (UDI) effect. It can be generally agreed that the UDI effect is commonly accompanied by UHI situation due to the rapid urbanization process. The lower urban humidity is mainly ascribed to the reduced urban evapotranspiration, which results in the weak latent heat release.

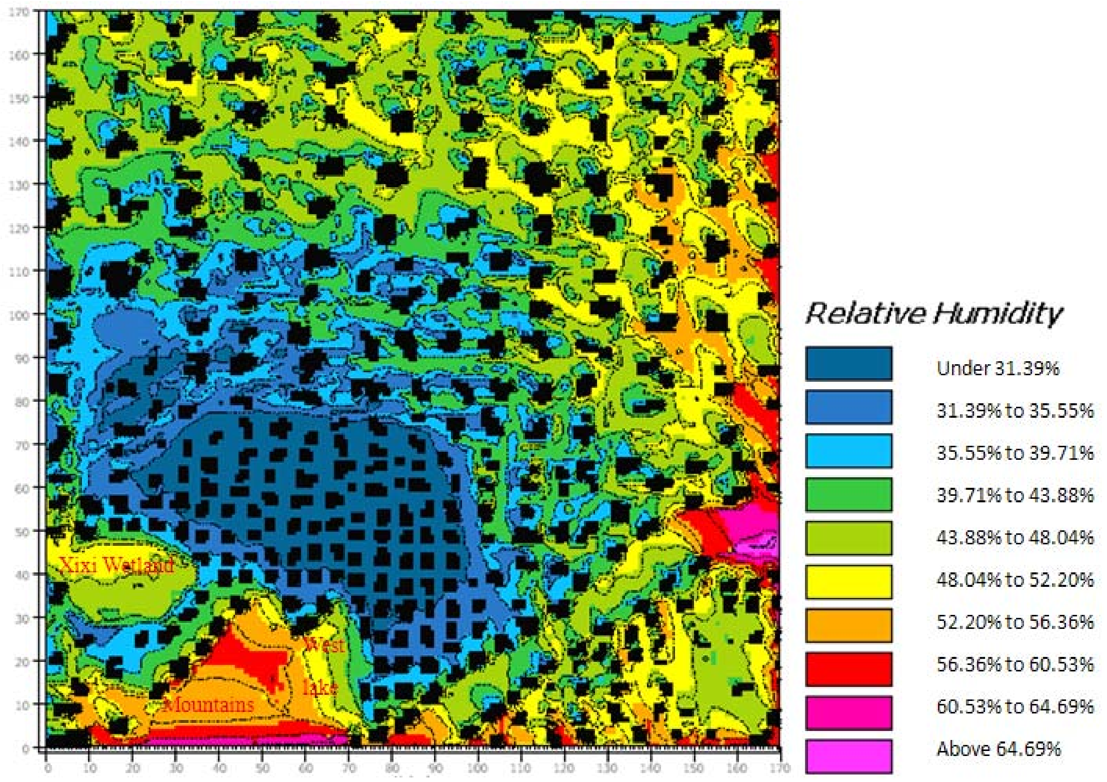

Fig.3.3: Relative humidity distribution in Hangzhou city centre at 13:00 23rd June 2011.

3.3.3 Wind speed distribution

As Figuerola and Mazzo [78], and Kidder and Essenwanger [79] demonstrated, wind speed is one of the most significant meteorological parameters that can influence the development of the UHI effect. Fig. 3.4 (a, b, c) show the wind speed distributions at 0, 10 and 30 m height in Hangzhou city at 13:00 on 23 June 2011 respectively. The prevailing wind direction is southeast in Hangzhou during summer period. On the basis of the comparison in Fig. 3.4 (a, b, c), it is obvious that the wind speed increases with height as building constructions cause obstructions to the flow of wind and modifies the encompassing wind environment. In general, mean urban wind speeds are consistently

20–30% lower than rural places, especially during the day [80]. In this model, the wind speed in urban centre area is roughly 25% lower than surrounding area.

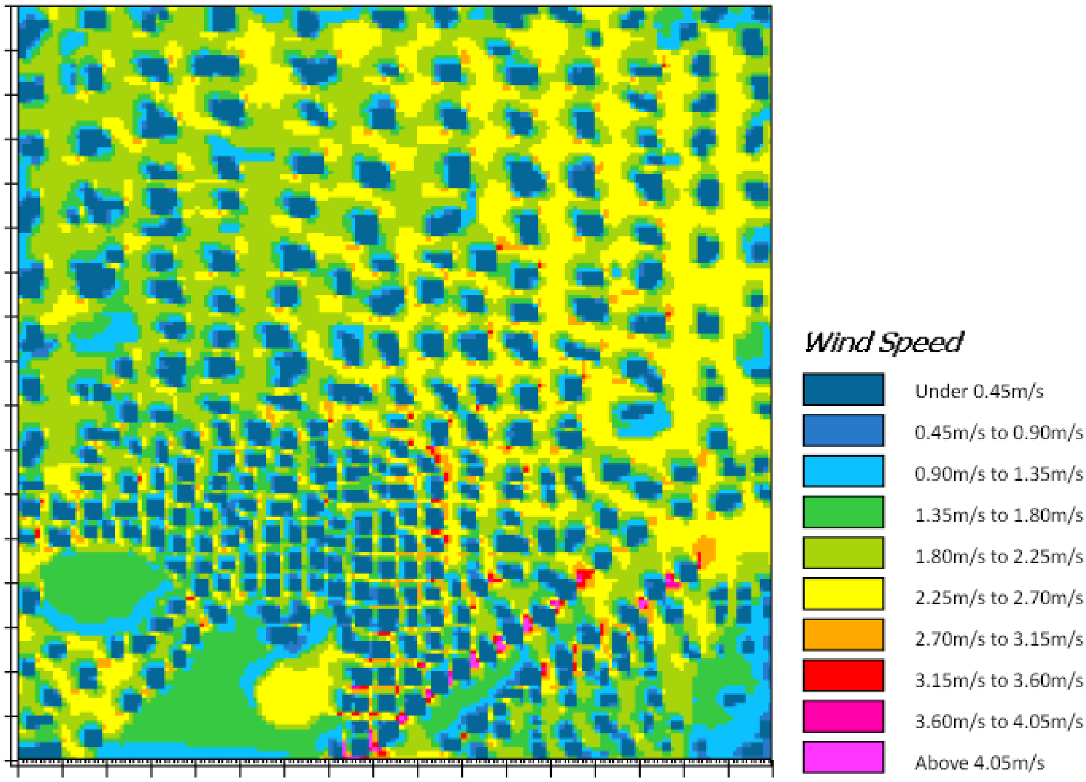

Fig. 3.4 (a)

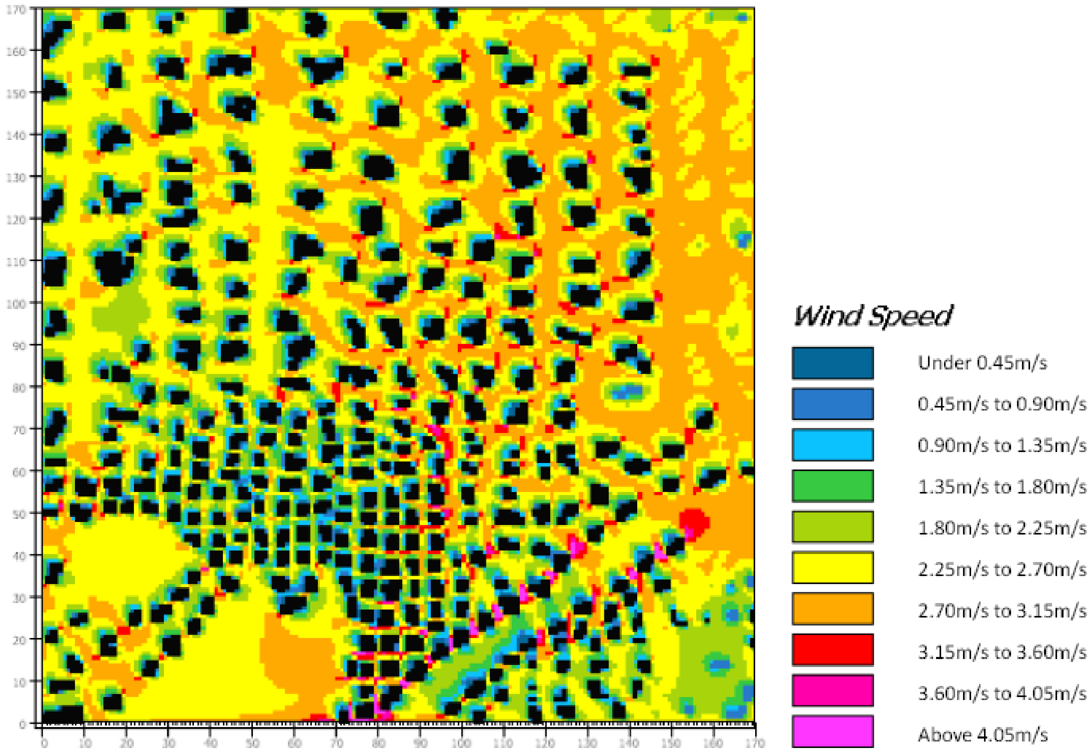

Fig. 3.4 (b)

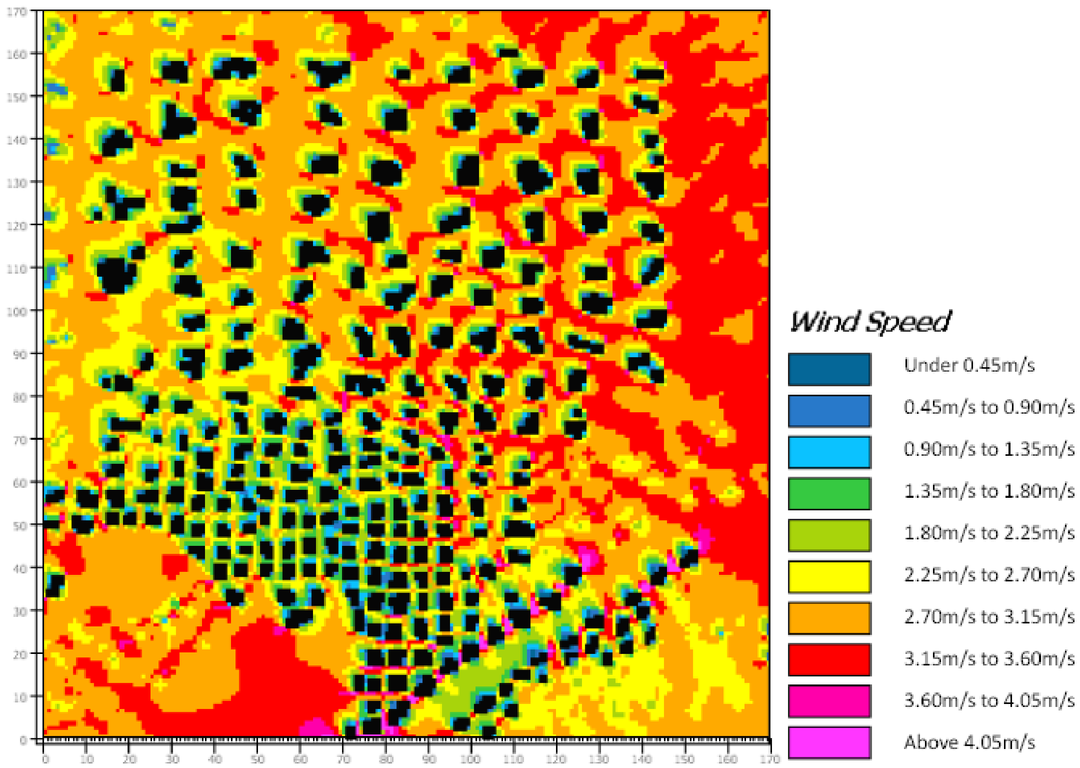

Fig. 3.4 (c)

Fig. 3.4: Wind speed distribution at (a) 0m, (b) 10m and (c) 30m height in Hangzhou city centre at 13:00 23rd June 2011.

3.3.4 Temperature comparison

West Lake and Xixi Wetland, as two natural underlying surfaces, are both full of water and vegetation. Apart from the ability of vegetation to lower surface temperatures by releasing water to the environment through evapotranspiration process, water space with great albedo can reflect more solar radiation to relieve the UHI effect. In order to further find out the impact of West Lake and Xixi Wetland on UHI situation in Hangzhou city centre, the research evaluates the scenarios if they are transformed into building construction areas. Fig. 3.5a shows the situation of West Lake and Xixi Wetland as they are; Fig. 3.5b shows the situation that the West Lake is transformed into building construction area; Fig. 3.5c shows the situation that Xixi wetland is transformed into building construction area and Fig. 3.5d shows both West Lake and Xixi Wetland transforming into building construction area.

According to the comparison, it can be noticed that the average air temperature or the UHI intensity in general urban area will be increased by 0.5°C roughly if both West Lake and Xixi Wetland are transformed into building areas. It seems that these urban natural ecological sources can mainly affect the area closing to these natural ecological resources, but cannot able to remedy the UHI situation in the whole city significantly.

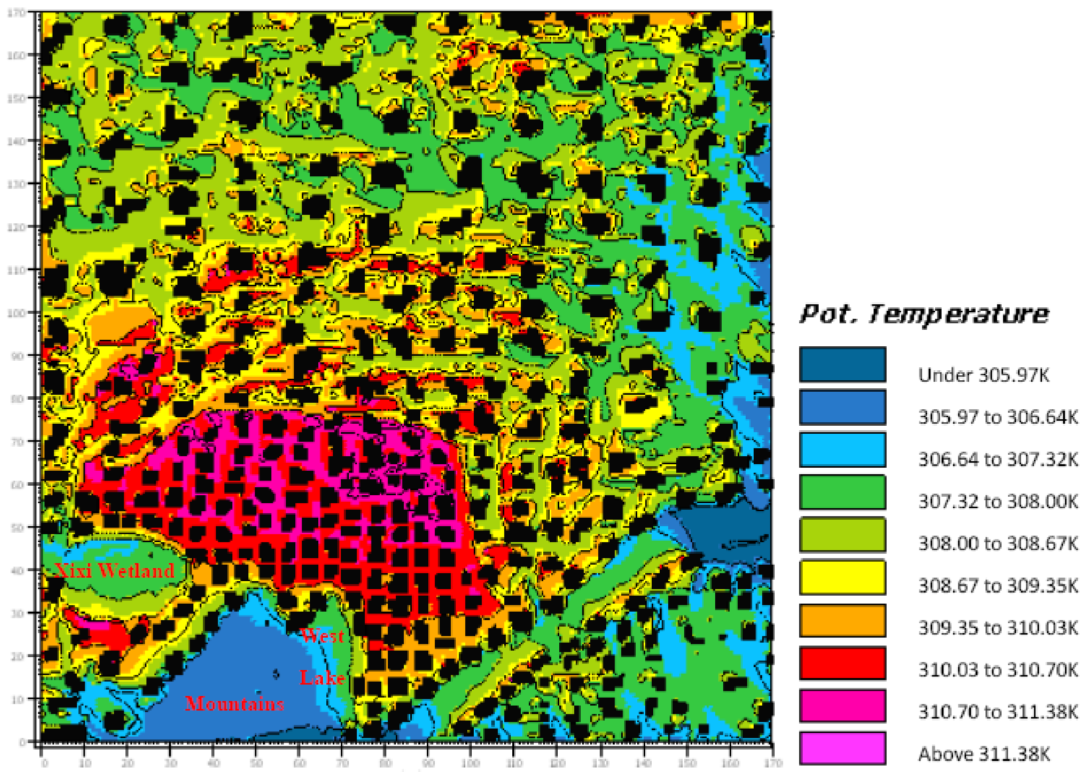

Fig. 3.5 (a): The air temperature distribution at the scenario that no transformation of West Lake and Xixi Wetland

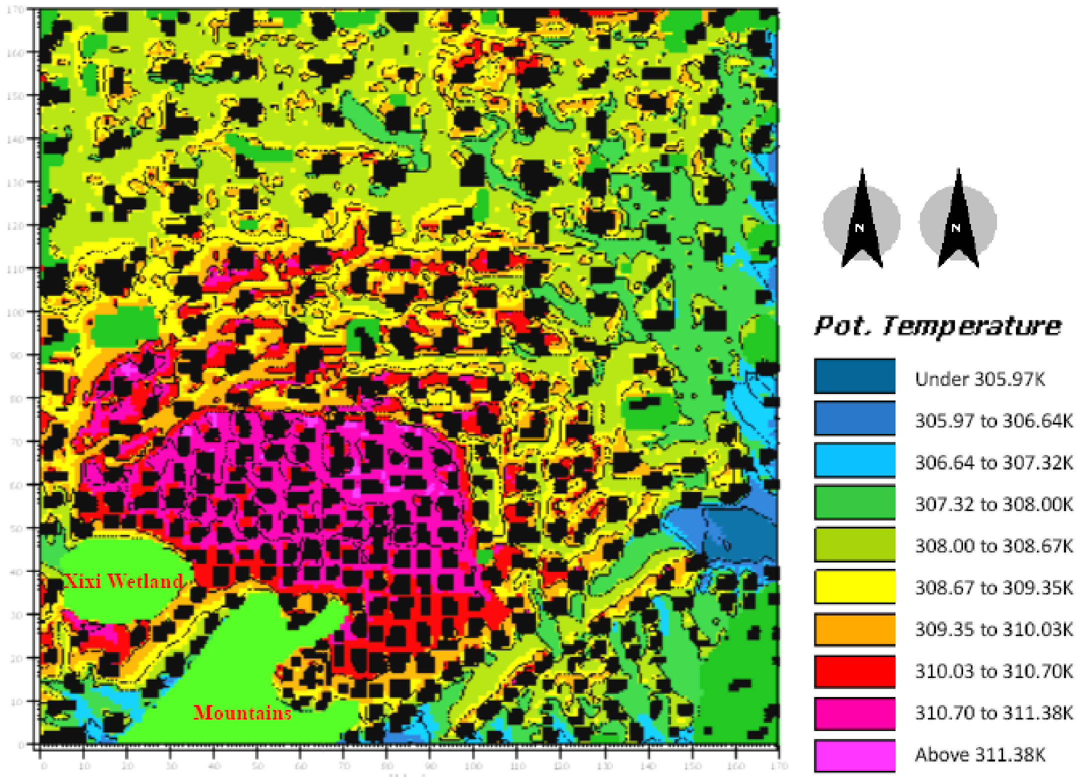

Fig. 3.5 (b): The air temperature distribution at the scenario that West Lake transformed into building construction area

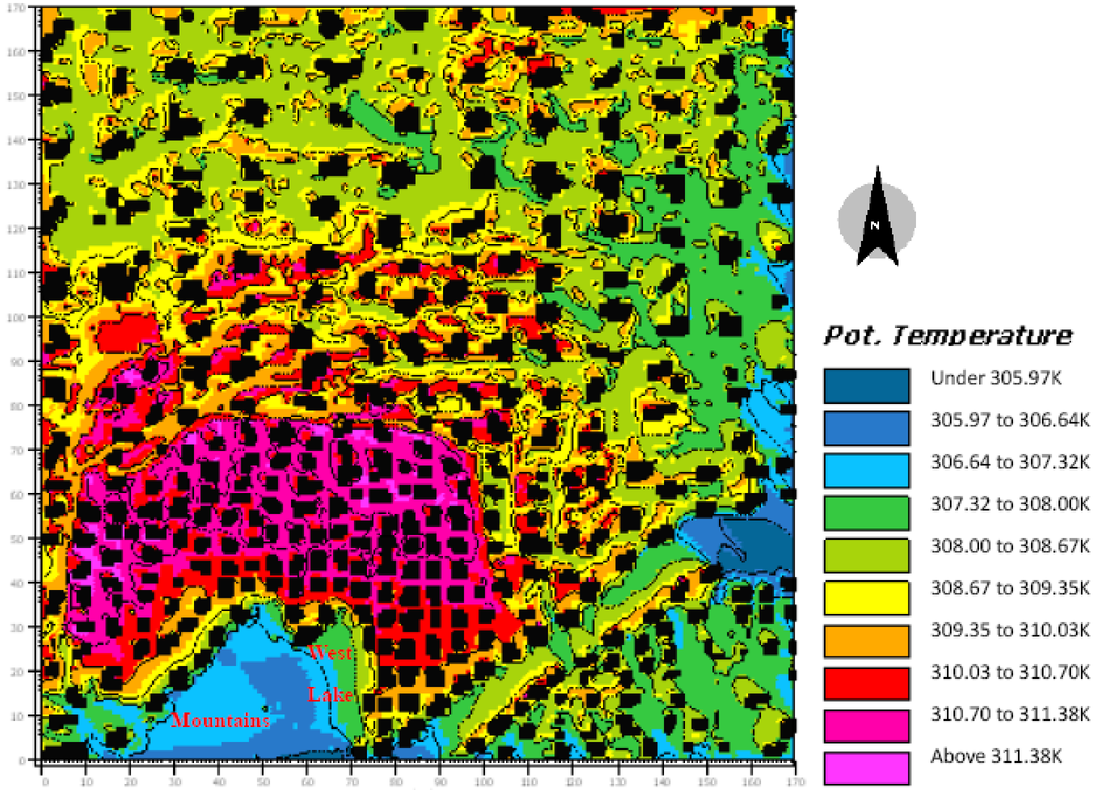

Fig. 3.5 (c): The air temperature distribution at the scenario that Xixi Wetland transformed into building construction area

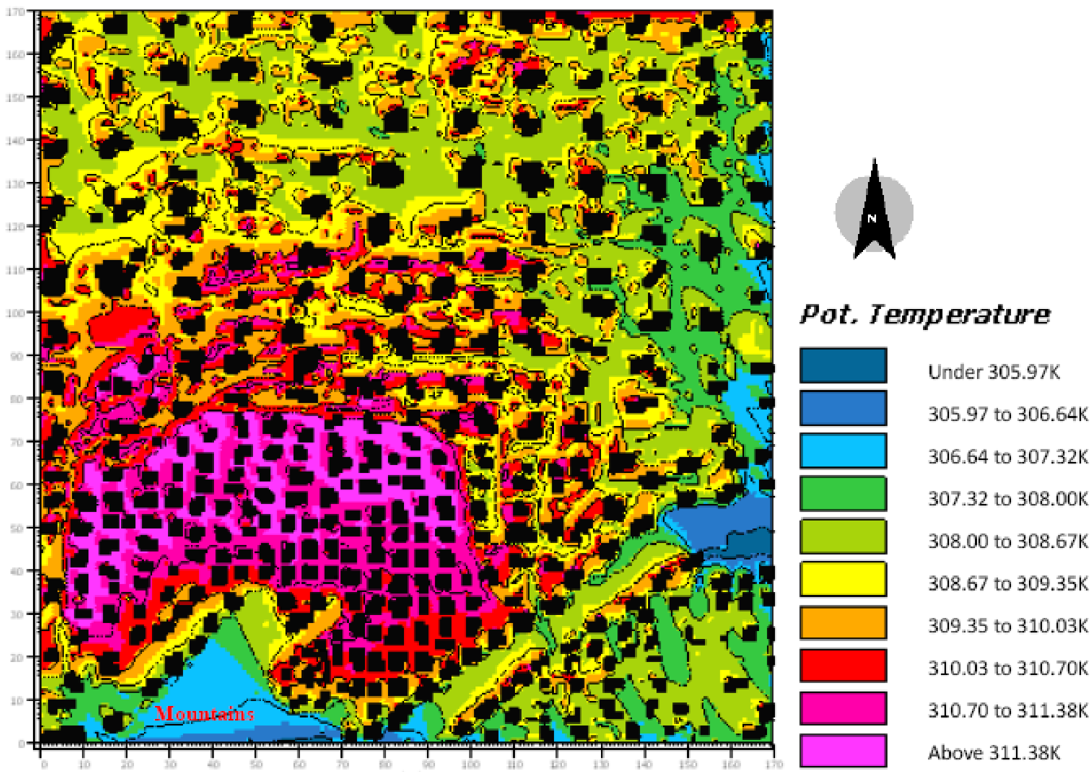

Fig. 3.5 (d): The air temperature distribution at the scenario that West Lake and Xixi Wetland both transformed into building construction area

3.4 Discussion

The following are the discussions from the results simulated by ENVI-met programme.

3.4.1 Impacts of West Lake and Xixi Wetland on UHI in Hangzhou

Urban expansion reduces much natural underlying surface and weakens the mitigation of the natural ecology on the heat island. West Lake and Xixi Wetland are two types of underlying surfaces containing a large amount of water by nature. The radiation process between the atmosphere, vegetation and soil surface, exchange of sensible and latent heat, and heat transfer of thermal conduction between soil and soil pore space occurring in the energy conversion may all directly or indirectly affect the micro-climate. Amongst these radiation processes, their cooling effect directly or indirectly affects the surrounding climate, which is conducive to improving the micro-climate of local urban areas and weakening the UHI effect.

However, the average UHI intensity is only reduced by 0.5℃ under the cooling effect of West Lake and Xixi Wetland in this simulation, which is far below expectation. The weak cooling effect of these two natural ecological sources is mainly caused by the weak wind-induced convective heat transfer between natural sources and urban construction area. According to Memon and Leung, 1 m/s increase in wind speed could roughly decrease the UHI intensity by 1.9 K [81]. As Fig. 3.4 (a–c) displays, the wind speed in urban area is lower than in urban boundary areas so that the convective heat transfer in dense building constructions is less effective. The wind speed at 10 meter above the ground in the prime simulation model is set as 2m/s. If the wind speed increases to 4m/s, the average air temperature appears to decrease by 1.5℃ and the UHI situation is also relieved more significantly, as Fig. 3.6 (a and b) displays.

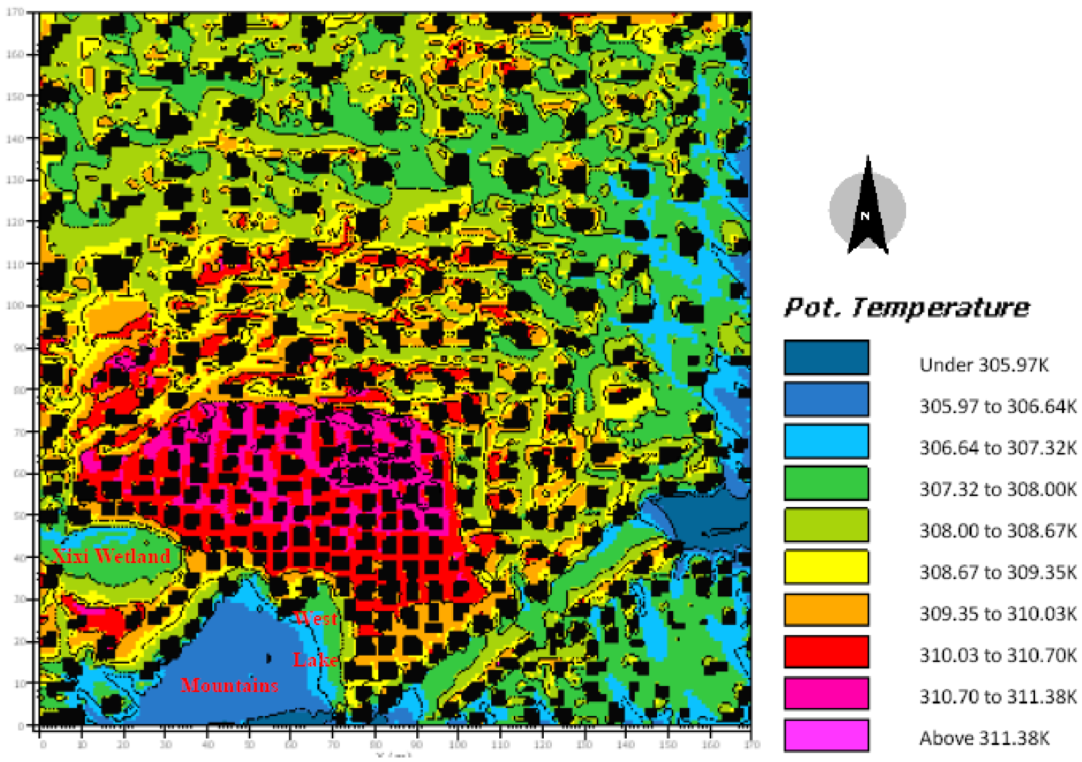

Fig. 3.6 (a)

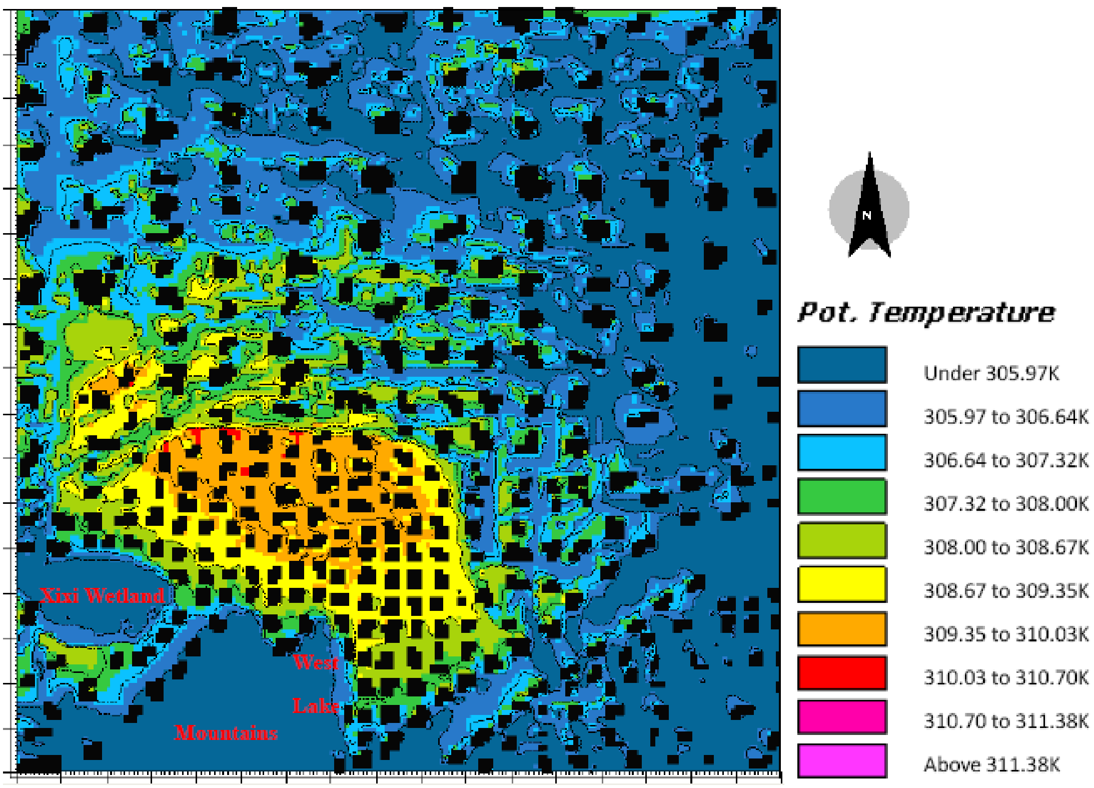

Fig. 3.6 (b)

Fig 3.6: Temperature distributions when wind speed is (a) 2m/s and (b) 4m/s at 13:00

The impact of wind speed on UHI can be also demonstrated by the vertical variation of UHI intensities. As Fig. 3.4 (a–c) shows, the wind speed at 30 m height is about twice greater than that on the ground. As a result, the UHI intensity at the bottom of the urban canopy is much higher than that on the top of the urban canopy, as Fig. 3.7 (a and b) displays.

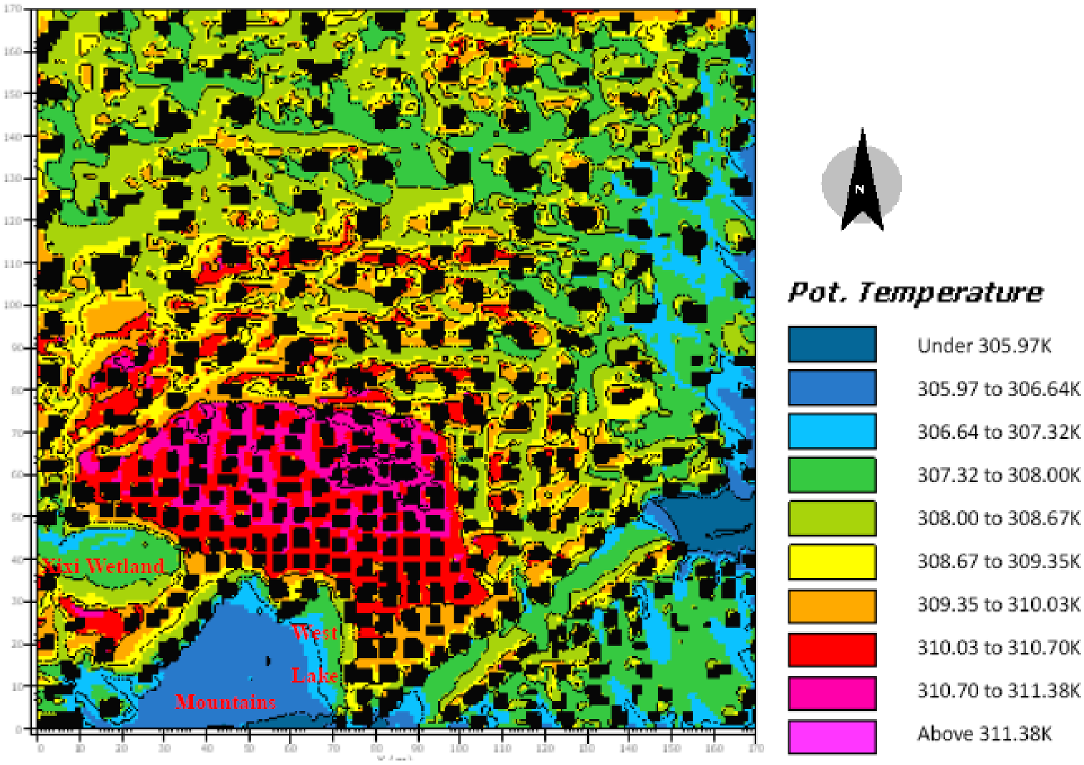

Fig. 3.7(a)

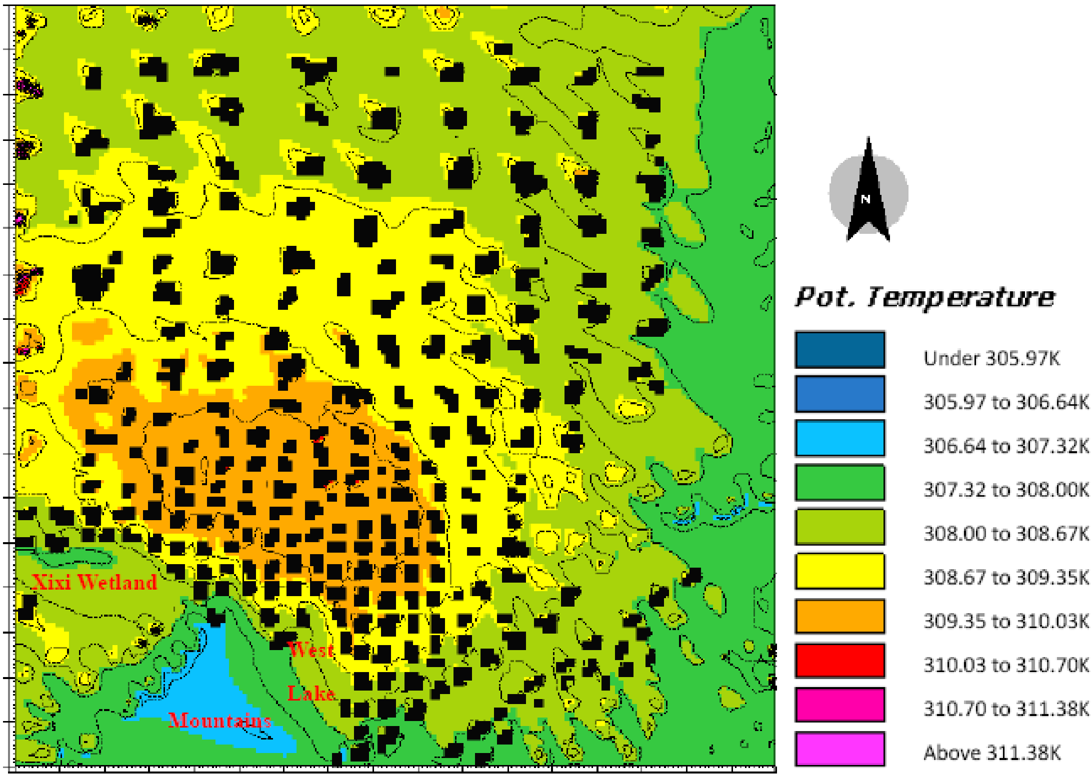

Fig. 3.7 (b)

Fig. 3.7: Temperature distributions at (a) 0m and (b) 30m height in Hangzhou city centre at 13:00 23rd June 2011

According to the comparisons mentioned above, there is a gradual decrease of UHII with increasing wind speed in urban area. Many studies have shown that wind flow characteristics are greatly affected by the building configurations and ambient wind directions [82]. Furthermore, urban planners and designers should consider gaps between adjacent buildings and arrangement of buildings, because for a given building height, larger gaps and identical arrangement induce more wind in urban canyons, thus improving ventilation process and relieving UHI effect.

The prevailing wind direction is southeast in Hangzhou during summer days;

nevertheless, both West Lake and Xixi Wetland are in the southwest part Hangzhou urban area. The southeast wind is not much effective in transporting the cool air generated in these natural sources, especially the West Lake, to the urban area. Furthermore, the cool air from the Qiantang River cannot be blown to the urban area either, because the buildings on the northeast side of the river are highest and block the cool wind into the urban area. Fig. 3.8 (a and b) shows the modified scenario where the wind direction changes to southwest and the comparison with the prime scenario. Although the general situation of UHI could not be mitigated greatly, the building area at the northeast side of West Lake is cooled significantly by the wind from West Lake. As the southeast prevailing wind direction cannot be easily altered, one possibility to mitigate the effects of UHI is to add some water or green spaces at the southeast part of dense urban area in Hangzhou.

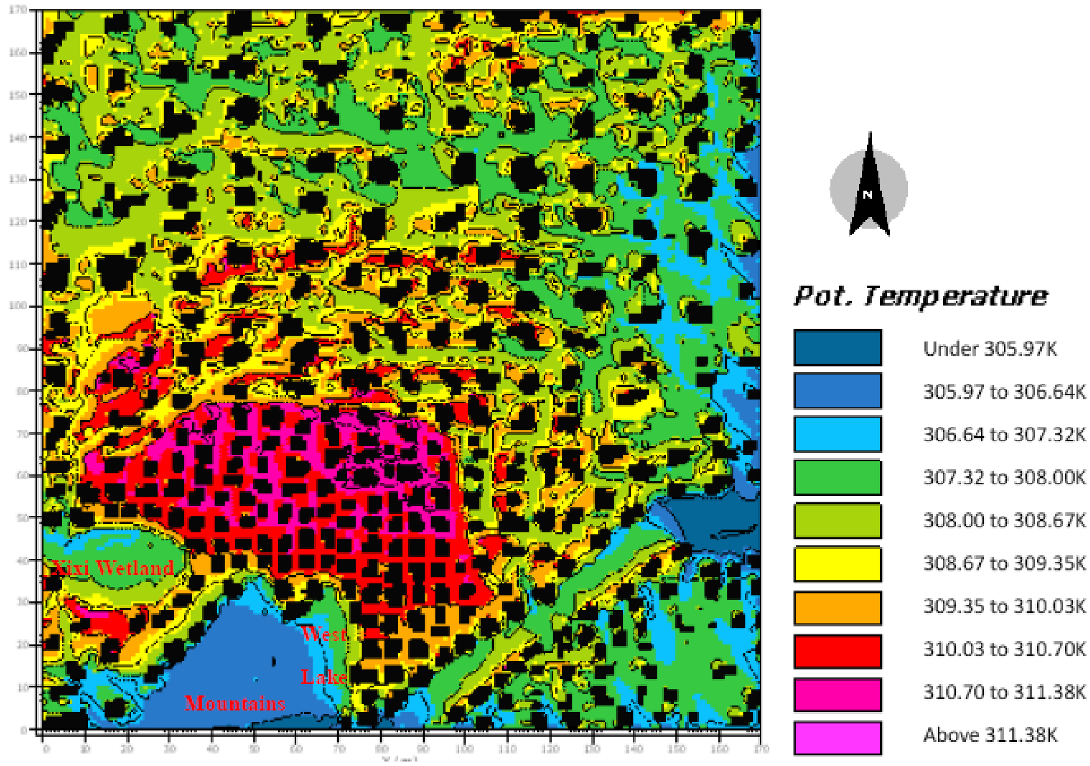

Fig. 3.8(a)

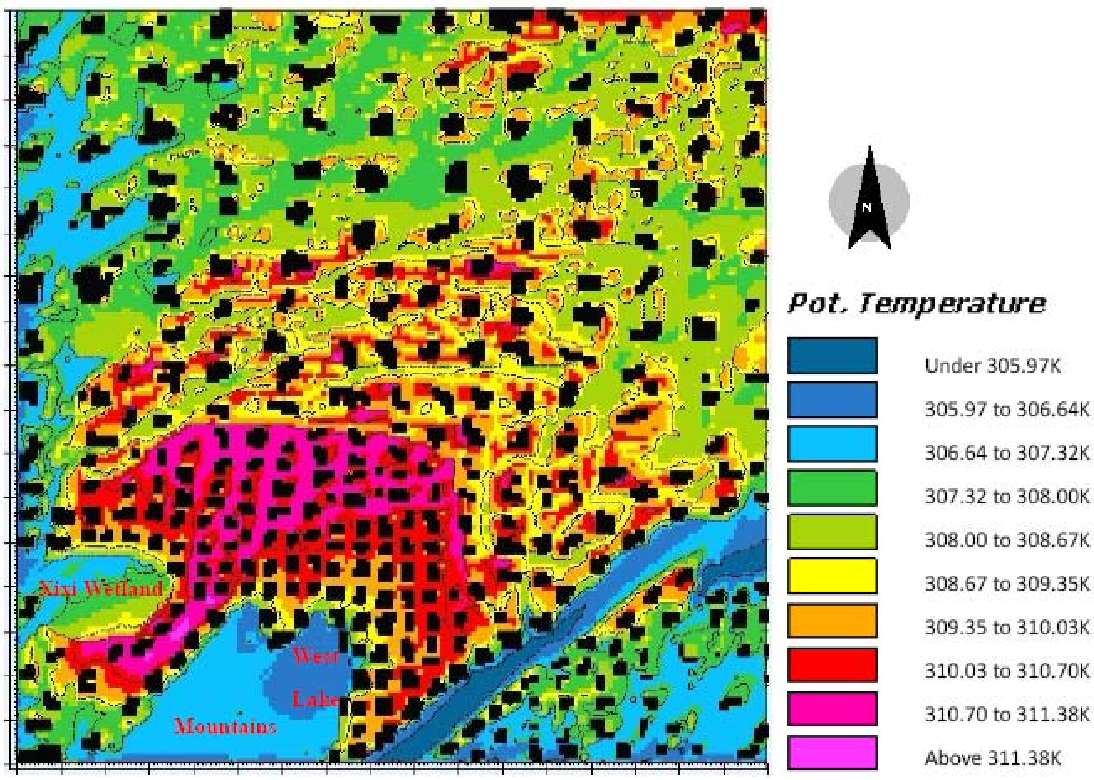

Fig. 3.8(b)

Fig. 3.8: Temperature distributions when wind direction is (a) southeast and (b) southwest at 13:00 23rd June 2011

On the other side, the gap between buildings also relates to another variable, sky view factor (SVF), which is a crucial indicator of the magnitude of urbanization of a city. Figure 3.9 shows that an area with low SVF can be normally recognized as urban area where UHI effect is significant. In principle, reductions in SVF can lead to an increase in UHI. This is because densely concentrated buildings in some developed areas with low SVF cannot easily release long-wave radiation into the open sky, and this traps the heat contributing to the UHI effect. For the areas with great SVF, their long-wave radiation cannot be trapped in large open area where the heat can be dispersed quickly by strong wind at night. As a result, widening the gap between adjacent buildings to improve SVF value is widely recommended for urban planning process to relieve the UHI effect.

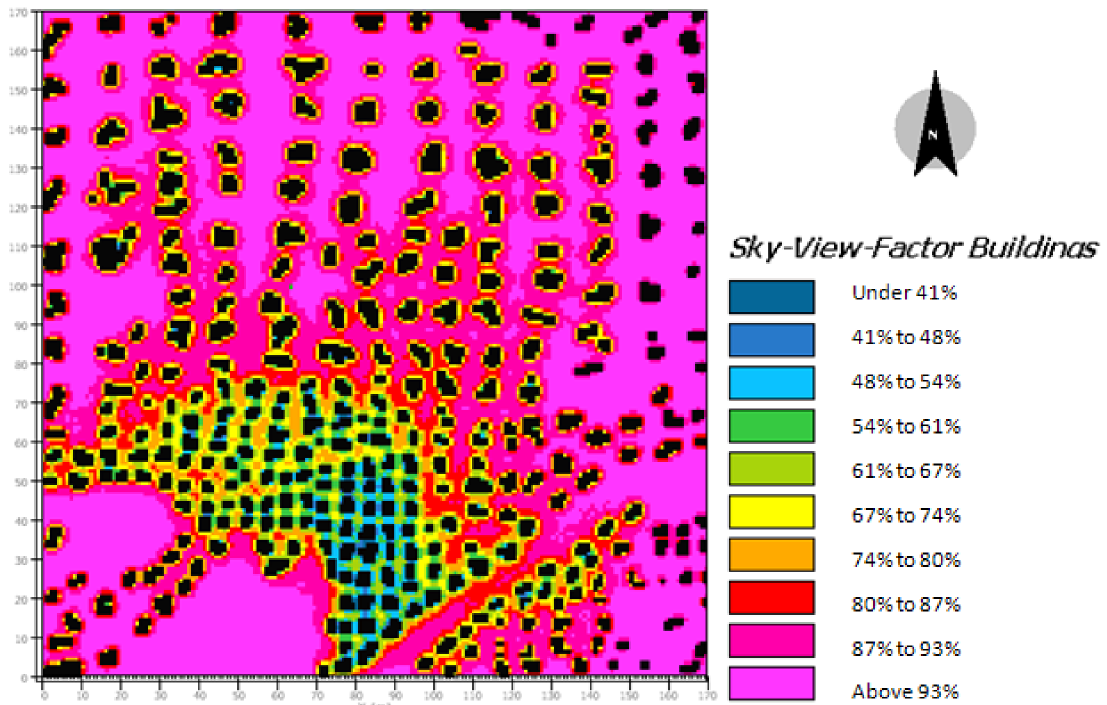

Fig. 3.9: Sky view factor distribution in Hangzhou city centre.

3.4.2 Limitations of ENVI-met programme for this study

The case study simulated the UHI situation in Hangzhou urban area through using ENVI-met programme. It mainly evaluated the impacts of natural ecological resources and wind speed on UHI formation. However, based on the experience of using ENVI-met programme, five main limitations of ENVI-met programme for this study were concluded as follows:

(1) The simplified 1-d atmospheric inflow model restricts the ability to dynamically simulate meso-scale thermal and turbulence exchanges that potentially effect microclimate. It would be problematic if regional weather conditions vary greatly over the model simulation period, but the simulated result from ENVI-met is probably very stable and this is unconvincing.

(2) Building facades throughout the model environment are parameterized with a single mean heat transmission value, which oversimplifies the heterogeneity of the urban environment.

(3) The programme is suitable for micro-scale model, but not for macro-scale model.

(4) The lack of horizontal soil transfer within the model potentially affects accurate calculations of soil heat storage.

(5) The weather data file of ENVI-met could not be changed or refined based on real situations.

Hence, if the ENVI-met programme is used for detailed simulation case study in future, it would be more beneficial to apply other research methods, such as experimental measurement and other simulation software, to reinforce the output of ENVI-met.

3.5 Concluding remark

Previous research has clarified that with the outward expansion of built-up urban area and the net increase in bare land, both of which have low ecosystem service functions, sustainable development must address the adverse impact of the loss of natural ecological resources due to drastic urbanization in Hangzhou [76]. From this case study, it has been demonstrated that protecting and expanding the natural ecological sources is a potential option for lowering urban air temperatures.

According to the simulation results from this case study, if the West Lake and Xixi Wetland are replaced by building constructions, the urban air temperature would increase by 0.5°C. Regarding the urban geometry, the larger gap between adjacent buildings and identical arrangement of buildings are recommended during the urban planning process to increase the wind speed and SVF in urban area. This strategy can lower the urban temperature and remedy the UHI situation effectively. As a result, for the purpose of making sustainable urban futures, government in the city-planning process has to make accurate decisions concerning land-use choices and development patterns.

In order to reinforce these initial findings from this case study, filed measurement of air temperature and other environmental parameters in Hangzhou city was proposed to be applied in further study. The following research

CHAPTER 4: FIELD MEASUREMENT OF UHI IN HANGZHOU AND NINGBO

4.1 Introduction

In addition to the simulation method presented in Chapter 3, this research applied field measurement as the main research methodology to study UHI effect. The bulk of this chapter is devoted to presenting the work of sensor network installation in research areas. After consideration and comparison, i-Button DS1923 data logger was selected to record air temperature and relative humidity in this research. The research also produced shields in order to present data loggers from direct solar radiation and rainfalls. The selection of measurement sites and the process of sensor installation are addressed in this chapter as well.

The location of the measurement sites, the positioning of the sensors and the harsh conditions in an urban environment could result in missing data and erroneous values. Missing data and erroneous values in micro-scale weather time series could produce bias in the data analysis, false correlations and wrong conclusions when deriving the specific local weather patterns. A simple Fourier serious method is therefore recommended and evaluated with its performance for replacing missing and erroneous values in urban weather time series in this chapter.

4.2 Installation of sensor network in Hangzhou and Ningbo

The UHI situations over Hangzhou (30^{o} 15’N 120^{o} 10’ E) and Ningbo (29^{o} 52’N 121^{o} 33’ E) in Zhejiang Province were examined by using hourly measurements of ambient air temperature and relative humidity 3-5 metres above ground level from experimental stations, installed in urban, suburban and rural places of these two cities, for a period of 22 months in Hangzhou and 24 months in Ningbo. The stations were strategically decided as a way to study areas with different land-uses, different Sky View Factors (SVF), different distances from the city centre and different surrounding albedo values in cities. Except surrounding albedo, all other parameters were actually measured by field measurement before site selection. Values of surrounding albedo were estimated based on the reference guide. Fig. 4.1 shows the network maps of sensors in Hangzhou and Ningbo. Detailed descriptions of each experimental station in Hangzhou and Ningbo are presented by Appendix 1. There are 26 experimental stations selected in Hangzhou. Among these stations, Hangzhou Mantou Mountain (HZ-NO.24) is chosen as the reference point, because this station is close to the National Datum Station and is nearly free from the UHI effect in Hangzhou. Hangzhou Tower Shopping Centre (HZ-NO.1) is regarded as the symbolic city centre of Hangzhou. Regarding to the field measurement in Ningbo, this research set up 29 experimental stations in Ningbo. Similar to the study of Hangzhou, Ningbo Lishe International Airport (NB-NO.27) is selected as reference site and Tianyi Square (NB-NO.1) is regarded as city centre of Ningbo.

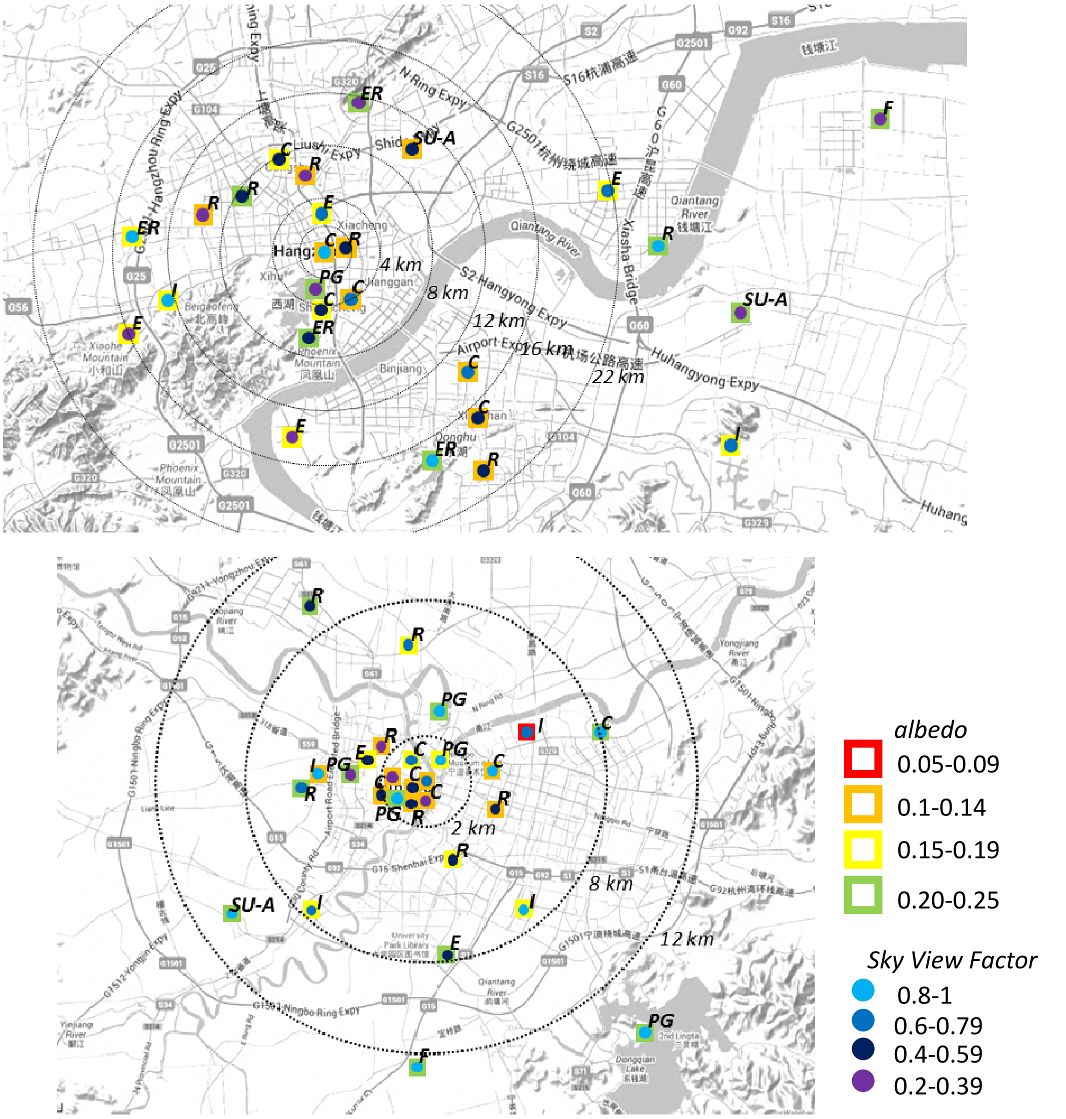

Fig. 4.1: The network maps of sensors for Hangzhou (top) and Ningbo (bottom).The box shapes' colouration gives an albedo estimation. The circles' colouration is descriptive of the SVF calculations on site. The letters nearby the sensors indicate the Land Use type as in the Local General Planning maps [77, 83]. The dotted lines show the distance from the city centre in kilometres.
C: Commercial, R: Residential, PG: Public Green, E: Educational, I: Industrial, ER: Ecological Reserve, F: Farmland, SU-A: Special use-Airport

4.2.1 Selection of sensors

The main experimental instrument in this research is data logger that can monitor air temperature and relative humidity simultaneously. The measurement of data loggers should be configured at an interval of every hour. Moreover, only battery powered devices is available for sensing and logging the measurements in this case. The lifetime of battery and the storage capacity of data loggers should guarantee that at least a whole year's data can be collected and stored safely. The small size and light weight of data loggers are recommended, since they should be attached and detached easily from the radiation shield for downloading data.

By considering above requirements, a small battery-powered temperature & humidity data logger named i-Button DS1923 was selected. A total of 8,192 8-bit readings or 4,096 16-bit readings taken at equidistant intervals ranging from 1s to 273 hrs can be recorded in a protected memory section. If selecting the low precision, 8-bit readings to record data at every hour, its storage capacity can afford 170 days' data collection. But if using the high precision, 16-bit readings, it can store 85 days' data information [84]. Fig. 4.2 displays the operation range of this i-Button data logger is from $-20℃$ to $85℃$ for air temperature and from 0 to 100% for relative humidity. A mission to collect data can be activated immediately or after a user-defined delay. According to the instruction from manufacturer, temperature accuracy is higher than $\pm 0.5℃$ from $-10℃$ to $65℃$ and the resolution can be as high as $0.0625℃$ [84]. Maxim's Quality Assurance Procedures acknowledged the accuracy of reference instrumentation in the test is less than $\pm 0.035℃$ over a range of $-100℃$ to $200℃$ [85].It is a coin-size device with thick of 6mm and diameter of 17mm. Its durable stainless steel package is highly resistant to environmental hazards such as dirt and moisture (see Fig. 4.3).

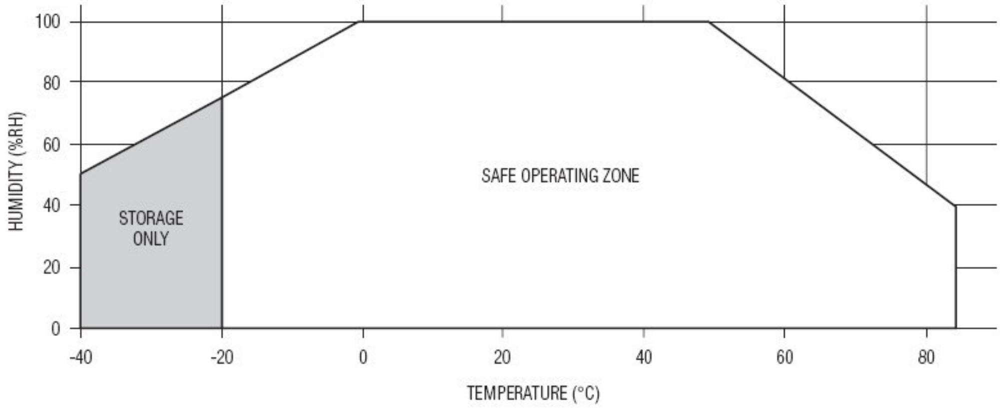

Fig. 4.2: Safe operation range of i-Button DS 1923 Data Loggers [84]

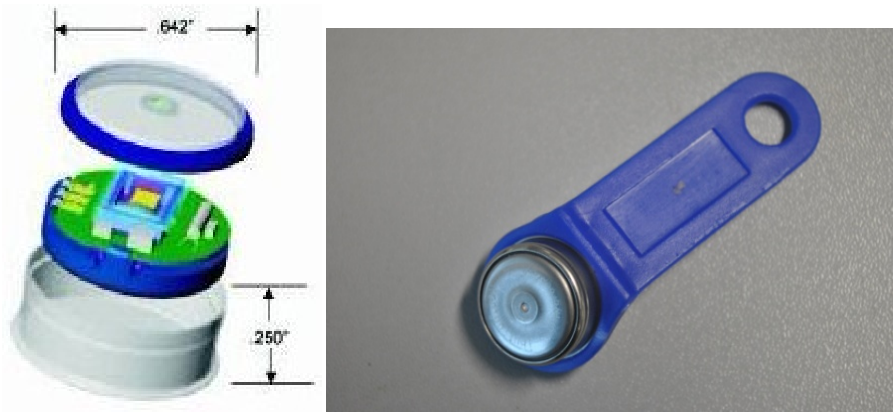

Fig. 4.3: Size of i-Button DS 1923 Data Loggers

The accuracy of i-Button DS1923 data loggers was tested in a laboratory chamber where user-defined environmental conditions can be set. All data loggers were placed on a table to measure inside temperature and relative humidity, and another two thermal couples were also placed nearby to measure exact air temperature, as Fig. 4.4 shows. The chamber temperature were set in the level of $10℃$, $0℃, -10℃$ and $40℃$. The data collection interval of data loggers was set as 1 minute.

Fig. 4.4: The arrangement of i-Button DS1923 data logger in the chamber

The detailed temperature and humidity results measured by these data loggers are listed in Appendix 2. The test result proves that the relative difference of measured temperature between these data loggers and the thermal couple is less than 2% (see Fig. 4.5). The difference of humidity between any two data loggers is ranging from 1% to 2% as well (see Fig. 4.6).

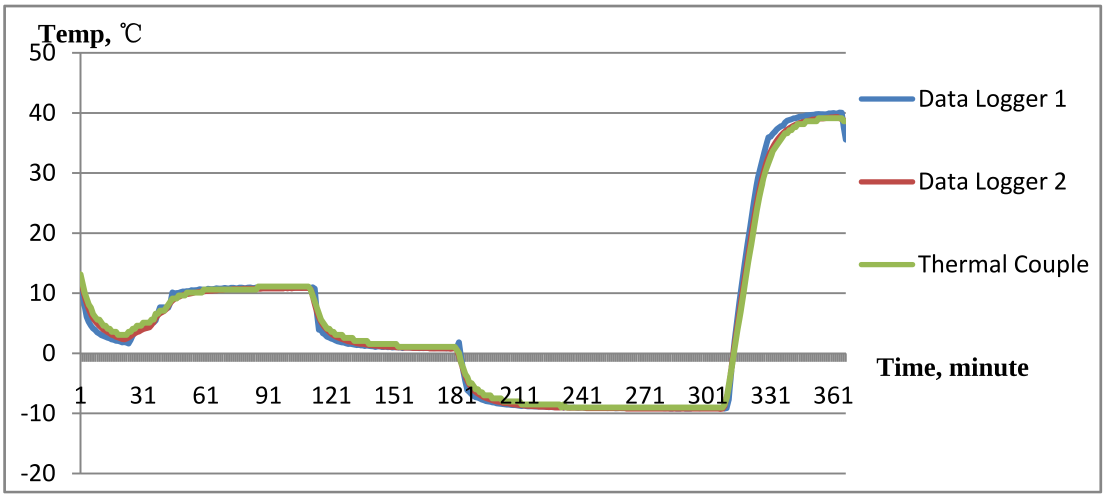

Fig. 4.5: The comparison of temperatures measured by two data loggers and one thermocouple

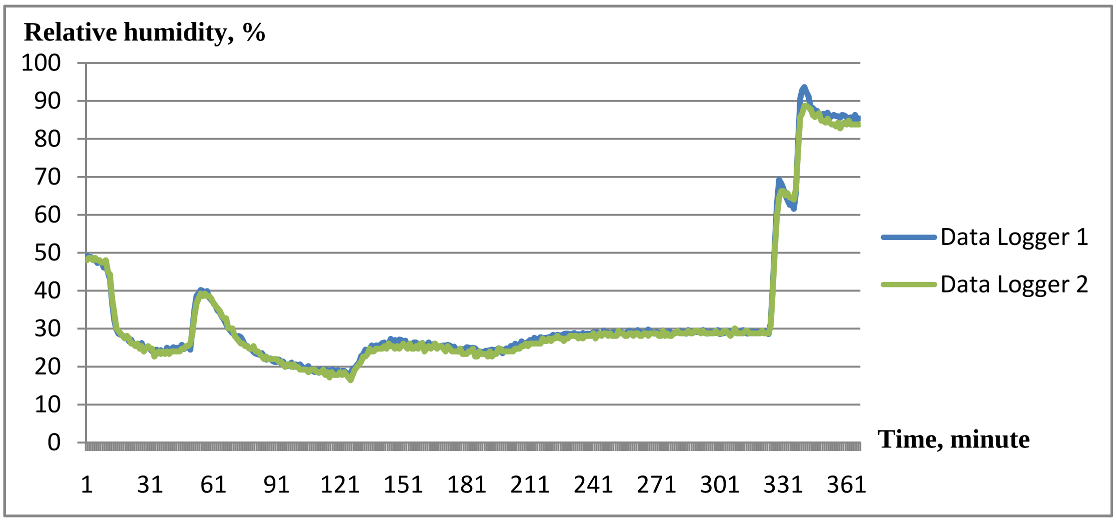

Fig. 4.6: The comparison of relative humidity measured by two data loggers

4.2.2 Fabricating the shield

In order to guarantee the accuracy of measurement and the safety of data loggers, shading protective devices are indispensable to shelter the data loggers from direct sunshine and rainfalls. For some common professional monitoring stations, Stevenson screen is used to protect sensors inside and greatly reduce influence of solar irradiance, as Fig. 4.7 illustrates. However, in this case Stevenson screen is too bulky to be mounted on a street lamppost column. As a result, a low cost and easily fabricated radiation shield should be designed to accommodate the miniature i-Button data logger. Dr. Cheung et al designed a simple shield with its miniature data logger to measure dry bulb air temperature in Great Manchester. Fig. 4.8 shows a sample of their radiation shield. The shield design and the i-Button sensors were tested to assure that the logged air temperature data are reliable and similar within an accepted accuracy to the data collected with the commonly used Stevenson screen design [86].

Fig. 4.7: Data loggers inside Stevenson screen [86]

Fig. 4.8: Original design of radiation shield

The majority accessory part of each radiation shield is 10 white plastic saucers of diameter 16cm. Although these 10 saucers should be arranged closely to shelter direct irradiance and rainfalls effectively, sufficient gap and vents are indispensable to avoid the accumulation of hot air inside the shield due to radiation. Apart from these saucers, a shield also contains three M6 studding of length 165mm, one round piece of alumina alloy of depth 2mm, one rectangular piece of alumina alloy arm of depth of 4mm and several fastening pieces. It has to be noted that all metal materials used in the radiation shield are corrosion proof.

On the basis of the original shield design, this study has improved the design in several ways. First of all, the data logger was attached on a metal plate which was then attached to a hook in their original design. Fig. 4.9 shows the hook with the metal plate and the data logger. The metal plate has high thermal conductivity, thus the metal surface temperature may affect the accuracy of data measurement. Hence, the data logger was designed to be fixed by plastic buckle (see Fig. 4.10). Second, all of the saucers, apart from the first two from the top, had a large hole to form a cavity for the data logger. A triangular aluminium plate, also with a large hole was placed at the bottom of the shield to provide strength. Nevertheless, a triangular aluminium plate was abandoned in new design and the large hole of bottom saucer was replaced by many small holes, as Fig. 4.11 shows. This design saves the cost of material, improves the strength of whole shield, guarantee the enough ventilation and prevent the data logger from falling. More detailed accessories specification of this radiation shield is listed in Appendix 3 and the manufacturing drawings for radiation shield are attached in

Appendix 4.

Fig. 4.9: Original hook design

Fig. 4.10: New plastic buckle design

Fig. 4.11: New design of radiation shield

The whole weight of one radiation shield without the arm is about 395g, so it can be safely fastened on a street lamppost column by two stainless steel clips with two rubber belts. Fig. 4.12 shows one stainless steel clip with one rubber belt. According to the manufacturing instruction, each stainless steel clip can bear the maximum weight of 20kg and the maximum drag force of 1200N.

Fig. 4.12: Stainless steel clip with one rubber belt.

4.2.3 Sensor installation process

At each measurement location, i-Button sensors with radiation shields were installed on road lamp posts to monitor air temperature and relative humidity (see Fig. 4.13). Tab. 4.1 lists the date of sensor installation and data collection in Hangzhou and Ningbo cities respectively. As mentioned before, all sensors were calibrated prior to installation and their readings were inter-compared in an environmental test chamber at the Centre for Sustainable Energy Technologies (CSET) at the University of Nottingham Ningbo. The data loggers were set to record hourly values for air temperature at a 8-Bit (0.8°C) resolution and relative humidity (RH) at a 8-Bit (0.6%) resolution. The memory capacity of 8kb allows to store up to 170 days of hourly data [87]. At the end of each 170 day period, the stored data should be downloaded to a computer and the sensors repositioned at the same location to continue recording.

Fig. 4.13: Sensor with radiation shield installation process

Tab. 4.1: Date of sensor installation and data collection in Hangzhou and Ningbo

City	**Sensor installation time**	**1st data collection & replacement time**	**2nd data collection & replacement time**	**3rd data collection & replacement time**	**4th data collection & replacement time**	**5th data collection& replacement time**
Hangzhou	16/12/2012	06/05/2013	23/10/2013	04/05/2014	01/10/2014	
Ningbo	24/09/2012	20/01/2013	01/05/2013	16/10/2013	15/04/2014	05/10/2014

The consultation report on meteorological observations at urban sites [88] that complements the World Meteorological Organisation's (WMO) Guide to Meteorological Instruments and Methods of Observation [89] standard provides extensive guidelines for the location selection and on-site installation of weather stations. The network installation and maintenance of the sensor network discussed here has proved so far that applying all the WMO recommendations is quite a challenging task in practice.

In situ installations had to strike a balance between being representative of the urban canopy layer and at the same time ensuring accessibility to the site and easy maintenance. The sensors are expected to be representative of the temperature and relative humidity of an area ranging from one hundred to several hundred meters in a direction upwind and around each sensor [88]. The locations were carefully selected to have homogeneous characteristics and the sensors were installed at sites with a reasonable distance to the fringe of different surface types.

The first problem encountered was that the local government did not consent to install objects on lamp posts on the grounds initially, as solar radiation shields would spoil street aesthetics and pose a risk to pedestrians. An experimental test was prepared to prove the firmness and safety of the installation. In the end, owing to the safety test report and the government's support to the research project, the Urban Administration Bureau of Hangzhou and Ningbo both approved the application for the network's installation. Despite the permissions and public information notes attached with the sensors, six solar radiation shields and the sensors within have been taken away since September 2012 (four in Ningbo and two in Hangzhou).

There were also some cases of private sites such as factory grounds and residential compounds where permission to install sensors were denied by the owners. The difficulty to convince the authorities and private owners to allow the use of the lamp posts in conjunction with the need for sites with easy access which at the same time, have to be free of obstructions make the current selection of sites the best possible choice. However, there are some cases where the sensors had to be positioned very close to airflow obstructions or in open park locations that may affect the representativeness of their readings for the local urban micro-climate conditions. Besides, the plastic shields were exposed outside for more than one year, the shields have had numerous breaks, as Fig. 4.14 shows.

Fig. 4.14: Radiation shield obstructed by direction board (left) and broken solar radiation shield (right)

4.3 Identifying missing and false values in collected dataset

False measurements or missing data due to malfunction of the sensors will distort the signal of site specific weather development, cause bias during the development of urban weather adaptation models and produce invalid correlations. Consequently, any false or missing values in the time series must be identified and effectively replaced. The weather data time series collected from the sensors' network were, in a first step, examined to identify any noise in the form of outliers in the dataset. It was found that relative humidity values were often above 100% regardless of the sensor and its location. When the i-Button reached high humidity levels it can become 'saturated', recording humidity levels >100% with the device needing time to normal recording levels, resulting in potentially extended higher readings. Device manufacturers acknowledged that humidity readings are most precise in controlled conditions and can lose accuracy in outdoor environments. The scatter and frequency of the erroneous relative humidity data indicates that the most probable cause is a sensor's drift due to pollution, water spray and general degradation. A simple algorithm was applied to cap the relative humidity values at 100% levels.

In a second stage, boxplots of the hourly air temperature distribution per week were created with IBM SPSS Statistics Ver.19 for each sensor's location in Hangzhou. These outliers were traced back to the data sample. Outliers that showed up in groups of subsequent hours or were common to all sensors at a specific time and day were not treated as potential errors. The remaining outliers were compared against the average hourly air temperature for the same week and the coldest and hottest days of this week respectively (Fig. 4.15). The range of hourly changes on each measurement site was also assessed against the hourly changes in weather data collected at Mantou Mountain, national datum station, as Fig. 4.16 shows. The box shows the range of air temperature change for the 50% of the values. The line inside the boxes is the median of the air temperature change distribution. The red stars denote the extreme outliers, changes in temperature at least three times larger than the range of change in the 50% of the values. The whiskers extend 1.5 times the height of the box or if there are not any values in that range then to the minimum and maximum values.

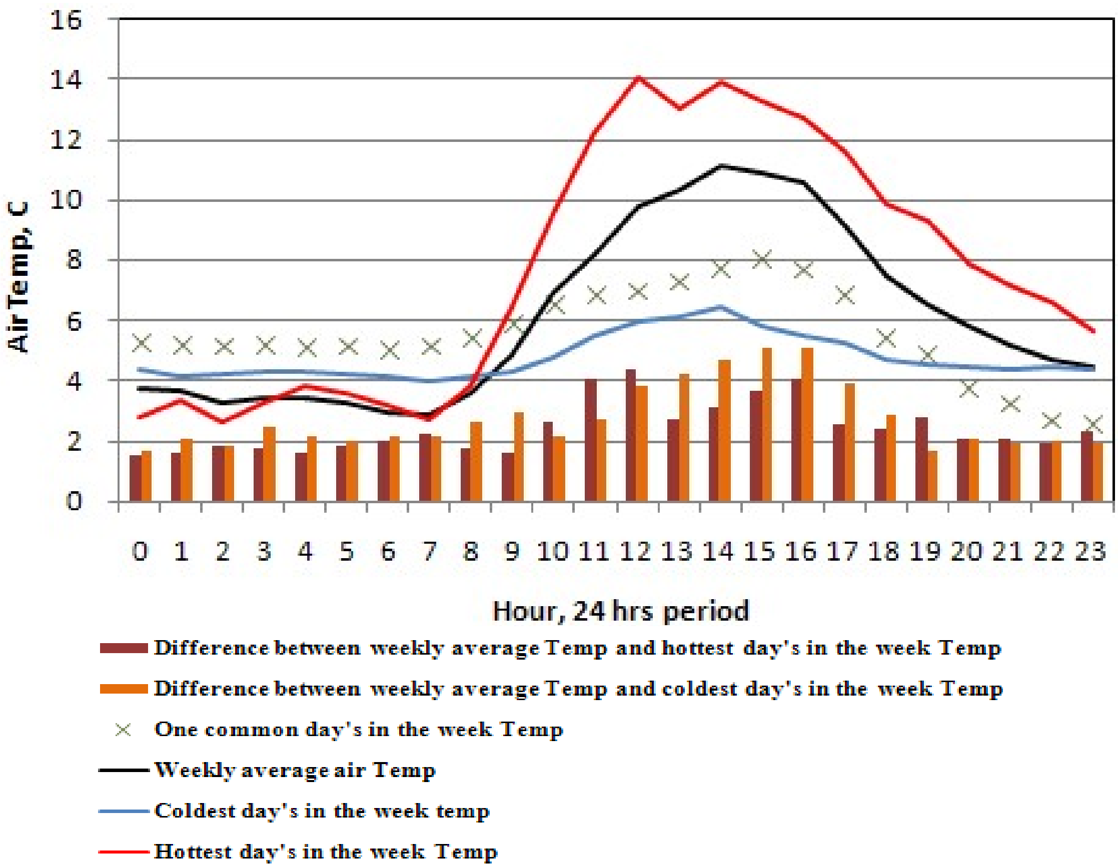

Fig. 4.15: Comparison of hourly air temperature to the weekly trend and extreme days in the week (Site: Yaqian industry area: 2013/01/22-2013/01/28).

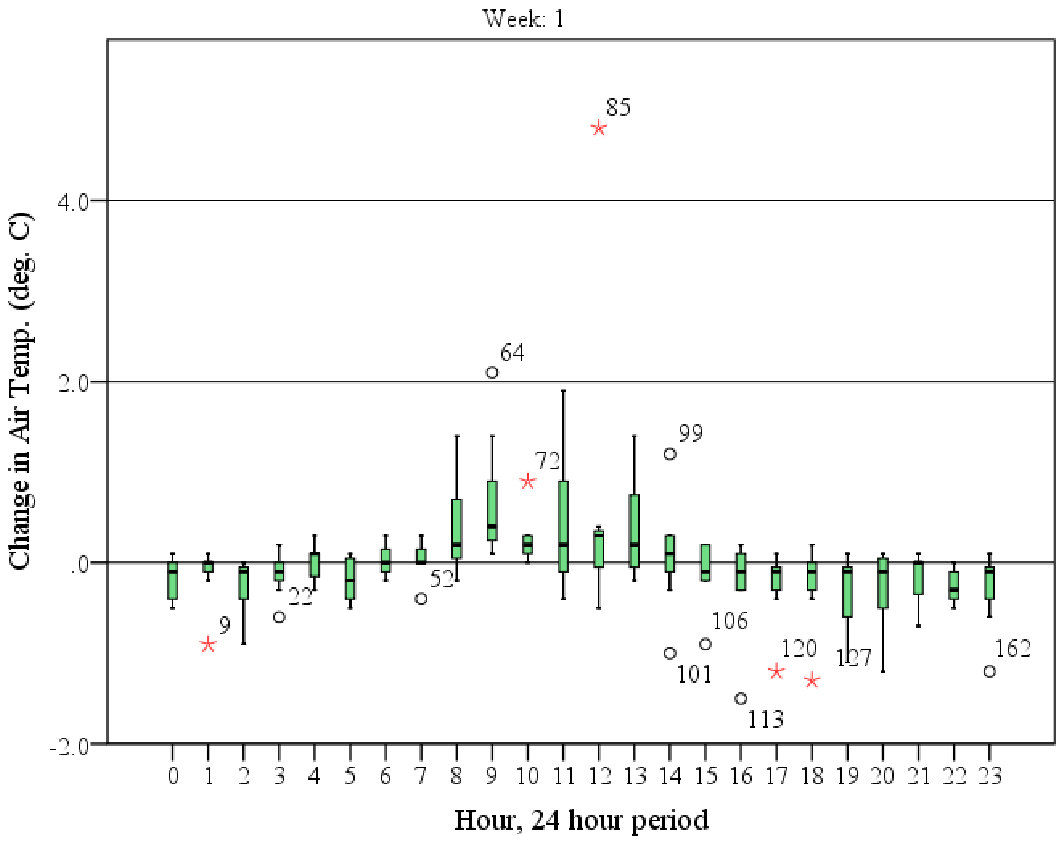

Fig. 4.16: The range of air temperature change collected at Mantou Mountain site

The air temperature collected on the measurement site of Hangzhou Xiaoshan International Airport was assessed against the official weather data collected at Hangzhou Xiaoshan International Airport's weather station (300 13′ N, 1200 26′ E, ZSHC) [90]. The Unary Linear Regression Model was created by SPSS to assess the accordance between these two different sources of weather data (see Fig. 4.17). In addition to that, the measured hourly air temperature at airport from 2013/01/01 to 2013/01/07 was also compared with official weather data (see Fig. 4.18).

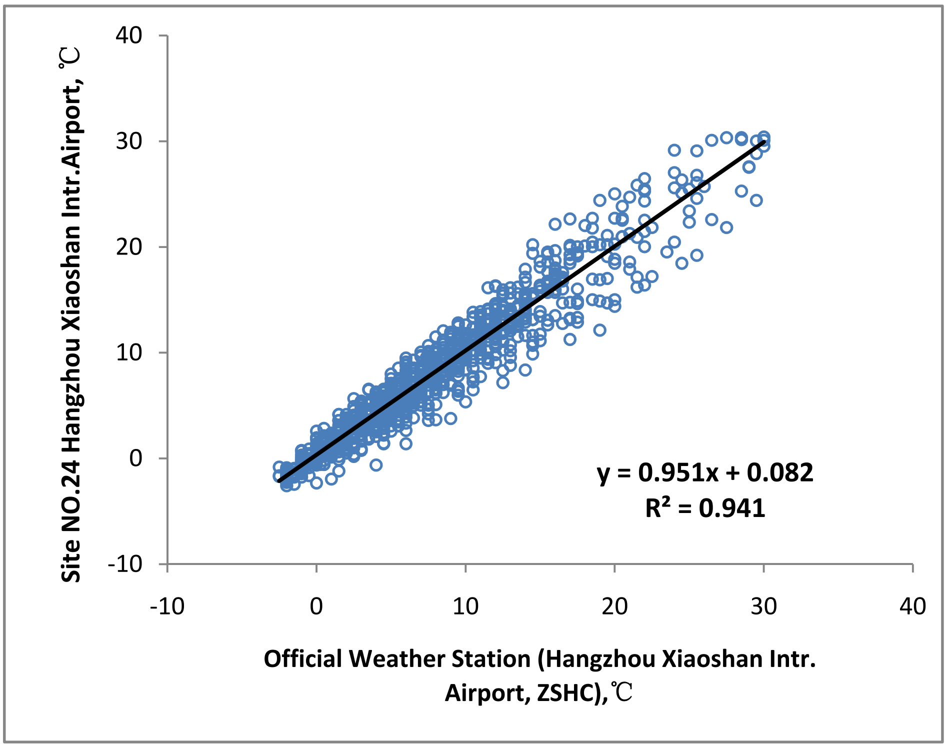

Fig. 4.17: The Unary Linear Regression Model of measured data and official data

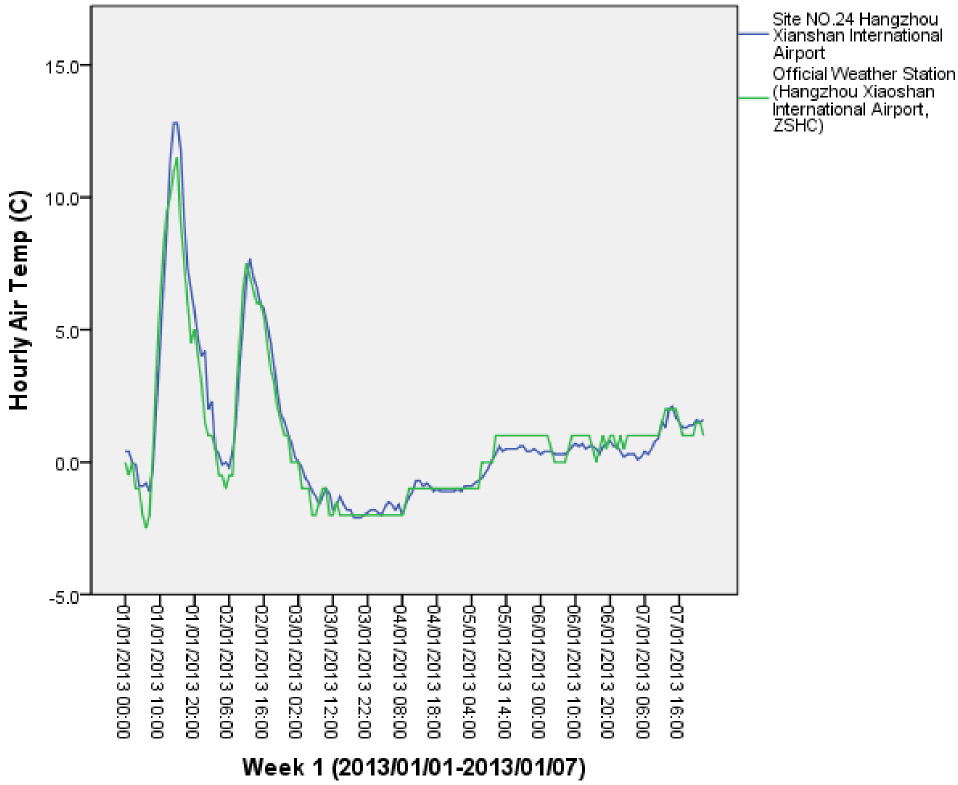

Fig. 4.18: The comparison between hourly measured air temperature and hourly official air temperature from 2013/01/01 to 2013/01/07.

4.4 Interpolation procedures for false and missing data

Actually, the great majority of weather data in the International Surface Weather Observations data base are at three-hour intervals [91]. This type of data has to be interpolated to one-hour intervals for adapting itself to thermal simulation work. The previous researchers have developed several statistical methods to interpolate the missing hours' data from the actual recorded data.

To interpolate missing and false dry-bulb temperatures in this research, Fourier series method is selected, because the change in dry-bulb temperature is periodic [91]. The Fourier series method is applied as below:

$$\theta(t) = a_0 + \sum_{n=1}^{N} \left(a_n \cos\frac{n\pi t}{12} + b_n \sin\frac{n\pi t}{12} \right) \tag{4.1}$$

where $a_0 = \frac{1}{8}\sum_{k=1}^{\infty}\theta(k)$

$$a_n = \frac{1}{4}\sum_{k=1}^{\infty}\theta(k)\cos\frac{n\pi t}{4}$$

$$b_n = \frac{1}{4}\sum_{k=1}^{\infty}\theta(k)\sin\frac{n\pi t}{4}$$

n = nth tern of the Fourier series

k = sequential number of observed dry-bulb temperature from 1 to 8 at three-hour intervals

$\theta(k)$ = kth observed dry-bulb temperature

t = local standard time, here meaning Beijing Standard Time.

The research evaluated that the Fourier series equation approximated measured dry-bulb temperatures most closely with n=3 or n=4, as Fig. 4.19 shows.

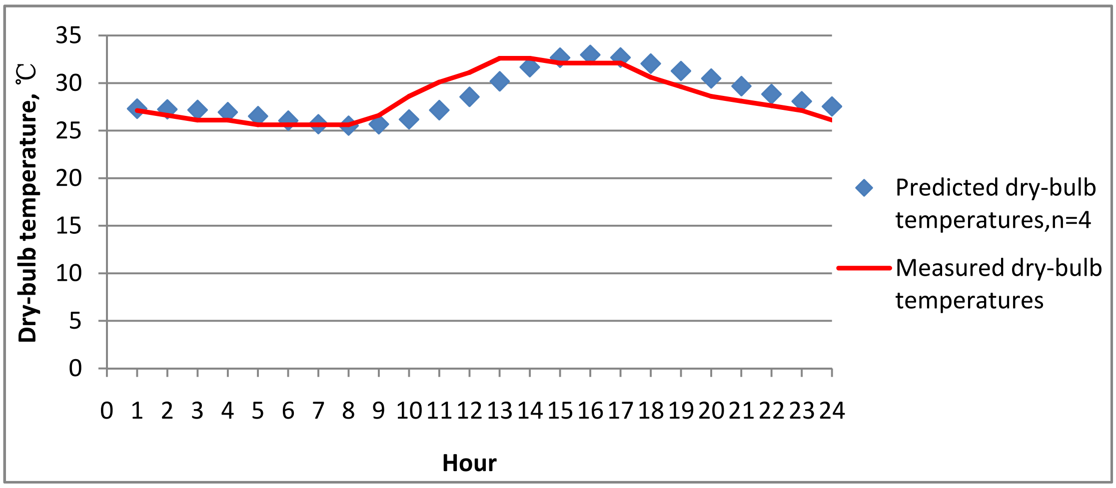

Fig. 4.19: Comparison between measured and predicted dry-bulb temperatures of Hangzhou city centre site at 21st June, 2013.

4.5 Concluding remark

This chapter has generally demonstrated the installation of sensor network in research areas, Hangzhou and Ningbo. The measurement sites were strategically decided as a way to study areas with different land-uses, different Sky View Factors (SVF), different distances from the city centre and different surrounding albedo values in cities.

The accuracy of i-Button DS1923 data loggers was initially tested in the laboratory and was proven with excellent performance. Afterwards, data loggers were installed with solar radiation shield on lamp posts to record the air temperature and relative humidity simultaneously more than one year. Although missing and erroneous collected data appeared to cause unrepresentative of the local microclimate, Fourier serious method can work effectively in interpolating missing and erroneous values in urban weather time series

CHAPTER 5: DATA ANALYSIS FROM THE FIELD MEASUREMENT IN HANGZHOU AND NINGBO

5.1 Introduction

This chapter is devoted to presenting the analysis work based on the data collected from the field measurement in Hangzhou and Ningbo. The measurement determined that the UHI situation in Hangzhou was more serious than in Ningbo. The chapter also covers the detailed analysis regarding how UHI effect highly impacted by factors, such as land-use, distance from city centre, surrounding albedo, SVF and other meteorological parameters.

The contributions of vegetation cover, urban building configuration and material properties, and human activities to UHI formation is discussed in this chapter. Finally, this chapter advocates mitigating UHI effect through three effective strategies, involving the application of cool materials on urban surfaces, modifying urban geometry to improve wind flow and expanding green space in urban areas.

5.2 Urban Heat Island situation

For the purpose of investigating the UHI situations in developed cites in China, two metropolitan cities, namely Hangzhou and Ningbo, were selected as research area. According to the collected air temperature and relative humidity data, the study first examined the UHI effect in Hangzhou and Ningbo comprehensively.

5.2.1 UHI situation in Hangzhou

Hangzhou experienced a significant rising of average temperature in the past 20 years [92]. During 2003-2006, up to 40-50 days of continuous high temperature appeared in the summer of Hangzhou, which made it one of the cities with the highest temperature in summer in China [93]. Climate change results in changes such as temperature, precipitation, and wind that may last for a long period of time. In addition to that, the impact from UHI and climate change may in fact be similar and cumulative [94]. Both have the capacity to rise temperature and increase energy demands, especially in summer.

The dependent variable for the UHI analysis is urban heat island intensity (UHII) which is defined as the temperature difference between a reference rural location and a place within Hangzhou urban area at a specific time in this research [95]. The weather station located at Mantou Mountain in Hangzhou is one of the national datum weather stations in China whose data collected were used for generating official typical weather year files [4]. The reference rural location was located close to this national datum station and is nearly free from the UHI effect. Fig. 5.1 marks the locations of reference station, national datum station and city centre in Hangzhou city.

Fig. 5.1: Locations of reference station, national datum station and city centre in Hangzhou

Fig. 5.2 manifests monthly average air temperature collected from all measurement sites during the period from May, 2013 to April, 2014 in Hangzhou. Each column stands for the monthly data collected at one measurement site. During the measurement period, the hottest months were July and August with the average air temperature of 32 - 33°C. The coldest months were November, January and February with the average air temperature of about 6°C.

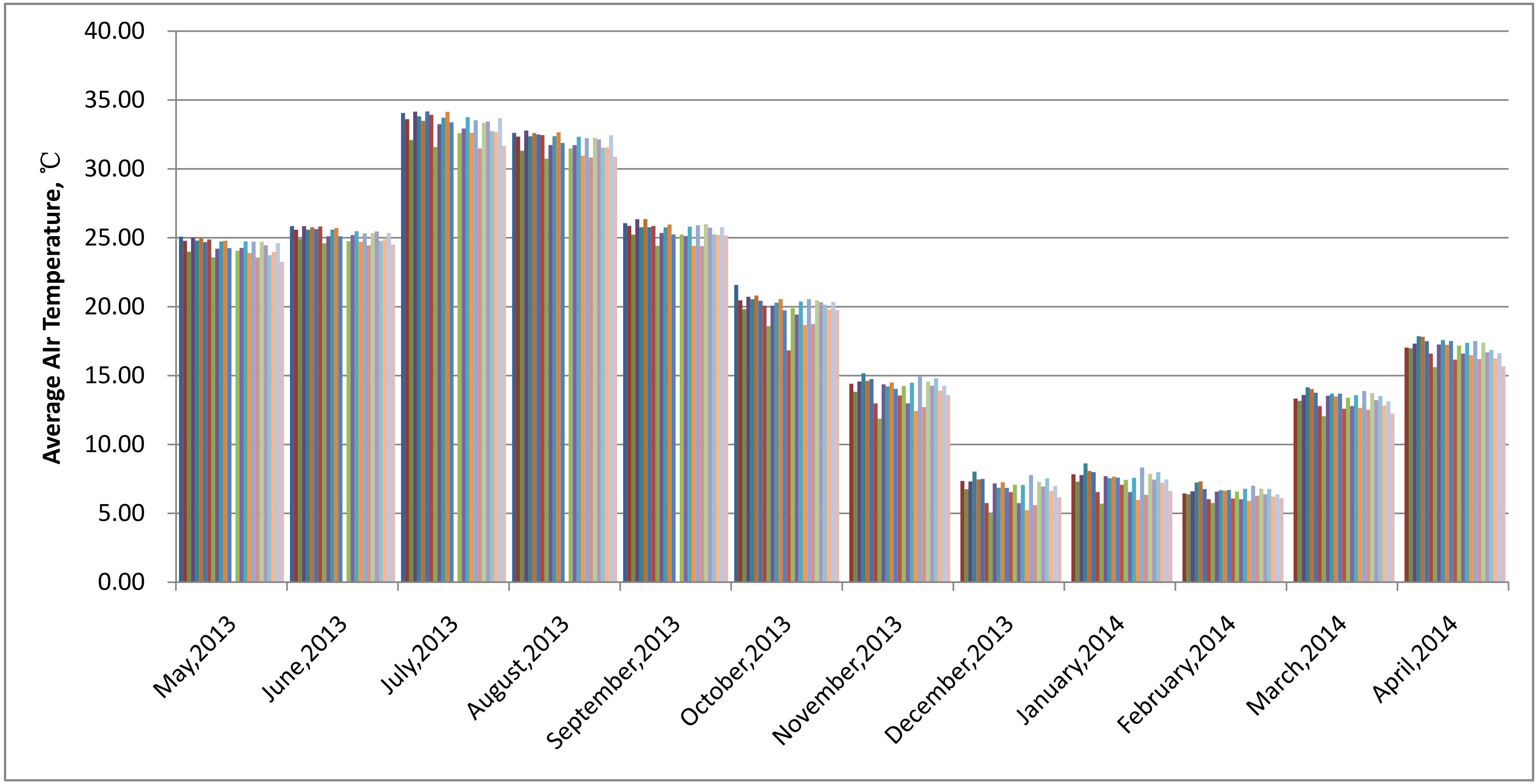

Fig. 5.2: Monthly average air temperature values of all measurement sites from May, 2013 to April, 2014 in Hangzhou.

Referring to relative humidity in Hangzhou, it can be observed from the measurement that Hangzhou has a humid climate with annual mean relative humidity of about 70%. Hangzhou is located in humid subtropical area where the climate should be characterized by long, hot, humid summers and chilly, cloudy and dry winters with occasional snow [96]. According to this observation, relative humidity is generally higher in winter, due to the low capacity of air to hold moisture in low temperatures (see Fig. 5.3).

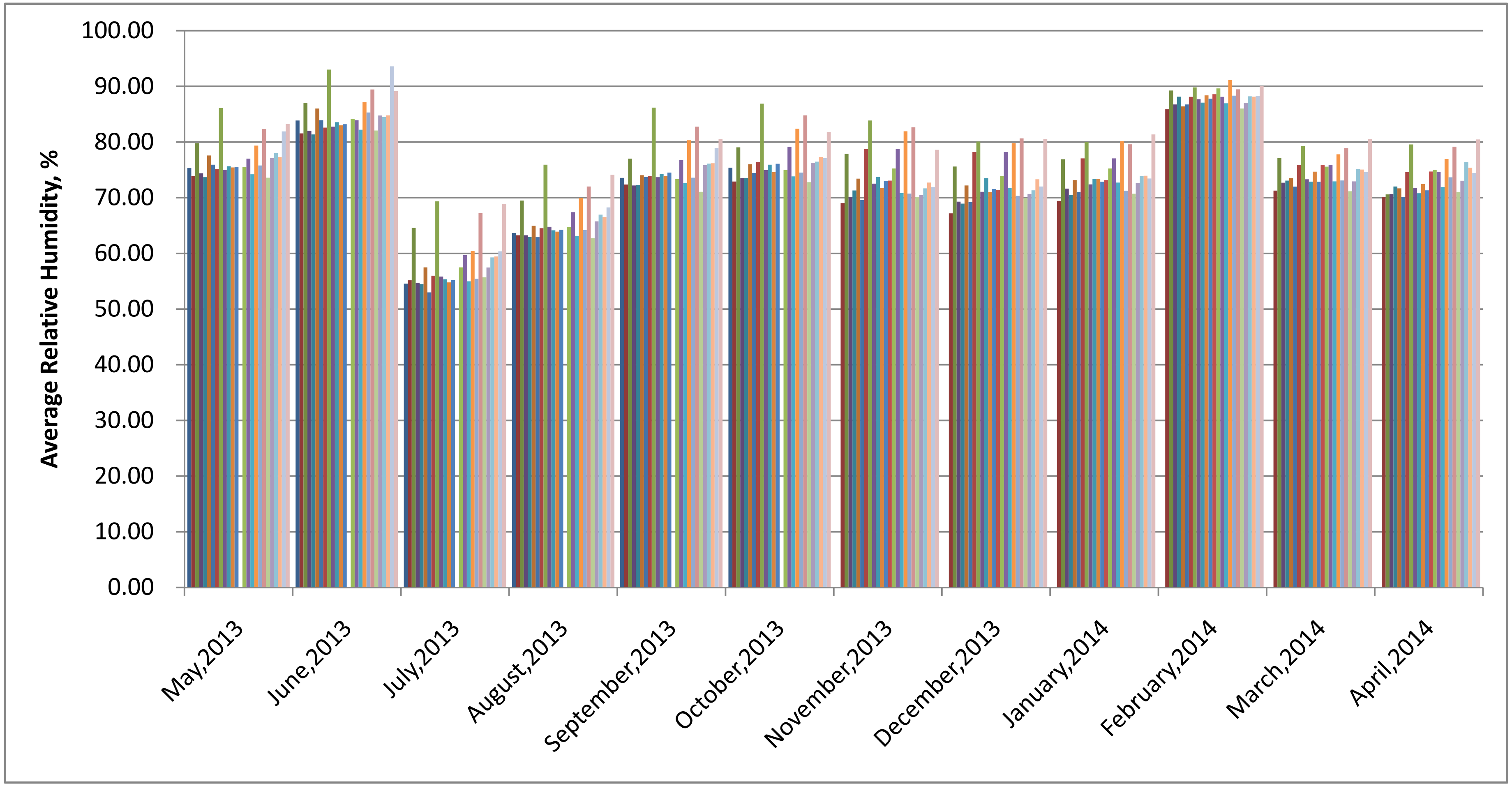

Fig. 5.3: Monthly average relative humidity values of all measurement sites from May, 2013 to April, 2014 in Hangzhou.

Fig. 5.4 illustrates monthly average UHII values of all measurement sites from May, 2013 to April, 2014 in Hangzhou. These positive UHII values demonstrate that UHI phenomenon exists in Hangzhou area. Moreover, UHI effect at some places of Hangzhou city in winter days is significantly pronounced with average UHII values higher than 3°C, as an example, the site of Hangzhou central railway station (Fig. 5.5).

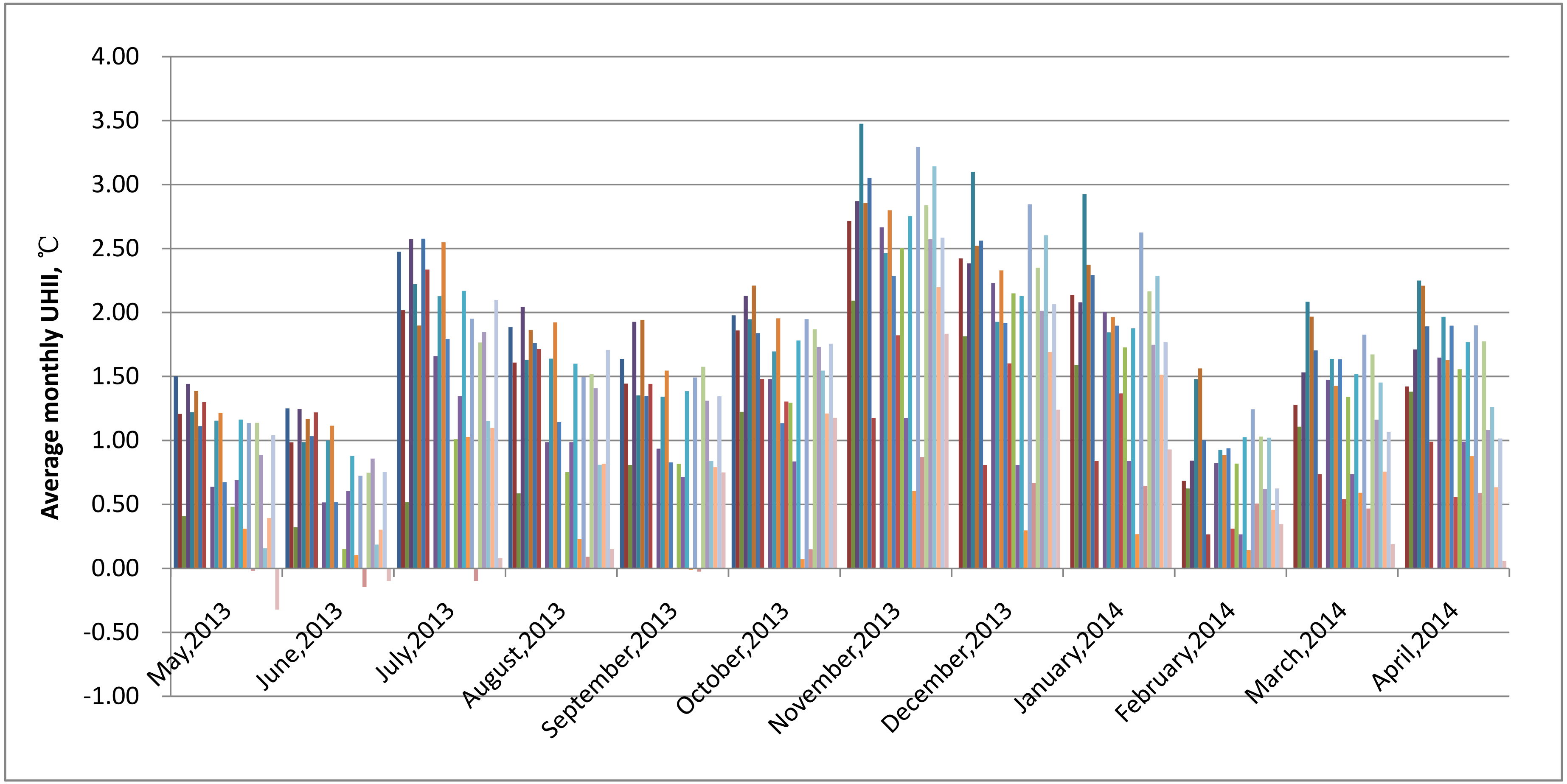

Fig. 5.4: Monthly average UHII values of all measurement sites from May, 2013 to April, 2014 in Hangzhou.

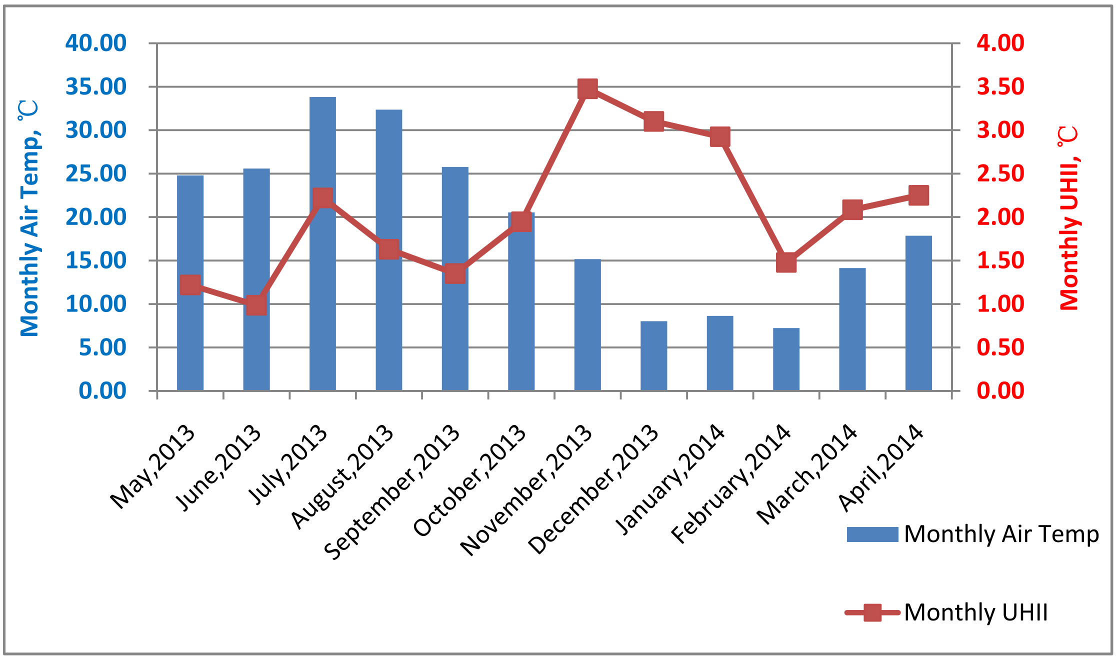

Fig. 5.5: Monthly average UHII and air temperature observed at the site of Hangzhou central railway station from May, 2013 to April, 2014.

5.2.2 UHI situation in Ningbo

Ningbo is the other city where the data collection exercise was carried out in this project. As the second developed city in Zhejiang province, Ningbo achieved an urbanization rate of 69% in 2013 that is only 4.5% lower than Hangzhou [97]. Although the land area of Hangzhou and Ningbo are not largest in Zhejiang Province, their Gross Domestic Products (GDP) values are highest (Hangzhou: 621.3 billion Chinese Yuan in 2012; Ningbo: RMB 395.1 billion Chinese Yuan in 2012) [97].

There is no national datum station, but only a national principle station in Ningbo. The surrounding environment requirement and data accuracy of national principle station is much lower than national datum station, which results in the data collected from national principle station could not be used for official typical weather year files generation [4]. Consequently, there is no availably official TMY or TRY weather dataset for Ningbo city. Besides, the location of Ningbo national principle station has been changed four times since the station was initially established in Ningbo at January 1st, 1953, because those previous locations were surrounded by dense high buildings due to rapid urbanisation in Ningbo [98]. Fig. 5.6 displays the previous and current locations of national principle station in Ningbo. The reference site was finally selected in the area of Ningbo Lishe International Airport which is about 10.5km away from Ningbo city centre.

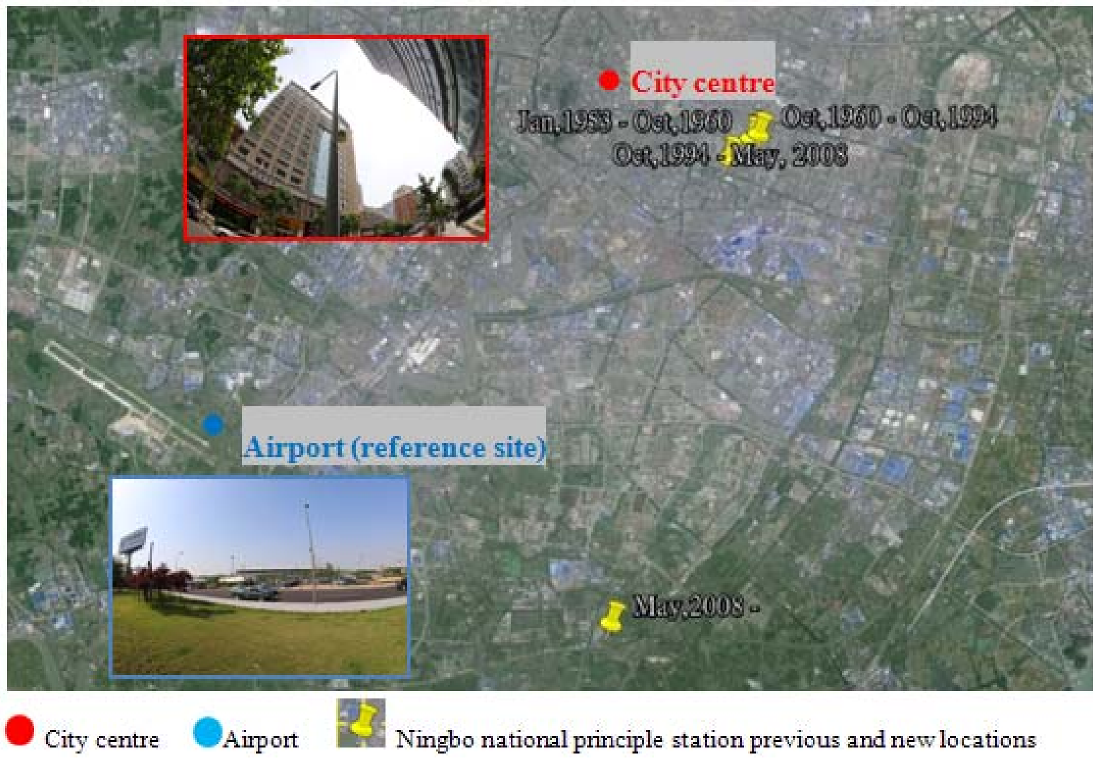

Fig. 5.6: Previous and current locations of national principle stations in Ningbo from Jan, 2013 to present.

The driving distance from Hangzhou city to Ningbo is only about 160km, thus, the climate of Ningbo is similar to Hangzhou. Compare Fig. 5.2 with Fig. 5.7, the average temperature in Ningbo is a little lower than in Hangzhou. As a port city, Ningbo is situated in the coastal plain on the Hangzhou Bay and its humidity is relatively higher (Fig. 5.8).

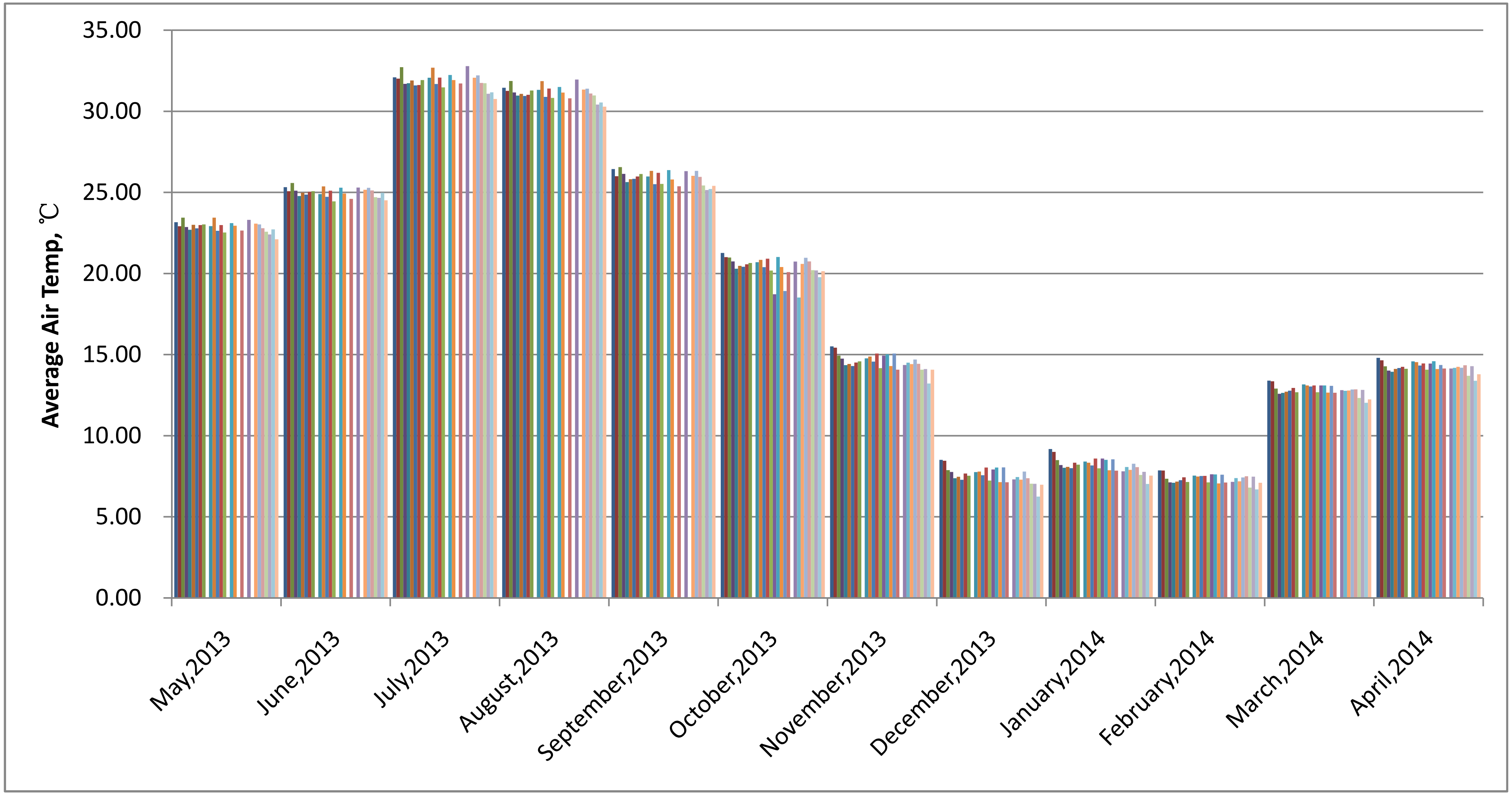

Fig. 5.7: Monthly average air temperature values of all measurement sites from May, 2013 to April, 2014 in Ningbo.

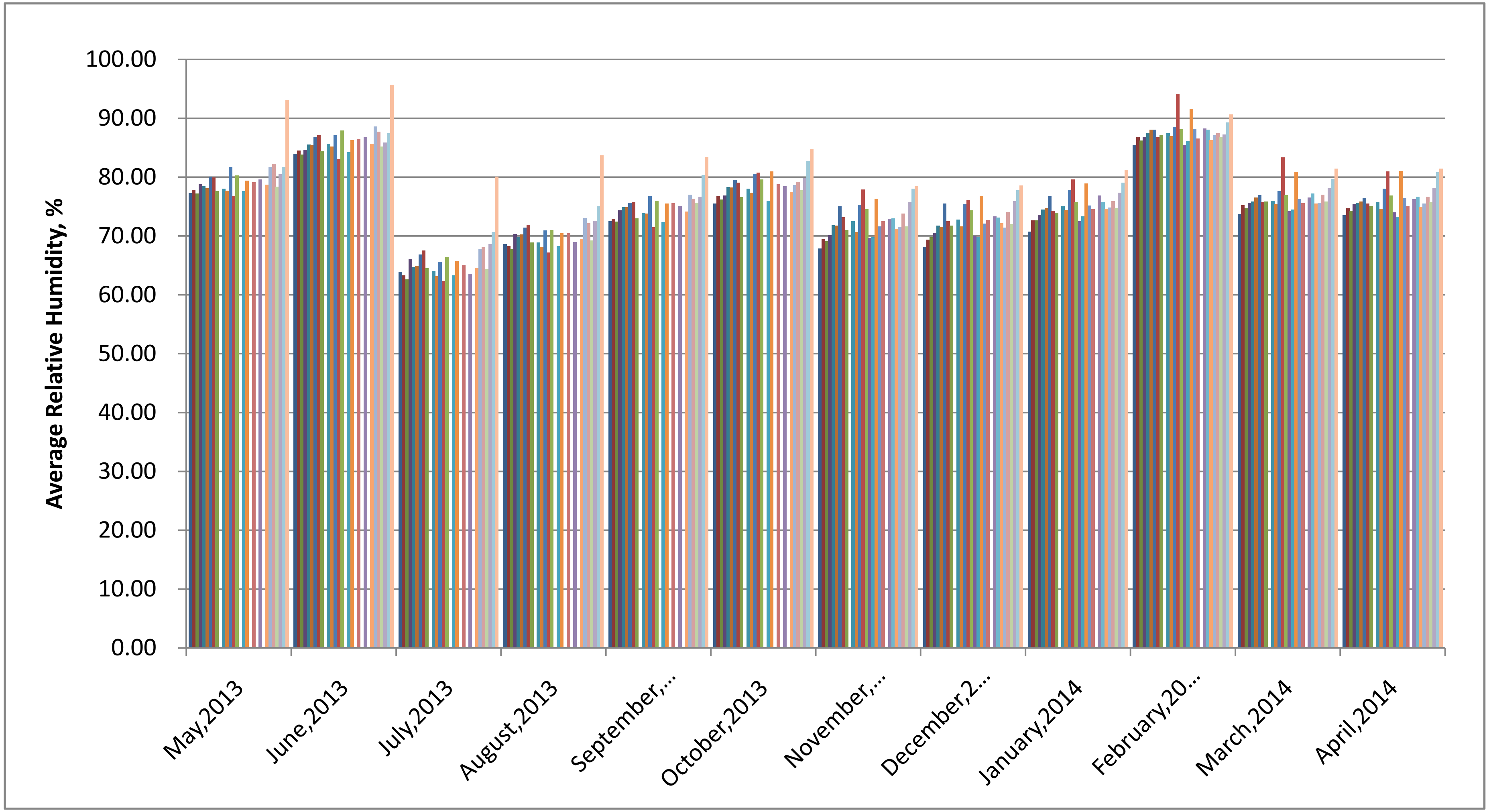

Fig. 5.8: Monthly average relative humidity values of all measurement sites from May, 2013 to April, 2014 in Ningbo.

As shown in Fig. 5.9, the highest monthly UHII of Ningbo measurement site is about 1.5°C. It should be noticed that the UHI effect of most measurement sites in Ningbo reduces exceedingly since February, 2014. The monthly average temperature values of most sites are continuously lower than the reference site in following measurement months from February, 2014 to October, 2014 (see Fig. 5.10). Comparing to the data measured in 2013, the UHII values observed in 2014 are extremely lower. It is virtually impossible that the UHI effect at Ningbo could be relieved so greatly or such an effective mitigation of UHI effect could be carried out suddenly. In addition to that, this sudden decrease in UHII was not caused by measurement error, because the data from October, 2013 to April, 2014 at each site was collected continuously by the same one i-Button sensor. The most feasible reason behind this situation is the variation of measurement environment at reference site and it is highly likely that the new construction work near the reference site provided additional anthropogenic heat of great extent and duration. The third phase of Ningbo Lishe International Airport expansion project started construction in the end of 2013 and was proposed to complete in 2016 [99].

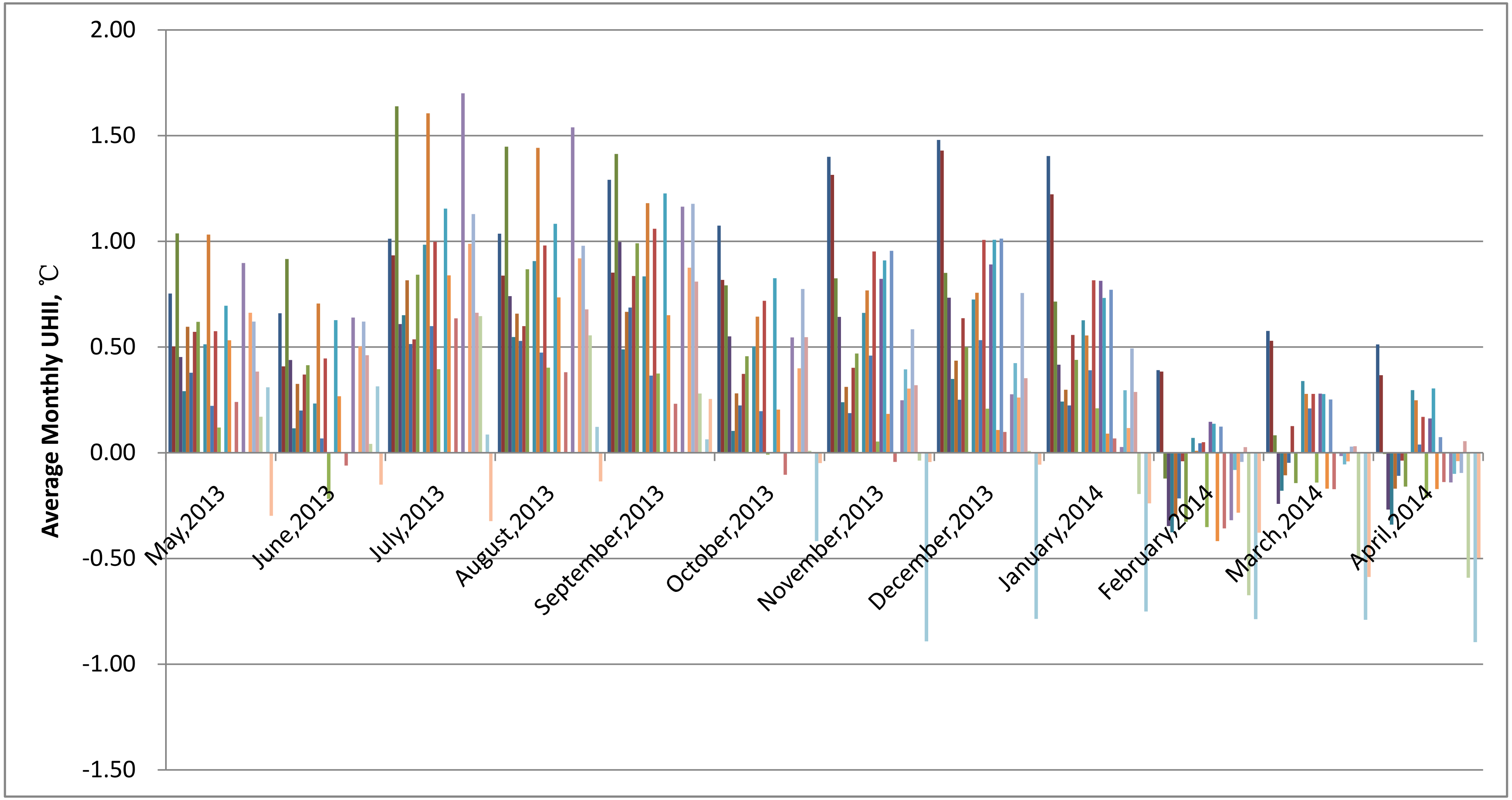

Fig. 5.9: Monthly average UHII values of all measurement sites from May, 2013 to April, 2014 in Ningbo.

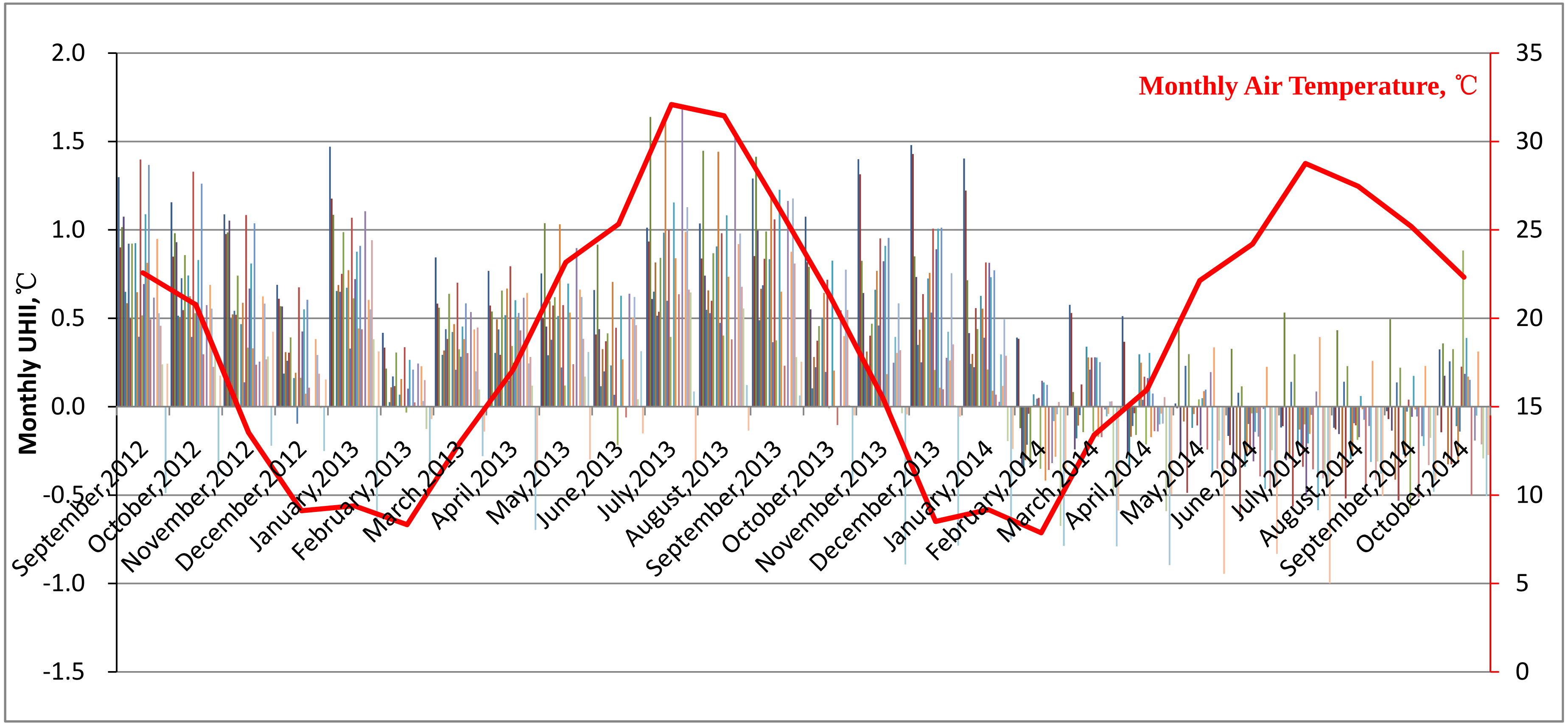

Fig. 5.10: Monthly average UHII values of all measurement sites from September, 2012 to October, 2014 in Ningbo.

5.3 Effects of urban design factors on UHI

5.3.1 Land-use

It is widely acknowledged that the growth of built-up land area is highly correlated with sociological and economic aspects, such as processes of industrialization and urbanization, the gross domestic product (GDP) and population growth. On the other hand, it would also lead to profound changes in ecological and environmental aspects, as an example, intensifying UHI effect.

5.3.1.1 Effect of land-use on UHI in Hangzhou

Most of Hangzhou metropolitan area is flat with a surface elevation ranging from 2 to 10 metres, and the urban spaces are located at elevations ranging from 2 to 3 metres. The hilly and mountainous regions account for 28.8% of Hangzhou metropolitan area [100].

As Fig. 5.11 illustrates, the built-up land area in Hangzhou metropolitan area increased from 319.4km^2 in 1978 to 861.9km^2 in 2008. In contrast, forest area, shrub land, fallow land, cropland and water space decreased nearly by 7.77 km^2/year, 18.92 km^2/year, 42.8 km^2/year, 51.7 km^2/year and 59 km^2/year on average [100]. It means that most newly emerging built-up land was converted from forest land, shrub land and other rural land cover types in recent years (see Fig. 5.12). Fig. 5.13 shows that shares of built-up land in land cover in sub-urban and rural regions of Hangzhou increased remarkably.

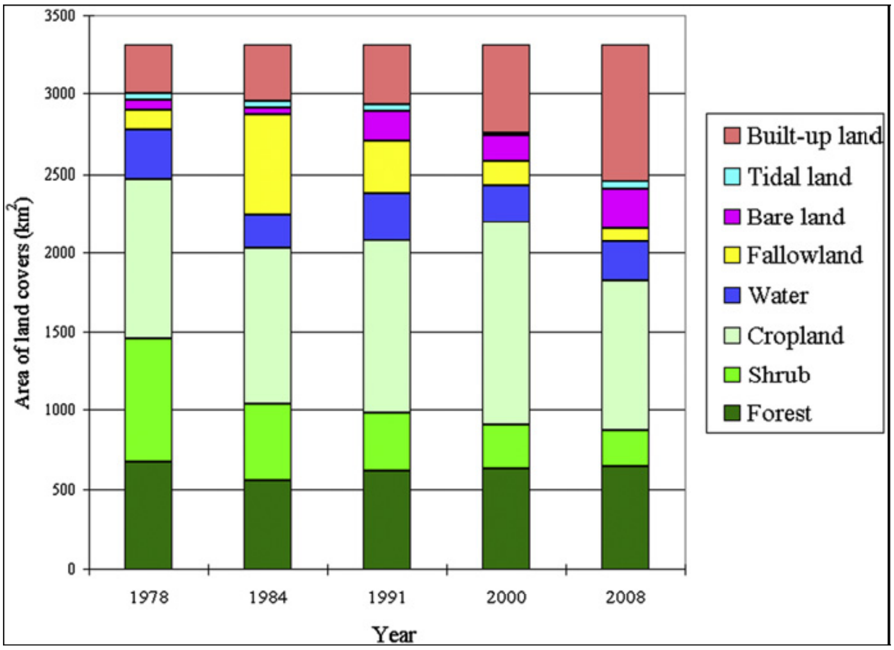

Fig. 5.11: Spatiotemporal patterns of land use in Hangzhou metropolitan area from 1978 to 2008 [100]

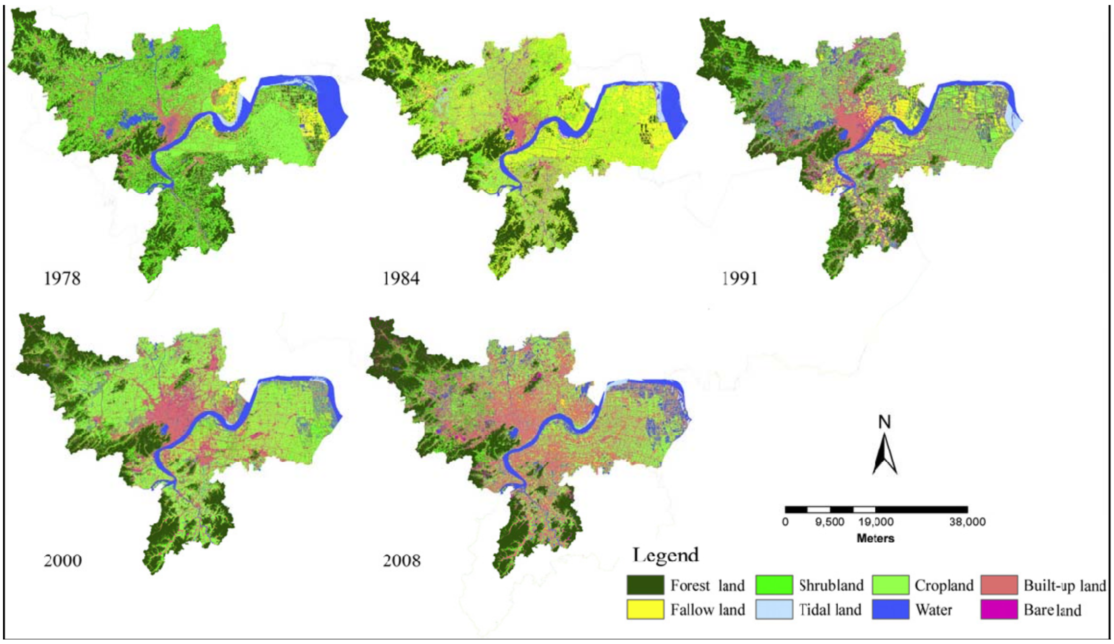

Fig. 5.12: Expansion patterns of Hangzhou metropolitan area from 1978 to 2008 [100]

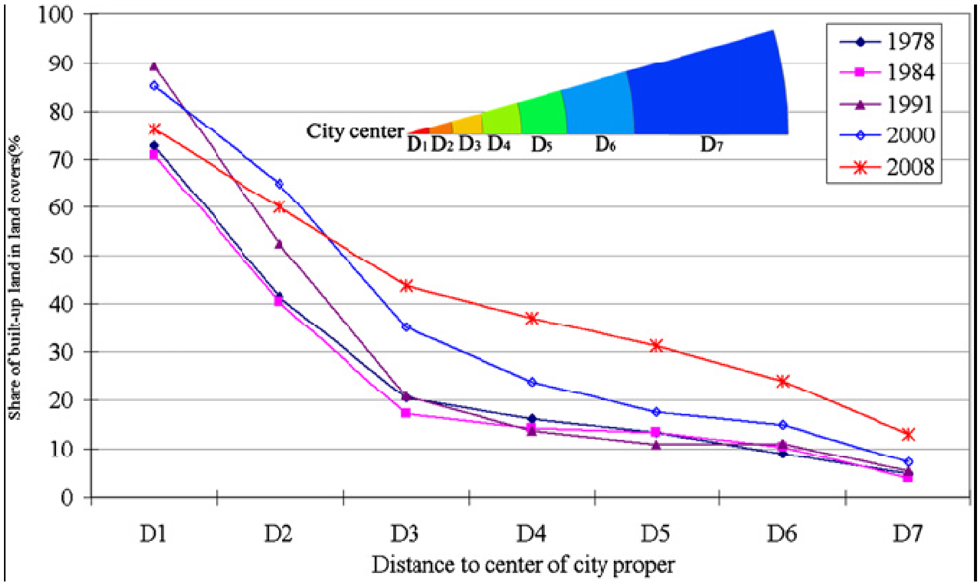

Fig. 5.13: Temporal pattern of land use in Hangzhou metropolitan area from 1978 to 2008 [100]

All the sensors were placed at locations with different types of land use and land cover, such as residential area, industrial area, green area, public area and others. As Fig. 5.14 shows, all these types of land use have been marked on the Hangzhou General Planning Map [77]. Each type of land use is characterised by presence of impervious surface (building roofs and pavements), vegetation cover, anthropogenic heat generation and surface characteristics (topography and elevation). The research examined the impacts of land use on Hangzhou UHI effect by examining the air temperature collected at various locations. Hangzhou Central Railway station located at the public core area of Hangzhou has the strongest UHI effect, whilst the UHI effect of Xixi Wetland and Yuhuang Mountain at green area is much weaker (see Fig. 5.15). Furthermore, although Yaqian Industrial Park was located at the boundary area of Hangzhou city, its UHI effect is significantly intense.

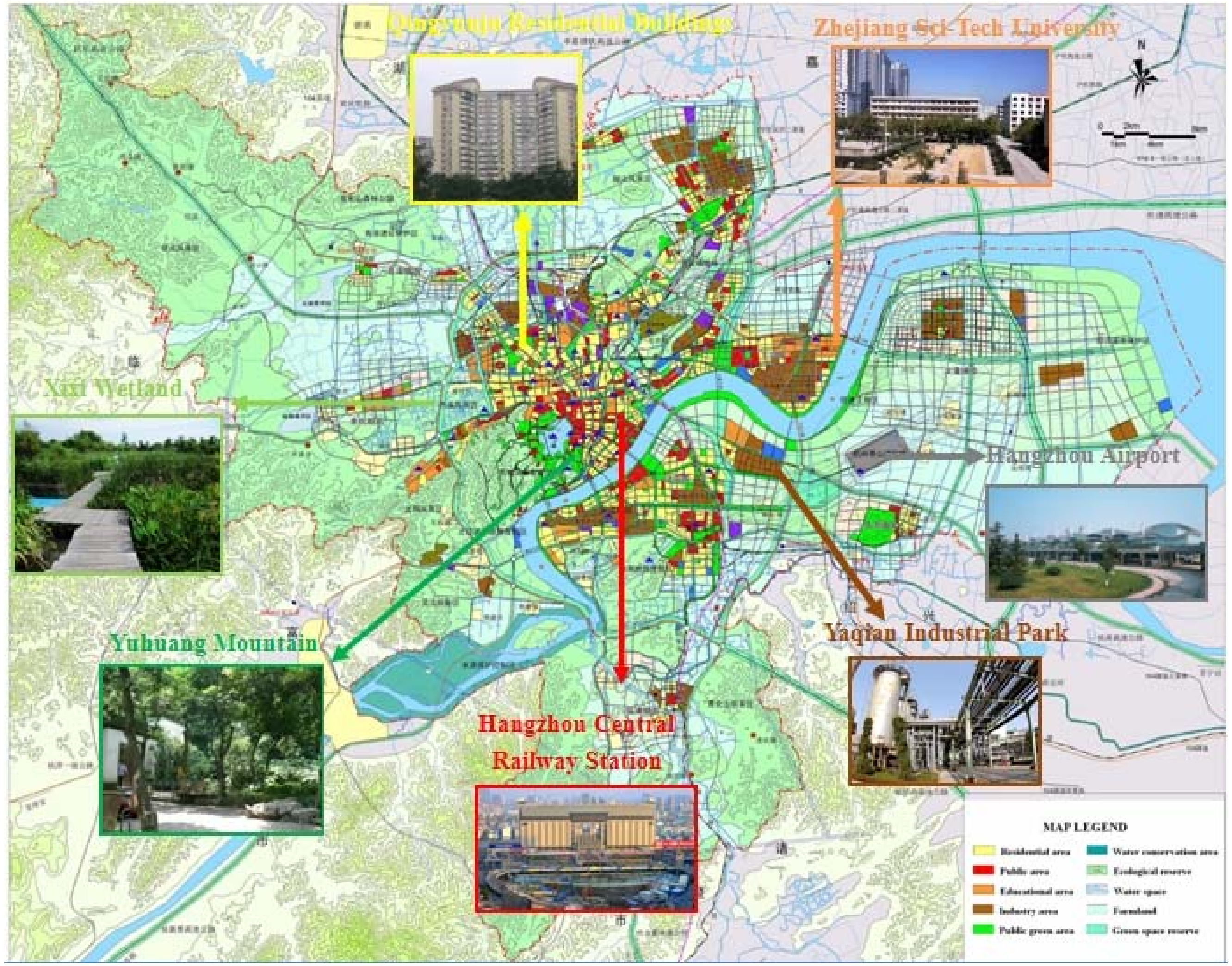

Fig. 5.14: Some measurement sites with different land use marked on Hangzhou general planning map [77]

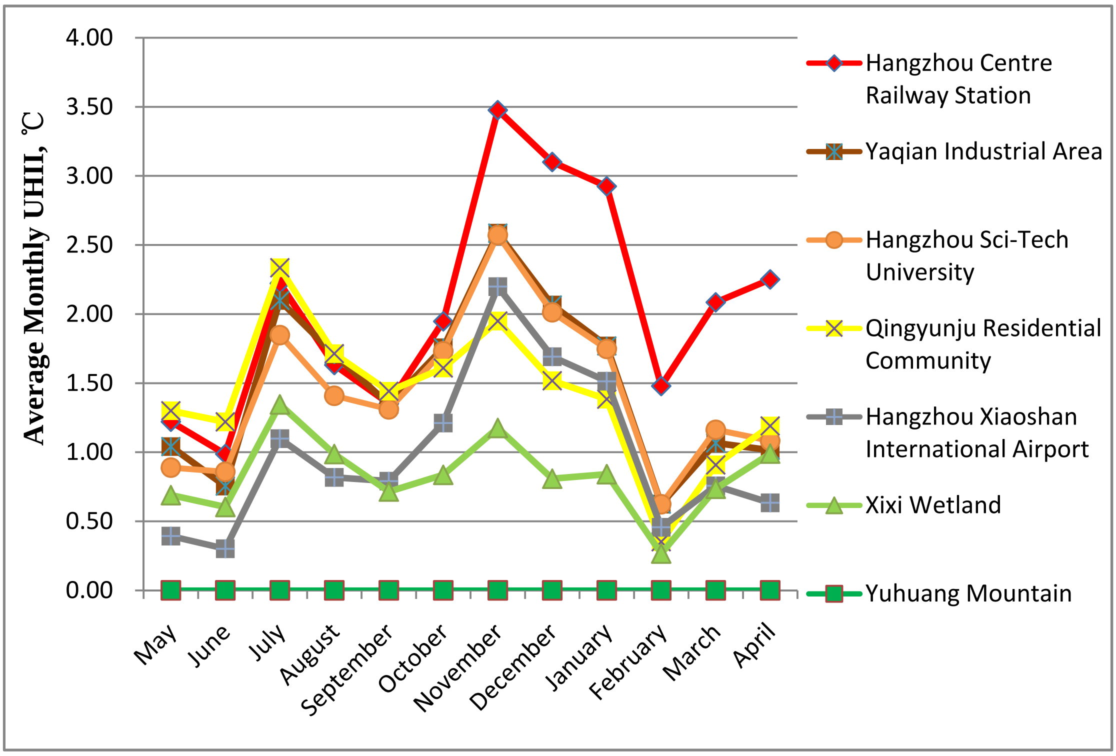

Fig. 5.15: Monthly average UHII measured at sites with different land use areas from May, 2013 to April, 2014.

The result shows that the land usage has impact on urban air temperature. The monthly average UHII values of five land use patterns (residential, industrial, public, educational and green area) are indicated by Fig. 5.16. In general, residential, industrial and public area have are higher mean ambient air temperature than educational and green spaces. The UHI effect at green area is the lowest among these five land use types.

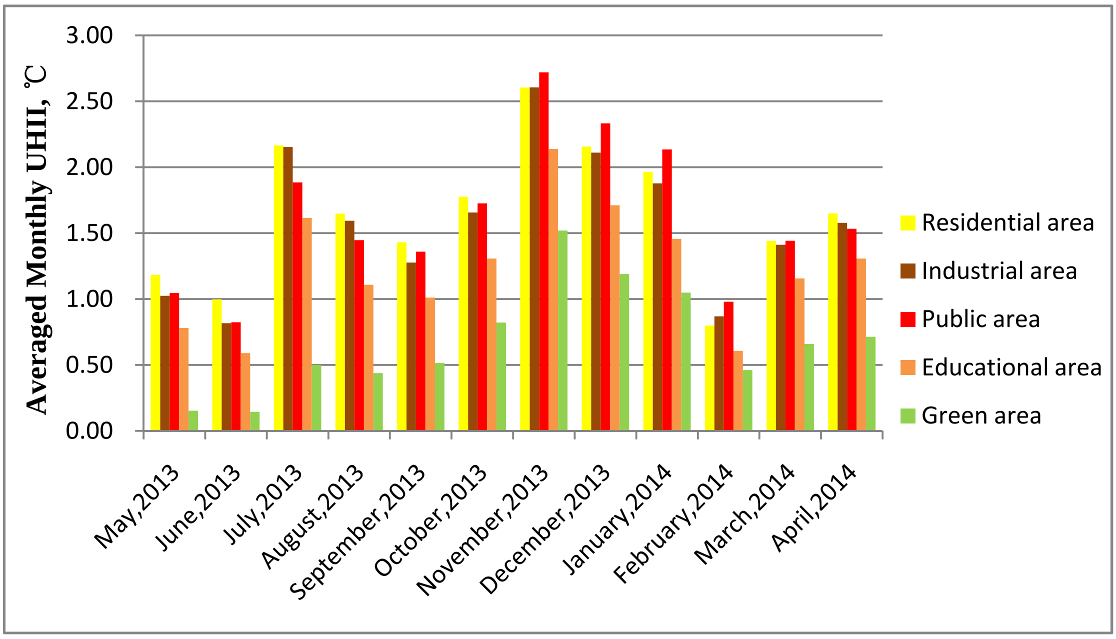

Fig. 5.16: Comparison of monthly average UHII in five land use areas from May, 2013 to April, 2014.

The detailed analysis was carried out to investigate the influence of various land use patterns on the UHI effect during day time as well as night time. For day time analysis, all the UHII values were extracted from the data collected from 6:00 to 17:00 each day. As Fig. 5.17 illustrates, the highest day time UHII values occurred in industrial area among different land use patterns. There are two main characteristics causing the intense UHI effect. Firstly, anthropogenic heat generated in industrial park in day time is extremely greater than other spaces. The second characteristic is industrial buildings are commonly designed with combination of metal pitched roofs and large exposed concrete surface. The industrial buildings are arranged close apart from one to another with no greenery in between (see Fig. 5.18). These contribute to the increase of ambient temperature because of the extensive use of heat absorbing materials, by decreasing of moisture available for evapotranspiration.

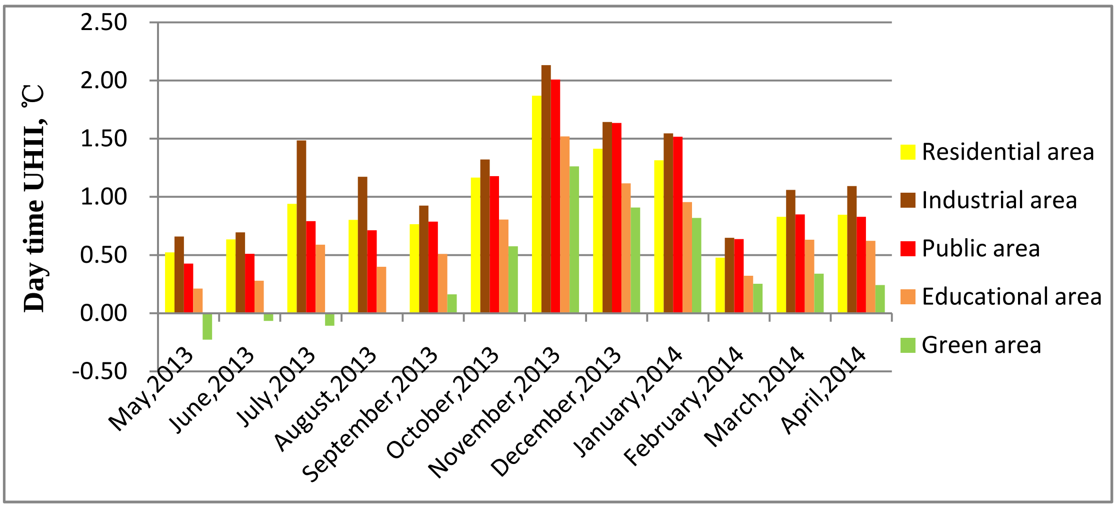

Fig. 5.17: Comparison of mean day time UHII in five land use areas from May, 2013 to April, 2014.

Fig. 5.18: The view of Yaqian industrial park

Following industrial area, intense day time UHI effect happens in residential and public spaces. This is also owing to the exceedingly large concrete area of roads and buildings. However, the residential area usually has open space of greenery area for small community parks which have an improvement of evaporating surfaces. Similar appearance can be noticed also in public area where a lot of high-rise commercial buildings consist. During day time period, due to the shading from those high-rise buildings, the roads and space between the towers are appears cool, even it is absence of plantation.

For educational area where buildings are much less congested and space of plants and sport field are larger (see Fig. 5.19), the air temperature at educational regions is relatively cooler than industrial, residential and public regions. It also proves again that sites near or surrounded by green area have less intense UHI effect than the one apart from green area. Owing to evapotranspiration process of plants, the day time UHII values at dense green area are definitely lowest.

Fig. 5.19: The view of Hangzhou Foreign Language School

Referring to the night time UHI situation at Hangzhou, all the data collected at measurement site were from 18:00 to 5:00. The order of UHII values in all land use types at night time is a bit different from the day time situation. As shown in Fig. 5.20, the night time UHII values of residential and public areas become higher than industrial area. There are two feasible reasons behind this change. In the first place, a quite few factories in the industrial park are closed at night, thus anthropogenic heat generation could be lowered significantly. The other point should be touched on is that concrete buildings at residential and public areas are excessively larger and more crowded comparing with industrial area. Concrete can function as thermal storage to absorb and store solar energy in the day time. The larger of the concrete volume, the larger the capacity is to store solar energy. The night time thermal environment around high-rise buildings would be effected by re-radiating the absorbed heat from the large area of concrete surface, when the ambient temperature cools down at night time.

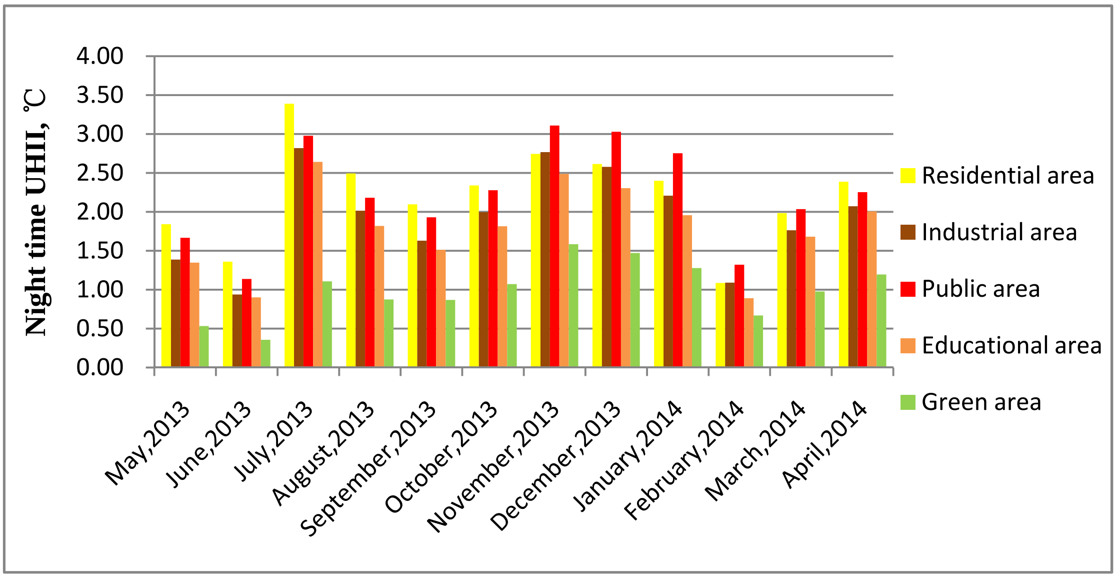

Fig. 5.20: Comparison of mean night time UHII in five land use areas from May, 2013 to April, 2014.

5.3.1.2 Effect of land-use on UHI in Ningbo

Alternatively, the effect of land use on UHI effect in Ningbo city was analysed by applying remote sensing technology. The land surface temperature distribution across different land use types was studied through comparison of land use types with Ningbo satellite images obtained from the Landsat Enhanced Thematic Mapper Plus (ETM+) sensor on board Landsat 7 satellite. The Landsat 7 satellite was successfully launched on April 15th, 1999 by the U.S. government. The ETM+ sensor on Landsat 7 has been recognised as the most stable, best characterized Earth observation instrument ever placed in orbit [101]. The Landsat ETM+ sensor can provide image data from the visible to thermal infrared spectral regions by nine spectral bands [102]. ETM+ bands 1-5 and 7 contain 30m resolution within the visible and infrared spectrum, and band 8 provides a 15m resolution panchromatic image. ETM+ band 6 (10.4-12.5μm) with the spatial resolution of 60m is usually used for thermal mapping. An approximate surface temperature could be extracted from the band 6 as well.

The extraction of the surface temperature data from the band 6 satellite image was based on recorded digital number (DN) values. The thermal band image data calibration is basically performed in two main steps as proposed by the Landsat 7 Science Data Users' Handbook [103]. The first step is converting digital number (DN) to radiance values, L, $(\mathrm{Wm^{-2}sr^{-1}\mu m^{-1}})$ using the bias and gain values, as follows:

$$\mathrm{L} = \mathrm{Gain} \times \mathrm{DN} + \mathrm{Bias} \tag{5.1}$$

The second step is to convert radiance to surface temperature, T in Kelvin using the following equation:

$$T = \frac{K_2}{\left\{\ln\left[\frac{K_1}{B(T_S)}+1\right]\right\}} \tag{5.2}$$

where K_1 is the calibration constant ($666.09 Wm^{-2}sr^{-1}\mu m^{-1}$), K_2 is the calibration constant (1282.71K) and B(Ts) is the atmospherically corrected value as radiance.

The Ningbo general planning map of land use (2004-2020), elaborated by Ningbo Urban Planning Bureau, divides the land uses in Ningbo city into 23 categories, as shown in Fig. 5.21 [83]. The region of Grid A on the planning map is the city core area of Ningbo where there is bare green space.

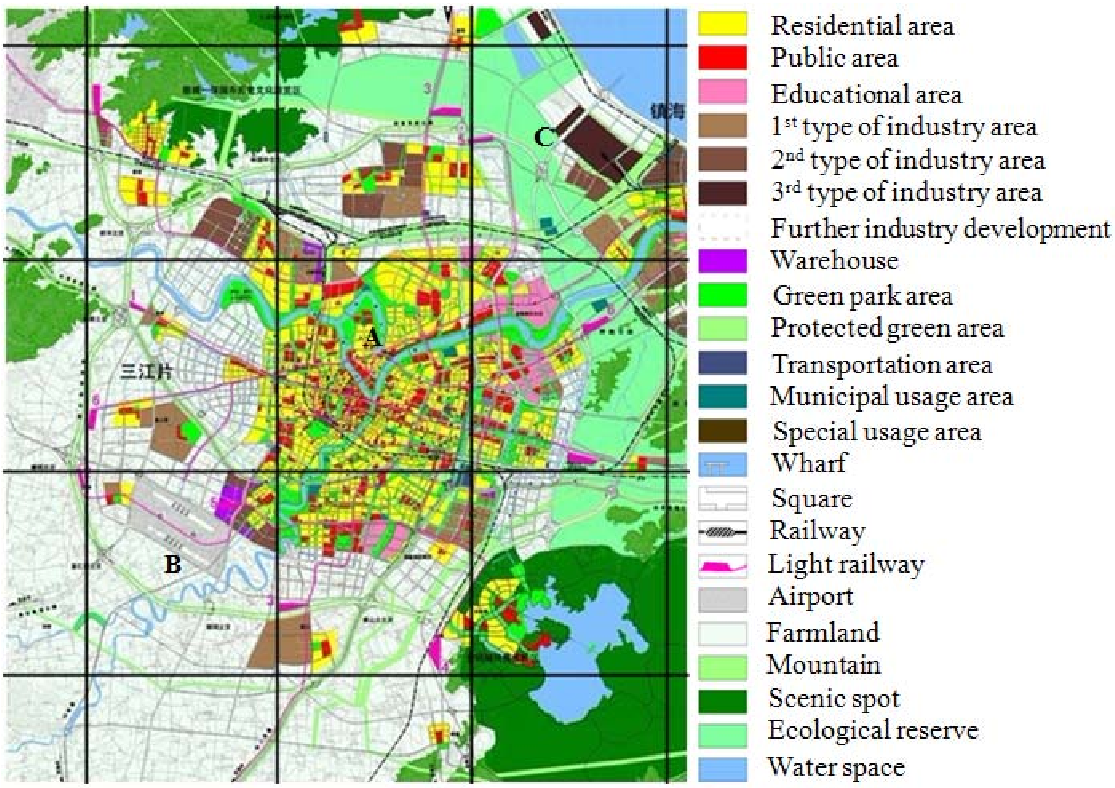

Fig. 5.21: Ningbo general planning map [83]

With the image processing software ENVI, the Landsat 7 ETM+ thermal image of the Ningbo city (longitude: 121.319-121.705E; latitude: 29.670-30.025N) were examined by the equations presented above. The thermal environment of Ningbo city at 13:35 on July 22, 2008 and at 13:40 on August 18, 2012 were performed respectively by band 6 thermal image of "LE71180392008204EDC00_B6_VCID_2" and "LE71180392012231EDC00_B6_VCID_2" (see Fig. 5.22 and Fig. 5.23).

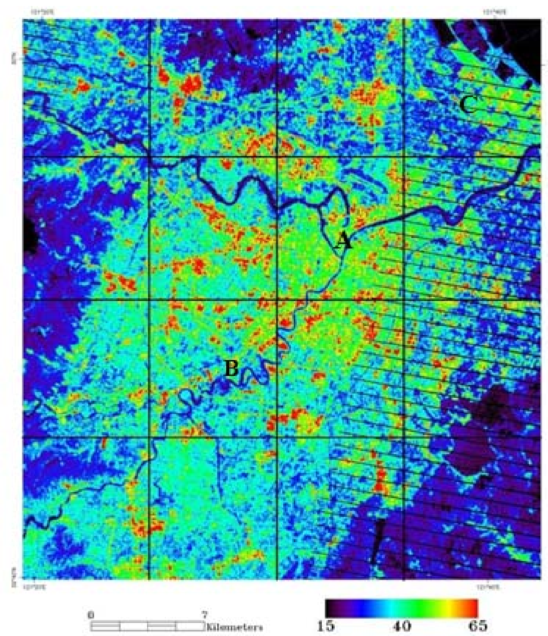

Fig. 5.22: Land surface temperature map of Ningbo city (longitude: 121.319-121.705E; latitude: 29.670-30.025N) at 13:35 on July 22, 2008

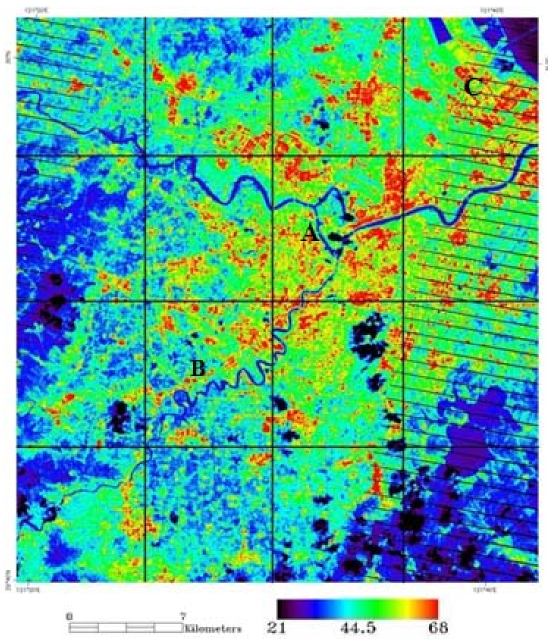

Fig. 5.23: Land surface temperature map of Ningbo city (longitude: 121.319-121.705E; latitude: 29.670-30.025N) at 13:40 on August 18, 2012

As Fig. 5.21 shows, there is rare green area and vast amount of built-up land area at the city centre of Ningbo (Grid A) where the surface temperature is significantly higher than surrounding areas. Indeed, green space and water space have lower surface temperature values, that is to say, they form cold islands in the whole area (see Fig. 5.22 and Fig. 5.23).

According to the historical temperature collected from the reference weather station at Ningbo Lishe International Airport (Fig. 5.24) [104], the temperature at airport at 13:35 on July 22, 2008 is similar as that at 13:40 on August 18, 2012. However, the surface temperature at Ningbo urban core area, Haishu District (Grid A) in 2012 has significant increase, comparing with the surface temperature in 2008, which proves the situation of surface UHI in Ningbo becomes intense. This phenomenon is most probably caused by the rapid development of building construction in the urban area. During the period from 2008 to 2012, the local building industry production at Haishu District of Ningbo city (Grid A) increased by about 2.3 billion RMB, from 0.956 billion RMB to 3.259 billion RMB, at an annual average rate of 36%, as Fig. 5.25 illustrates. Buildings commonly locate at the urban core area and the narrow arrangement of buildings along the streets from urban canyons that inhibit the escape of reflected radiation from most of the urban surface to space. This may imply that if there is more vegetation in urban core areas, the UHI effect can be mitigated effectively.

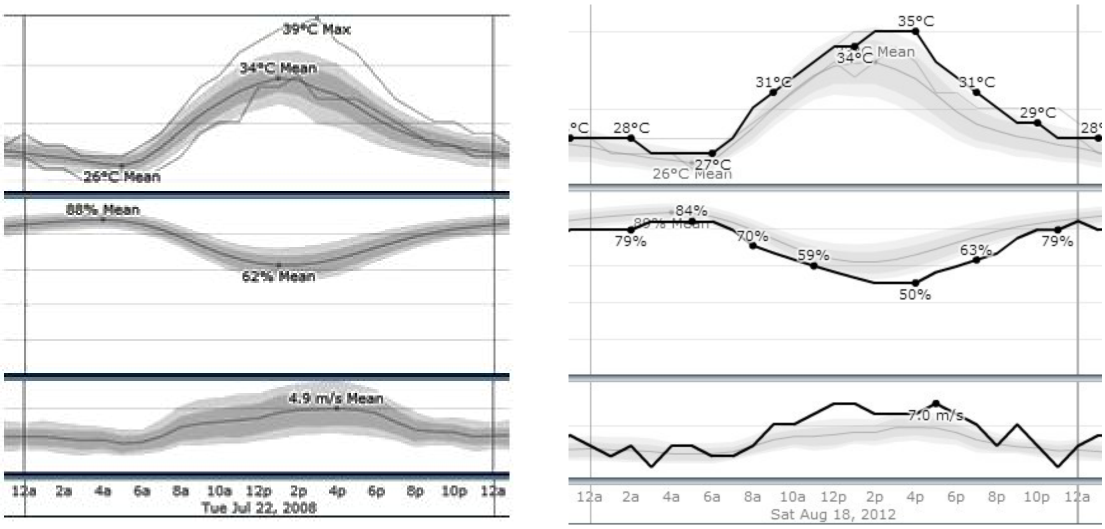

Fig. 5.24: Historical weather condition information at July 22, 2008 (left) and August 18, 2012 (right) collected from Ningbo Lishe International Airport [104].

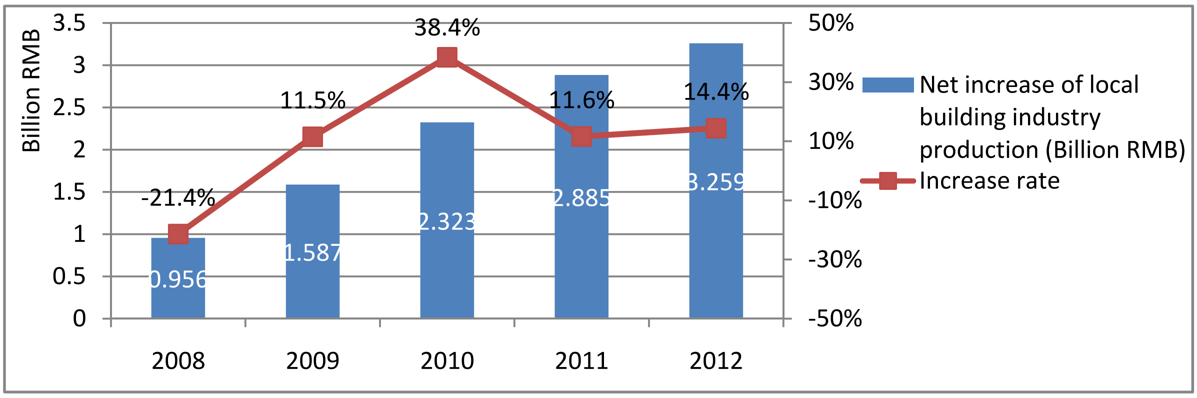

Fig. 5.25: Development of local building industry production at Haishu District of Ningbo from 2008 to 2012 [105]

Comparing Fig. 5.22 with Fig. 5.23, the UHI space has expanded towards the east and northeast part of Ningbo, closing to the East China Sea. This UHI expansion occurs in Ningbo city is the response to the policy made by local government. Ningbo, as a port city, focuses on developing coastal industry upon marine resources in accordance with

China's 11th (2006-2010) and 12th (2011-2015) Five year Plans [106, 107] . For example, Zhenhai District (Grid C), locates by the East China Sea and relies on marine industry, has developed faster than the average level of Ningbo since 2009 (see Fig. 5.26) [108].

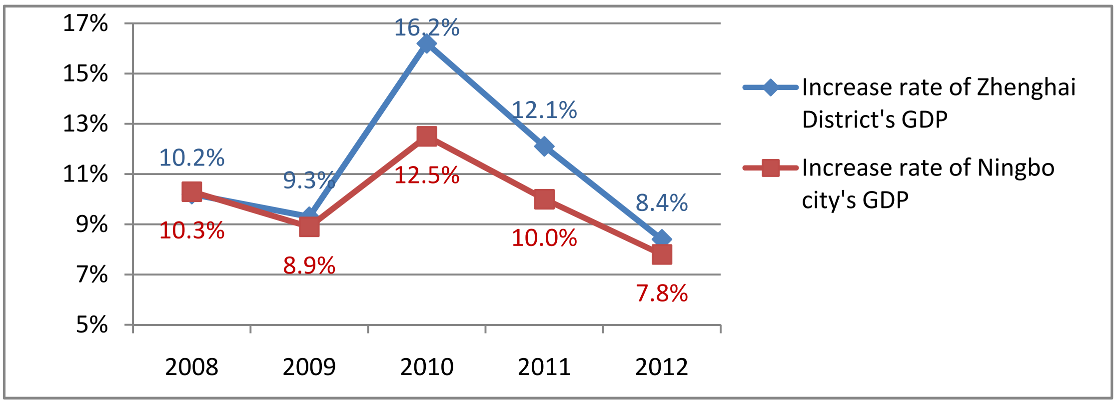

Fig. 5.26: Comparison between the GDP increase rates in Zhenhai District (Grid C) and Ningbo City (Grid A) (2008-2012)

5.3.2 Distance from city centre

It has been proved that the UHI effect is most intense at the city centre where buildings are densely concentrated. The observation determined that UHII patterns are dominated by a strong linear and negative relationship between UHII and distance from the city centre, which is in agreement with previous studies [9].

5.3.2.1 Effect of distance from city centre on UHI in Ningbo

It is shown by Fig. 5.27 that UHII values gradually decreased with increasing distance from city centre of Ningbo. This phenomenon has also been observed both in day time and night time situations (see Fig. 5.28). Several factors become the cause of this situation, such as shortage of green space, low wind velocity due to high-building density and the extensive usage of building materials at city centre area. As Fig. 5.29 shows, the population density in the study area of Ningbo gradually decreased with increasing distance from city centre as well. The average population density in urban core area is about 10299persons/km^2 that is 15 times greater than in suburban and rural area in 2013 [109].

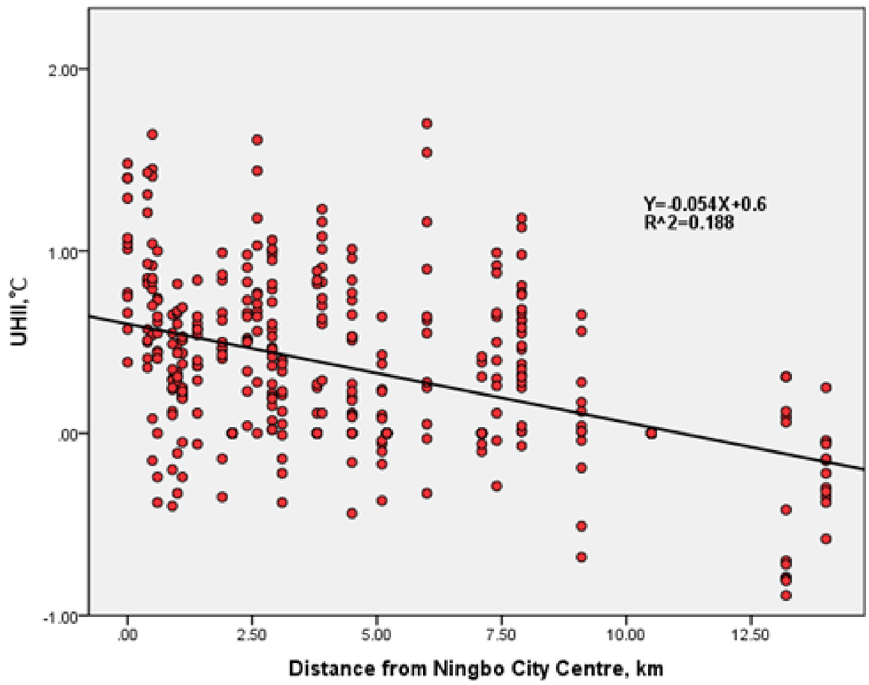

Fig. 5.27: Monthly average UHII against distance from Ningbo city centre

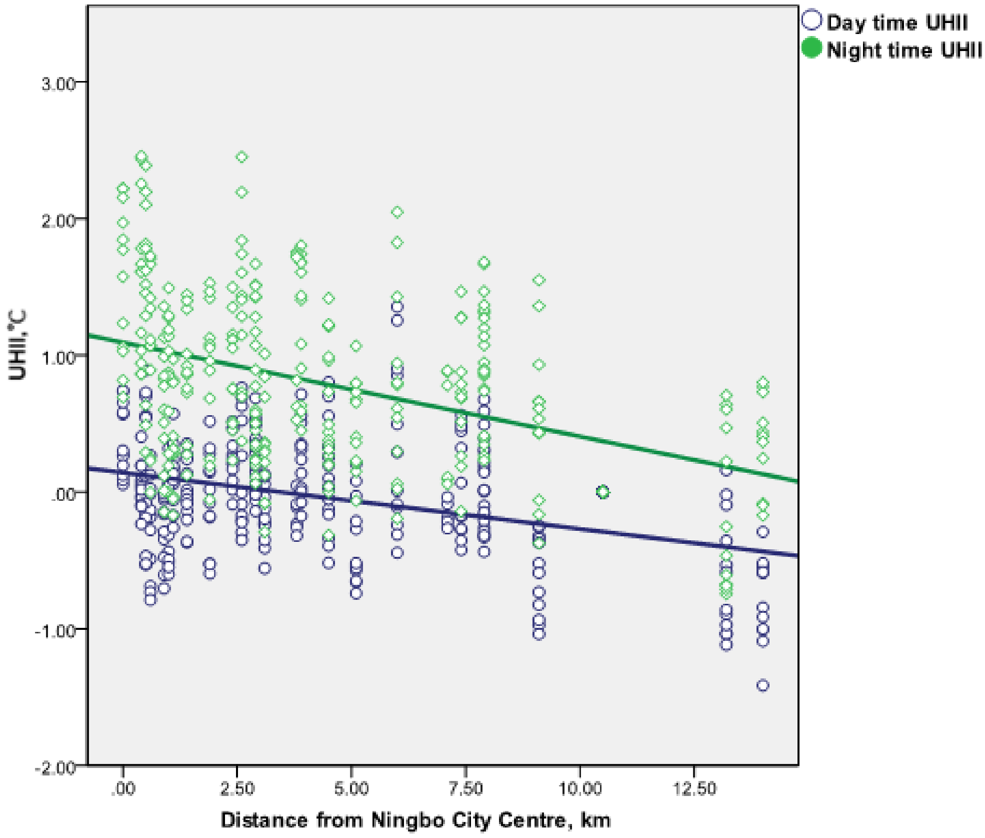

Fig. 5.28: Average day time and night time UHII against distance from Ningbo city centre

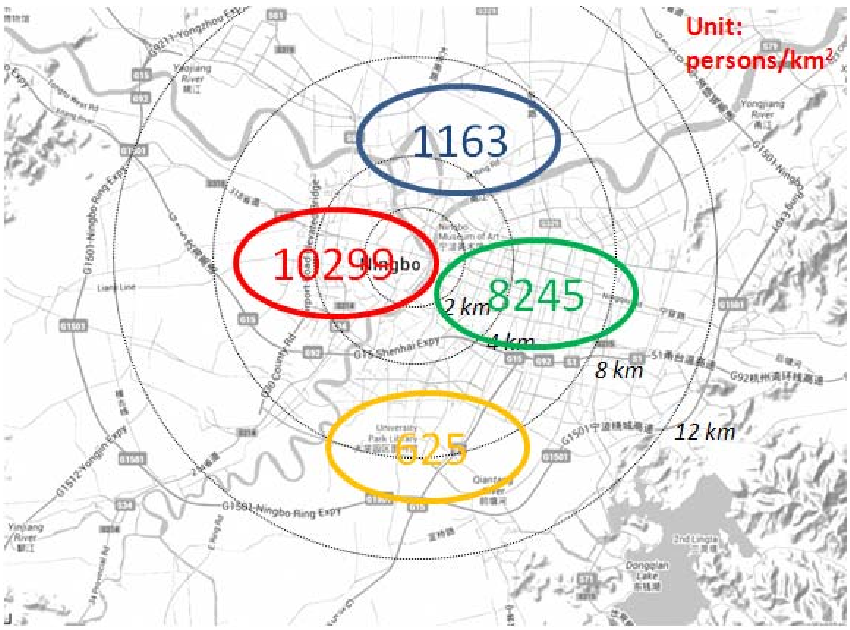

Fig. 5.29: Average population density in different regions of Ningbo [109]

5.3.2.2 Effect of distance from city centre on UHI in Hangzhou

As Fig. 5.30 shows, the negative relationship between UHII and distance from city centre in the case of Hangzhou is not as perceptible as in Ningbo, due to the special landform of Hangzhou city. West Lake (30°15′N; 120°10′E) is a famous tourist lake, locating west of the city centre of Hangzhou. The distance from the West Lake to Hangzhou city centre is only 1.4km. It is a small shallow lake with an average depth of only 1.56m, but its area is 5.66km^2. Xixi National Wetland Park also locates in the west part of Hangzhou city, only 6km from the city centre and 5km from the West Lake (see Fig. 5.31). Xixi Wetland covered an area of about 60km^2 historically and currently, the overall area of the protected Xixi Wetland is about 11.5km^2.

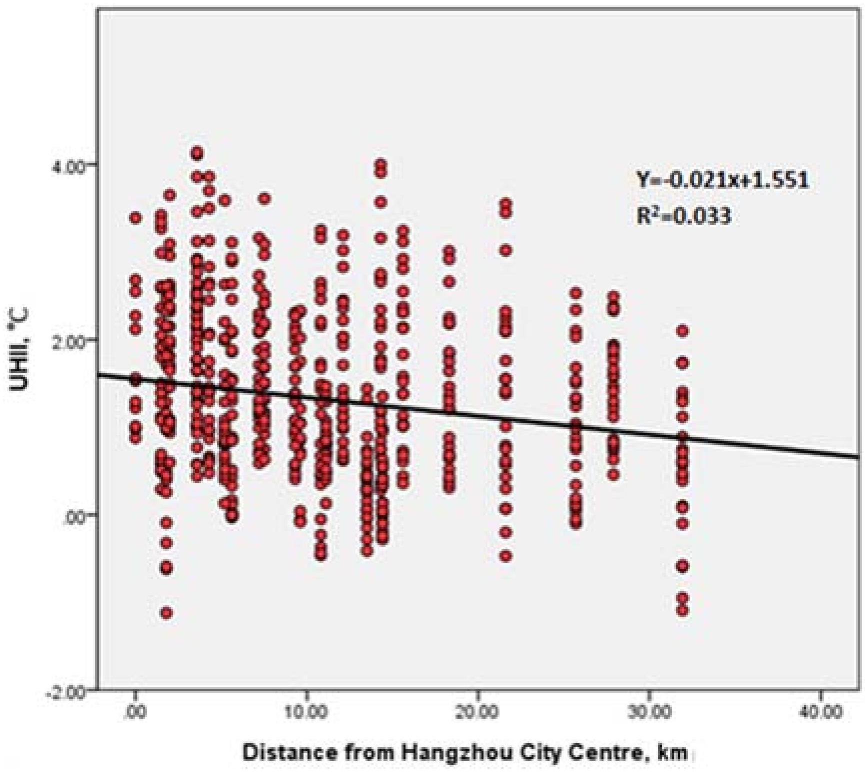

Fig. 5.30: Monthly average UHII against distance from Hangzhou city centre

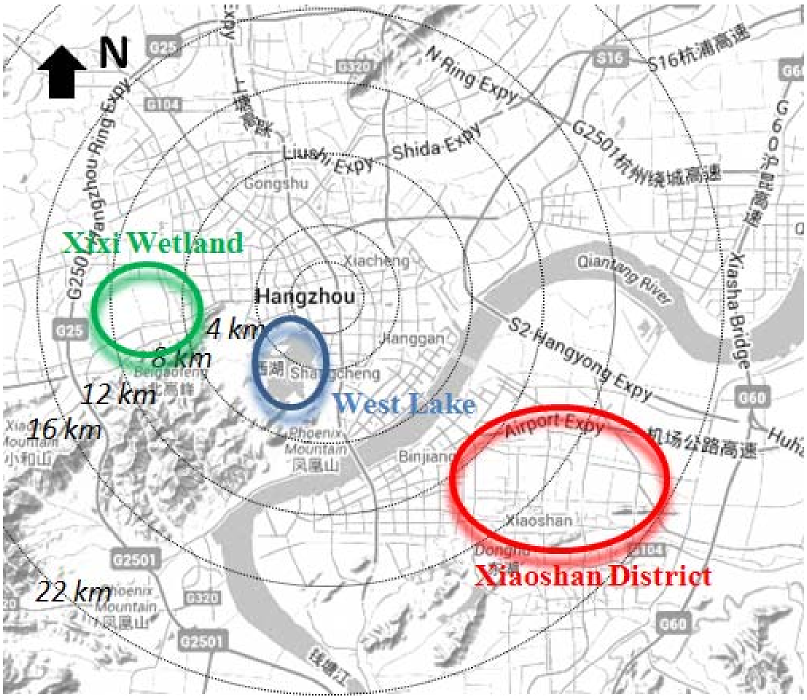

Fig. 5.31: Locations of West Lake, Xixi Wetland and Xiaoshan District in Hangzhou

It has also been evaluated by previous ENVI-met simulation case study that West Lake and Xixi Wetland, as large urban ecological resources in Hangzhou urban area, they can serve similar functions and complement each other in lowering urban temperature in Hangzhou. There are few metropolitan cities in the world have this similar size of natural ecological space in urban core area. Additionally, Xiaoshan district, as one of the most developed districts of Hangzhou city, locates between Hangzhou urban area and Hangzhou Xiaoshan International Airport. As Fig. 5.31 displays, Xiaoshan's urban area is more than 10km away from Hangzhou's city centre, nevertheless, the density of high-rise buildings and the urbanisation rate is not lower than Hangzhou. Bearing these two reasons in mind, it is possible that air temperature collected from some measurements closing to Hangzhou city centre sometimes might similar or even lower than sites far away from city centre.

5.3.3 Surrounding albedo

Albedo plays a crucial role in the thermal behaviour of pavement and other ground surface. Stull defines the term of albedo as: “the ratio of total reflected to total incoming solar radiation (i.e., average over all solar wavelengths)”[110]. Surface material with higher albedo is able to absorb less radiation and maintain a lower surface temperature under sunshine. Earth surface has an effective albedo of approximately 0.3, since about 30% of the annually received solar radiation is reflected or scattered [111]. Rural surfaces commonly have 2-5% higher albedo values than urban spaces at the same latitude[112]. Many numerical simulations and field measurements indicated that increasing albedo of surface can be effective in reducing the surface and air temperatures near ground [113, 114]. Fig. 5.32 shows the simulated outside wall surface temperature for a south wall in July for Washington, D.C. [115]. In that research, the cooling energy of a house in Sacramento, California, was reduced by 18.9% by painting the house white to increase its surface albedo from 0.25 to 0.9. If the albedo of house’s surrounding surface could be increased to 0.4 simultaneously, the reduction in energy use could be as large as 62% [115].

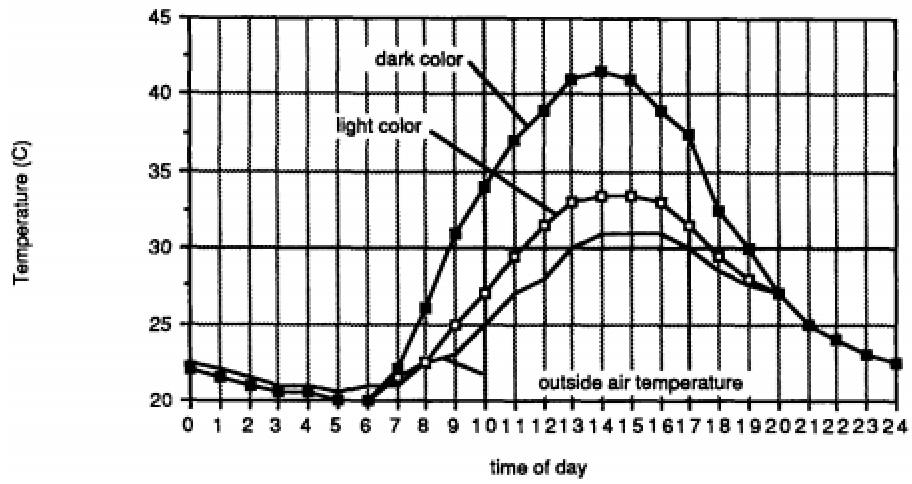

Fig. 5.32: Exterior surface temperature on insulated residential building's south wall in July day time in Washington, D.C. [115]

In this study, the albedo value of each measurement site is estimated by a simple questionnaire survey based on the following guide (Tab. 5.1) [24], because there are no available equipments that could be used to measure the exact albedo value of exposed surfaces in this research.

Tab. 5.1: Albedo of surface material samples [24]

Non-urban		Urban		
Surface	**Albedo**	**Surface**	**Material**	**Albedo**
Soils	0.05-0.40	Roads	Asphalt	0.05-0.20
Desert	0.20-0.45	Walls	Concrete	0.10-0.35
Grass	0.16-0.26		Brick	0.20-0.40
Agricultural crops & tundra	0.18-0.25	Roofs	Tar and gravel	0.08-0.18
Deciduous forest	0.15-0.20		Tile	0.10-0.35
Coniferous forest	0.05-0.15	Windows	Glass, zenith angle <40	0.08
Snow	0.40-0.95		Glass, zenith angle 4080°	0.09-0.52
Water, small zenith angle	0.03-0.10	Paints	Whitewash	0.50-0.90
Water, large zenith angle	0.10-1.00		Black	0.02-0.15

The study evaluated that both in Hangzhou and Ningbo cities, places with higher surface albedo usually have less intense UHI effect (see Fig. 5.33 and Fig. 5.34). It should be noticed that the determination coefficients of R^2 in most linear regression in this study are much lower than 1, it is mainly because there are many uncontrolled factors impact UHII simultaneously in the real filed measurement. Fig. 5.35 also shows that the linear and negative relationship between UHII and surrounding albedo not only occurred in day time situation, but also in night time situation. Although higher reflective ability of surrounding surface with higher albedo does not beneficial when there is no sun light at night, surfaces with higher albedo would absorb less radiation during day time and release less heat during night time. As a result, there is also a great potential of reflective materials to mitigate UHI effect at night.

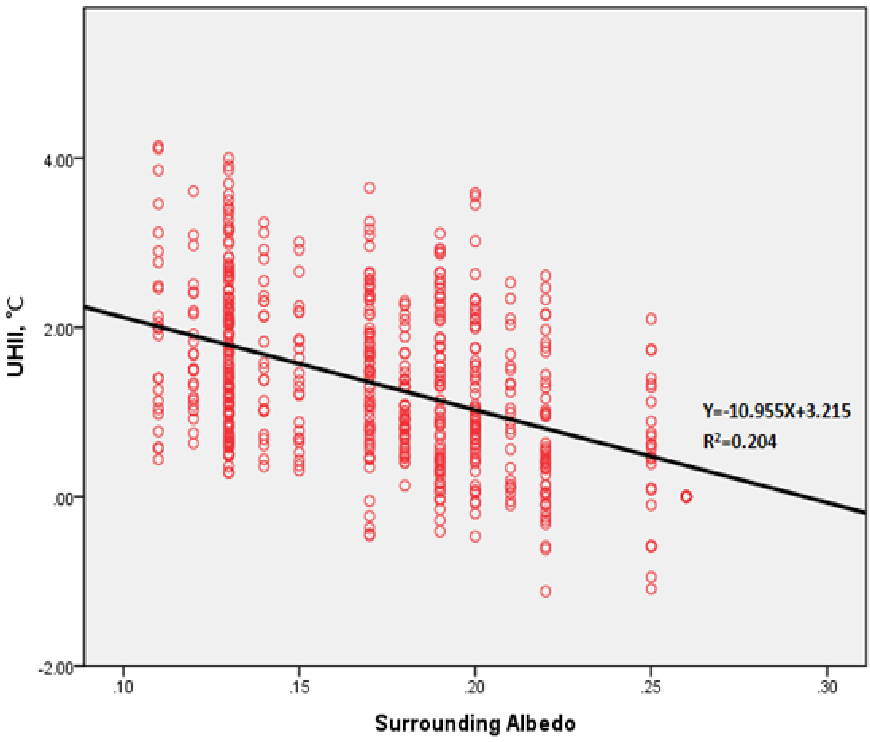

Fig. 5.33: Monthly average UHII against surrounding albedo of Hangzhou sites

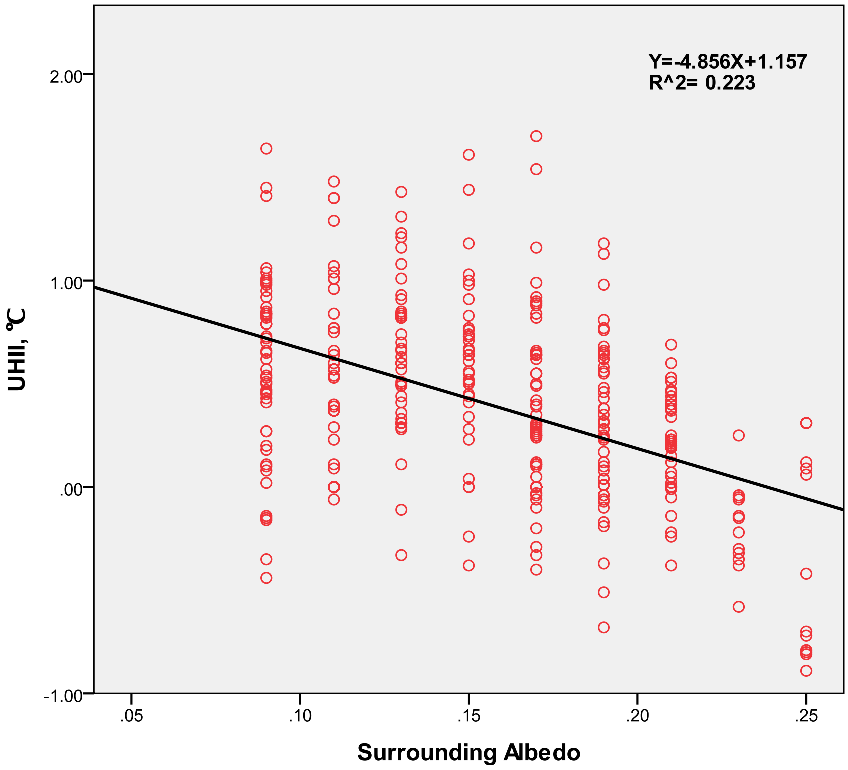

Fig. 5.34: Monthly average UHII against surrounding albedo of Ningbo sites

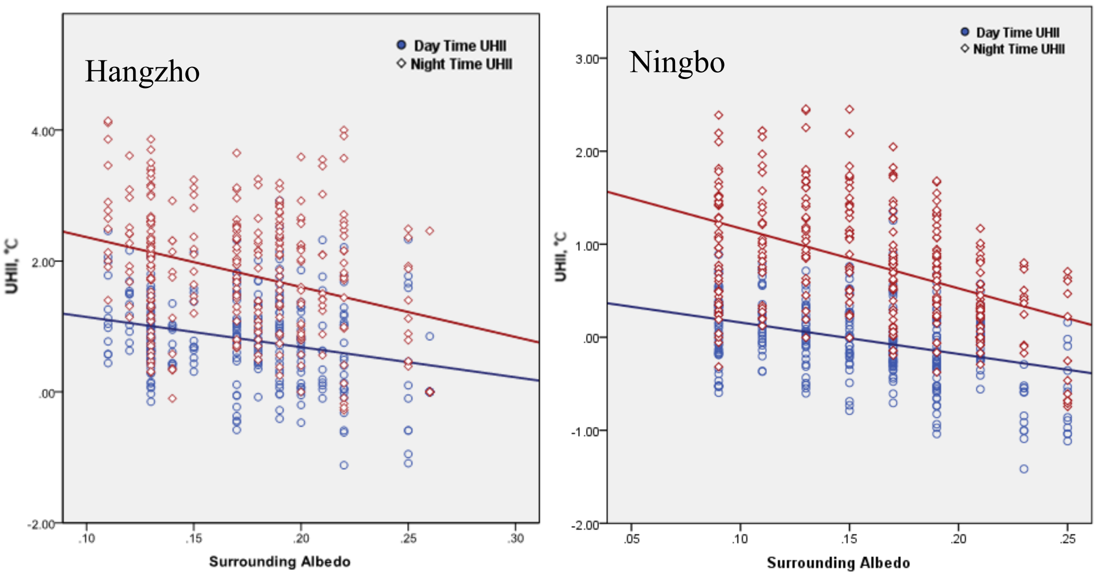

Fig. 5.35: Average day time and night time UHII against surrounding albedo of Hangzhou and Ningbo sites

As a quintessential example, Hangzhou Institute of Technology, Hangzhou Foreign Language School and Zhejiang Business College, as educational land use pattern, are all located at places with similar distance away from Hangzhou city centre (see Fig 5.36). Nevertheless, because the site of Hangzhou Foreign Language School is surrounded by more green plants and white colour surface material, its surrounding albedo is a bit higher than other two educational sites. As Fig. 5.37 demonstrates, it is one of important reasons leads to a less intense UHI effect of Hangzhou Foreign Language School. Accordingly, the measurement result in this study validated that the extensive use of high-albedo materials in cities can be advocated as an effective way to mitigate UHI effect.

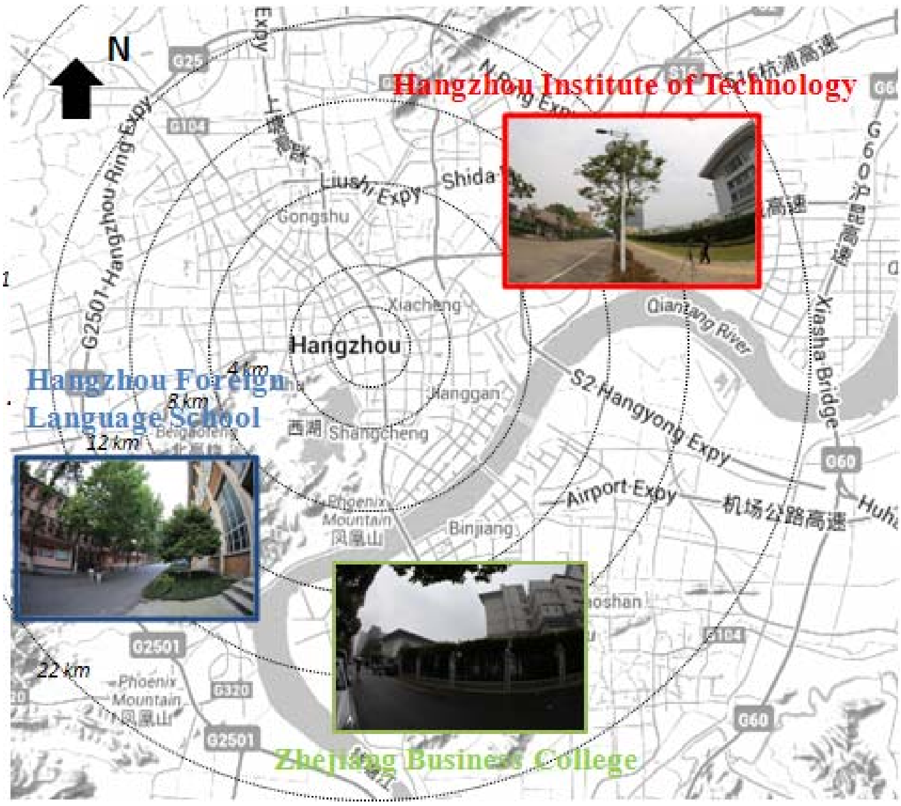

Fig. 5.36: Locations of Hangzhou Institute of Technology, Hangzhou Foreign Language School and Zhejiang Business College in Hangzhou metropolitan area.

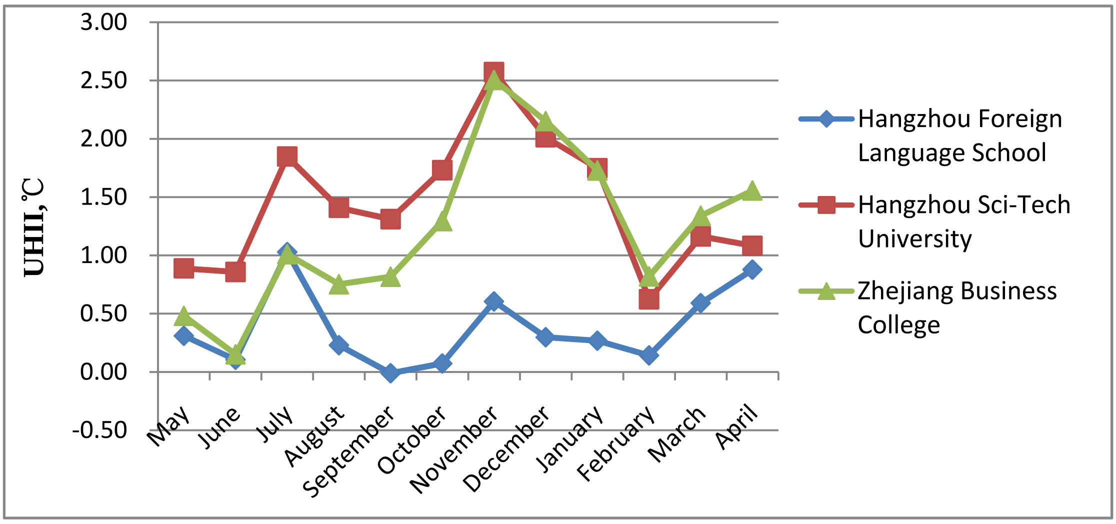

Fig. 5.37: Monthly average UHII values of Hangzhou Institute of Technology, Hangzhou Foreign Language School and Zhejiang Business College from May 2013 to April 2014.

It can be observed from Fig. 5.38 that surrounding albedo plays more critical role in determining the intensity of UHI in sunny days, comparing to cloudy and rainy days. The impact of surface albedo on UHII is most impotent in rainy days. The result infers that when solar radiation is strong, surrounding albedo can have dominant impact on UHI formation.

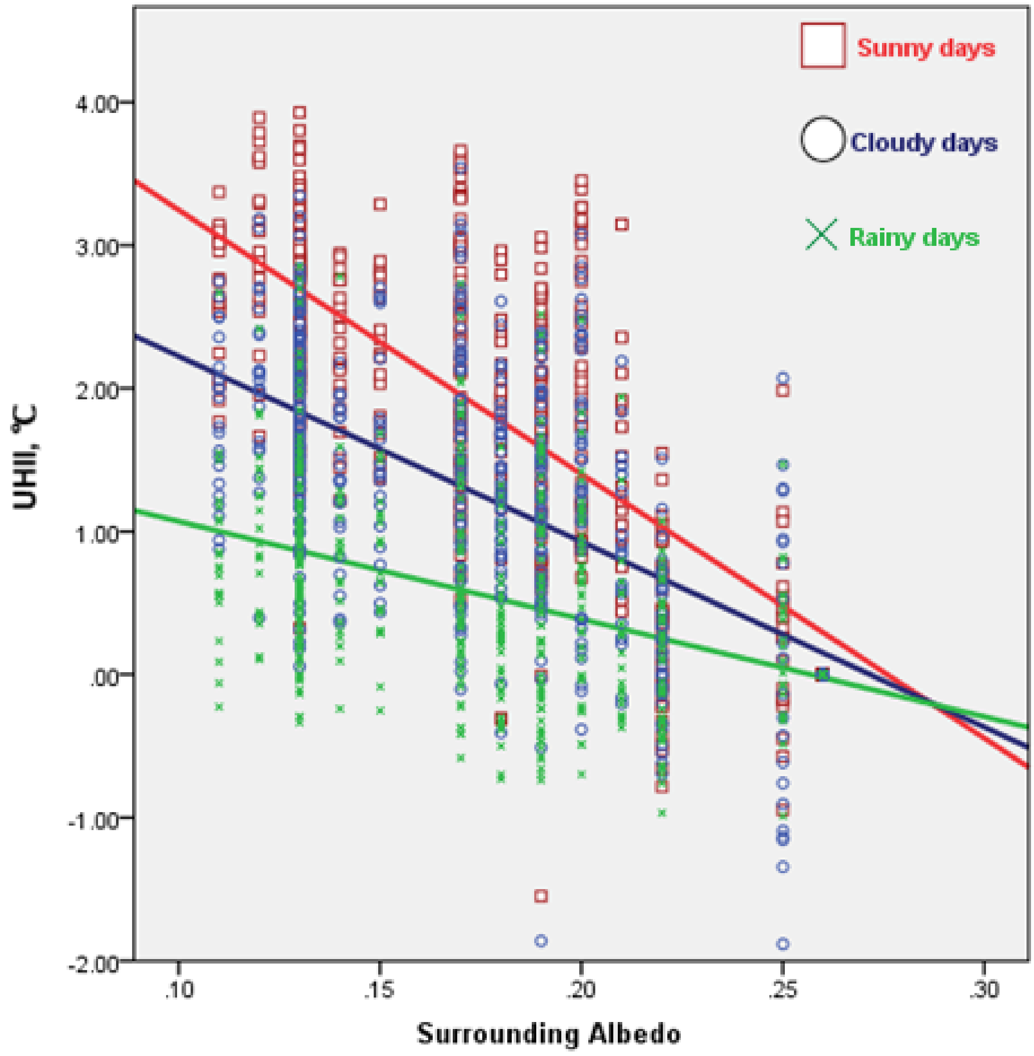

Fig. 5.38: Monthly average UHII values against surrounding albedo of Hangzhou sites in sunny, cloudy and rainy days respectively from July 2013 to September 2013.

5.3.4 Sky view factor (SVF)

Watson and Johnson [13] defined the Sky View Factor (SVF) as the ratio of radiation received by a planar surface from the sky to that received from the entire hemispheric radiating environment (see Fig. 5.39). SVF is determined by size and layout of building structures and it can be widely used to measure the visible sky. A number of previous studies [116, 117] have emphasized that SVF is a useful indicator of the effect of building geometry on radiation exchange in urban environment and UHI phenomenon. In principle, lower SVF would increase the shadow effect in day time. On the other hand, it leads to increasing absorption of solar radiation onto surfaces, decreasing terrestrial radiation loss, decreasing total turbulent heat transport and reducing wind speeds, which all result in increased ambient air temperature directly [118].

Fig. 5.39: Sky view factor image taken by fish-eye camera at Site No. 26 in Ningbo

The methods for estimating SVF in urban environment can be classified into four ways: geometrical calculation using the angles measured to the tops and sides of buildings [119, 120]; manual and computer evaluation of fish-eye photos [121, 122]; Global Positioning System (GPS) method [123]; computer evaluation of a 3D database describing surface geometric elements [124]. This study has taken SVF photos of all experimental sites by a fish-eye camera, and then applies a model named Sky View Factor Calculator which is developed by University of Gothenburg to compute the value of SVF [125]. The model is written in MATLAB computing language and can estimate SVF from fish-eye images based on two methodologies developed by Holmer et al (2001) [126] and Johnson & Watson (1984) [120]. Because the SVF photo was taken under the radiation shield, the lamppost with radiation shield is deleted from the original SVF image by Photoshop program before the calculation process of SVF (see an example in Fig. 5.40).

Site No.26 in Ningbo	Holmer et al (2001)	Johnson & Watson (1984)
SVF values	0.427	0.464

Fig. 5.40: SVF values of Site No. 26 in Ningbo calculated by Sky View Factor Calculator [125]

Although it has been stated by many researchers [117, 119] that urban canyons with reduced SVF would decrease the long wave radiation loss and trapped the heat that contributes to the UHI effect, according to the measurement and observation in this research, the practical impact of SVF on UHI effect is not as simple as that.

As Fig. 5.41 illustrates, there is a strong linear and negative relationship between night time UHII and SVF values of Ningbo sites. This measurement result validated the argument of some previous studies that more intense UHI effect is formed at places with lower SVF values. Nevertheless, the similar negative relationship between UHII and SVF of Ningbo measurement sites does not appear in the situation of day time (see Fig. 5.42). The measurement infers that there is little or nothing impact of SVF on the day time UHI effect change in the case of Ningbo.

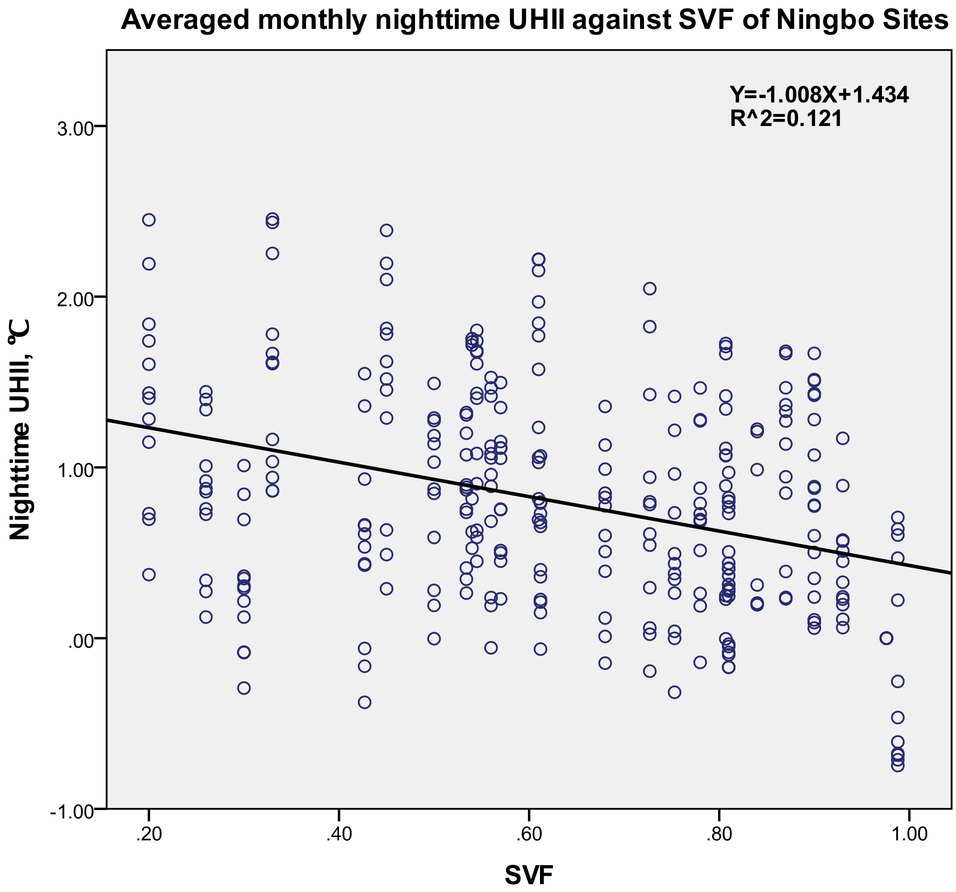

Fig. 5.41: Monthly average night time UHII against SVF of Ningbo sites

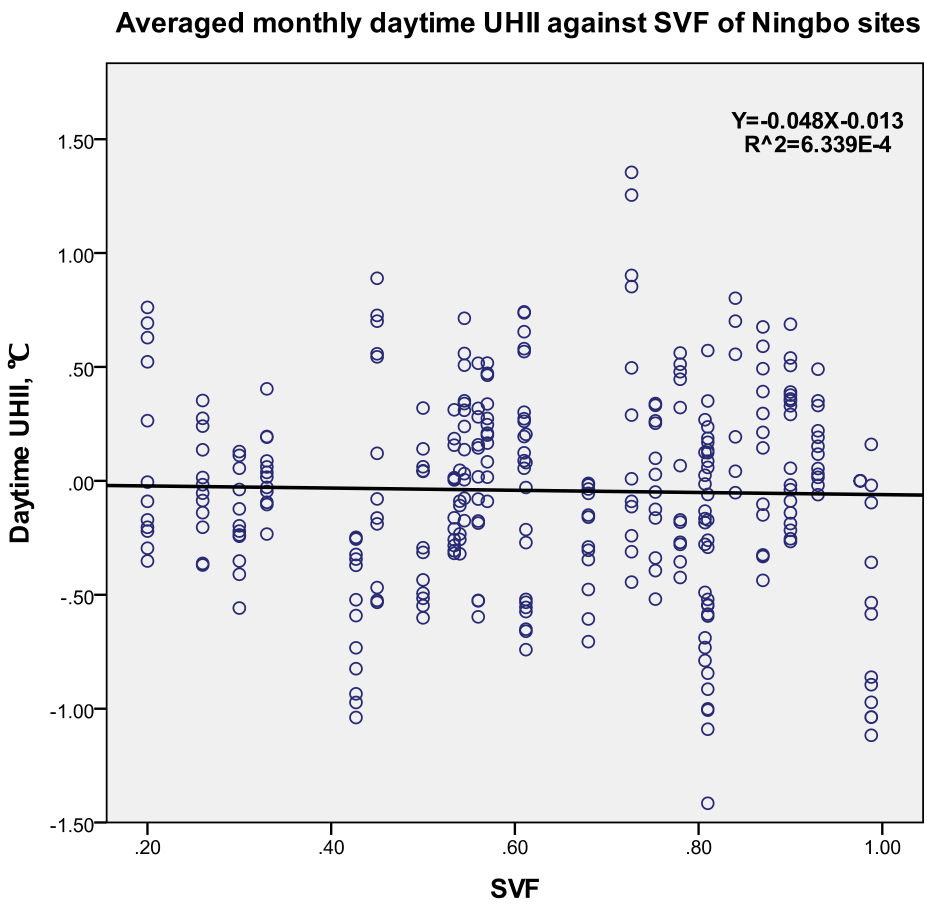

Fig. 5.42: Monthly average day time UHII against SVF of Ningbo sites

In the case of Hangzhou, the linear and negative relationship between night time UHII and SVF is not as outstanding as that in the case of Ningbo. As Fig. 5.43 manifests, reducing SVF of sites only increases their night time UHII slightly. Besides, the correlation between UHII and SVF of Hangzhou sites changes from negative to positive in day time (see Fig. 5.44). It implies that the spaces of high-rise buildings sometimes may have lower temperature than open space.

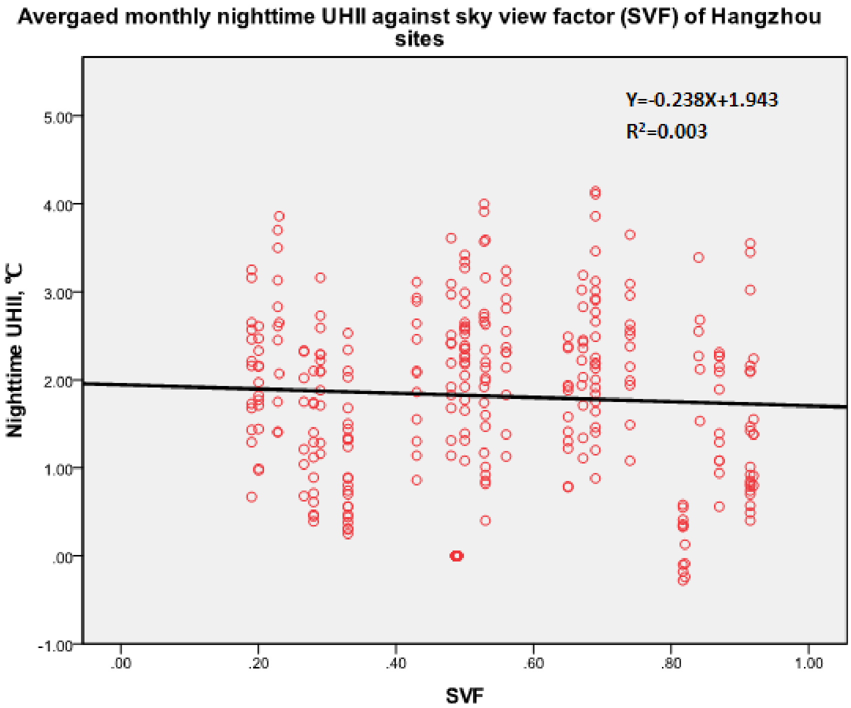

Fig. 5.43: Monthly average night time UHII against SVF of Hangzhou sites

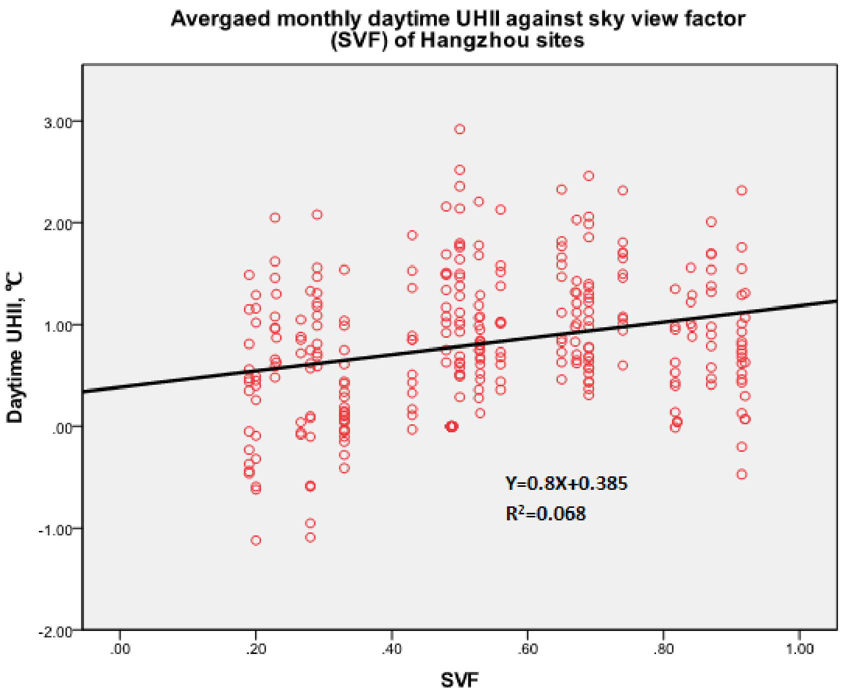

Fig. 5.44: Monthly average day time UHII against SVF of Hangzhou sites

Bearing the above measurement results in mind, the conclusion inferred from this study does not comply with arguments of previous researchers overwhelmingly. It can be determined from this research that the reduction in SVF would lead to an increase in UHI effect at night time, which is expected to happen. The reason behind this is that areas of dense and high-rise buildings can absorb and trap much more heat in concretes during day time, and afterwards release more heat to improve ambient air temperature correspondingly at night time. Unlike the situation at night time, the direct solar radiation is the main source of heat during day time. Most direct solar radiation would be blocked by surrounding high buildings in dense infrastructure area. Accordingly, the sites in the shadow area may have relatively lower air temperature than other open space where it is completely exposed to direct solar radiation.

Sun path diagrams can conveniently represent annual changes in the path of the sun through the sky within a single 2D diagram. The photos taken by fish eye lens combined with sun path diagram can be applied to determine the times of the day and year in which the sun will be available on a particular site. Alternatively, it can be used to check solar access by casting shadows onto a site plan [127]. For instance, the site of Fumao Mansion in Ningbo is surrounded by high-rise buildings and its SVF value is only 0.33, as Fig. 5.45 shows. According to the 3D simulation model made by Ecotect (Fig. 5.46), the measurement site at Ningbo Fumao Mansion is virtually impossible exposed to direct solar radiation for a long period. As Fig. 5.47 demonstrates, the time when the measurement site at Fumao Mansion is covered by the shadow occupies about

60% of a whole year. Nevertheless, for some other sites like Sun Lake Park, it is nearly exposed to solar radiation whole year (see Fig. 5.48).

Fig. 5.45: SVF photo of Fumao Mansion taken by fish eye lens

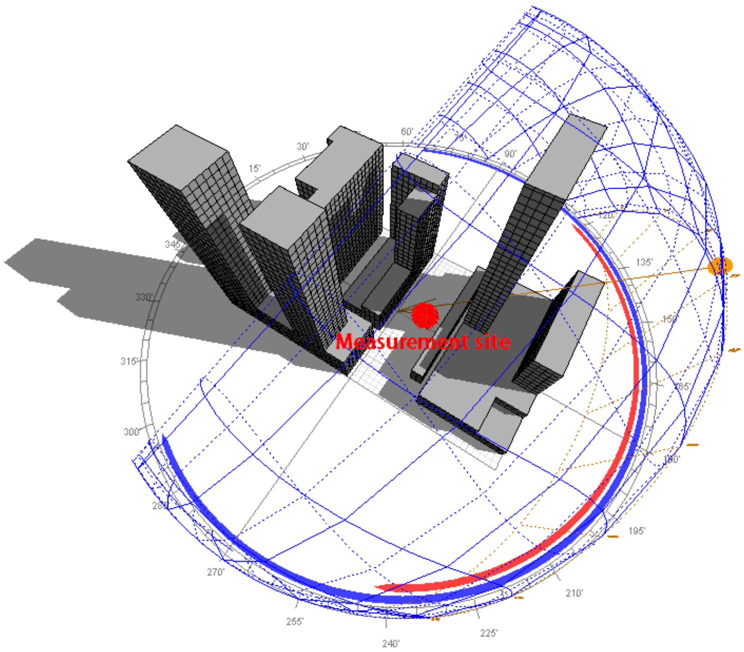

Fig. 5.46: 3D representation of sun path diagram at the measurement site of Ningbo Fumao Mansion at 10:45 am, January 1st.

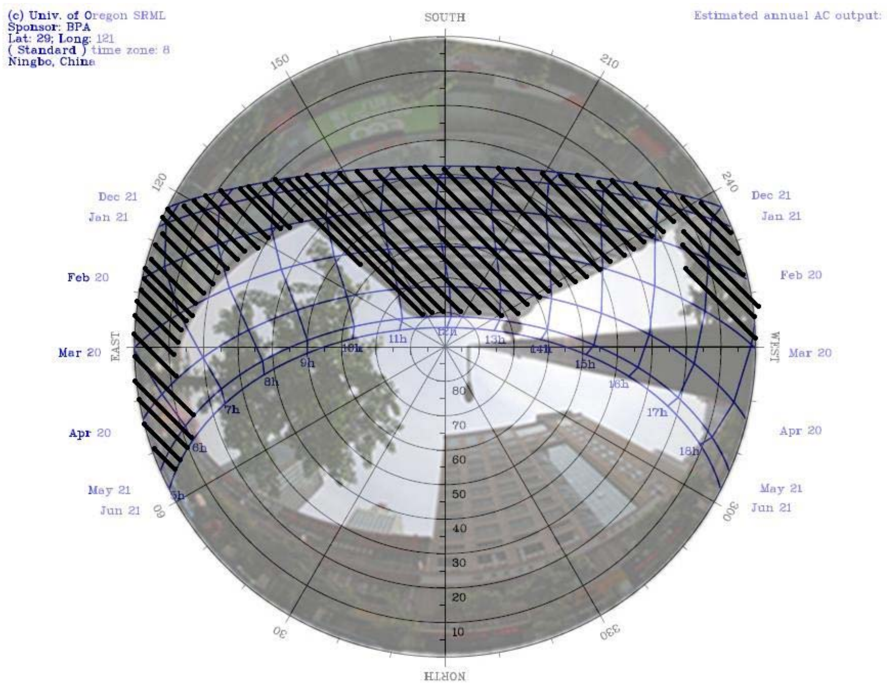

Fig. 5.47: 2D representation of sun path diagram at the measurement site of Ningbo Fumao Mansion [127].

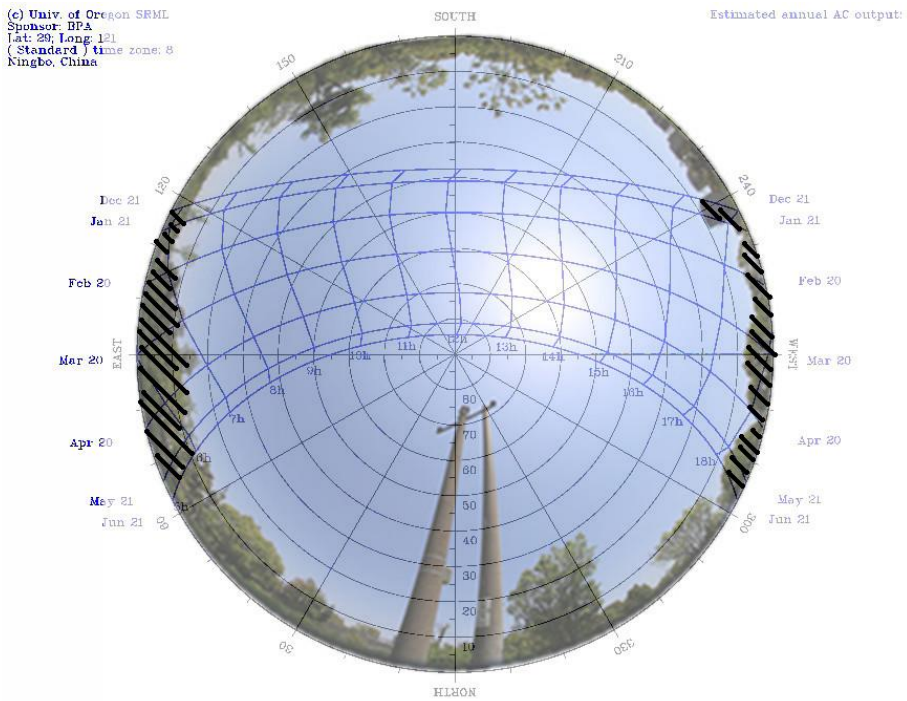

Fig. 5.48: 2D representation of sun path diagram at the measurement site of Ningbo Sun Lake Park [127].

Comparing the hourly temperature between Ningbo Fumao Mansion and Ningbo Sun Lake Park, there is a great disparity between day time temperature difference and night time temperature difference. As mentioned before, the night time air temperature at Ningbo Fumao Mansion where the SVF is lower is extremely higher than Ningbo Sun Lake Park where the SVF is higher. In contrast, the day time air temperature at Ningbo Fumao Mansion is sometimes lower than Sun Lake Park, especially in the period from 10:00 to 14:00 when the solar radiation is strongest (see Fig. 5.49). In addition, the day time air temperature of Fumao Mansion is greatest lower than Sun Lake Park in cloudless and sunny days. When the solar radiation is weak in cloudy or rainy days, there is a marked reduce in the day time air temperature difference between Fumao Mansion and Sun Lake Park.

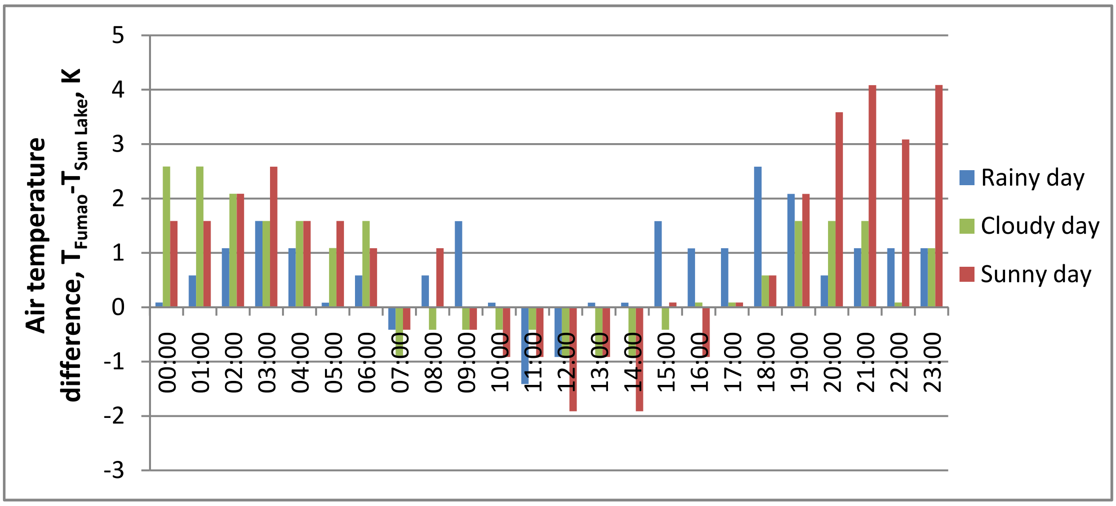

Fig. 5.49: Hourly air temperature difference (**T_{Fumao} - $T_{Sun\ Lake}$**) between Ningbo Fumao Mansion and Sun Lake Park in rainy, cloudy and sunny days.

5.3.5 Other meteorological parameters

5.3.5.1 The seasonal variation

The hypothesis demonstrated by Howard [9] in 1833 that the phenomenon of UHI is greatest in cold months. However, there are some cities experiencing more intense UHI effect in summer, rather than winter. As an example, Giannaros and Melas discovered higher UHI intensity during the night and during the warm period of the year at Thessaloniki city, Greece [128]. Maximum values of UHII were also observed in summer days in other non European cities with tropical and subtropical climates, such as Shanghai, China [129], Muscat, Oman [130] and as well as in some large cities of Korea [131]. It seems that UHI effect varies prodigiously according to existing researches in terms of the maximum intensity occurrence. In theory, the maximum UHII appears in winter or summer is mainly determined by the thermal balance of the city which relates to sensible and latent heat storage and release, strength of solar radiation, surface albedo, anthropogenic heat generation, urban geography and heat convection. Obviously, in addition to the aforementioned reasons related to climatic feature and thermal balance of cities, usage of different measurement methods, monitoring tools and selection of reference site would also largely effect the calculation of UHII.

According to the data measurement in Hangzhou, the peak monthly UHII values of most sites occurred in cold months from November to January. During summer days, for instance, July when the mean air temperature is highest, its UHI effect is also pronounced but still a bit lower than in winter (see Fig. 5.50). It can be clearly observed from Fig. 5.51 that when the air temperature cools down since October, there is a critical increase in UHII at Hangzhou city centre. When the mean air temperature reaches in 35°C in July, the UHII at Hangzhou city centre is about 1 - 2°C lower than the value measured in winter when the air temperature is 0°C.

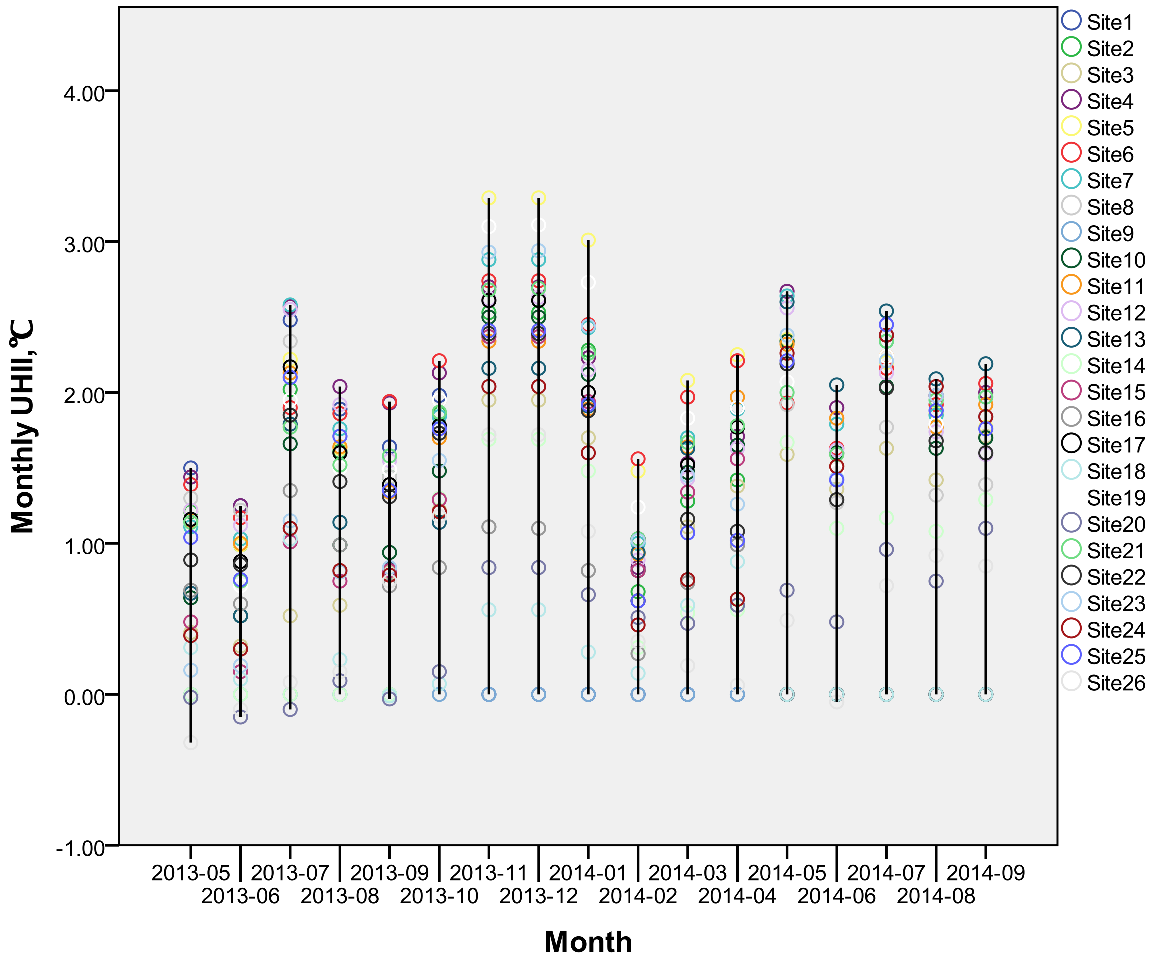

Fig. 5.50: Monthly average UHII of all sites in Hangzhou from May, 2013 to September, 2014

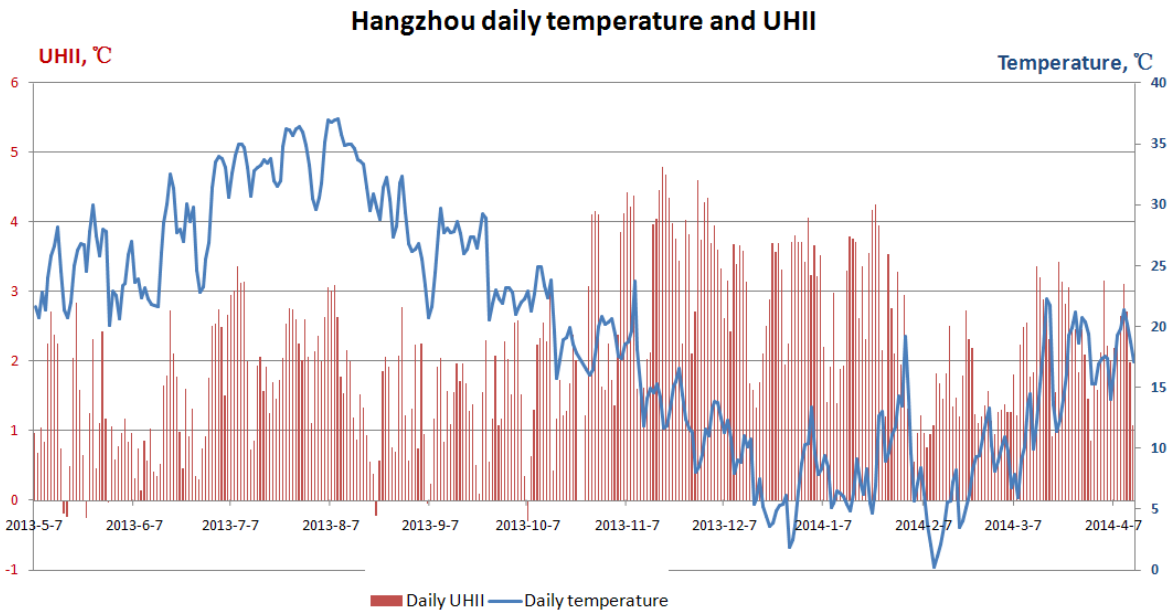

Fig. 5.51: Daily UHII of Hangzhou city centre varies with daily air temperature from May, 2013 to July, 2014.

Comparing to the UHI situation in Hangzhou, the peak UHII of sites in Ningbo seem to appear in cold months from November to January as well (see Fig. 5.52). Similarly, if the city centre site of Ningbo is selected to investigate, the variety of daily UHII with seasonal change is same as the situation of Hangzhou city centre site (see Fig. 5.53). Once the weather in Ningbo became cold in winter, the UHI effect at Ningbo city centre was being more intense. The gap of air temperature between winter and summer in Ningbo can be more than 40°C. The mean UHII of Ningbo city centre at winter days is approximate 0.5°C – 1°C higher than at summer days. Consequently, the measurement results proved that the daily UHI effect at all sites of Hangzhou and Ningbo exhibited seasonal variability, with higher values corresponding to winter months and lower values in summer.

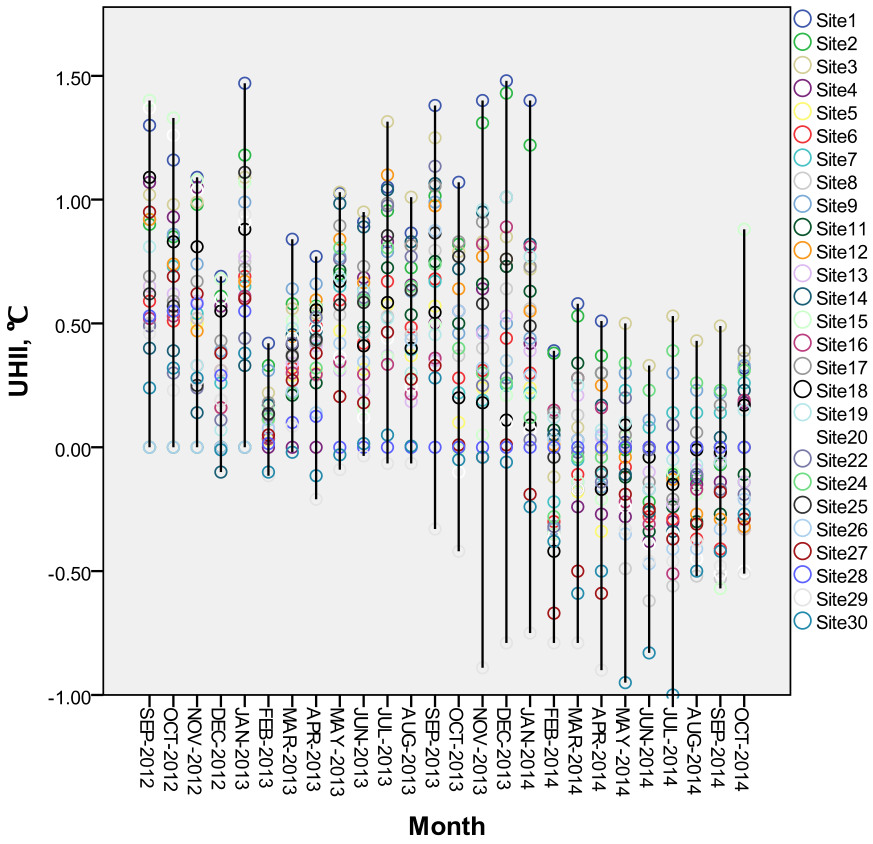

Fig. 5.52: Monthly average UHII of all sites in Ningbo from April, 2013 to March, 2014

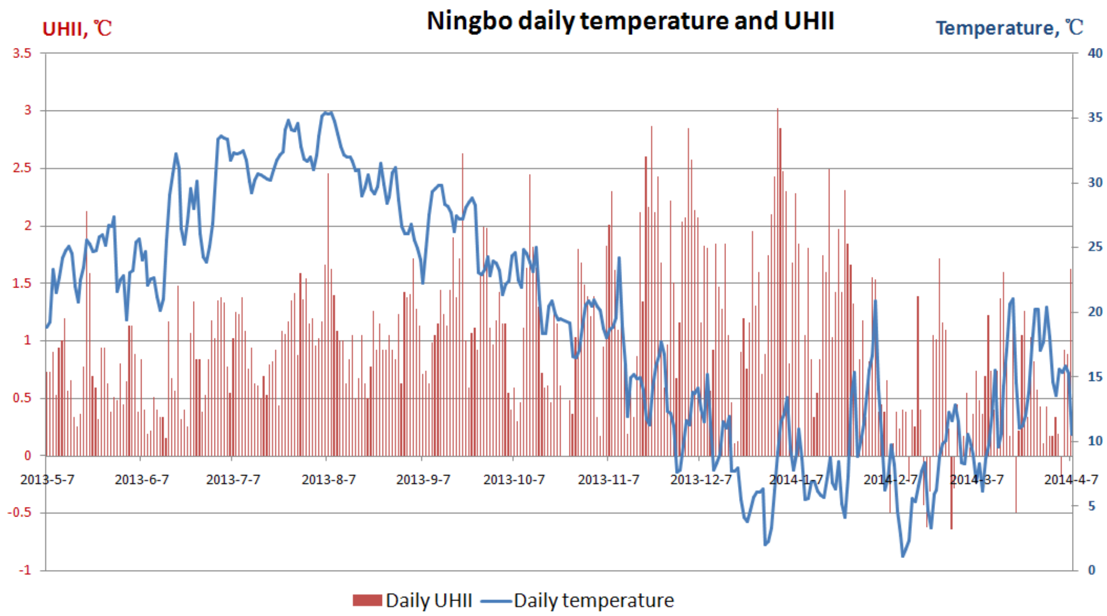

Fig. 5.53: Daily UHII of Ningbo city centre varies with daily air temperature from May, 2013 to July, 2014.

There are two main reasons for causing this seasonal variation of UHI effect in Hangzhou and Ningbo cities. The first and foremost point is the serious air pollution and high concentration of Particulate Matter (PM) in winter days in China. As Fig. 5.54 indicates, China suffered heavily from the most serious atmospheric pollution of particulate matter in China from the end of 2013 to the beginning of 2014, which has received intense international attention. Fig. 5.55 and Fig. 5.56 display the distributions of PM2.5 in China in August, 2014 and January, 2015 respectively. Based on the comparison of PM2.5 distribution in China between summer and winter months, it is clear that the concentration of PM2.5 is extremely higher and also the distribution of PM2.5 is extremely broader in January. Additionally, as Tab. 5.2 lists, there is a seasonal trend in Air Quality Index (AQI) and the concentrations of polluted matters, involving PM2.5, PM10, SO_2, CO, NO_2 and O_3. As Fig. 5.57 demonstrates, the peak concentrations of PM2.5 and PM10 both appear in winter months. The atmospheric pollution of particulate matters will aggravate UHI effect, because the high concentration of particulate matters will weaken the thermal circulation and intensify thermal accumulation in the city.

Fig. 5.54: The atmospheric pollution of particulate matter in Hangzhou, China in winter 2013.

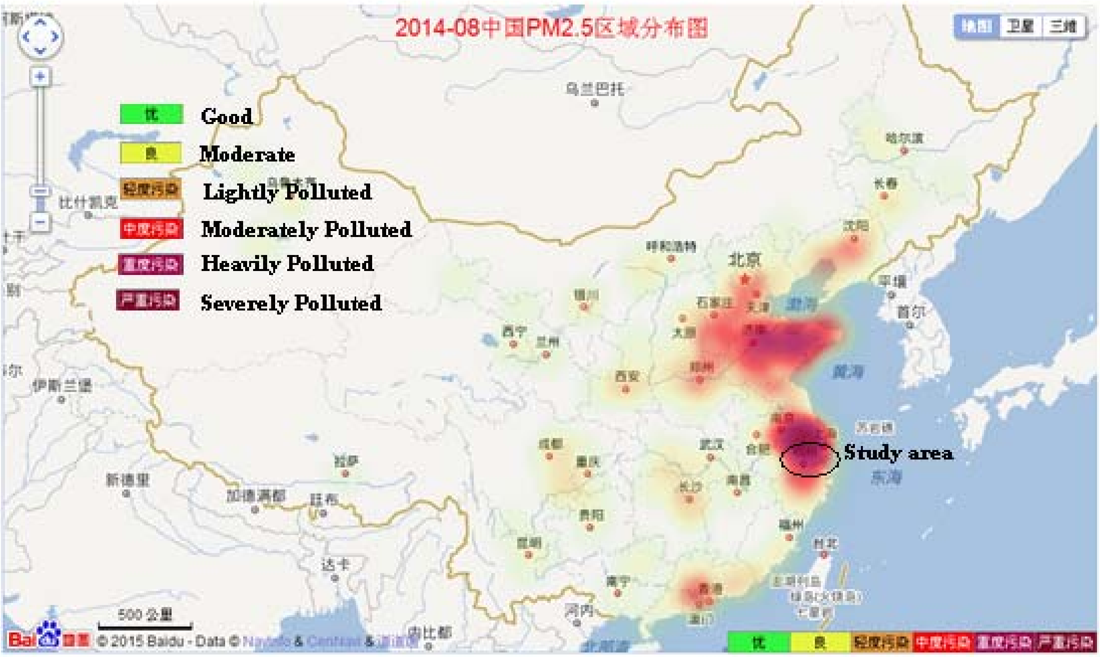

Fig. 5.55: Distribution of PM2.5 in China in August, 2014 [132]

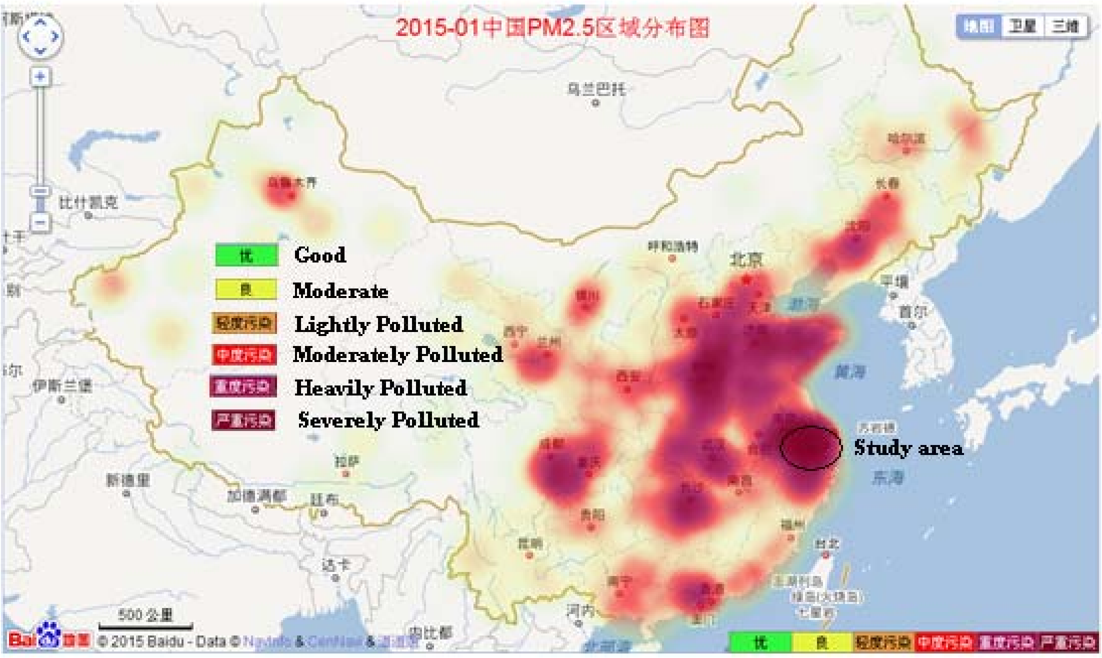

Fig. 5.56: Distribution of PM2.5 in China in January, 2015 [132]

Tab. 5.2: Mean monthly Air Quality Index (AQI) and concentrations of air pollution over Hangzhou city from December, 2013 to April, 2015 (unit of CO: mg/m^3; unit of others: μg/m^3) [132]

Month	AQI	PM2.5	PM10	SO_2	CO	NO_2	O_3
Dec-2013	174	140.3	189.9	44.7	1.616	79.1	23.2
Jan-2014	137	104.3	142.5	33.2	1.16	61.2	27.9
Feb-2014	83	60.7	71.3	19	0.884	40.1	35.5
Mar-2014	84	59.7	95.3	22.6	0.82	49.8	47.3
Apr-2014	85	60.1	95.7	21.7	0.775	51.2	52.6
May-2014	89	58.6	113.2	19.4	0.825	46.5	71.6
Jun-2014	80	53.1	87.4	12.5	0.802	40.2	71.8
Jul-2014	71	44	72.7	9.8	0.774	33.6	67.6
Aug-2014	68	45.5	69.9	12.3	0.906	35.3	67.4
Sep-2014	68	45.3	69.3	14.6	0.816	34.5	66.3
Oct-2014	86	58.8	98.4	20.9	0.853	46.9	73.3
Nov-2014	103	75.3	107.4	22	1.058	59.3	37.5
Dec-2014	103	72.7	116.8	31.3	1.011	61	28.9
Jan-2015	119	88.4	119.1	24.3	1.222	61.2	29.1
Feb-2015	90	65.3	87.4	13.5	0.952	39.2	48.6
Mar-2015	78	53.6	81.2	15	0.843	48	48.2
Apr-2015	79	53.2	88.7	16.7	0.855	48.9	67.5

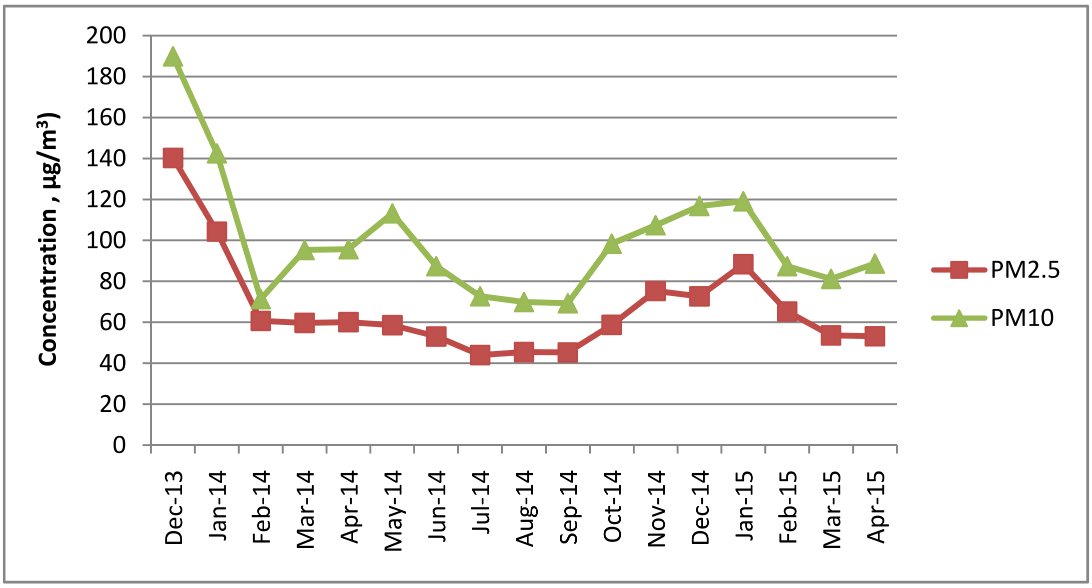

Fig. 5.57: Monthly average concentrations of PM2.5 and PM10 for the period from December, 2013 to April, 2015.

There is one more reason referring to wind speed should be touched on. It has been generally agreed that wind speed can significantly influence the formation of the UHI effect. Mean annual wind speeds at city centres are often 20-30% lower than in surrounding rural areas, which is one of most paramount reasons forming UHI effect in city [80]. Based on the Test Meteorological Year (TMY) weather dataset of Hangzhou, wind rose graphs show the distributions of wind direction and speed in summer and winter respectively (see Fig. 5.58 and Fig. 5.59). The wind rose graphs indicate that the wind speed over Hangzhou is relatively high in summer.

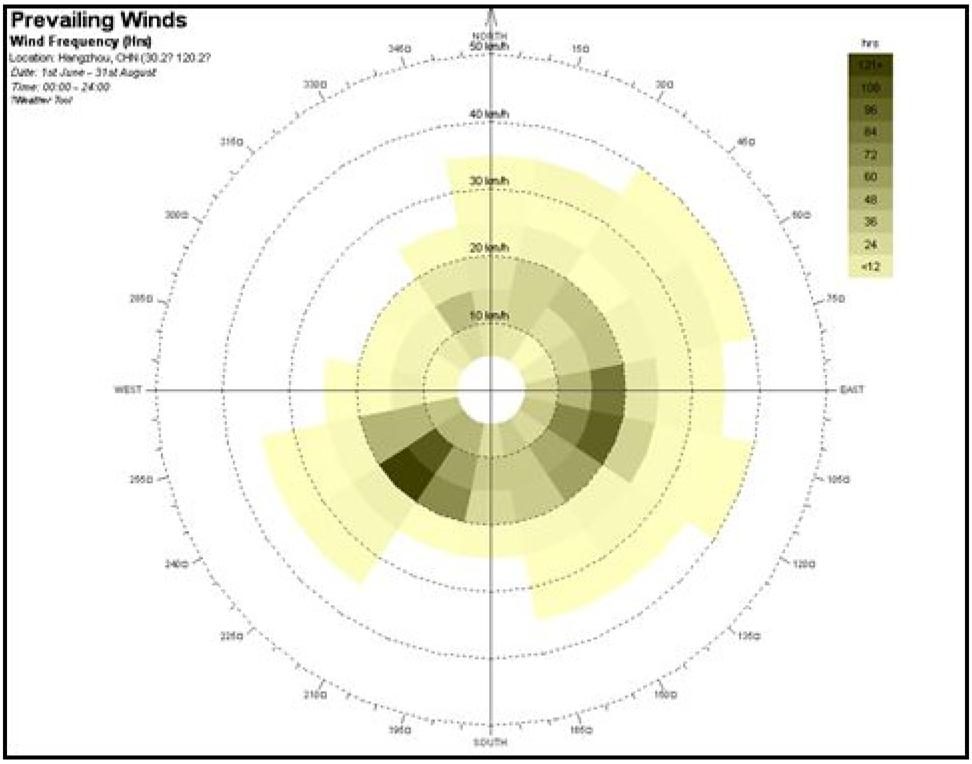

Fig. 5.58: Wind rose graph of wind direction and speed distributions over Hangzhou in summer

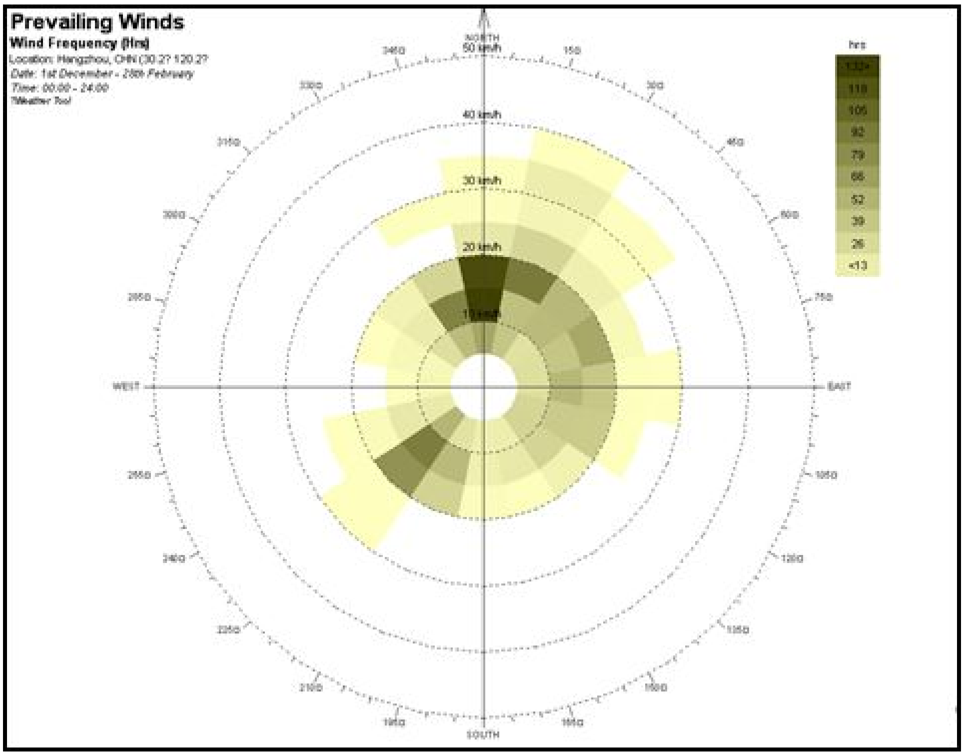

Fig. 5.59: Wind rose graph of wind direction and speed distributions over Hangzhou in winter

December 9th, 2012 and December 10th, 2012 are both cloudless sunny days and have similar air temperature range in Ningbo. Nevertheless, the wind speed in December 9th is greatly larger than December 10th (see Fig. 5.60) [104]. Meanwhile, Fig. 5.61 indicates that the average daily UHII of all measurement sites on December 9th is about 40% lower than the UHII values on December 10th. The result validates that calm wind can foster the formation of UHI, because calm wind decreases atmospheric mixing and thermal convection. Consequently, since it has determined that the wind speed is lower in winter days, it is reasonable that UHI effect in winter is more intense than in summer.

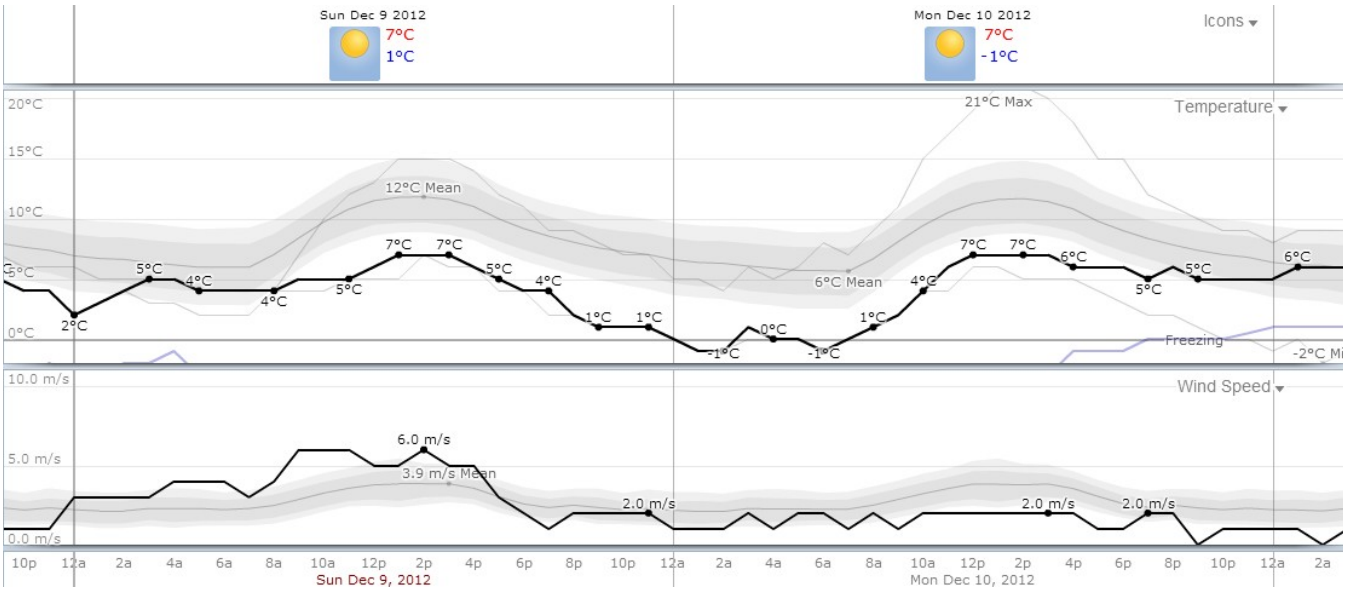

Fig. 5.60: Comparison of weather conditions between on December 9th, 2012 and December 10th, 2012 in Ningbo [104, 133]

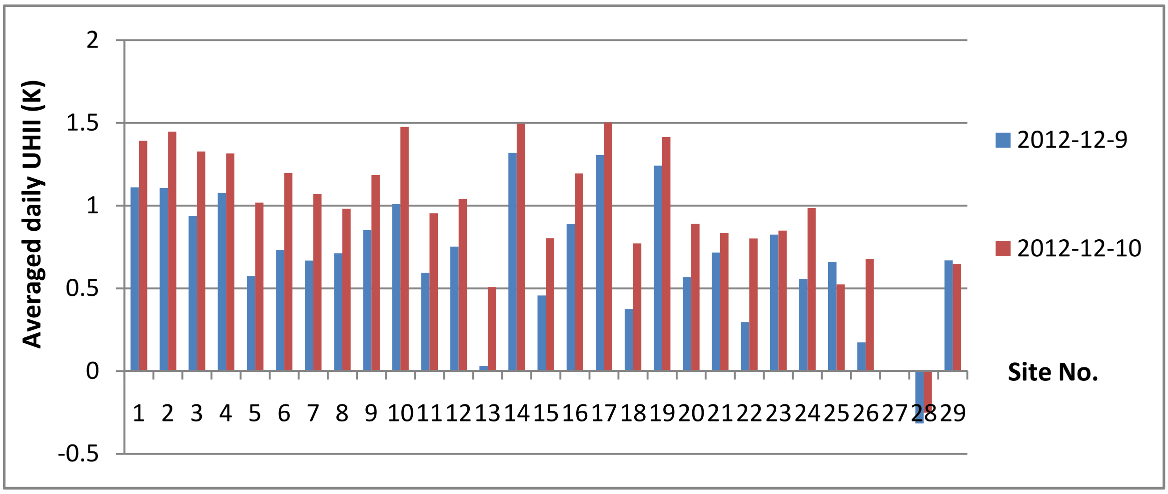

Fig. 5.61: Comparison of average daily UHII of all sites in Ningbo measured on December 9th, 2012 and December 10th, 2012

5.3.5.2 The diurnal variation

The study has determined there is a diurnal variation of UHI effect in day time (6:00 –

17:00) and night time (18:00 – 5:00). Fig. 5.62 displays the temporal variation and trend of hourly UHI effect at all Ningbo measurement sites in July. It is clear that there is a sudden reduce in UHII of all Ningbo sites when the run rises at about 5:00 a.m. and an increase when the sun sets at about 18:00 p.m. in July. As Fig. 5.63 and Fig. 5.64 show, there is a negative correlation between hourly air temperature and hourly UHII the specific sites of Hangzhou and Ningbo city centre. When the air temperature cools down after the sun set, the UHI effect at these two sites are aggravated.

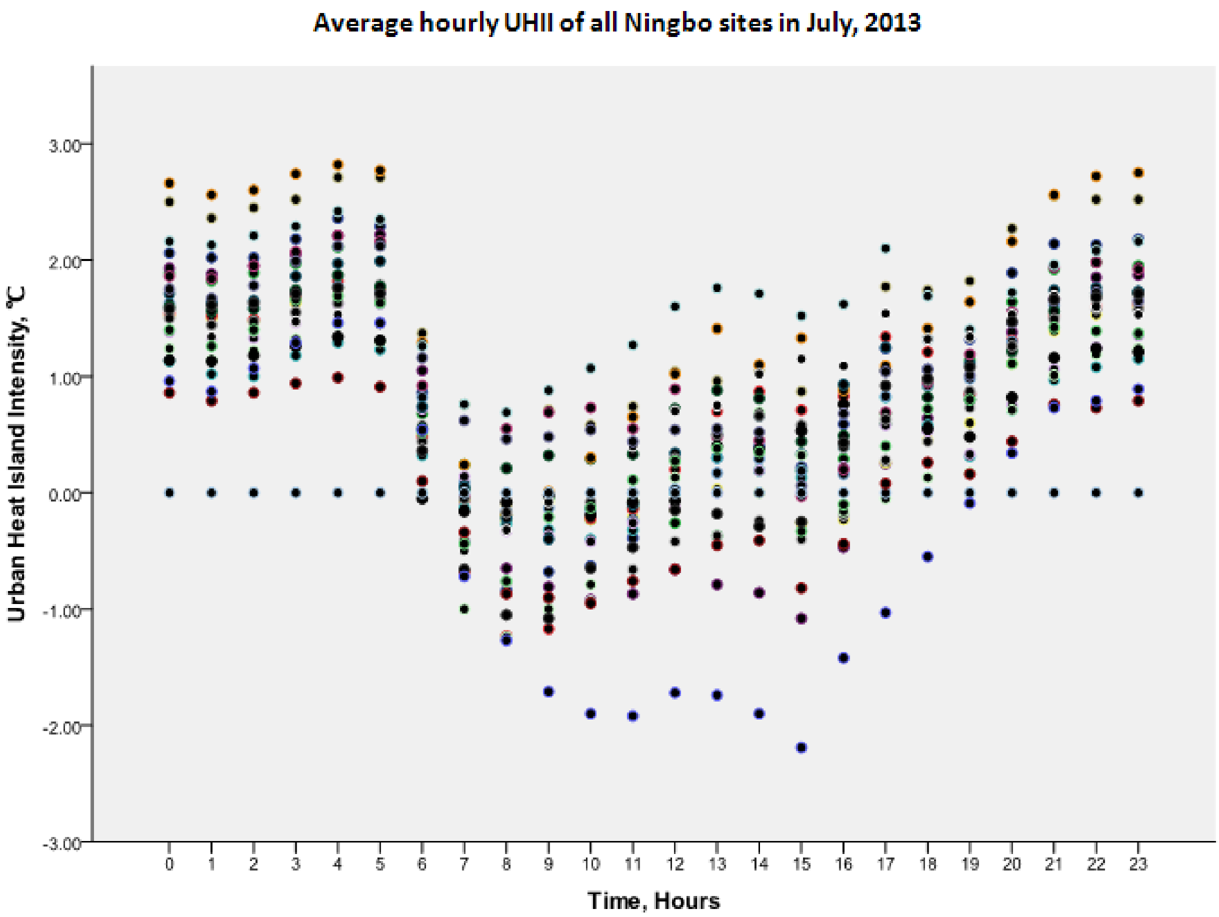

Fig. 5.62: Hourly variation in UHII at all measurement sites of Ningbo in July

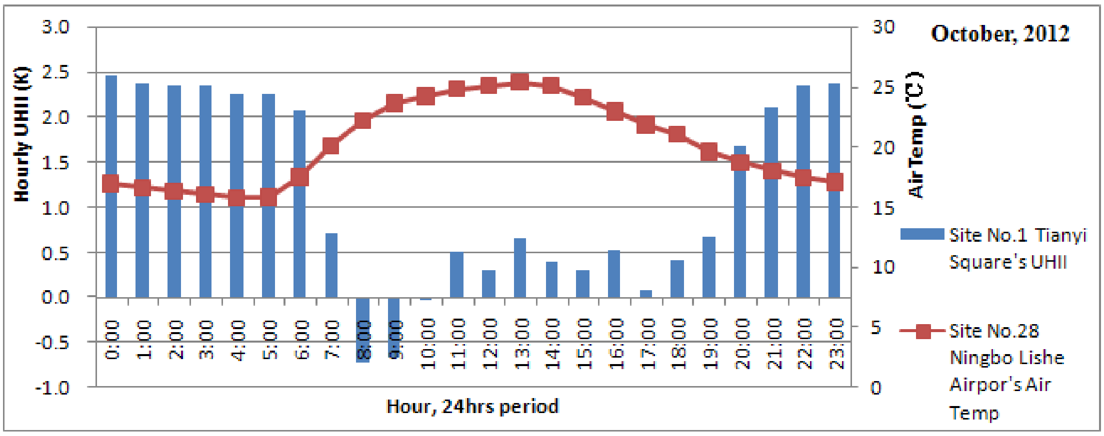

Fig. 5.63: Hourly UHII changes with air temperature at Ningbo city centre in October, 2012

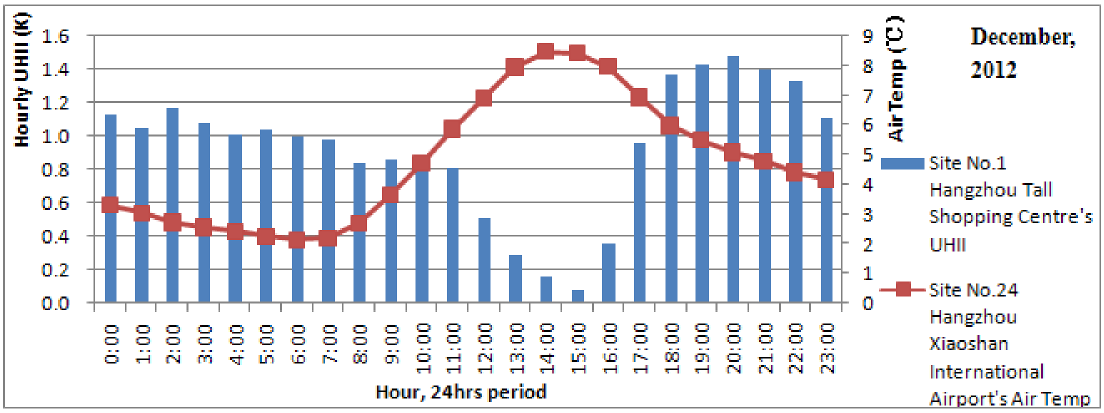

Fig. 5.64: Hourly UHII changes with air temperature at Hangzhou city centre in December, 2012

Fig. 5.65 and Fig. 5.66 exhibit the comparisons of monthly day time and night time UHII at city centres of Hangzhou and Ningbo respectively. In the view of comparison, the night time UHII measured at both cities of Hangzhou and Ningbo are exceedingly more intense than their day time UHII in every month. Additionally, it can be observed from Fig. 5.67 that there is a large percentage of night time UHII over

Hangzhou around the value of 2.5°C in both summer and winter days, in contrast, most day time UHII in summer and winter days close to 0°C.

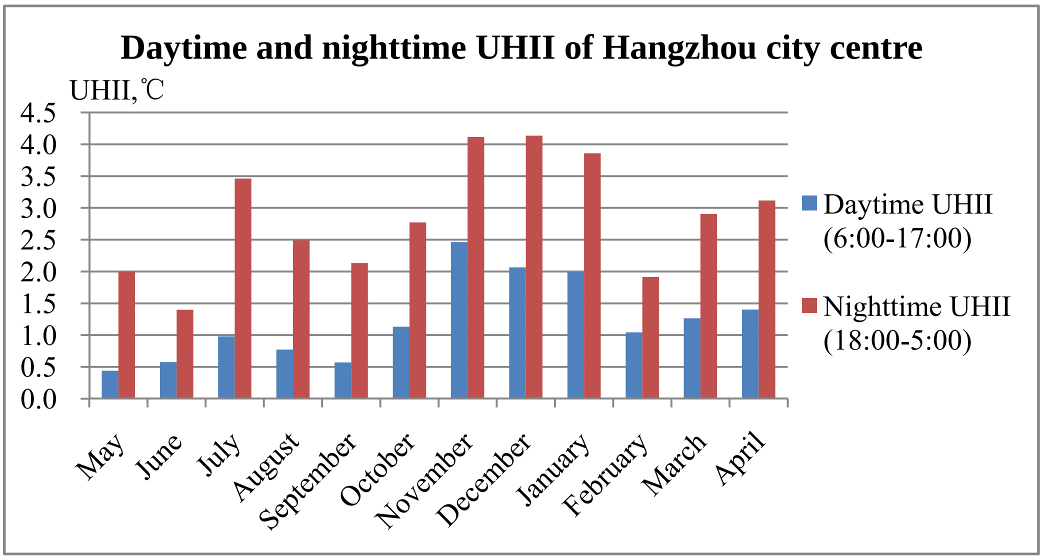

Fig. 5.65: Comparison of monthly day time and night time UHII at Hangzhou city centre

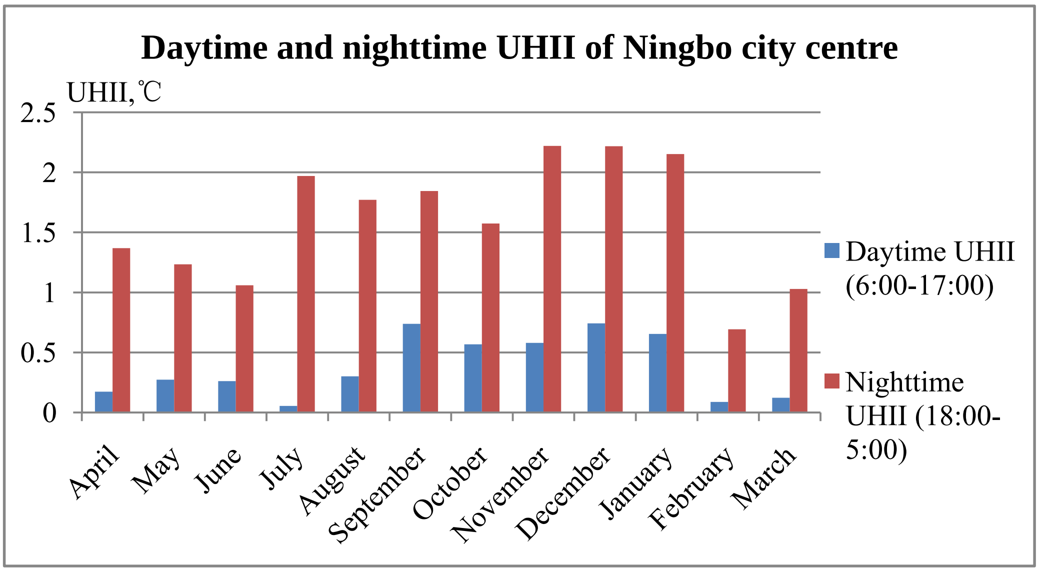

Fig. 5.66: Comparison of monthly day time and night time UHII at Ningbo city centre

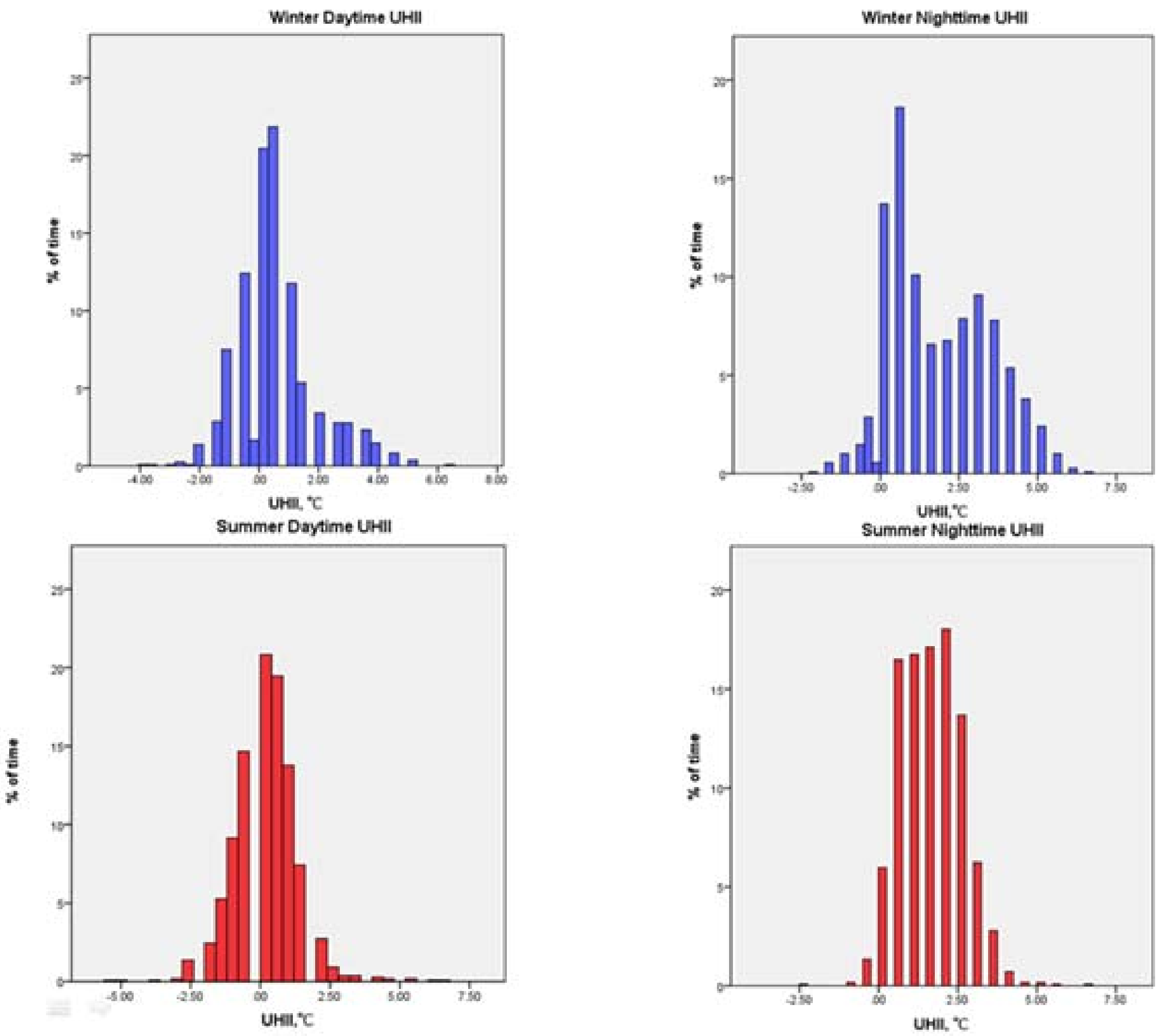

Fig. 5.67: Distribution of UHII values in winter day time, winter night time, summer day time and summer night time.

The main causes of UHI formation are defined as the decreased long-wave radiation loss and the increased release of heat stored in urban materials [134]. UHI effect is formed because high heat capacities of urban surfaces result to high heat storage at day time and high heat release at night time. During night time, the radiative deficit at urban place can be largely compensated by the great release of heat stored in urban surface materials. Besides, winds at night tend to be lighter than during the day due to decreased solar heating and less atmospheric mixing. These are why the maximum UHII most likely appears during night time rather than day time.

5.3.5.3 Relative humidity

The other key thermo-hygrometric variable, hourly relative humidity (RH) was monitored at all measurement sites of Hangzhou and Ningbo by sensors simultaneously with air temperature. As Fig. 5.68 and Fig. 5.69 illustrate, Hangzhou and Ningbo both have humid climate around the year with the average relative humidity higher than 70%. According to the measurement result, there is no distinct variation of relative humidity in these two cities over the year. Relatively speaking, summer days have a bit lower humidity values and winter days have higher relative humidity values.

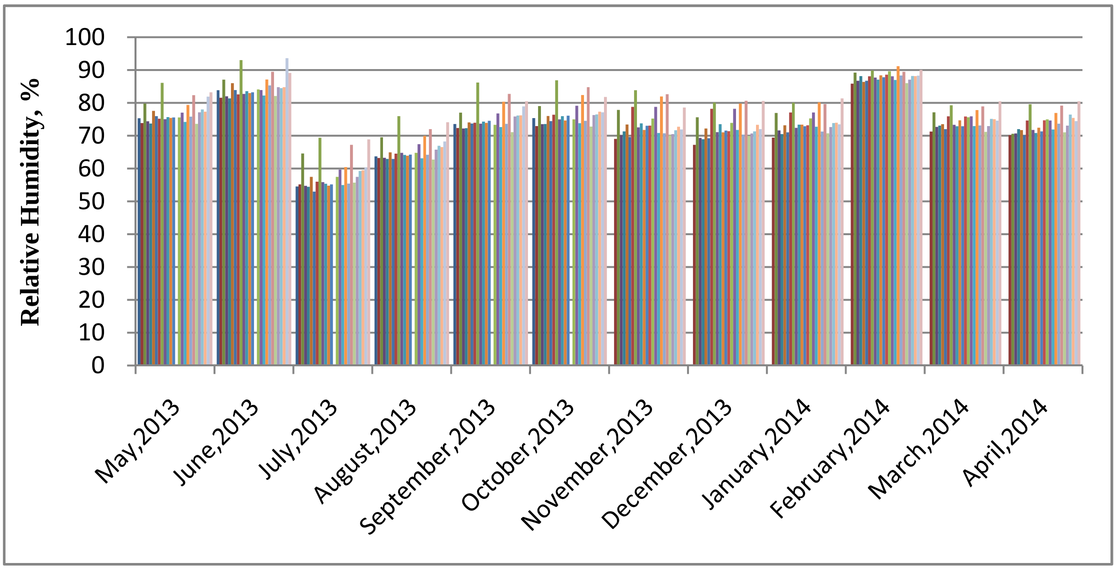

Fig. 5.68: Monthly relative humidity values of all measurement sites in Hangzhou from May, 2013 to April, 2014

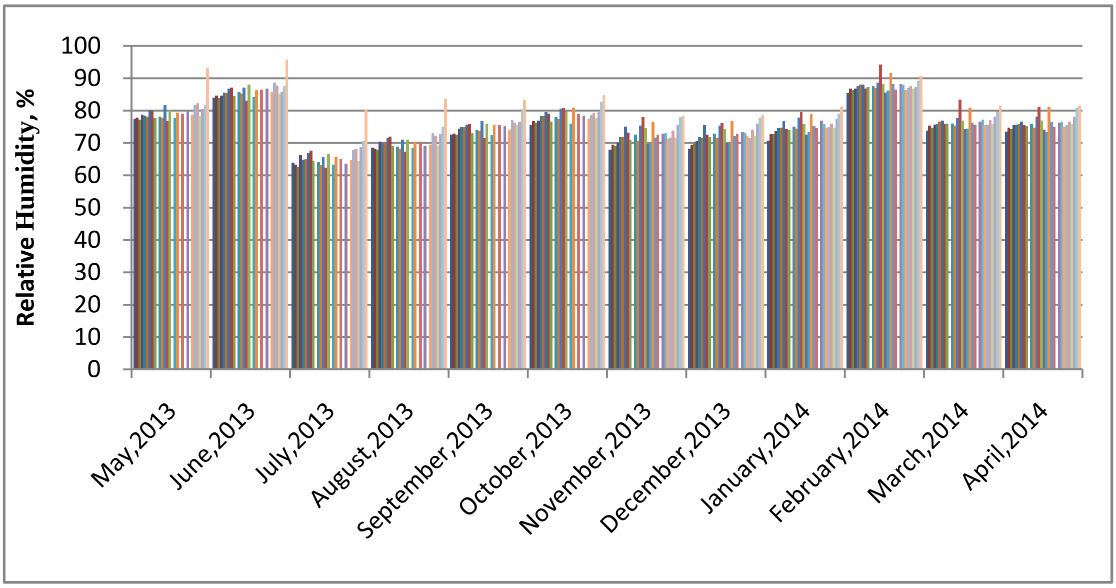

Fig. 5.69: Monthly relative humidity values of all measurement sites in Ningbo from May, 2013 to April, 2014

In contrast, the difference in relative humidity between urban and rural places is distinct. The higher relative humidity is always caused by higher evapotranspiration effect in green zones. As Fig. 5.70 shows, the relative humidity of Hangzhou city centre is about 10% to 20% lower than the reference site of Hangzhou Yuhuang Mountain. Thus, the higher air temperature and lower relative humidity are recorded at the city centre compared to that observed at rural places.

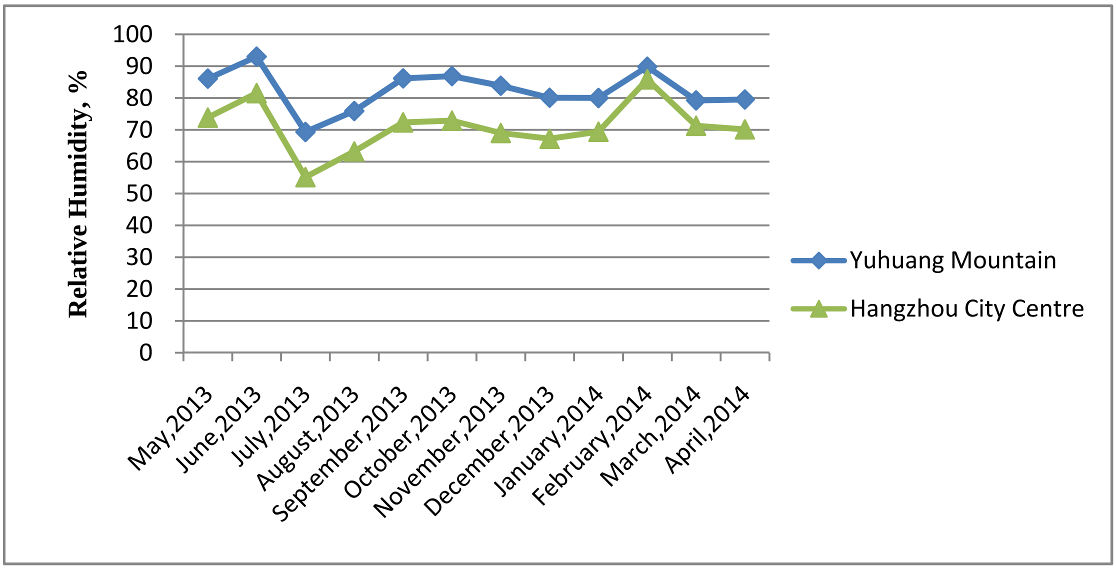

Fig. 5.70: Comparison of relative humidity between Hangzhou city centre and Yuhuang Mountain sites

In this study, the UHII variation was determined to be inversely proportional to the relative humidity, as Fig. 5.71 and Fig. 5.72 manifest. The result infers that places with higher relative humidity have better cooling effect. It verified the result obtained from Envi-met simulation work that the UHI effect is commonly accompanied by low humidity situation. The average hourly relative humidity difference was determined by subtracting the average hourly relative humidity of the rural area from that of the urban area. Fig. 5.73 also displays the negative correlation between UHII and the relative humidity difference between Ningbo city centre and reference site, which suggests the decrease of UHII, is associated with an increase in relative humidity difference. It is because at a place where the ambient relative humidity is higher, the solar radiation can have a greater possibility to cause the evapotranspiration process. The evapotranspiration phenomenon can effectively promote the latent heat release in atmosphere to reduce the ambient air temperature. Consequently, the finding showed a strong cooling tendency imposed by the thick vegetation cover at city centre to improve the ambient moisture

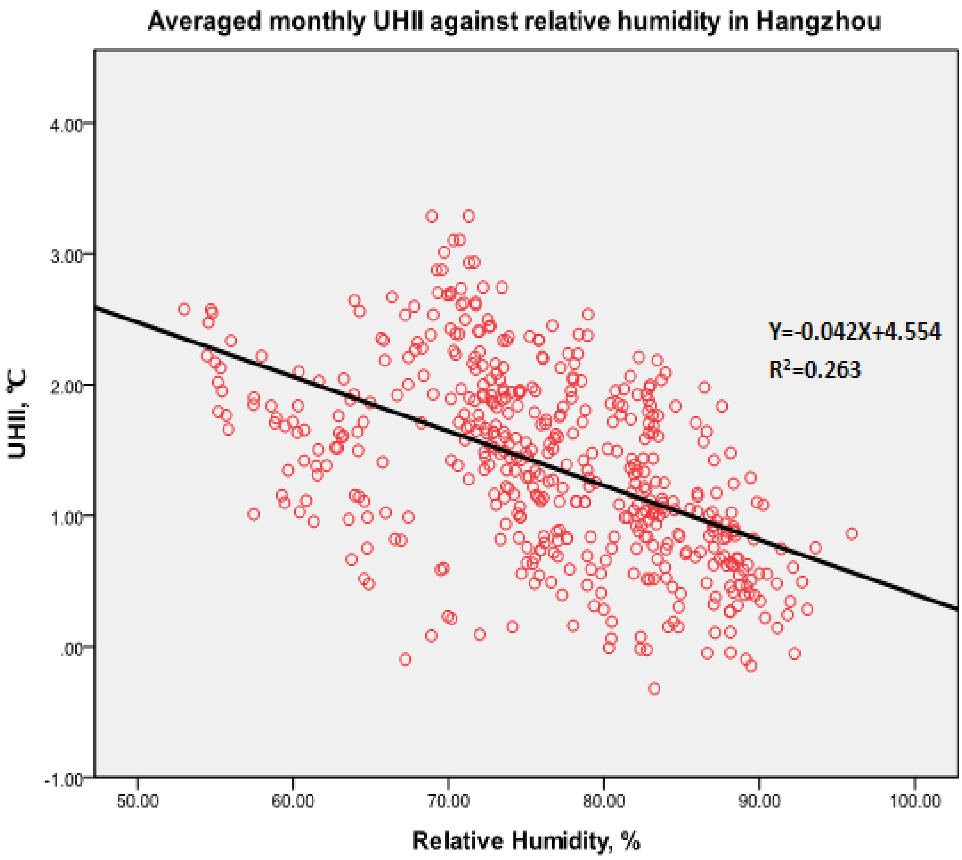

Fig. 5.71: Correlation between monthly UHII and relative humidity in Hangzhou

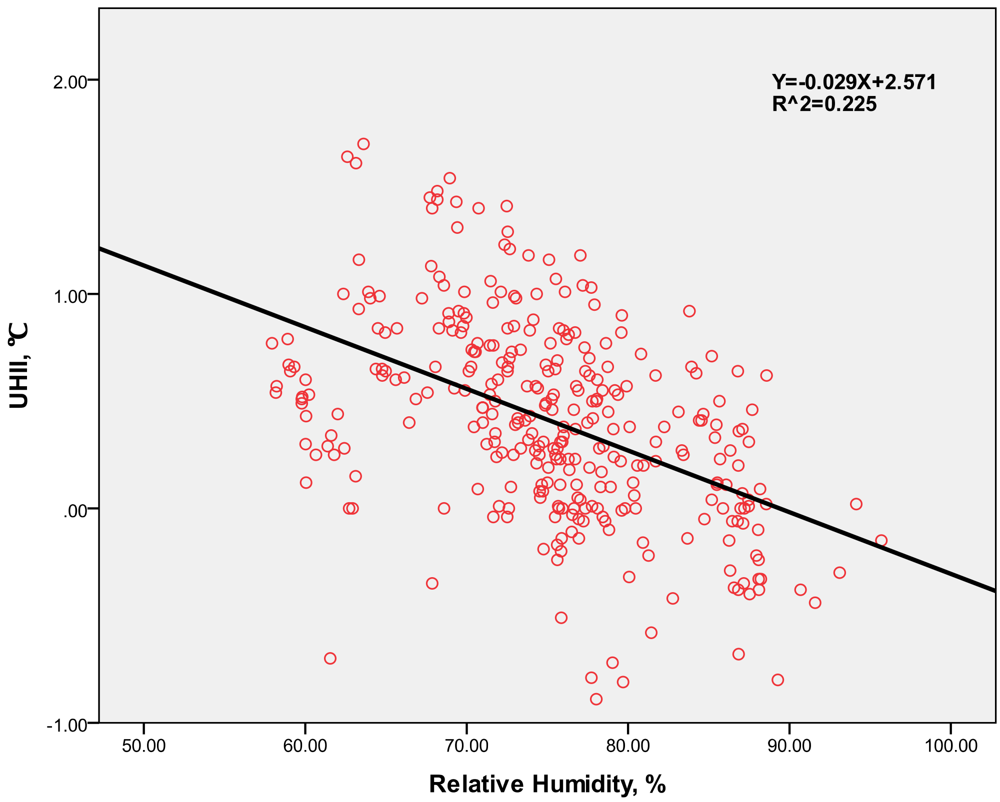

Fig. 5.72: Correlation between monthly UHII and relative humidity in Ningbo

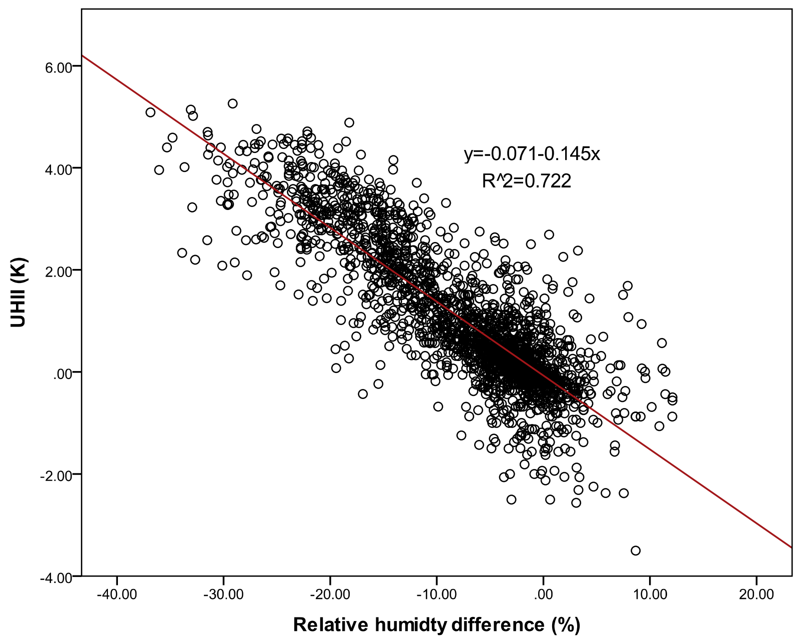

Fig. 5.73: Correlation between hourly UHII and relative humidity difference of Ningbo city centre in summer

5.3.5.4 Weather conditions

Weather conditions such as air temperature, wind speed, solar radiation and cloud cover, which are all worthy of investigation for the development of UHI. Considerable evidence listed above in this study has indicated that the strong UHI effect appears more frequently under calm and weak wind conditions at night, and its intensity is affected by day time and night time circulations. In comparison to the weak UHI appearing in summer days, the research also evaluated that the most intense UHI effect commonly occurs in winter.

In addition to that, solar radiation and cloud cover are critical factors that can influence the formation of UHI situation as well. Weather conditions in this study fall into three basic categories: rainy, cloudy and sunny. As an example, The temperature range in November 5th, 2012, November 22nd, 2012 and November 24th, 2012 are all from 8°C to 18°C and the wind speed are all less than 4m/s in Ningbo city [135]. The only major difference among these three days is that November 5th, 2012 is sunny and cloudless in whole day, November 22nd, 2012 is rainy in whole day and November 24th, 2012 is cloudy in whole day. As Fig. 5.74 illustrates, the measurement results found that average daily UHII of all Ningbo measurement sites in the sunny and cloudless day is higher than that in the rainy and cloudy days. In general, the average daily UHII values measured at sunny and cloudless days with strong solar radiation are highest (see Fig. 5.75). Whilst, the UHI effect is weaken in rainy days when the solar radiation is weak and cloud cover is heavy. It can surmise that the synoptic weather patterns that involve stable weather with strong solar radiation, high visibility and a cloudless sky are suitable for UHI development.

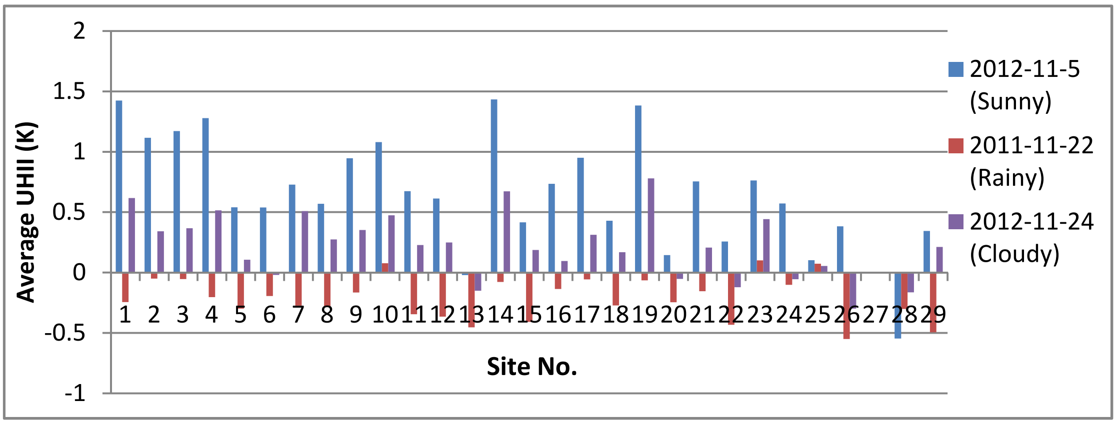

Fig. 5.74: Comparison of average daily UHII measured at sunny, rainy and cloudy days in Ningbo

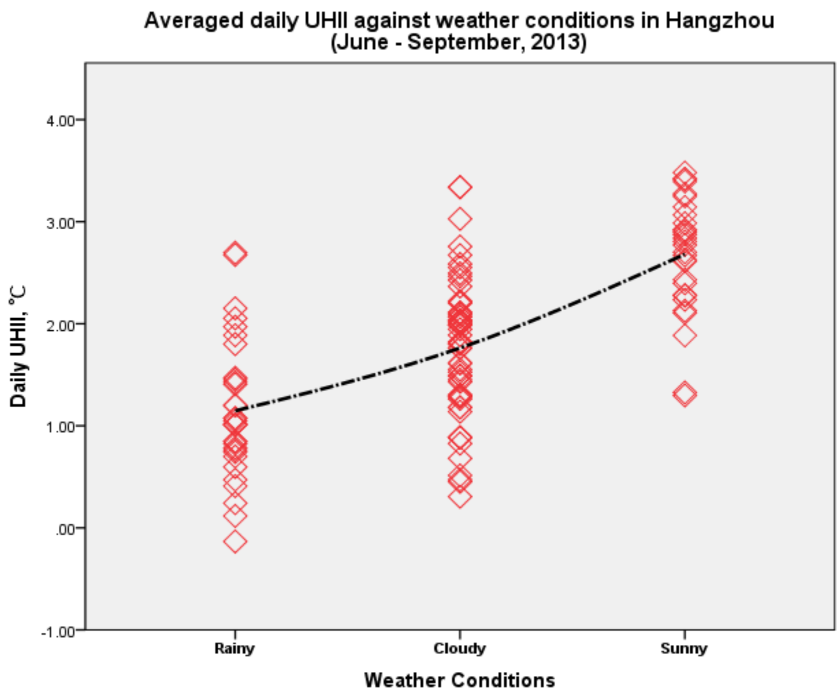

Fig. 5.75: Daily UHII range in rainy, cloudy and sunny days over Hangzhou

5.4 The factors contribute to UHI formation

The vegetation cover, surface material properties and human activities are three main factors that can contribute to UHI formation.

5.4.1 Vegetation cover

Trees and vegetation can reduce surrounding air temperature by evapotranspiration process and providing shade. In contrast, impervious surface are paved and covered with buildings, which results in less shade and moisture to elevate surface and air temperature. Fig. 5.76 shows that urban area has less surface moisture available for evapotranspiration than natural ground cover [136].

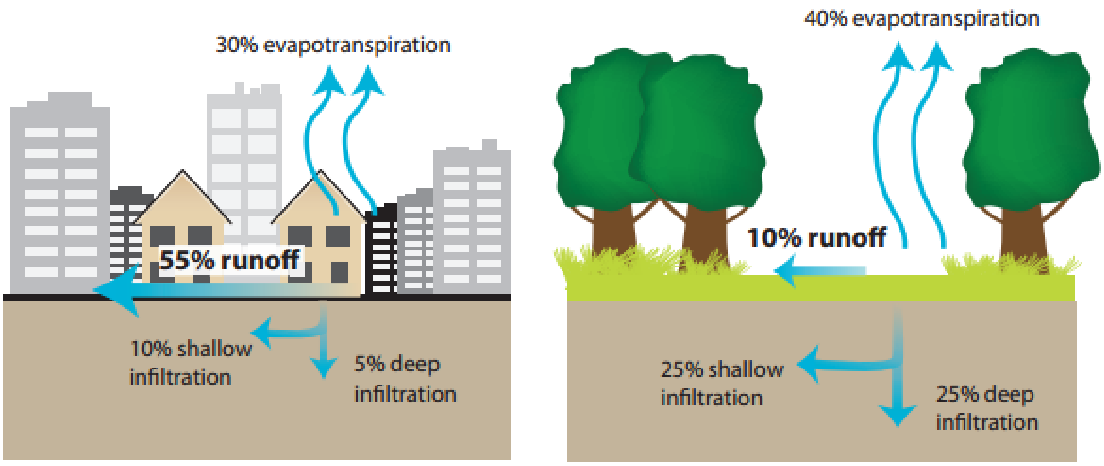

Fig. 5.76: Comparison of moisture balance between urban and rural places [136]

As Fig. 5.77 displays, distances from Hangzhou city centre to sites of Xiang Lake and

Chonghua Residential Community are similar. The main difference between these two closing sites is the vegetation cover. Xiang Lake area with more vegetation covered has much lower UHII than Chonghua residential community area where the ground surface is impervious, as Fig. 5.78 shows.

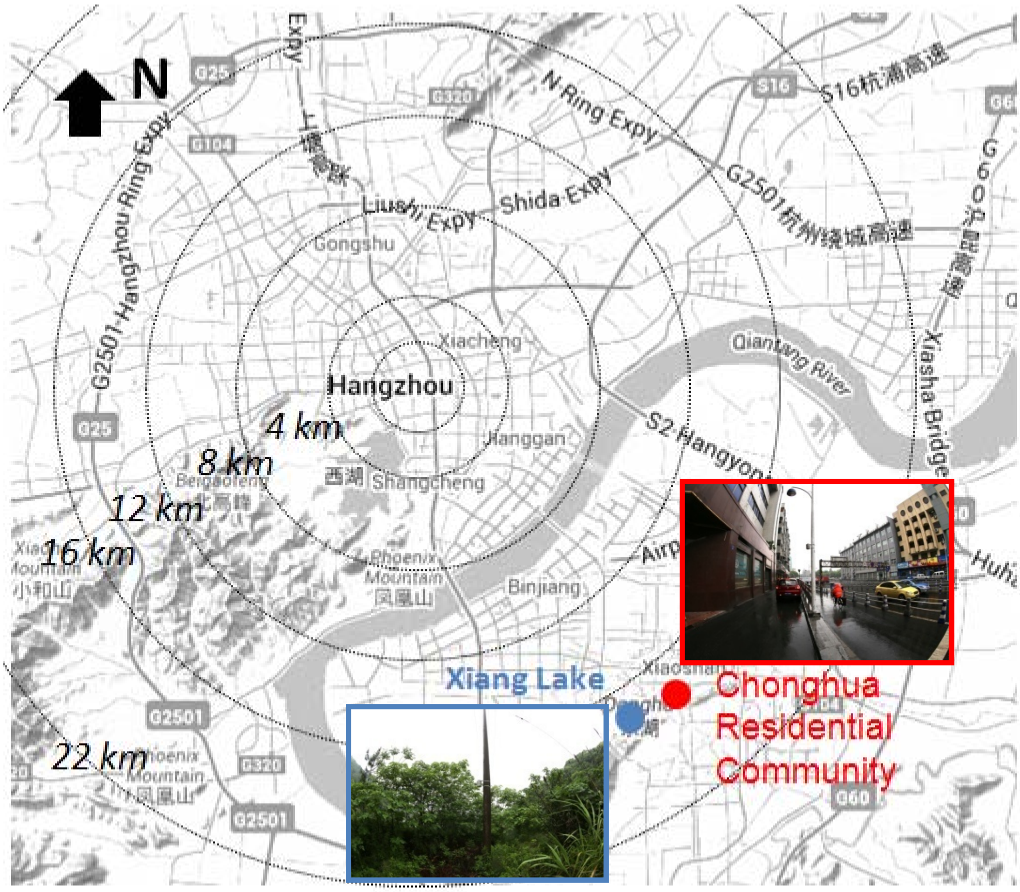

Fig. 5.77: Locations of Xiang Lake and Chonghua Residential Community

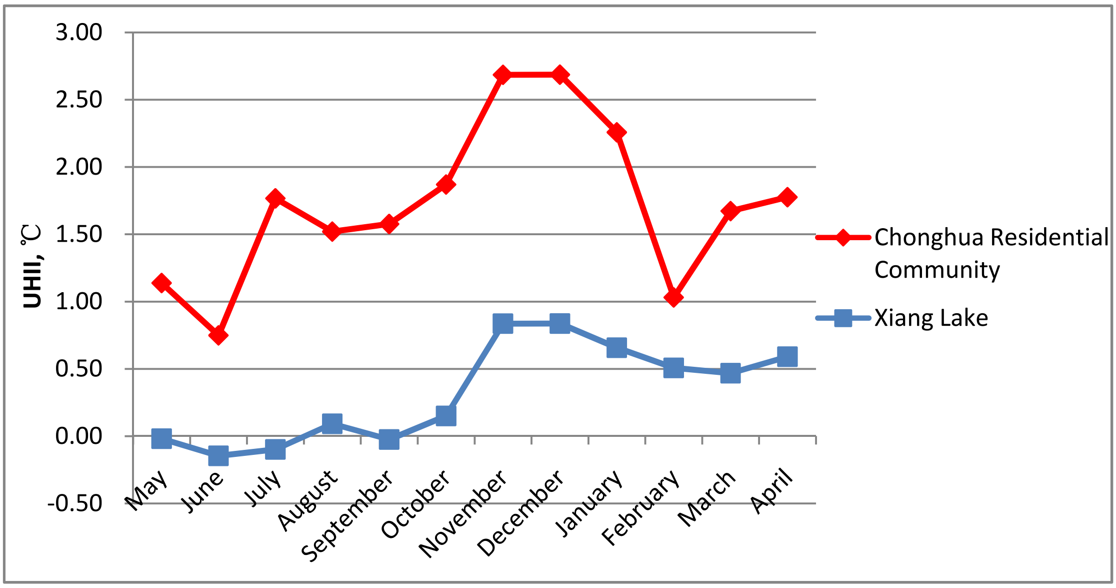

Fig. 5.78: UHII of Xiang Lake and Chonghua Residential Community

5.4.2 Urban building configuration and material properties

The urban building configurations including the ratio of building height to street width, building shape, orientation and surface roughness, are amongst parameters highly influencing urban wind flow. Generally, densely concentrated high-rise buildings cause less air circulation and more trapped heat energy in the urban canopy layer and therefore, more intense UHI effect.

Thermal emissivity, heat capacity, solar reflectance and other properties of surface material are highly related to the UHI formation, because they determine the amount of solar energy reflected, emitted and absorbed.

It has been mentioned that solar reflectance, or albedo, is the ratio of solar radiation reflected by a surface to the total radiation reaching that surface. Albedo can play the dominate role in the thermal behaviour of pavement and other ground surface. Albedo is generally correlated with colour of surface material. Lighter surfaces tend to have higher solar reflectance values than darker surfaces [133].

In addition to solar reflectance, thermal emissivity also determines a surface temperature. Surface with high emissivity can emit long-wave radiation (infrared) more readily to keep surface low temperature. Indeed, typical construction materials generally have high emissivity values, so that they can dissipate heat quickly [136]. Another surface property that can influence formation of UHI is heat capacity of material, which refers to its ability to store heat [133]. Rural surface materials, such as dry sand and soil, have much lower heat capacities than typical urban surface materials, such as asphalt, concrete and brick. The amount of heat absorbed and stored in urban metropolitan spaces can be twice greater compared to their surrounding rural areas during the day time [137].

It can be discovered from Fig. 5.79 that the distance from Ningbo South Station to Moon Lake Park is only 0.6km. However, according to the guide [24], it estimates that albedo value of Moon Lake Park space is twice as great as the value of Ningbo South Station area. Therefore, the UHI effect at Ningbo South Station is expected to be more intense than Moon Lake Park site (see Fig. 5.80).

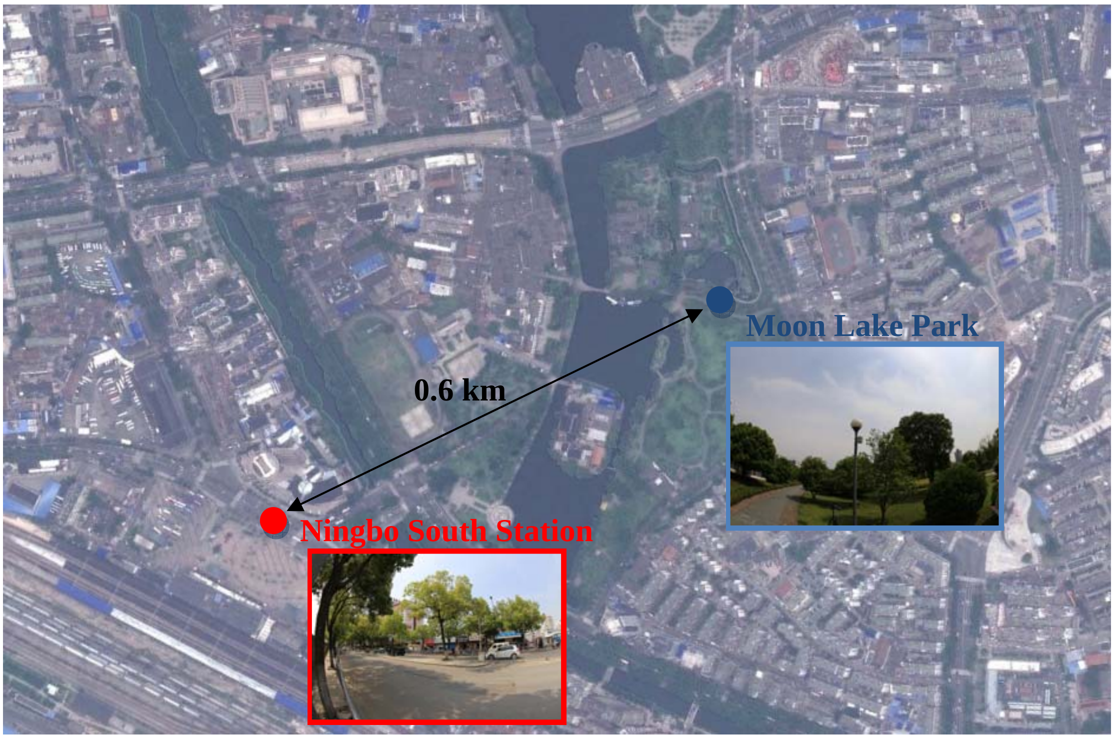

Fig. 5.79: Locations of Ningbo South Station and Moon Lake Park

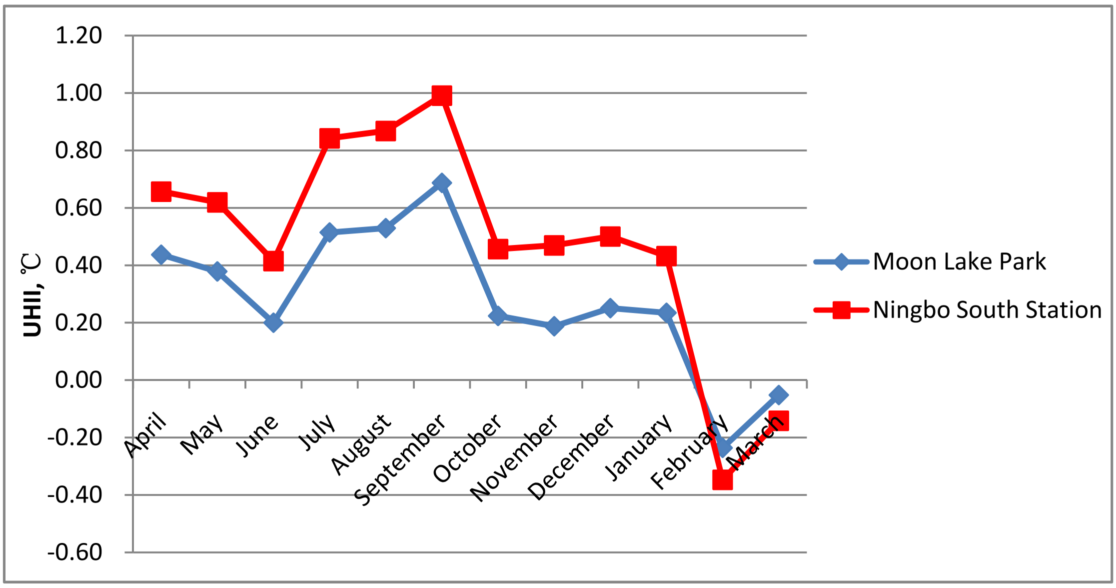

Fig. 5.80: UHII of Ningbo South Station and Moon Lake Park

5.4.3 Human activities

Air conditioning, manufacturing, transportation, and other human activities are discharging heat into urban environments, which contributes to atmospheric heat island. Anthropogenic heat typically is not a concern in rural spaces, but varies by urban infrastructure and activities, with more energy-intensive buildings and transportation producing more heat [138].

Chinese Spring Festival is the most paramount traditional festival and a public holiday in China, which falls on February 19, 2014. The study determined that UHII measured at majority urban sites, especially for industrial area, were relieved markedly in February, because majority factories were closed during Spring Festival. On the contrary, situation of UHI at rural places was not impacted by public holiday, as Fig. 5.81 shows. The locations of Xiang Lake, Yaqian Industrial area and Liuxia Industrial area are marked on the below map (see Fig. 5.82).

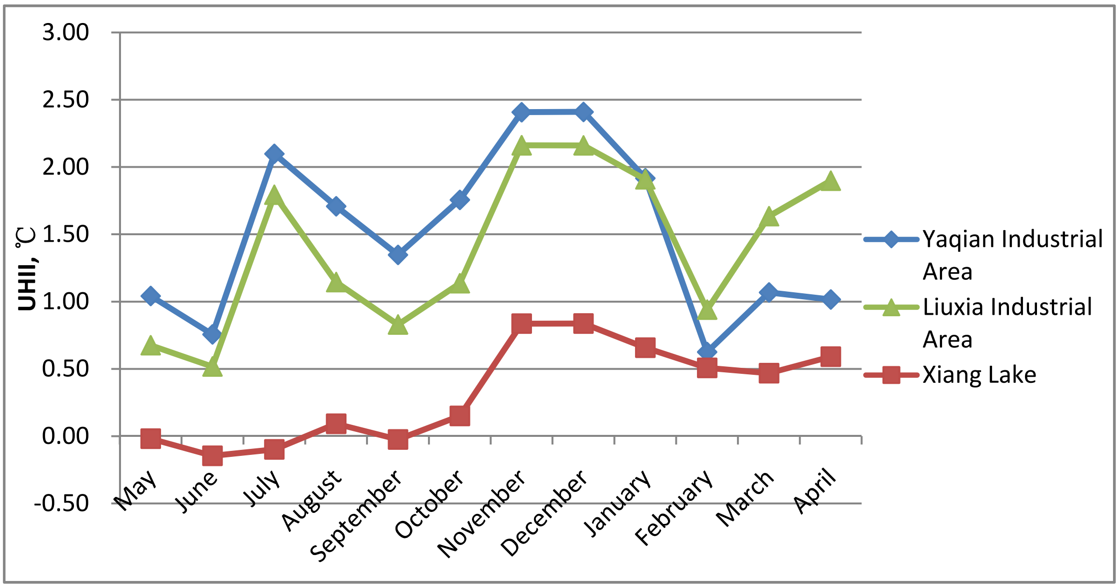

Fig. 5.81: UHII of Xiang Lake, Yaqian Industrial Area and Liuxia Industrial Area

Fig. 5.82: Locations of Xiang Lake, Yaqian Industrial Area and Liuxia Industrial Area

5.5 Mitigation of UHI

The development and adverse impacts of UHI effect have been demonstrated in the previous study, several innovative strategies, such as cool material application on urban surface, modify urban geometry to improve wind flow within cities and green space expansion in urban zones, are addressed to have substantial potentials to mitigate UHI effects and improve thermal performance of the building.

5.5.1 The application of cool materials on urban surfaces

It has been noticed in this research that surface albedo is a critical factor in shaping local climates through the radiation energy budget, because albedo values can determine the proportion of solar radiation of all wavelengths reflected by a body to the amount incident upon it. The surface with higher albedo values can absorb less and reflect more incoming solar radiation, thus the stored thermal energy in urban structures and ambient urban temperature can be reduced as well. The increase of the albedo in the built environment can be achieved by using high reflectance surfaces in roofs, pavements and other urban surfaces. Numerous studies considered in principle the value of surface albedo is determined by the colour and the roughness of materials [139]. As reported in other researches, after different pavement materials are comparatively measured, the result evaluates the tiles with rough surface are hotter than tiles with smooth and flat surface [140]. As Tab. 5.1 exhibits, surfaces with white painting can present an albedo value to 0.5 – 0.9, on the contrary, black surfaces have an albedo only close to 0.02 [24]. It means that improved albedo of light colour and smooth surface can increase its spectral reflectance in the visual spectrum of solar radiation.

In addition to the improved surface albedo and reflectivity, cool surfaces are also characterised by the using the latent heat of water evaporation to decrease their surface and ambient temperature. Green roof is a representative mitigation way whose working principle is based on the latent heat release by strong water evaporation. Green roofs are fully or partially covered with vegetation and a growing medium over a waterproofing membrane. There are two common types of green roofs are available: one is intensive roofs which are heavy constructions and can support small trees and shrubs, and the other one is called extensive roofs which are covered by a thin layer of vegetation [141]. Besides vegetated cover on surfaces, irrigation on surfaces is an effective way to cool the surfaces by increasing ambient moisture. It has been expounded in foregoing paragraphs that places with higher relative humidity have less intense UHI effect. Consequently, the research advocates popularising green surfaces and water retention surfaces to mitigate UHI effect in metropolitan areas.

5.5.2 Modify urban geometry to improve wind flow

It has been reported that calm wind would aggravate the intensity of UHI effect (see

Fig. 5.83). Because most wind speed values measured from June to September are located around 2m/s and not evenly distributed, it decreases the determination coefficient of R^2 greatly. It has also been proved by the simulation work in Chapter 3 that the cooling effect of the strong wind can mitigate the adverse impacts of UHI on the micro climate effectively. The wind pattern is not only the result of natural weather conditions, but also related to the buildings situated in urban settlements. The configuration and layout of a city can also assist wind circulation and affect wind speed which in turn influences the urban air temperature variations. The movements of the wind within a city can be impacted by city morphology directly, depending on city shape, city design, open space, and orientations and distributions of the roads within the city.

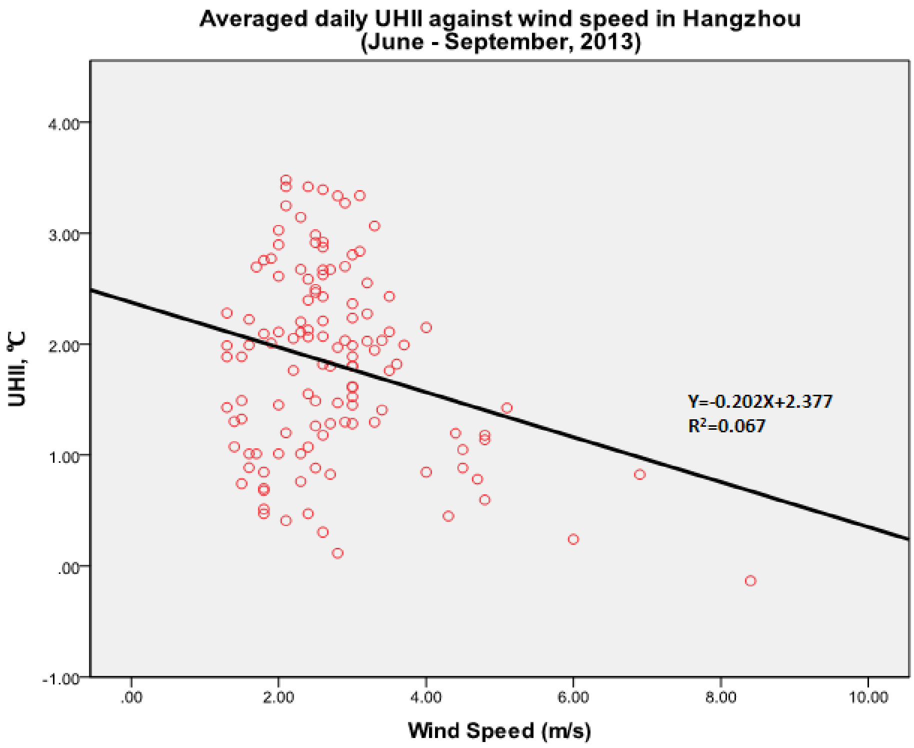

Fig. 5.83: Average daily UHII against wind speed over Hangzhou from June, 2013 to September, 2013

It has been examined that the urban configuration where windward buildings are lower than leeward buildings can enhance the wind flow in urban area effectively [142]. The interaction between the prevailing wind and this step-up urban configuration is displayed by Fig. 5.84. This urban configuration can effectively distribute the wind evenly and can allow the wind to reach the leeward side of each building.

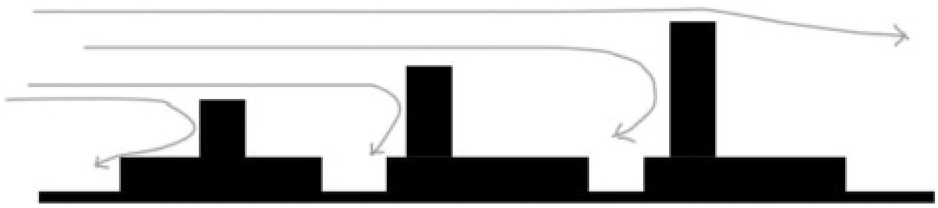

Fig. 5.84: Display of step-up urban configuration with prevailing wind

In addition, during the initial urban planning process, less ventilated urban area is recommended to be shaded by trees or covered by vegetations. The connection joint between two adjacent groups of building blocks is especially less ventilated. The research suggests building green space at this connection joint to break two adjacent groups of building configuration. In this way, shading and evapotranspiration provided by green space can compensate the thermal discomfort in this typical urban area with lower wind speed. As Fig. 5.85 shows, the green space, located at the leeward side of previous building towers, can work as a buffer region for the next group of urban set-up configuration and can be most effective to offer thermally comfortable zone.

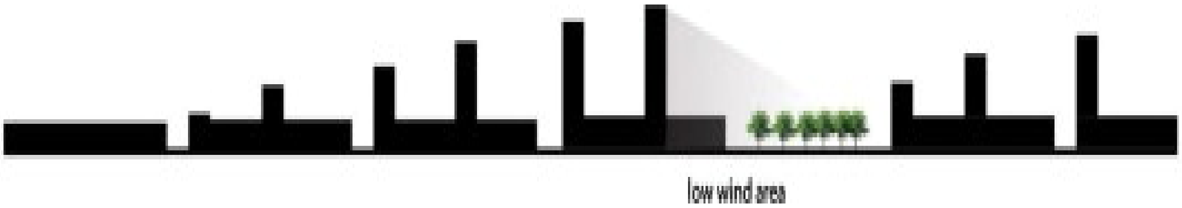

Fig. 5.85: The arrangement of building blocks and green space

5.5.3 Green space expansion in urban areas

Green space in the urban environment is recognised in this research as the most effective strategy that can contribute to the mitigation of UHI. Green space can provide cooling effect by its evapotranspiration process. Meanwhile, the relative humidity of surrounding areas can be improved as well to relieve the UHI effect. Other beneficial effects of urban green areas are related to fresh air supply, air pollution and noise pollution mitigation.

Hangzhou is a metropolitan city that has a unique natural geographical environment. As Fig. 5.86 displays, the large ecological space of West Lake, lies in the west part of Hangzhou city, has a significant influence in cooling temperature on surrounding urban areas. According to the comparison between the sites within 1km and 2-3 km from West Lake region, the result indicates that the average UHII of sites far away from West Lake are at least twice the UHII of sites near West lake (see Fig. 5.87). For most of cities over the world, there are no large natural ecological spaces in the urban area. The research advocates building small green area such as tiny green park, green parking lots and grassland in densely urbanised area.

Fig. 5.86: Geographic environment in Hangzhou city

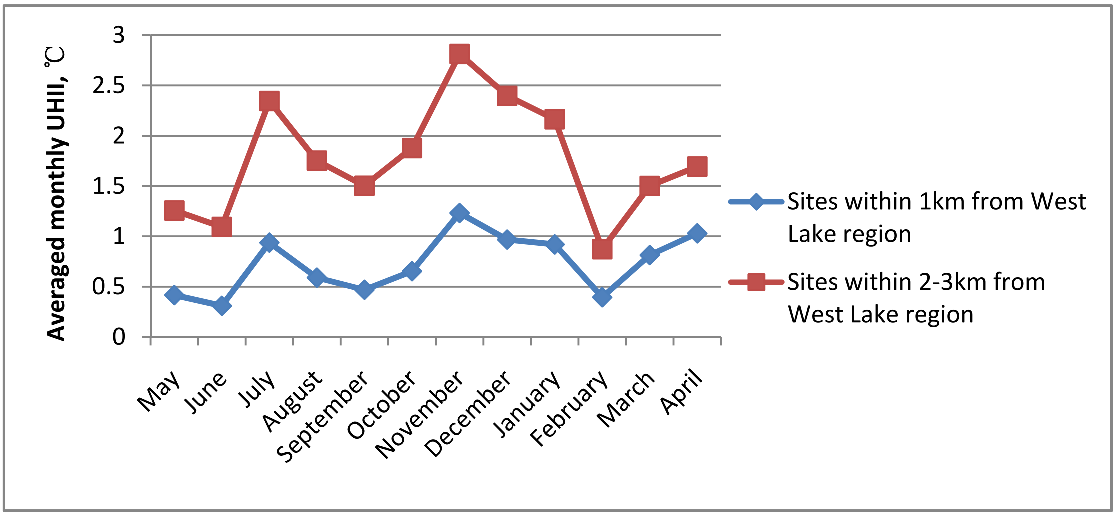

Fig. 5.87: Comparison of the monthly average UHII measured between the sites within 1km and 2-3 km from West Lake region

5.6 Concluding remark

The observation has determined that the UHI effect in Hangzhou is more intense than that in Ningbo. The monthly average UHII values in Hangzhou ranged between 1℃ and 4℃, whilst the highest monthly average UHII in Ningbo is only as high as 1.5℃.

Based on the field measurement, this chapter has focused on evaluating how UHI effect impacted by urban design factors, such as land-use, distance from city centre, surrounding albedo and sky view factor (SVF). Due to the serious air pollution, high concentration of Particulate Matter (PM) and low wind speed in winter days in China, the UHI effect is most serious in winter days. Furthermore, the night time UHI effect is significantly more intense than the day time UHI effect. Referring to the impacts of other meteorological parameters on UHI effect, for instance, the UHII variation has been evaluated to be inversely proportional to the relative humidity. Solar radiation and cloud cover are critical factors that can influence the formation of UHI situation as well. It can be concluded that the synoptic weather patterns that involve stable weather with strong solar radiation, high visibility and a cloudless sky are suitable for UHI development.

The study has also evaluated the contributions of vegetation cover, urban building configuration and material properties, and human activities to the UHI formation. Though UHI effect is unavoidable, there are feasibilities to reduce its impact on urban environment. The study has suggested to mitigating the UHI effect by three effective strategies, involving the application of cool materials on urban surfaces, modifying urban geometry to improve wind flow and expanding green space in urban areas.

CHAPTER 6: THE IMPACT OF UHI ON BUILDING ENERGY

6.1 Introduction

This chapter is divided into three main sections. The first section introduces the TMY weather dataset generation in China, especially the dataset in research areas of Hangzhou and Ningbo. The second section proposes three methods to modify currently available TMY weather dataset by considering the UHI effect. The last section is to evaluate energy performance of urban buildings with UHI effect by using Energy-plus software.

6.2 Typical Meteorological Year (TMY) weather dataset in China

Precise data information of local weather is indispensable for accurate estimation of building energy consumption. The weather data involves dry bulb temperature, relative humidity, wind speed, solar radiation data, etc. Although weather conditions change greatly from year to year, Typical Meteorological Year (TMY) weather dataset is derived as a customised weather dataset that can intelligently represent the long term average weather conditions over a year. Currently, TMY weather dataset are most commonly used in building simulations to predict the annual energy consumption. The generation of TMY weather dataset of each city in the world basically relies on the available meteorological data recorded from reference weather stations during a certain period. As an example, meteorological dataset of 270 cities in China were created based on real data collected from 270 national weather stations.

Most of these national weather stations are located in suburbs and far away from buildings, in order to satisfy the regulation referring to the selection of Meteorological Facilities and stations' locations [5].

Much of the research in building service engineering have realised the problem that the impact of UHI is often neglected in current building energy simulation practices when TMY weather data is applied. Hassid et al. mentioned that the cooling energy and peak power in the western Greater Athens are both underestimated if the simulation is only based on the TMY data without taking the UHI effect into account [143]. Chan determined that there was around a 10% increase in air-conditioning demand caused by the UHI effect in Hong Kong [144]. An increase of up to 10% in electricity for air-conditioning also occurs in metropolitan centres due to the UHI effect in the country of Bahrain [145]. On the other hand, a previous study showed that total energy consumption of urban buildings in Tokyo was decreased by the UHI effect, because decreases of energy consumption in space heating and water-heating were greater than the increase in cooling energy consumption [146].

In one word, UHI has critical impacts on building energy consumption and indoor thermal comfort in urban area. If the UHI effect is considered, the designed requirement of energy consumption, especially air-conditioning demand of urban buildings, will change greatly due to the increase in urban air temperature. It is indispensable, therefore, to take into account the UHI effect in building design and in simulations of the thermal performance of buildings. There are several methods, such as field measurement [144] and establishing computational mode [147, 148], have been dedicated to modify the currently available TMY weather files by taking into account the effect of UHI.

6.2.1 TMY weather dataset for Hangzhou

All kinds of ground weather data from national datum stations and national principle stations are involved in the national ground climatic observation network that is the origin of TMY weather dataset generation. There are 136 national principle stations and 134 national datum stations that were rebuilt in succession based on national principle stations since 1987 [4]. The national datum stations provide 1-hour interval observation data while the national principle stations provide 6-hour intervals observation data [4].

The weather station located at Mantou Mountain in Hangzhou is the national datum station of Hangzhou city. It is about 5km away from the city centre of Hangzhou (see Fig. 6.1). Its temperature record started in January, 1951 and solar radiation started in January, 1961 [149]. The currently available TMY weather dataset was generated based on the data collected from this station with a time spam from 1971 to 2003. The station is mainly surrounded by grass and trees, with little blocks see Fig. 6.2.

Fig. 6.1: Locations of city centre and national datum station

Fig. 6.2: View of national datum station at Mantou Mountain of Hangzhou

Geographically, the national datum station of Hangzhou city is not far away from city centre and locates in urban area, however, due to the particular landform of Hangzhou, the location of station is on a small mountain. Thus, the surrounding thermal environment of weather station is entirely different from the urban thermal environment. It causes the significant difference of daily air temperature collected at between Hangzhou city centre and national datum station. As Fig. 6.3 demonstrates, the air temperature of Hangzhou urban core area is about 1-2℃ higher than the national datum station. It reveals that the UHI effect would not be involved by the TMY weather data.

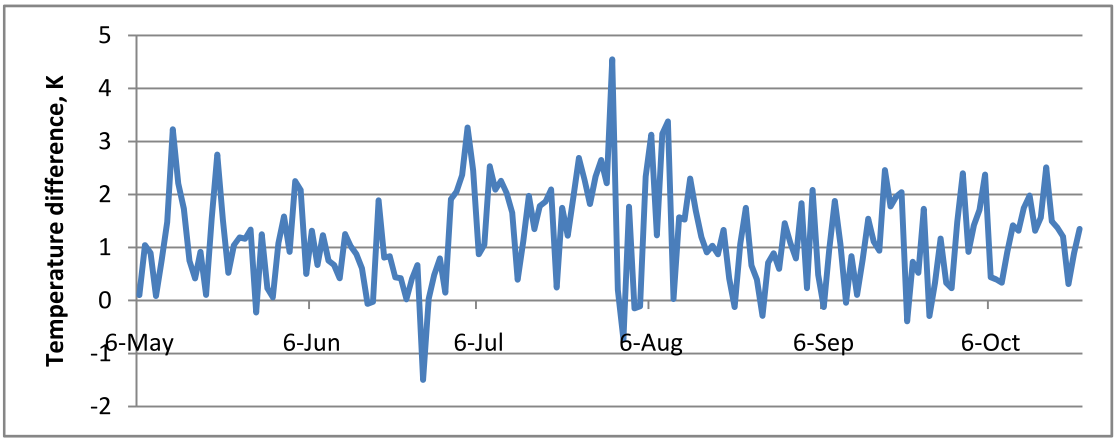

Fig. 6.3: The difference of daily air temperature collected at between Hangzhou city centre and national datum station from May to October, 2013

6.2.2 TMY weather dataset for Ningbo

As mentioned before, there is no national datum station constructed in Ningbo and no available TMY weather dataset for Ningbo. The precision of meteorological data collected from the national datum station is highest among all patterns of national stations in China. The official meteorological station in Ningbo only achieves the standard of national principle station. The data collected at Ningbo national principle station was not recorded hourly, but rather at six hour intervals. The more serious problem regarding Ningbo meteorological station is that the location of Ningbo station has varied four times since it was initially established at January 1st, 1953 [98]. The reason behind this phenomenon is also related to the unsustainable urban planning and rapid urbanisation in Ningbo. Once the place of weather station is surrounded by high buildings closely or its SVF is no longer great enough, the collected meteorological data would be influenced by surrounding urban environment.

The current national principle station has been built in Ningbo suburb area that is about 10km away from the location of initial Ningbo weather station at city centre. Fig. 6.4 compares the mean monthly air temperature collected from the site close to initial Ningbo weather station with the temperature collected from the site near current Ningbo weather station. The result verifies that the thermal environment at the initial Ningbo weather station is at least 1°C warmer than the current one.

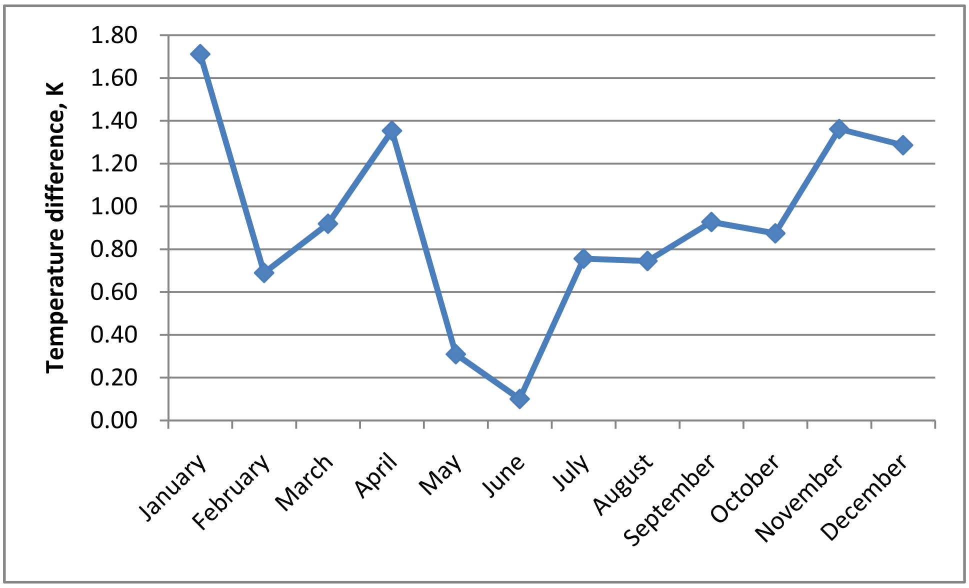

Fig. 6.4: The difference of mean monthly air temperature collected at between Ningbo initial weather station area and Ningbo current weather station area.

6.3 The modification of the existing TMY weather dataset

The research proposed a problem that it is probably not accurate if simply using current TMY weather file for evaluating the thermal and energy performance of buildings located in urban areas with a UHI effect, and it may greatly underestimate the average cooling energy consumption of these urban buildings in summer.

The impacts of UHI on the energy consumptions of buildings have been investigated by various studies. As an example, in the investigation of UHI effect in Greater Athens, the research applied the weather data of the years 1997 and 1998 to simulate the air conditioning load of local urban buildings by software DOE2.1 E. That research evaluated that the cooling energy and peak power load of urban buildings in Athens simulated based on official TMY weather dataset without considering UHI effect were both underestimated [143]. A similar research was conducted in London in 2000. The research indicated that a rural reference office building only required 84% cooling energy demand compared to an urban office building [150]. In addition to the UHI effect, climate change would also threaten the precision of TMY weather dataset and influence the prediction of building thermal performance. A previous study in Bahrain evaluated that the weather file generated based on far past data (before 1991) tends to underestimate the electricity consumption of local buildings by 14.5% and misrepresented the cooling load by 5.9-8.9% [151].

Consequently, it is indispensible to derive a modified TMY weather dataset for research target cities by taking the UHI effect into account based on the collected hourly air temperature and relative humidity. An appropriate solution should be adopted to incorporate the UHII into a standard TMY weather dataset. In simple terms, it can incorporate the UHI effect into the existing TMY weather dataset by three methodologies.

Firstly, the modified weather data file could be generated by adding the hourly UHII values (the temperature difference between city centre site and reference site) to the existing TMY weather data file, as listed in equation 6.1:

$$\mathrm{T_1 = T_0 + UHII_{hourly}} \tag{6.1}$$

where T_1 is the modified hourly air temperature and T_0 is the existing hourly air temperature.

Secondly, the paper proposes to generate the modified weather data file by adding the mean monthly UHII (mean monthly temperature difference between city centre site and reference site) to the existing TMY weather dataset, as listed in equation 6.2:

$$\mathrm{T_2 = T_0 + UHII_{\,monthly}} \tag{6.2}$$

where T_2 is the modified hourly air temperature and T_0 is the existing hourly air temperature.

In addition to the above two methodologies, there is another shared methodology developed by Belcher et al. called Morphing [152]. They developed this method initially to produce design weather data for building thermal simulations that account for changes of climatic conditions. The method includes stretching and shifting the climatic variables in the currently available weather dataset to produce the updated version of weather dataset which encapsulates the average climate change. Meanwhile, the physically realistic weather sequence of the source data is preserved. By using this simple and effective method, the measured UHI intensities could be involved in the existing TMY weather dataset. The methodology of morphing the weather dataset has three common algorithms: (i) a shift; (ii) a linear stretch; (iii) a combination of shift and stretch, as listed in equations 6.3 – 6.5 [144]:

$$x = x_0 + \Delta x_m \tag{6.3}$$

$$x = \alpha_m x_0 \tag{6.4}$$

$$x = x_0 + \Delta x_m + \alpha_m \times (x_0 - (x_0)_m) \tag{6.5}$$

where x is the modified hourly climatic variable, x_0 is existing hourly climatic variable, Δx_m is absolute change in monthly mean climatic variable for the month m, α_m is fractional change in monthly mean climatic variable for month m, $(x_0)_m$ is climatic variable x_0 average over month m.

For equation 6.1, a shift adds a monthly change to the current hourly weather data parameter. One common example of this approach is to adjust atmospheric pressure. For equation 6.2, it is to stretch current hourly weather data which scales the existing hourly data with a mean monthly change of the weather data. This equation is mainly used for adjusting wind speed. Referring to the equation 6.3, it combines a shift and a stretch, a current hourly weather data is shifted by adding an absolute mean monthly change and stretched by a monthly variation of the parameter. This method is most appropriate for adjusting the air temperature. In previous research, it applied the measured monthly difference of the daily mean, minimum and maximum air temperatures in order to integrate predicted variation of the diurnal cycle [144].

The approach of a combination of a shift and a stretch was adopted to morph the hourly air temperature rise due to the UHI effect in this study, as equation 6.6 lists:

$$T_3 = T_0 + UHII_{monthly} + \alpha_m \times (T_0 - (T_0)_m) \tag{6.6}$$

where T_3 is the modified hourly air temperature, T_0 is the existing hourly air temperature, $UHII_{monthly}$ is the mean monthly UHII (mean monthly temperature difference between city centre site and reference site), $(T_0)_m$ is the mean monthly air temperature in month m of the existing TMY weather dataset. The fractional change of α_m was calculated by dividing the difference between monthly maximum UHII and monthly minimum UHII by the difference between mean daily maximum and mean daily minimum air temperature of the original TMY weather dataset. Tab. 6.1 lists the values of $UHII_{monthly}$, α_m and $(T_0)_m$ that were calculated by the prediction of UHII from field measurement.

Tab. 6.1: Values of $\mathrm{UHII}_{\mathrm{monthly}}$, α_m and $(T_0)_m$ for input into a morphing algorithm: combination of a shift and a stretch (Equation 6.6)

	Jan	Feb	Mar	Apr	May	Jun	Jul	Aug	Sep	Oct	Nov	Dec
$\mathbf{UHII_{monthly}}$	2.14	0.68	1.28	1.42	1.21	0.99	2.02	1.61	1.44	1.86	2.72	2.42
$\boldsymbol{\alpha_m}$	0.69	0.92	0.77	1.13	0.75	0.89	0.82	0.71	0.81	0.58	0.56	0.70
$\mathbf{(T_0)_m}$	5.20	6.62	10.76	16.33	23.34	24.61	31.60	30.74	24.42	19.39	12.68	6.52

6.4 Evaluation of energy performance of urban buildings with UHI effect by using Energy-plus software

With the measured data of UHII values, modified TMY weather files for Hangzhou were generated based on the methods mentioned above, taking into account of the UHI effect. For the purpose of investigating the impact of the UHI effect on building energy performance with the modified TMY weather dataset, a typical office building in Hangzhou city had been modelled for the present study.

6.4.1 Description of the model building

China Telecom Business Office Building, located at the city centre of Hangzhou, is close to the measurement site was selected as the target research building (see Fig. 6.5). The building is 15 stories high and fully air conditioned. The first floor is the business hall and the rest of the floors are for office accommodation. The code of Design

Standard for Energy Efficiency of Public Buildings in Zhejiang Province (DB33/1038 – 2007) was developed by the Department of Construction of Zhejiang Province in 2007 [153]. With the combination of Zhejiang local weather conditions, the code was enforced to reduce the energy consumption of public buildings by improving the internal thermal environment and improving the efficiency of heating, cooling, ventilation and lighting systems.

Fig. 6.5: Locations of the target building and the measurement site at city centre of Hangzhou.

The study assumes that the criteria of this building were designed based on the code of DB33/1038 – 2007. According to the standard, Tab. 6.2 lists the requirement of envelop elements in the fully air-conditioned buildings. The required electric power to achieve a recommended lighting lever is about $11\mathrm{W/m^2}$ and the gross required power of electric equipments is about $20\mathrm{W/m^2}$. The occupant load of this building is supposed to be 4m^2 net floor area per person. The comfort range of fully air-conditioned buildings in Zhejiang Province is set as 18℃ to 26℃, as Tab. 6.3 shows.

Tab. 6.2: The envelop element requirements for fully air-conditioned building in the code DB33/1038-2007 [153]

Building Elements	**Required U-value W / (m^2·K)**	
Roof	≤0.50	
External Walls	≤0.70	
Ground Walls	≤0.70	
Windows	U-value W/（m2·K）	Shading ratio
Ratio of window to wall≤0.2	≤3.3	—
0.2＜Ratio of window to wall≤0.3	≤2.5	≤0.40 / —
0.3＜Ratio of window to wall≤0.4	≤2.1	≤0.35 / 0.40
0.4＜Ratio of window to wall≤0.5	≤2.0	≤0.32 / 0.40
0.5＜Ratio of window to wall≤0.7	≤1.8	≤0.28 / 0.35
0.7＜Ratio of window to wall≤0.8	≤1.4	≤0.25 / 0.28
Transparent Roof	≤2.0	≤0.28

Tab. 6.3: Design requirement for the fully air-conditioned building [153]

Criteria		Winter	Summer
Air Temp (℃)	Typical rooms	20	26
	Hall / Corridor	18	≥26 And the indoor and outdoor temperature difference ≤10
Wind speed (v) (m/s)		0.10≤υ≤0.20	0.15≤υ≤0.30
Relative humidity (%)		30 ~ 60	40 ~ 65

In order to satisfy the requirement of the building code, characteristics of envelop elements should be designed as below (Tab. 6.4):

Tab. 6.4: Design thermal properties of construction materials in this building

Wall	Materials	Thickness (m)	Density (Kg/m^3)	Conductivity (W/m × K)	Specific Heat (J/kg × K)	U Value (W/m^{2}K)
Updated External Wall	Medium Brick Masonry	0.11	2000	0.711	836.8	0.3637
	Air Gap	0.075	1.3	5.56	1004	
	Fibrous Wool	0.11	96	0.043	840	
	Plaster	0.01	1250	0.431	1088	

Roof	Materials	Thickness (m)	Density (Kg/m^3)	Conductivity (W/m × K)	Specific Heat (J/kg × K)	U Value (W/m^{2}K)
Updated External Roof	Roof Membrane	0.0095	1121.29	0.16	1460	0.2296
	Roof Insulation	0.2105	265	0.049	836.8	
	Metal Decking	0.0015	7680	45.006	418.4	

External floor	Materials	Thickness (m)	Density (Kg/m^3)	Conductivity (W/m × K)	Specific Heat (J/kg × K)	U Value (W/m^{2}K)	Admittance (W/m^{2}K)
External Floor	Soil	1.5	1300	0.837	1046	0.5195	6
	Concrete	0.1	3800	0.753	656.9		

6.4.2 Result and discussion

The cooling and heating demands of this office building model were evaluated by using a renowned building energy simulation software named Energy Plus, developed by the US Department of Energy [154]. The original and modified TMY hourly weather files were used as the weather data input in the simulations. The analysis and comparison of the simulation results are detailed below.

Owing to the climate conditions in Hangzhou, space heating is a not a basic provision in most buildings in winter. Cooling demands are immensely required in hot months from May to October in Hangzhou. Software simulations of monthly building energy consumptions based on original and modified TMY weather data files were carried out. Tab. 6.5 lists the required cooling energy consumptions of this target office building in hot months estimated by using original TMY weather dataset (T_0), modified TMY weather dataset with hourly UHII added (T_1), modified TMY weather dataset with monthly UHII added (T_2), and morphing modified TMY weather dataset (T_3). The result is plotted in Fig. 6.6 to compare the monthly cooling energy consumptions of the office building based on original and modified weather dataset.

Tab. 6.5: Monthly and gross cooling energy of the target office building during hot period based on original and modified TMY weather data

Cooling energy (kWh)	**May**	**Jun**	**Jul**	**Aug**	**Sep**	**Oct**	**Gross**
Original TMY (T_0)	241000	394000	553000	546000	349000	182000	2265000
Modified TMY (T_1)	268000	440000	633000	605000	391000	212000	2550000
Modified TMY (T_2)	294000	450000	685000	639000	415000	247000	2730000
Modified TMY (T_3)	291000	446000	691000	652000	411000	249000	2740000
Percentage of increase ($\frac{T_1-T_0}{T_0}$)	11.2%	11.7%	14.5%	10.8%	12.0%	16.5%	12.6%
Percentage of increase ($\frac{T_2-T_0}{T_0}$)	22.0%	14.2%	23.9%	17.0%	18.9%	35.7%	20.5%
Percentage of increase ($\frac{T_3-T_0}{T_0}$)	20.8%	13.2%	25.0%	19.4%	17.8%	36.8%	21.0%

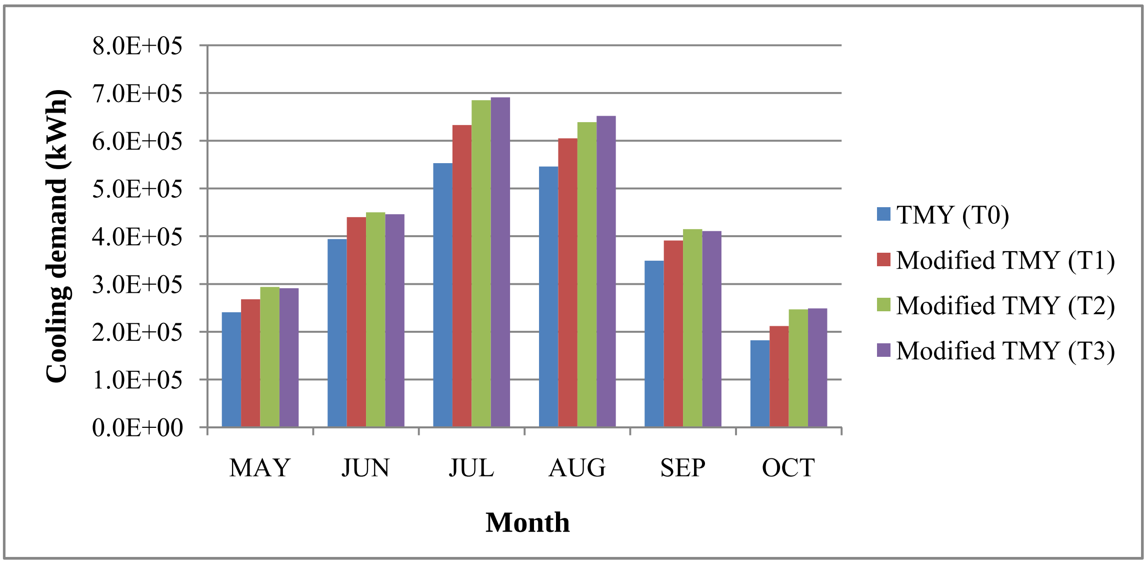

Fig. 6.6: Comparison of cooling energy of the target office building during hot months

As shown in Fig. 6.6, the office building in Hangzhou urban core area consumes more cooling energy under the impact of the UHI effect. Compared with using original weather dataset, the gross cooling energy consumption of this target building is increased by 12.6% in hot months through using the modified TMY weather dataset with hourly UHII added. However, if the TMY weather dataset is modified by adding monthly UHII or morphing method, the percentage of increase in cooling energy is about 20%, starting from 14% in June up to a peak value of 36% in October.

In order to examine the exact cooling energy consumption of this target office building during summer months in 2013, this study run the simulation again by using the actual weather data (T_4) collected at Hangzhou city centre in 2013. As Tab. 6.6 demonstrates, the office building consumes the highest amount of cooling energy in July when the air temperature in highest. The actual gross cooling energy consumption of the target building in 2013 is 3.5million kWh that is extremely higher than the values simulated by previous modified weather dataset (T_1, T_2 and T_3). It is because under the impact of climate change and global warming, the average air temperature in 2013 summer is significantly higher than the temperature recorded in TMY weather dataset average over 1971 to 2003. In one word, through building energy computer simulations using the modified TMY weather dataset, taking into account the impact of UHI effect, the result reveals that there is a significant increase in building cooling demand in office buildings under the climatic conditions of Hangzhou.

Tab. 6.6: Monthly and gross cooling energy of the target office building during hot period based on collected weather data.

Cooling energy (kWh)	May	Jun	Jul	Aug	Sep	Oct	Gross
Original TMY (T_0)	241000	394000	553000	546000	349000	182000	2265000
Modified TMY (T_4)	432000	494000	1033000	837000	469000	247000	3512000
Percentage of increase ($\frac{T_4-T_0}{T_0}$)	79.3%	25.4%	86.8%	53.3%	34.4%	35.7%	55.1%

Referring to the heating energy consumption of this office building, based on the original TMY weather data file, the simulation predicts that the gross heating demand in cold months required by this building is only 184,539 kWh that occupies 8.1% of gross cooling energy consumption. Due to the specific climatic conditions of

Hangzhou, in contrast to cooling, heating is not a basic provision in most buildings in Hangzhou city. Nevertheless, as Tab. 6.7 and Fig. 6.7 show, UHI effect can work effectively to reduce the heating energy consumptions of this office building. There is at least 20% of heating energy will be over-designed if the previous design work is based on the original TMY weather dataset.

Tab. 6.7: Monthly and gross heating energy of the target office building during cold period based on original and modified TMY weather data

Heating energy (kWh)	**JAN**	**FEB**	**MAR**	**APR**	**NOV**	**DEC**	**Gross**
Original TMY (T_0)	69700	47700	20800	47	4800	41500	184539
Modified TMY (T_1)	52100	42500	15000	0	3700	32600	145900
Modified TMY (T_2)	47600	42900	13800	0	3100	32500	139900
Modified TMY (T_3)	46100	43100	13300	0	3200	32000	137700
Percentage of increase ($\frac{T_1-T_0}{T_0}$)	-25.3%	-10.9%	-27.9%	0.0%	-22.9%	-21.4%	-20.9%
Percentage of increase ($\frac{T_2-T_0}{T_0}$)	-31.7%	-10.1%	-33.7%	0.0%	-35.4%	-21.7%	-24.2%
Percentage of increase ($\frac{T_3-T_0}{T_0}$)	-33.9%	-9.6%	-36.1%	0.0%	-33.3%	-22.9%	-25.4%

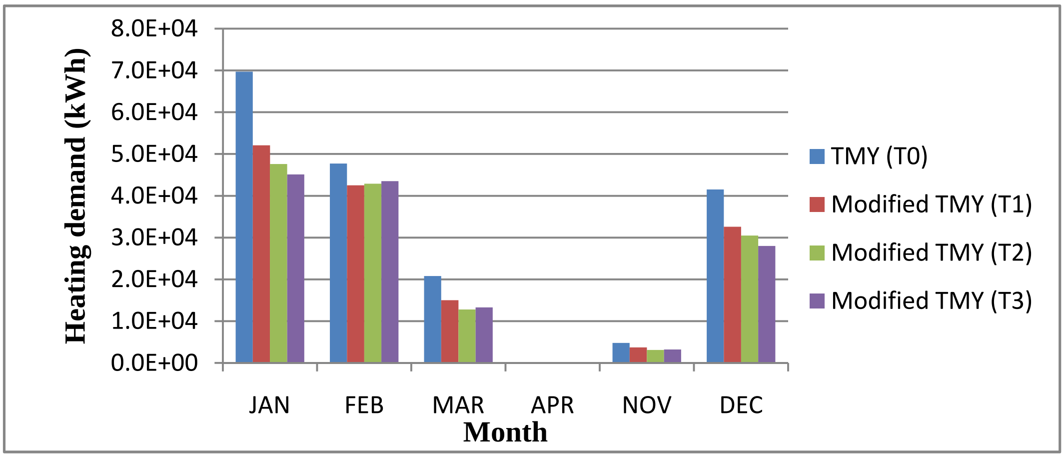

Fig. 6.7: Comparison of heating energy consumptions of the target office building during cold months

As a result, the study insists on the point that original TMY weather dataset cannot give a precise evaluation of building energy performance, because the meteorological data selected to generate the TMY weather dataset is mainly obtained from rural weather stations. It is because a great temperature difference between urban and rural areas will be caused by UHI effect. The result has revealed that the cooling demands of building located in urban areas will be under-estimated and the heating demands will be over-estimated if the currently available weather dataset is applied. The study also implies that there is a great potential to save urban building energy consumptions by using various UHI mitigation strategies.

6.5 Concluding remark

It can be summarised that the currently available TMY weather dataset generated from rural stations without considering UHI effect cannot be used to represent the local urban microclimate. This chapter therefore has advocated three methods to modify the existing TMY weather dataset by adding the UHI effect.

The Energy-plus simulation has determined that for an example office building located at Hangzhou city centre, there was about a 20% cooling demand underestimated in hot days and about a 25% heating demand overestimated in cold days. Referring to the total annual energy consumption, it would be underestimated by about 17.5%. The result has also implied that there is a great potential to reduce the building energy consumption as well as greenhouse gas emission considerably by various UHI mitigation strategies.

CHAPTER 7: UHII PREDICTION MODEL

7.1 Introduction

The undesired side impacts of UHI effect on increasing urban air temperature, increasing building energy consumption in summer and damaging outdoor air quality have been realised by the public and also been widely studied by researchers. The most shared methodologies to predict UHI effect are field measurement and satellite remote sensing technology. On the other hand, to date, there are limited studies that have been carried out to explore the use of different statistical and numerical methods in predicting UHI effect [155]. The prediction of UHI behaviour by simulation models should be gained a significant attention.

The statistical methods have the advantages of being faster and simpler in the prediction applications. The traditional models are mainly driven based on the regression approach that has been widely applied for the purposes of predicting and forecasting. A non-linear or linear correlation between a dependent variable and one or more independent variables is expected in regression models [156]. The work theory of the statistical method in this study is to predict the intensity of UHI by linking the complex interaction between values of UHII and related influence parameters. This chapter introduces two statistical model, artificial neural network and genetic programming, to achieve this target.

7.2 Artificial Neural Network (ANN)

Because extreme values cannot be always captured in the predictions of linear regression models, the large masses of data can have huge effect on the linear regression by decreasing the accuracy of the prediction [155]. Considering the highly complex relation between UHII and other environmental and time parameters, the non-linear regression model is a more efficient way to find the relation.

Artificial Neural Network (ANN) is recognised as one of most effective methods for approximating non-linear model function [155]. ANN is known as a kind of biologically inspired computer programmes that can mimic the behaviour of human brain. A neural network is a distributed processor composed of massively simple elements operating in parallel that have a natural tendency for storing experiential knowledge [157]. A neural network can be trained to perform a complex function in various fields by adjusting the values of the connections and weights between elements. Currently, neural networks have been developed to solve problems that are difficult for conventional computers or human beings [158]. ANN has been widely applied in a number of prediction studies that involve atmospheric time series data. Daily maximum ozone levels in Texas metropolitan areas was predicted by a standard three-layer ANN model with nine inputs and four hidden nodes. The result proves the accuracy of ANN prediction is superior to statistical methods [159]. Another ANN model with three layers and 17 inputs was developed to predict the air pollution levels of Chinese cities [160]. Additionally, many researchers also predicted the urban heat island effect by using ANN with the adequate input weather data [49, 50, 161, 162]. As an example, a previous study presented the applicability of ANN and learning paradigms for UHII prediction in Athens, Greece. The data of time, ambient temperature and global solar radiation are used to train and test the different models [163].

The performance of ANN model can be improved by normalizing data before training the model. The use of original data with large divergence may cause a convergence problem, because mixing variables with large magnitudes and small magnitudes will confuse the learning algorithm on the importance of each variable and may force it to finally reject the variable with the smaller magnitude [157]. The input parameter including air temperature, relative humidity and difference of relative humidity dataset, therefore, normalised in the range of [-1,1] by dividing the difference between the actual value x and the minimum value x_{min} by the difference between the maximum value x_{max} and the minimum value x_{min}, i.e.

$$x_{nor} = \frac{x - x_{min}}{x_{max} - x_{min}} \tag{7.1}$$

The main goal of data normalisation is to guarantee the quality of the data before it is fed to the learning algorithm. Furthermore, through combing with the weight initialisation, normalisation is to allow the squashed activity function to work at least at the beginning of the learning phase [163]. Normalisation is an effective strategy to avoid the gradient, which is the derivative of the non-linearity, being zero. At the end of each algorithm, the outputs should be transformed into its original data format.

7.2.1 ANN model design

In general, a complete ANN model consists of three main steps, such as the neural network design, learning or training process, and testing process. In this study, an ANN model was also appropriately designed and tested to predict the UHII based on the data collected in one year period from September 2012 to October 2013 in Ningbo city. The input parameters of the ANN model are all measured environmental and time data, as follows:

(a) Reference air temperature (°C) collected from the reference site
(b) Reference relative humidity (%) collected from the reference site
(c) Real relative humidity (%) collected from the target measurement site
(d) Difference of relative humidity (%) between the reference site and the target measurement site
(e) Date to represent the yearly climatic variations (the date is converted into the number of days starting from January 1^{st}) and ranges within [1,365]
(f) Hourly time to represent the solar position

Multi-layer feed-forward backprop neural network was selected in this study. The feed-forward neural network has all of the data information flows in one direction. The neurons of one later are connected with the neurons of the following layer and there is no feedback [163], as Fig. 7.1 shows. The ANN model was running based on the MATLAB toolbox with the version of 7.10.0.499 (R2010a) and the license number of 161051 [164].

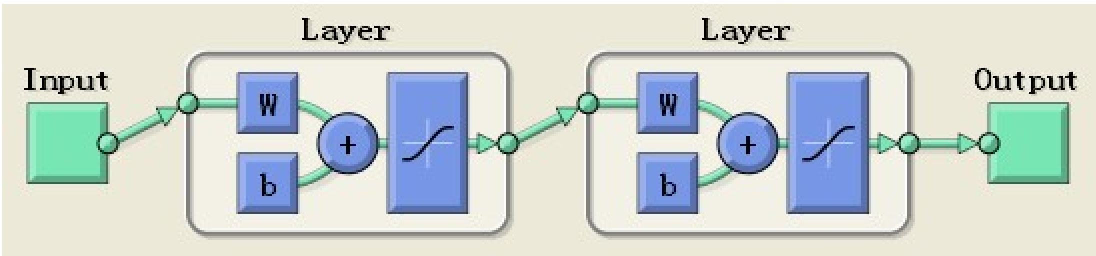

Fig. 7.1: The structure of neural network

7.2.2 The learning and training process of ANN model

For each difference neural network mode, the training function, adaption learning function, performance function, transfer function, hidden layers and number of neurons are key factors to determine the accuracy of prediction. The training process of this ANN prediction model is performed by using the data collected during the period from September 27th to December 21st, 2012. The neural network in this case was created by following characteristics:

Training function: Trainlm (*Trainlm is a network training function that updates weight and bias values according to Levenberg-Marquardt optimization. Trainlm is often the fastest back propagation algorithm in the toolbox, and is highly recommended as a first-choice supervised algorithm, although it does require more memory than other algorithms.*[165])

Adaption learning function: Learngdm *(Gradient descent with momentum weight and bias learning function* [165]*)*

Performance function: Mean squared normalized error performance function (MSE)

Number of hidden layers: 2

Number of neurons in Layer 1: 10

Transfer function of Layer 1: Logistic Sigmoid (Tansig) $f(x) = \frac{1}{1+e^{-x}}$

Transfer function of Layer 2: Logistic Sigmoid (Tansig) $f(x) = \frac{1}{1+e^{-x}}$

7.2.3 The testing process of ANN model

The purpose of the testing process is to examine the accuracy of the ANN prediction model. The scatter plot of test data is given in Fig. 7.2. It presents the ANN predicted UHII values versus the calculated UHII values of the site of Tianyi Square based on the data collected from September 27th to December 21st, 2012.

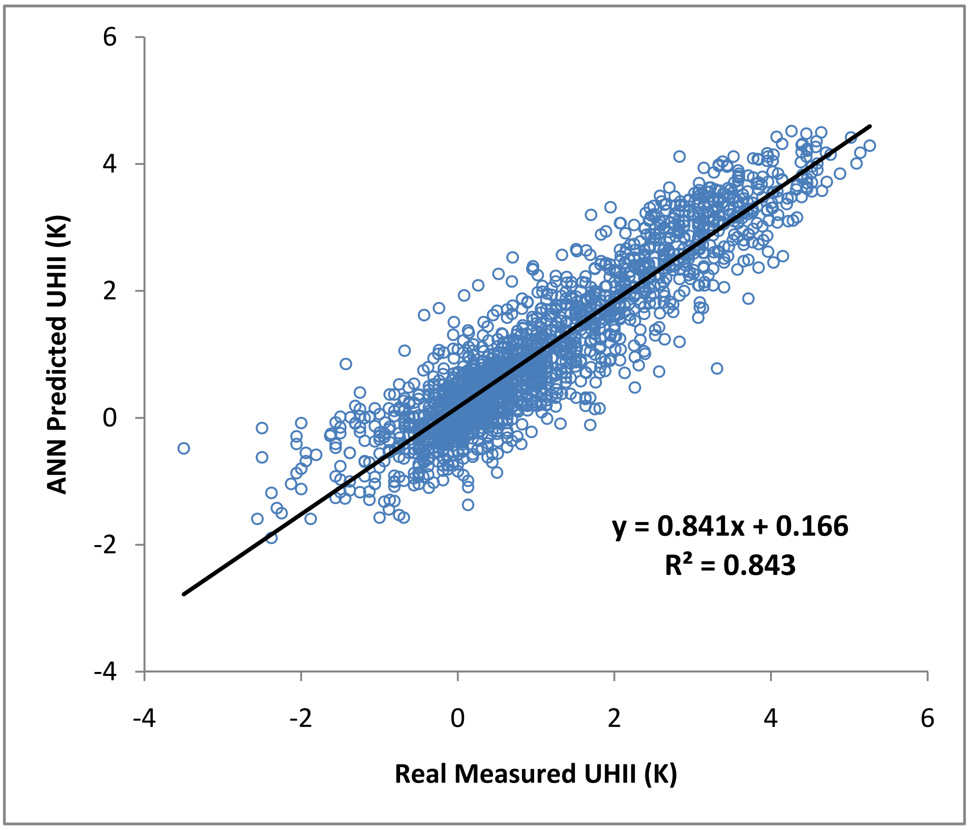

Fig. 7.2: Comparison between real measured UHII and ANN predicted UHII for Tianyi Square from September 27th to December 21st, 2012

The percentage error can be utilised to calculate the difference between the measured and the predicted UHII values (see equation 7.2). The mean percent error of ANN model is about 32.6%. Moreover, MSE is also used to examine the prediction accuracy of ANN, defined as equation 7.3. The result determined that the MSE of ANN model in this prediction case is about 0.32.

$$\text{Percent Error} = \frac{\text{Measured value} - \text{Predicted value}}{\text{Predicted value}} \times 100\% \tag{7.2}$$

$$\text{MSE} = \frac{\sum_{i=1}^{N}(\text{Measured value}_i - \text{Predicted value}_i)^2}{N} \tag{7.3}$$

Fig. 7.3 compares the measured UHII and ANN predicted UHII of the site of Tianyi Square in the month of October, 2012. Fig. 7.4 compares the measured hourly UHII and the predicted hourly UHII of the site of Tianyi Square on October 1st, 2012. The result presented in this study showed the feasibility of predicting UHII by using ANN model based on a limited data series.

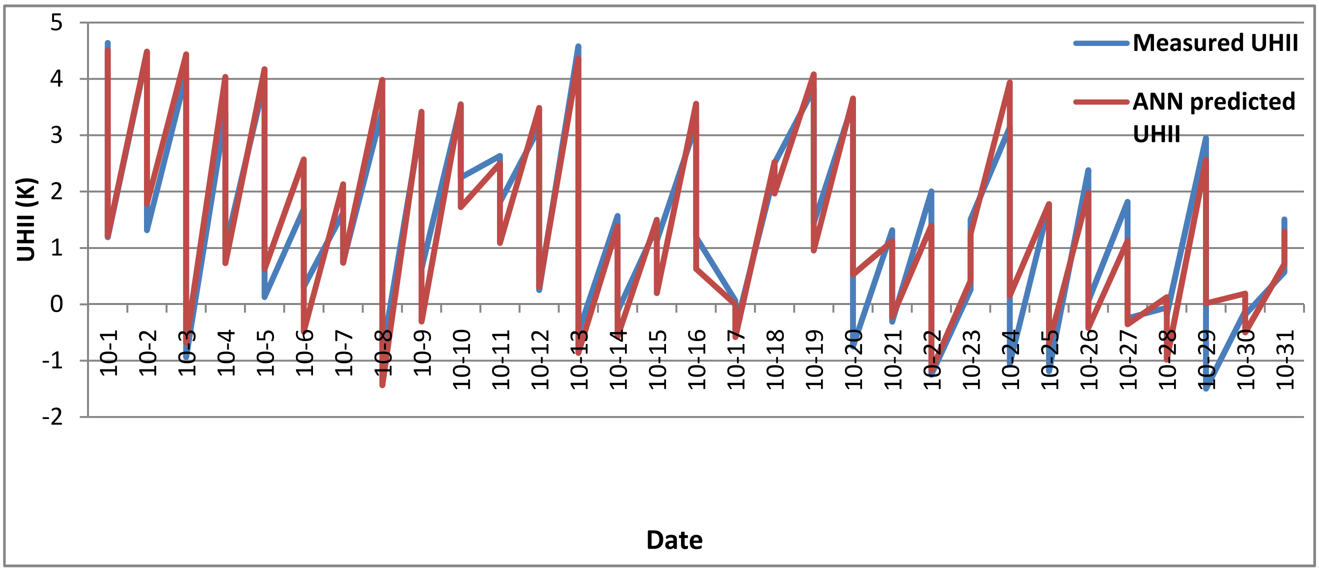

Fig. 7.3: Comparison between measured UHII and ANN predicted UHII of the site of Tianyi Square in October, 2012

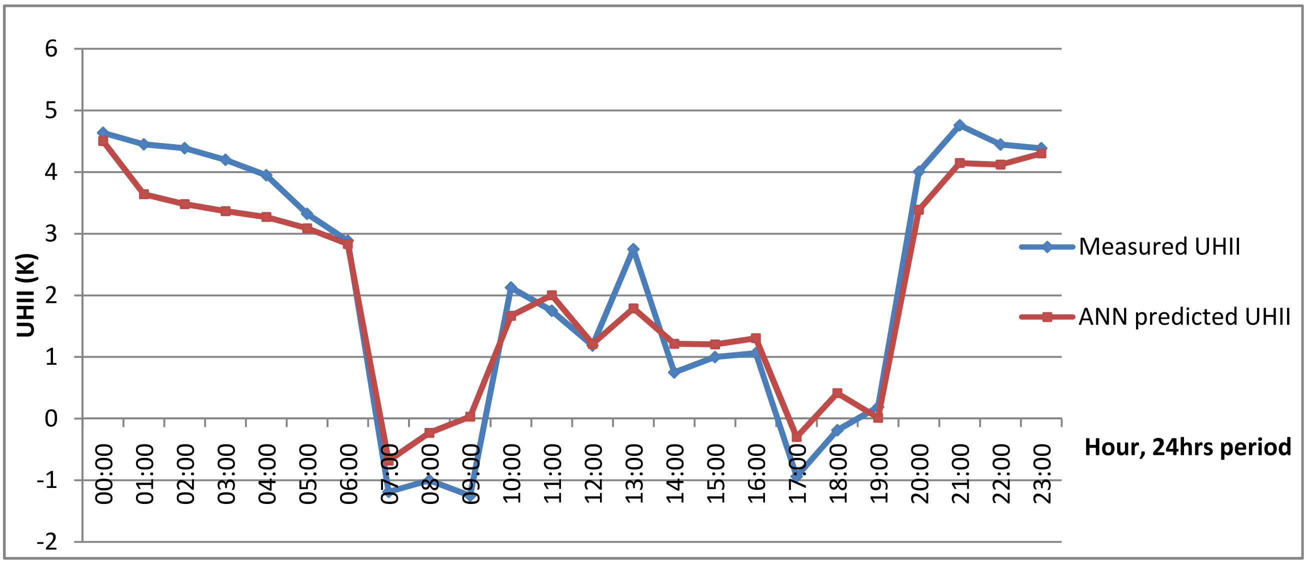

Fig. 7.4: Comparison between measured hourly UHII and ANN predicted hourly UHII of the site of Tianyi Square on October 1st, 2012

7.3 Genetic Programming (GP)

In addition to ANN model, modelling could also be carried out with another shared computational intelligence tool, namely genetic programming (GP). GP is an evolutionary computation (EC) technique inspired by biological processes. GP has been pronounced as a new strong soft computing technique to solve a wide range of modelling problems in recent years [166-169]. Unlike ANN models, the GP model can complete prediction without assuming any a priori structure of functions and relies on theoretically grounded factorization of data [170]. According to the literature review, the GP model is evaluated to be more powerful in prediction performance in smaller dataset owing to its higher diversity both in terms of the functional form as well as the variables defining the models [171].

A regression model over a series of generations and programmes based on the Darwinian principle of natural selection is involved in GP method [172]. After certain number of generations, GP can transform populations of programmes into new and better programmes. The general idea of GP is described as follows [168]: GP model starts with solving a problem by creating massive amount of simple random functions in a population pool, and then it runs each individual programme to evaluate the quality which is called the fitness. Next, one or two programme(s) will be probabilistically selected based on its fitness in order to participate the genetic operations. Normally there are two genetic operations, one is called crossover and another is called mutation. The crossover operation is used to create a new child programme (called offspring) by choosing some random parts from the two selected programmes (called parents) and combining them together. The mutation operation is used to create a new child programme by choosing some random parts from one selected programme and altering them. After the new individuals are created, their fitness will be calculated again, and the genetic operations will also be performed again. This whole process is repeated until an acceptable solution is found or other termination criterion is satisfied (usually up to some certain number of generations). The best individual will be returned as the solution. A typical GP system consists of the following components [168]:

Terminal Set: It is the inputs of the programme, which could be the variables, the constants or the functions with no arguments.

Function Set: It is the primitive functions used by the programme that consists of arithmetic operators (i.e. $+, -, \times, \div$) and mathematical functions (sin, cos, exp, ln, etc). GP model can select functions and terminals randomly and automatically to reach minimum error. The complexity of GP model is determined by function selection; for example, by selecting $(+, -)$ as a function one reaches to a linear model and by selecting (exp, sin,) one arrives at a non-linear model.

Fitness measure: It is used to evaluate the accuracy of the prediction model. There are many possible ways to calculate the fitness, for example it can be through the calculation of the error between the output of the programme and the desired output, or through the calculation of the accuracy of the programme in recognizing patterns. As an example, equation 7.4 can be accepted as a simple fitness function.

$$\text{fitness} = \sum_{i=1}^{N} |\text{target values} - \text{ouput values}| \tag{7.4}$$

GP parameters: These are used to control the whole GP system. Some common parameters include the population size, the maximum programme size.

Termination criterion: Usually it is a desired solution found, or the maximum number of generations reached.

7.3.1 GP model design

In this research, GP model is applied to predict the UHII values based on the data collected in the period from September to December, 2012 in Ningbo as well. GP model uses the function set specified in Tab. 7.1 randomly. The prediction of GP model is generated by best programme that is obtained after several generations. In contrast to ANN model, the input parameters in GP model are different. GP model employs the urban design related parameters as input data instead of environmental parameters used in ANN model. Basically, the GP prediction model runs relied on the following function (equation 7.5):

$$f(\boldsymbol{x}_1,\ \boldsymbol{x}_2,\ \boldsymbol{x}_3,\ \boldsymbol{x}_4,\ \boldsymbol{x}_5) = \text{UHII} \tag{7.5}$$

where$\boldsymbol{x}_{1,..,5}$ denote the input parameters, including land-use, distance from city centre, sky view factor (SVF), surrounding albedo and relative humidity respectively. The structure

Other related characteristics of this GP prediction model can be observed in Tab. 7.1. As mentioned before, GP method performs more accurate in handling small size of dataset. For each month, this study trains the GP model individually. Because it has been validated that UHI effect has different performances in day time or night time, the GP model was proposed to run different functions according to the selection of day time or night time. The basic structure of GP prediction model in this study is displayed by Fig. 7.5. The input parameters such as Time, Land-use, Distance from

City Centre, SVF, Albedo and relative humidity, are desired to predict the UHII of a specific site,

Tab. 7.1: GP prediction model parameters

Parameter name	Parameter specification
Terminal set	$\boldsymbol{x}_1 - \boldsymbol{x}_5$ and one random constant are in the range of [−3, 3].
Function set	$+, -, \times, \div, \%, \mathrm{abs}$ (Protected division, the denominator cannot be 0).
Fitness measure	The difference between the actual result and the computed result
Termination criterion	The fitness measure is 0 or up to 100 generations.
Population size	500
The maximum length of the programme	1000
Probability of mutation operation	80%
Probability of crossover operation	10%

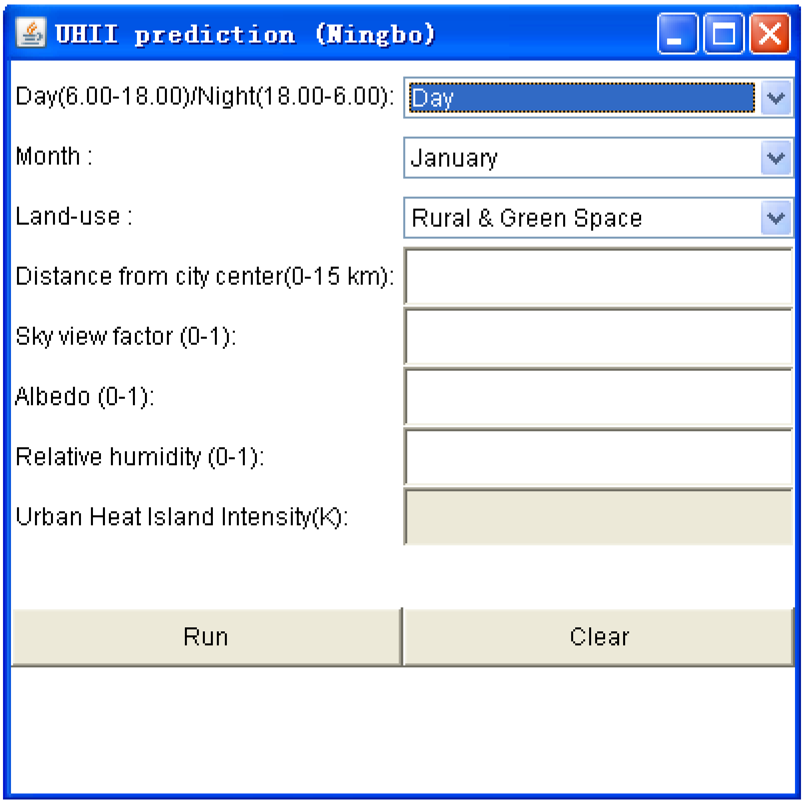

Fig. 7.5: The structure of UHII prediction GP model

7.3.2 Results

The GP approach was tested and developed for predicting the UHII values by applying C language programming. As mentioned before, GP method performs more accurate in handling small size of dataset. The whole-year collected data was initially divided into twelve months, afterwards, each month data was again divided into day time and night time data. For each group of data, this study trains the GP model individually. There is a simplified GP generated function for the data collected during day time in October, see as below:

$$UHII = (X4 * ((X2 - ((X1 - X5) * X4)) - (X2 * ((X3 * (X5 - (((((((X4 * X5) * ((X3 *$$

$$((X4 + X5) + (X5 / X2))) * (((X4 / X3) * (X4 * X2)) * ((X2 - (X4 * X4)) - (X1 * X1))))) / X4) / X4) - (X1 * ((((X1 / X4) + X2) / ((((X4 * (((X4 * X4) - (((((X5 + ((X2 * X5) - X4)) - X5) * (((((((((X3 - X2) * (X5 + (X5 * X2))) - X4) * X4) * (X4 / (X2 / (X3 / X1)))) / ((X3 + ((X5 * X1) / (X1 + X5))) + X2)) + (((X2 - X2) - X4) / ((X4 / (X5 + ((0.53 + (((X4 / X3) + X1) / ((X4 * X1) / X4))) / (X2 * (0.53 / X2))))) - (X5 * X2)))) * (X4 * X4)) * (((X1 / X4) + X2) / (X5 - 0.53))) * (X1 * X4))) * X4) - X3)) * ((X2 - (X4 * X4)) - (X1 * X1)))) * X4) / (((0.53 - X4) * X3) + ((X5 * X3) + X4))) - (X5 / 0.53))) / (X3 + X3)))) + (((X3 * X1) + (X2 + X3)) * X1)) - X4))) / ((((X1 / X4) + X2) / (X2 / ((((X1 * (((((X5 / X5) / ((((((X5 * (X4 / X2)) / (X1 + X2)) + X4) / X3) + X1) + X1)) - (((0.53 / X4) / (X5 * X1)) - X1)) / (((X5 - 0.53) * (X5 * X2)) + X4)) - X4)) + X1) * X2) / ((X4 * X4) - (((((0.53 - X5) / ((X2 / X4) - (X1 * X2))) * ((((((((((((X1 / X4) + X2) / (X5 - 0.53)) - (((X1 * ((X4 / X4) / (X3 + X3))) / ((((X3 + X3) * X4) / (((0.53 - X4) * X3) + ((X5 * X3) + X4))) \ldots \qquad (7.6)$$

The scatter plot of test data collected at day time and night time are given in Fig. 7.6 and Fig. 7.7 respectively. Linear fit line function with $y = C_1x + C_2$ is applied to validate the accuracy of GP model in the figure. The GP model can be proved with higher accuracy, if the closer the linear fit line function gets to $y = x$ and the determination coefficient value of R^2 approaches 1. One result that can be inferred from comparing Fig 7.6 and Fig. 7.7 is that the accuracy of GP model predicting night time dataset is higher than predicting day time dataset, because the night time UHII values are more remarkable.

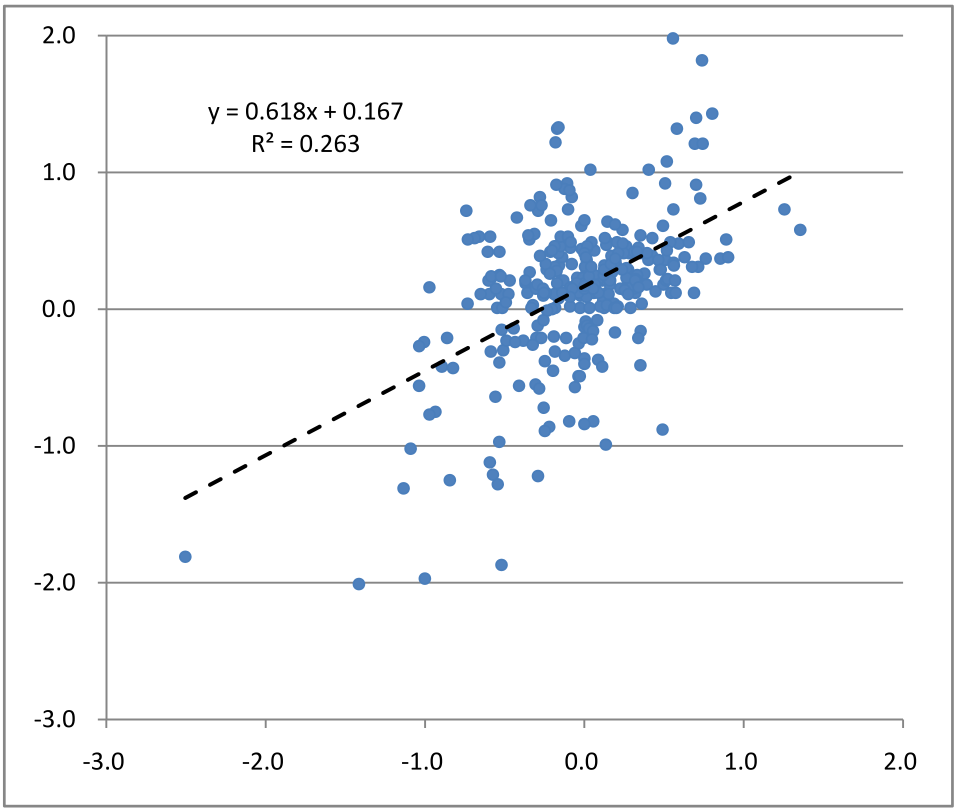

Fig. 7.6: Observed versus predicted day time UHII of Ningbo measurement sites

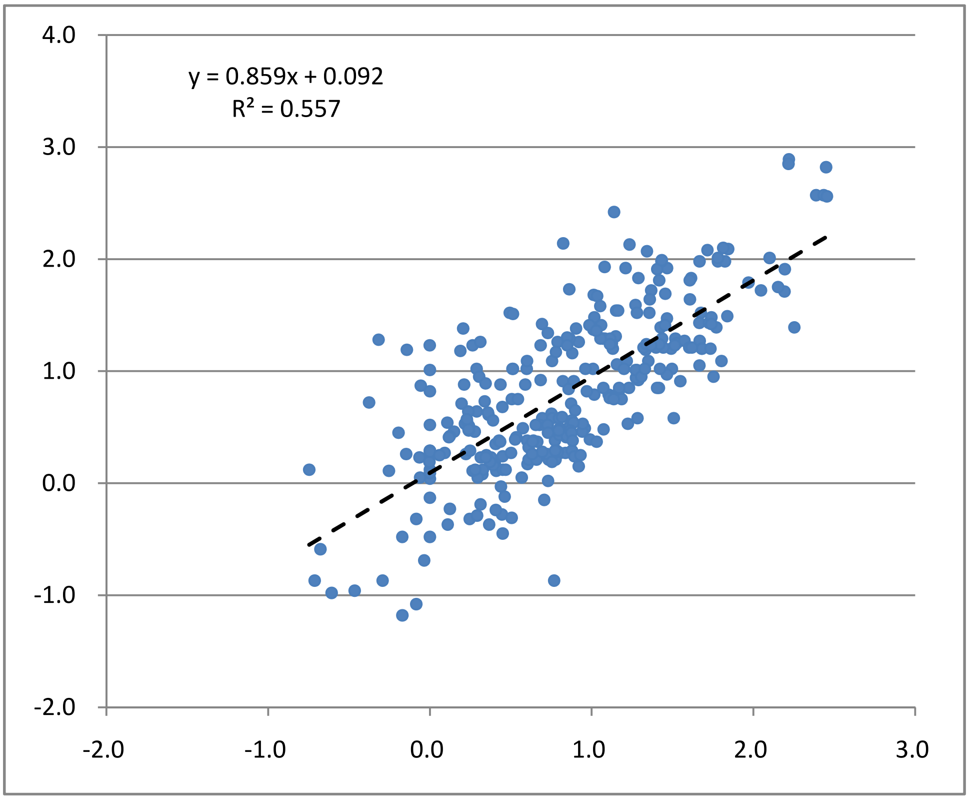

Fig. 7.7: Observed versus predicted night time UHII of Ningbo measurement sites

7.4 Concluding remark

This chapter has applied artificial neural network (ANN) and genetic programming (GP) models to predict UHII based on the data collected from field measurement. The good agreement between the prediction and the measured data demonstrated their capability of approximating nonlinear relations. The mean percent error of ANN model is about 32.6% and the MSE of ANN model is about 0.32. Regarding GP model, the index of agreement (IA = 0.618 or 0.859) and the coefficient of determination (R^2 = 0.263 or 0.557) indicate an acceptable satisfactory relationship between the forecasted and observed values as well.

CHAPTER 8: CONCLUSION AND FUTURE WORK

8.1 Conclusion

An extensive literature review has been carried out to study UHI effect. It can be concluded that UHI is a universal problem that exists in Hangzhou and Ningbo cities. The UHI effects in both two cities have been investigated by the field measurement method which applies i-Button data loggers to measure air temperature and relative humidity at strategically selected sites. This study has also addressed challenges of interpreting collected weather data and found a possible solution to interpolate missing and false weather data in this research. The observation has determined that the UHI effect in Hangzhou is more intense than that in Ningbo. The monthly average UHII values in Hangzhou ranged between 1℃ and 4℃, whilst the highest monthly average UHII in Ningbo is only as high as 1.5℃.

The main reason for the emerging of UHI is because the rapid urbanisation process causing the change of natural landscape and environment. According to the ENVI-met simulation, the natural ecological resources like West Lake and Xixi Wetland, can act as passive thermal comfort systems in improving the outdoor environment and mitigating the UHI effect in Hangzhou.

This study has examined how UHI effect impacted by urban design factors, such as land-use, distance from city centre, surrounding albedo and sky view factor (SVF). Additionally, the study has evaluated that the UHI effect is most pronounce in winter days, because there is serious air pollution, high concentration of Particulate Matter (PM) and low wind speed in winter days in China. The result has also proved that there is a diurnal variation of UHI effect in day time and night time. The night time UHI effect is significantly more intense than the day time UHI effect. The main causes of UHI formation are defined as the decreased long-wave radiation loss and the increased release of heat stored in urban materials. Referring to the impacts of other meteorological parameters on UHI effect, for instance, the UHII variation has been determined to be inversely proportional to the relative humidity. Solar radiation and cloud cover are critical factors that can influence the formation of UHI situation as well. It can surmise that the synoptic weather patterns that involve stable weather with strong solar radiation, high visibility and a cloudless sky are suitable for UHI development.

The study has also evaluated how vegetation cover, urban building configuration and material properties, and human activities contribute to UHI formation. Though UHI effect is unavoidable, there are feasibilities to reduce its impact on urban environment. The study has suggested to mitigating UHI effect by three effective strategies, involving the application of cool materials on urban surfaces, modifying urban geometry to improve wind flow and expanding green space in urban areas.

The main task of scholars studying in this field is to prevent the problems related to UHI from increasing the building energy consumption and the amount of CO_2

emissions. According to the analysis in this study, the urban building energy consumption would be increased by UHI effect in two aspects. In the first way, UHI effect has the capacity to increase urban building cooling energy demand in summer as the urban local microclimate is warmed by UHI effect. In the other way, because the currently available weather dataset used in building simulation software mainly comes from weather stations located in remote and rural areas, the urban buildings would be inappropriately designed based on the currently available weather dataset without considering the impact of UHI. Thus, the designed urban buildings are inability to adapt the real local micro climate and may require more energy demands.

Owing to the hourly air temperature and relative humidity collected from sites around the city, modified TMY weather dataset has been developed. The study has revealed that the cooling demand in a typical office building located in urban area of Hangzhou city will be underestimated and its heating demand will be overestimated if the currently available TMY weather dataset applied. Building energy simulation has been performed to evaluate the cooling and heating loads of a modelled office building. It determines that there is about a 20% increase in the cooling demand in the hot months and a 25% decrease in the heating demand in the cold months for the office building located in urban areas as compared to buildings in rural areas. The result has also implied that there is a great potential to reduce the building energy consumption as well as greenhouse gas emission considerably by various UHI mitigation strategies.

Based on the existing measured data, artificial neural network (ANN) and genetic programming (GP) techniques have been used for the prediction of UHII in this study. The good agreement between the prediction and the measured data demonstrated their capability of approximating nonlinear relations. The mean percent error of ANN model is about 32.6% and the MSE of ANN model is about 0.32. Regarding GP model, the index of agreement (IA = 0.618 or 0.859) and the coefficient of determination (R^2 = 0.263 or 0.557) indicate an acceptable satisfactory relationship between the forecasted and observed values as well.

In general, the accurate awareness of the existence of UHI effect and positively remedying the UHI effect are indispensible for saving urban building energy consumptions and improving the living environment in Hangzhou and Ningbo.

8.2 Future work

The research carried out in this thesis revealed some unsolved problems and new tasks about UHI study. Further research would involve following aspects:

- It is significant to promote this research methodology to other parts of China where the climate is unlike Zhejiang province. The promotion work will examine the UHI effect in different parts of China and may find out more particular relationships between UHI development and local climate and urbanisation.

- The study has evaluated that parameters, such as wind speed and solar radiation, have critical impacts on UHI development. However, due to the lack of equipments, those two important parameters have not been measured simultaneously with air temperature and relative humidity. In general, there is a need to identify the impacts of wind speed and solar radiation on UHI effect based on the accurate field measurement data.

- Because the impact of UHI effect on urban building energy consumption is only simulated by software in this research and the simulated result has not been validated by real measurement, the study suggests to observe the actual energy consumption of an example urban building in future. The observed result can not only evaluate the accuracy of the simulation model, but also support improving the energy efficiency of buildings.

- The accuracy of prediction model for UHII can be noticeably improved by advanced ANN model or GP model. The advanced model requires more input parameters and computations, therefore the advanced can be a bit more time consuming to initialize. However, the advantages of the advanced model will greatly outweigh its drawbacks. The better agreement between the prediction made by advanced model and the measured data can be clearly demonstrated.

- The prediction of the UHI distribution is possible through the simulation of the current situation in an urban area. Therefore, it is feasible to create a UHI map that can help to distinguish the vulnerable regions of a city in further research.

REFERENCES

1. CIA. *The World Factbook*. 2013 Apr 19, 2013; Available from: https://www.cia.gov/library/publications/the-world-factbook/fields/2212.html.
2. Fortuniak, K., K. Kłysik, and J. Wibig, *Urban–rural contrasts of meteorological parameters in Łódź.* Theoretical and Applied Climatology, 2006. **84**(1-3): p. 91-101.
3. Song, F., et al., *METEOROLOGICAL DATA SET FOR BUILDING THERMAL ENVIRONMENT*, in *Building Simulation*. 2007. p. 9-16.
4. xiong;, A., et al., eds. *Meteorological data set for building thermal environment analysis in China*. 2005, China Architecture & Building Press: Beijing. 165.
5. *Regulation on the Protection of Meteorological Facilities and Meteorological Observation Environment*, in *Order No. 623 of the State Council*, S. Council, Editor. 2012: Beijing.
6. *Zhejiang Statistical Yearbook*. 2013, Beijing: China Statistics Press.
7. *Top 10 hottest cities in China*, in *China Polotical & Defence Forum*. 2010.
8. Yao, J. and N. Zhu, *Enhanced supervision strategies for effective reduction of building energy consumption—A case study of Ningbo.* Energy and Buildings, 2011. **43**(9): p. 2197-2202.
9. Howard, L., ed. *The Climate of London*. Gerald Mills ed. Vol. 2&3. 1833, International Association for Urban Climate. 700.
10. Mills, G., *Luke Howard and The Climate of London.* Weather, 2008. **63**: p. 153-157.
11. Yeon-Hee, K.I.M. and B. Jong-Jin, *Spatial and temporal structure of the urban heat island in Seoul.* Journal of applied meteorology (1988), 2005. **44**(5): p. 591-605.
12. Magee, N., J. Curtis, and G. Wendler, *The Urban Heat Island Effect at Fairbanks, Alaska.* Theoretical and Applied Climatology, 1999. **64**(1-2): p. 39-47.
13. Arrau, C.P. and M.A. Peña. *URBAN HEAT ISLANDS (UHIs)*. 2010 August 26, 2011; Available from: http://www.urbanheatislands.com/.
14. Rizwan, A.M., L.Y.C. Dennis, and C. Liu, *A review on the generation, determination and mitigation of Urban Heat Island.* Journal of Environmental Sciences, 2008. **20**(1): p. 120-128.
15. Harman, I.N., *The energy balance of urban areas*, in *Department of Meteorology*. 2003, The University of Reading: Reading. p. 169.
16. Oke, T.R., *The urban energy balance.* Progress in Physical Geography, 1988. **12**(4): p. 471-508.
17. Sass, R.L. *IT'S NOT COOL TO BE HOT IN HOUSTON*. [cited 2013; Available from: http://www.ruf.rice.edu/~sass/UHI.html.
18. Harman, I.N. and S.E. Belcher, *The surface energy balance and boundary layer over urban street canyons.* Q. J. R. Meteorol. Soc., 2006. **132**: p. 2749–2768.
19. Monteith, J.L., *Evaporation into the atmosphere: Theory, history and applications, Wilfried H. Brutsaert, D. Reidel Publishing Co., 1982. No. of pages; vii-299. Price: $34.95.* Journal of Climatology, 1983. **3**(2): p. 213-213.
20. Swinbank, W.C., *Long-wave radiation from clear skies.* Quarterly Journal of the Royal Meteorological Society, 1963. **89**(381): p. 339-348.
21. B. OFFERLE, C.S.B. GRIMMOND, and K. FORTUNIAK, *HEAT STORAGE AND ANTHROPOGENIC HEAT FLUX IN RELATION TO*

THE ENERGY BALANCE OF A CENTRAL EUROPEAN CITY CENTRE. INTERNATIONAL JOURNAL OF CLIMATOLOGY, 2005. **25**: p. 1405-1419.

22. HOSLER, C.L. and H.E. LANDSBERG, *The effect of localized man-made heat and moisture sources in mesoscale weather modification.* Energy and Climate, 1977.
23. Taha, H., *Urban climates and heat islands: albedo, evapotranspiration, and anthropogenic heat.* Energy and Buildings, 1997. **25**: p. 99-103.
24. Oke, T.R., *Boundary layer climates 2nd Edition*. 1987, Cambridge: University press.
25. GRIMMOND, C.S.B. and T.R. OKE, *Heat Storage in Urban Areas: Local-Scale Observations and Evaluation of a Simple Model.* Journal of Applied Meteorology, 1999. **38**: p. 922-940.
26. Schmugge, T., *ASTER observations for the monitoring of land surface fluxes*, in *Geoscience and Remote Sensing*. 1997, IEEE International p. 1236-1238.
27. Berliner, P.R., *Contribution of heat dissipated at the soil surface to the energy balance of a citrus orchard*. 1988: Hebrew University of Jerusalem.
28. ROBERTS, S.M., et al., *Comparison of four methods to estimate urban heat storage.* JOURNAL OF APPLIED METEOROLOGY AND CLIMATOLOGY, 2006. **45**: p. 1766-1781.
29. Grimmond, C.S.B., H.A. Cleugh, and T.R. Oke, *An objective urban heat storage model and its comparison with other schemes.* Atmospheric Environment. Part B. Urban Atmosphere, 1991. **25**(3): p. 311-326.
30. Masson, V., *A Physically-Based Scheme For The Urban Energy Budget In Atmospheric Models.* Boundary-Layer Meteorology, 2000. **94**(3): p. 357-397.
31. Peikorz, G., *Die Energiebilanz einer stadtischen Struktur*, in *Department of Meteorology*. 1987, Rheinische Friedrich-Wilhelms-Universität,: Bonn, German.
32. Pigeon, G., et al., *SEA-TOWN INTERACTIONS OVER MARSEILLE – PART II : CONSEQUENCES ON ATMOSPHERIC STRUCTURE NEAR THE SURFACE.* Theoretical and Applied Climatology, 2003. **84**: p. 171-178.
33. Wong, N.H. and C. Yu, *Study of green areas and urban heat island in a tropical city.* Habitat International, 2005. **29**(3): p. 547-558.
34. Giridharan, R., S.S.Y. Lau, and S. Ganesan, *Nocturnal heat island effect in urban residential developments of Hong Kong.* Energy and Buildings, 2005. **37**(9): p. 964-971.
35. Schwarz, N., S. Lautenbach, and R. Seppelt, *Exploring indicators for quantifying surface urban heat islands of European cities with MODIS land surface temperatures.* Remote Sensing of Environment, 2011. **115**(12): p. 3175-3186.
36. Giridharan, R. and M. Kolokotroni, *Urban heat island characteristics in London during winter.* Solar Energy, 2009. **83**(9): p. 1668-1682.
37. Huang, J., R. Wang, and Y. Shi, *Urban climate change: A comprehensive ecological analysis of the thermo-effects of major Chinese cities.* Ecological Complexity, 2010. **7**(2): p. 188-197.
38. Gu, C., et al., *Climate change and urbanization in the Yangtze River Delta.* Habitat International, 2011. **35**(4): p. 544-552.
39. Skinner, M.W., R.G. Kuhn, and A.E. Joseph, *Agricultural land protection in China: a case study of local governance in Zhejiang Province.* Land Use Policy, 2001. **18**(4): p. 329-340.
40. Hua, Y. and D. Wei, *Restructing for growth in urban China: Transitional institutions, urban development, and spatial transformation.* ScienceDirect, 2012.
41. *Statistical yearbook of Hangzhou*. 2011, Beijing: China Statistical Press.

42. Huang, C., et al., *Relevance Analysis of Hangzhou Hot Island Effect and Urban Functional Layout*. 2011, Zhejiang University of Technology: Hangzhou.
43. Liu, R.Z. and A.G.L. Borthwick, *Measurement and assessment of carrying capacity of the environment in Ningbo, China.* Journal of Environment Management, 2011: p. 2047-2053.
44. *Ningbo 2011 population report issued*, in *Ningbo Government*. 2011.
45. *Ningbo Statistical Yearbook 2011*. 2011, Ningbo: China Statistics Press.
46. Tang, Y.-T., F.K.S. Chan, and J. Griffiths, *City profile: Ningbo.* Cities, 2015. **42, Part A**: p. 97-108.
47. Ding, Y., Y. Chen, and H. Huang, *Characteristics of Urban Heat Island Intensity Changes in Ningbo* 2006, Ningbo Meterological Bureau: Ningbo.
48. Chen, Y., et al., *Research on Urban Spatial Thermal Environment Using Remotely Sensed Data*. 2004, Beijing Normal University Beijing.
49. GIOULI MIHALAKAKOU, et al., *Application of Neural Networks to the Simulation of the Heat Island over Athens, Greece, Using Synoptic Types as a Predictor.* Journal of Applied Meteorology, 2002. **41**(5): p. 519-527.
50. Kolokotroni, M., et al., *A validated methodology for the prediction of heating and cooling energy demand for buildings within the Urban Heat Island: Case-study of London.* Solar Energy, 2010. **84**(12): p. 2246-2255.
51. Sundborg, Å., *Local Climatological Studies of the Temperature Conditions in an Urban Area.* Tellus, 1950. **2**(3): p. 222-232.
52. Saitoh, T. and I. Yamada. *Effect Of Energy Consumption On Urban Atmosphere*. in *Energy Conversion Engineering Conference, 1990. IECEC-90. Proceedings of the 25th Intersociety*. 1990.
53. Saitoh, T.S., T. Shimada, and H. Hoshi, *Modeling and simulation of the Tokyo urban heat island.* Atmospheric Environment, 1996. **30**(20): p. 3431-3442.
54. Li, J.-j., et al., *Remote sensing evaluation of urban heat island and its spatial pattern of the Shanghai metropolitan area, China.* Ecological Complexity, 2009. **6**(4): p. 413-420.
55. Wooster, M. (2011) *Introduction to Urban Remote Sensing*. Environmental Monitoring & Modelling Research Group.
56. Tran, H., et al., *Assessment with satellite data of the urban heat island effects in Asian mega cities.* International Journal of Applied Earth Observation and Geoinformation, 2006. **8**(1): p. 34-48.
57. Chen, X.-L., et al., *Remote sensing image-based analysis of the relationship between urban heat island and land use/cover changes.* Remote Sensing of Environment, 2006. **104**(2): p. 133-146.
58. Mirzaei, P.A. and F. Haghighat, *Approaches to study Urban Heat Island - Abilities and limitations.* Building and Environment, 2010: p. 2192-2201.
59. Hu, Z., et al., *Numerical investigation on the urban heat island in an entire city with an urban porous media model.* Atmospheric Environment, 2011(0).
60. Mochida, A., et al., *CFD analysis of mesoscale climate in the Greater Tokyo area.* Journal of Wind Engineering and Industrial Aerodynamics, 2004. **67-68**(0): p. 459-477.
61. Fahmy, M. and S. Sharples, *On the development of an urban passive thermal comfort system in Cairo, Egypt.* Building and Environment, 2009: p. 1907-1916.
62. Takahashi, K., et al., *Measurement of thermal environment in Kyoto city and its prediction by*

CFD simulation. Energy and Buildings, 2004. **36**(8): p. 771-779.

63. Erell, E. and T. Williamson, *Simulating air temperature in an urban street canyon in all weather conditions using measured data at a reference meteorological station.* International Journal of Climatology, 2006. **26**(12): p. 1671-1694.
64. Bruse, M. and H. Fleer, *Simulating surface–plant–air interactions inside urban environments with a three dimensional numerical model.* Environmental Modelling & Software, 1998. **13**(3–4): p. 373-384.
65. Fahmy, M. and S. Sharples, *On the development of an urban passive thermal comfort system in Cairo, Egypt.* Building and Environment, 2009. **44**(9): p. 1907-1916.
66. Okeil, A., *A holistic approach to energy efficient building forms.* Energy and Buildings, 2010. **42**(9): p. 1437-1444.
67. Thapar, H. and S. Yannas, *Microclimate and Urban Form in Dubai*, in *PLEA 2008 – 25th Conference on Passive and Low Energy Architecture*. 2008: Dublin.
68. Hedquist, B.C., et al., *RESULTS FROM THE PHOENIX ARIZONA URBAN HEAT ISLAND EXPERIMENT*, in *The seventh International Conference on Urban Climate*. 2009: Yokohama, Japan.
69. Kolokotroni, M., et al., *London's urban heat island: Impact on current and future energy consumption in office buildings.* Energy and Buildings, 2012(0).
70. Agarwal, M. and A. Tandon, *Modeling of the urban heat island in the form of mesoscale wind and of its effect on air pollution dispersal.* Applied Mathematical Modelling, 2010: p. 2520-2530.
71. Su, Y., G.M. Foody, and K. Cheng, *Spatial non-stationarity in the relationship between land cover and surface temperature in an urban heat island and its impacts on thermally sensitive populations.* Landscape and Urban Planning, 2012: p. 172-180.
72. Lin, C.-Y., et al., *Urban heat island effect and its impact on boundary layer development and land–sea circulation over northern Taiwan.* Atmospheric Environment, 2008. **42**(22): p. 5635-5649.
73. Mirzaei, P.A. and F. Haghighat, *Approaches to study Urban Heat Island – Abilities and limitations.* Building and Environment, 2010. **45**(10): p. 2192-2201.
74. Ali-Toudert, F. and H. Mayer, *Numerical study on the effects of aspect ratio and orientation of an urban street canyon on outdoor thermal comfort in hot and dry climate.* Building and Environment, 2006. **41**(2): p. 94-108.
75. Yang, X., et al., *Evaluation of a microclimate model for predicting the thermal behavior of different ground surfaces.* Building and Environment, 2013. **60**(0): p. 93-104.
76. Wu, K.-y., et al., *Impacts of land use/land cover change and socioeconomic development on regional ecosystem services: The case of fast-growing Hangzhou metropolitan area, China.* Cities, 2013. **31**(0): p. 276-284.
77. *Hangzhou General Planning Map*. 2006, Hangzhou Academy of Urban Planning & Design: Hangzhou, China.
78. Figuerola, P.I. and N.A. Mazzeo, *Urban-rural temperature differences in Buenos Aires.* International Journal of Climatology, 1998. **18**(15): p. 1709-1723.
79. Kidder, S.Q. and O.M. Essenwanger, *The Effect of Clouds and Wind on the Difference in Nocturnal Cooling Rates between Urban and Rural Areas.* Journal of Applied Meteorology,

1995. **34**(11): p. 2440-2448.

80. Lee, D.O., *The influence of atmospheric stability and the urban heat island on urban-rural wind speed differences.* Atmospheric Environment (1967), 1979. **13**(8): p. 1175-1180.

81. Memon, R.A. and D.Y.C. Leung, *Impacts of environmental factors on urban heating.* Journal of Environmental Sciences, 2010. **22**(12): p. 1903-1909.

82. Bady, M., et al., *An experimental investigation of the wind environment and air quality within a densely populated urban street canyon.* Journal of Wind Engineering and Industrial Aerodynamics, 2011. **99**(8): p. 857-867.

83. *Ningbo General Planning Map (2004-2020)*. 2003, Ningbo Urban Planning Bureau: Ningbo, China.

84. Maxim, *DS1923 iButton Hygrochron Temperature/Humidity Logger with 8KB Data-Log Memory*. 2013, Maxim Integrated Products, Inc.: San Jose, USA.

85. MAXIM, *International Certificare of Validation*. 2011, Dallas.

86. Cheung, H.K., G.J. Levermore, and R. Watkins, *A low cost, easily fabricated radiation shield for temperature measurements to monitor dry bulb air temperature in built up urban areas.* Building Services Engineering Research and Technology, 2010. **31**(4): p. 371-380.

87. Integrated, M. *iButton Temperature / Humidity Logger with 8 kb Data Logger Memory*. Available from: http://www.maximintegrated.com/products/ibutton/data-logging/.

88. Oke, T.R., *Initial Guidance To Obtain Representative Meteorological Observations at Urban Sites*`. Instruments and observing methods (WMO/TD-No. 1250), 2006. **47**.

89. Organisation, W.M., *Guide to Meteorological Instruments and Methods of Observation. Sixth Edition*, in *WMO-No. 8*. 1996: Geneva.

90. Steremberg, A., J. Masters, and T. Skinner. *Hangzhou Weather Data from Xiaoshan International Airport's WMO-listed Weather Station*. The Weather Underground [cited 2013; Available from: http://www.wunderground.com/.

91. Zhang, Q.Y., Y.J. Huang, and S.W. Lang, *Development of typical year weather data for Chinese locations.* Transactions of the American Society of Heating, Refrigerating and Air-Conditioning Engineers, Inc., 2002. **108, Part 2**.

92. Chun-ye, W. and Z. Wei-ping, *Analysis of the Impact of Urban Wetland on Urban Temperature Based on Remote Sensing Technology.* Procedia Environmental Sciences, 2011. **10, Part B**(0): p. 1546-1552.

93. Xu, M. and D. Guo, *Research on characteristics of ecological system in floodplain wetlands of Fen River and*
its protection. Sci/Tech Information Development & Economy, 2005. **21**(15): p. 2.

94. Agency, U.S.E.P. *Reducing Urban Heat Islands: Compendium of*
Strategies (1-6). 2008; Available from: http://www.epa.gov/heatisld/resources/pdf/compendium.htm.

95. Kolokotroni, M. and R. Giridharan, *Urban heat island intensity in London: An investigation of the impact of physical characteristics on changes in outdoor air temperature during summer.* Solar Energy, 2008. **82**(11): p. 986-998.

96. Chen, F., X. Yang, and W. Zhu, *WRF simulations of urban heat island under hot-weather synoptic conditions: The case study of Hangzhou City, China.* Atmospheric Research, 2014. **138**(0): p. 364-377.

97. Zhu, C., *Zhejiang Statistical Yearbook 2013*. 2013, Beijing: China Statistics Press.

98. Guoping, H. 2013 [cited 2013; Available from: http://www.nbqx.gov.cn/.

99. Fan, H. *The announcement of the construction prgramme with Termial 2 of Ningbo Lishe International Aiprot* 2013 [cited 2014; Available from: http://news.cnnb.com.cn/system/2013/07/04/007771878.shtml.

100. Wu, K.-y. and H. Zhang, *Land use dynamics, built-up land expansion patterns, and driving forces analysis of the fast-growing Hangzhou metropolitan area, eastern China (1978–2008).* Applied Geography, 2012. **34**(0): p. 137-145.

101. NASA. *Landsat Science*. 2013 July 31, 2013; Available from: http://landsat.gsfc.nasa.gov/.

102. Chen, F., et al., *Recovering of the thermal band of Landsat 7 SLC-off ETM+ image using CBERS as auxiliary data.* Advances in Space Research, 2011. **48**(6): p. 1086-1093.

103. NASA. *Landsat 7 Science Data Users Handbook*. 2011 March 11, 2011; Available from: http://landsathandbook.gsfc.nasa.gov/.

104. WeatherSpark. *Historical Weather*. Available from: http://weatherspark.com/.

105. *2012 Statistics Bulletin of the National Economic and Social Development of Haishu District*. 2013 [cited 2013 June 6]; Available from: http://www.nbhstj.gov.cn/info.aspx?id=251415.

106. *Ningbo Marine Economy Development Plan (2006-2010)*. 2007, Ningbo Municipal Government: Ningbo.

107. *Ningbo 12th Five Year Marine Economy Development Plan*. 2011, Ningbo Development and Reform Commission: Ningbo p. 1-56.

108. *Hangzhou Statistical Year Book 2012*. 2012, Hangzhou Municipal Statistics Bureau: Hangzhou.

109. *Ningbo Population Development* Ningbo China 2014; Available from: http://gtoc.ningbo.gov.cn/art/2014/3/10/art_10478_1070471.html.

110. Stull, R., *Meteorology for scientists and engineers, 2nd ed.* 2000, Pacific Grove, CA: Brooks/Cole. 502.

111. Ahrens, C.D., *Meteorology Today: An Introduction to Weather, Climate, and the Environment*. 7 ed. 1902, Belmont, CA, USA: Brooks/Cole. 624.

112. Spångmyr, M., *Global effects of albedo change due to urbanization*, in *Department of Earth and Ecosystem Sciences*. 2010, Lund University: Lund, Sweden. p. 30.

113. Taha, H., D. Sailor, and H. Akbari, *High-albedo materials for reducing building cooling energy use*, in *Other Information: PBD: Jan 1992*. 1992. p. Medium: ED; Size: 73 p.

114. Shahmohamadi, P., et al., *The Impact of Anthropogenic Heat on Formation of Urban Heat Island and Energy Consumption Balance.* Urban Studies Research, 2011. **2011**.

115. Taha, H., et al., *Residential cooling loads and the urban heat island—the effects of albedo.* Building and Environment, 1988. **23**(4): p. 271-283.

116. Kikegawa, Y., et al., *Impacts of city-block-scale countermeasures against urban heat-island phenomena upon a building's energy-consumption for air-conditioning.* Applied Energy, 2006. **83**(6): p. 649-668.

117. Yamashita, S., et al., *On relationships between heat island and sky view factor in the cities of Tama River basin, Japan.* Atmospheric Environment (1967), 1986. **20**(4): p. 681-686.

118. Chun, B. and J.M. Guldmann, *Spatial statistical analysis and simulation of the urban heat island in high-density central cities.* Landscape and Urban Planning, 2014. **125**(0): p. 76-88.

119. Oke, T.R., *Canyon geometry and the nocturnal urban heat island: Comparison of scale model*

and field observations. Journal of Climatology, 1981. **1**(3): p. 237-254.

120. Johnson, G.T. and I.D. Watson, *The Determination of View-Factors in Urban Canyons.* Journal of Climate and Applied Meteorology, 1984. **23**(2): p. 329-335.
121. Grimmond, C.S.B., et al., *Rapid methods to estimate sky-view factors applied to urban areas.* International Journal of Climatology, 2001. **21**(7): p. 903-913.
122. Chapman, L., et al., *Potential Applications of Thermal Fisheye Imagery in Urban Environments.* Geoscience and Remote Sensing Letters, IEEE, 2007. **4**(1): p. 56-59.
123. Chapman, L., J.E. Thornes, and A.V. Bradley, *Sky-view factor approximation using GPS receivers.* International Journal of Climatology, 2002. **22**(5): p. 615-621.
124. Brown, M.J., S. Grimmond, and C. Ratti, *Comparison of methodologies for computing sky view factor in urban environments*, in *International Society of Environmental Hydraulics Conf.* 2001: Tempe, AZ.
125. Lindberg, F. and B. Holmer, *Sky View Factor Calculator User Manual - Version 1.0*. 2010, University of Gothenburg.
126. Holmer, B., U. Postgård, and M. Eriksson, *Sky view factors in forest canopies calculated with IDRISI.* Theoretical and Applied Climatology, 2001. **68**(1-2): p. 33-40.
127. *Sun path chart program*. 2007 July 12, 2013; Available from: http://solardat.uoregon.edu/index.html.
128. Giannaros, T.M. and D. Melas, *Study of the urban heat island in a coastal Mediterranean City: The case study of Thessaloniki, Greece.* Atmospheric Research, 2012. **118**(0): p. 103-120.
129. Tan, J., et al., *The urban heat island and its impact on heat waves and human health in Shanghai.* International Journal of Biometeorology, 2010. **54**(1): p. 75-84.
130. Charabi, Y. and A. Bakhit, *Assessment of the canopy urban heat island of a coastal arid tropical city: The case of Muscat, Oman.* Atmospheric Research, 2011. **101**(1–2): p. 215-227.
131. Kim, Y.H. and J.J. Baik, *Daily maximum urban heat island intensity in large cities of Korea.* Theoretical and Applied Climatology, 2004. **79**(3-4): p. 151-164.
132. Wang, J. *Chinese Air Quality Online Observation & Analysis*. 2014 [cited 2015; Available from: http://aqistudy.sinaapp.com/.
133. Wong, E., *Reducing Urban Heat Islands: Compendium of Strategies* Urban Heat Island Basics, ed. K. Hogan, J. Rosenberg, and A. Denny. Vol. 6. 2011, Washington, D.C: United States Environmental Protection Agency.
134. Schrijvers, P.J.C., et al., *Breakdown of the night time urban heat island energy budget.* Building and Environment, 2015. **83**(0): p. 50-64.
135. *Chinese Weather*. Ningbo Weather 2011 [cited 2013 August 7]; Available from: http://www.weather.com.cn/.
136. Matricardi, D., *The role of paved surfaces in the Urban Heat Island phenomenon: Assessment of fundamental thermal parameters and finite element analysis for UHI mitigation*, in *SCUOLA DI INGEGNERIA E ARCHITETTURA*. 2015, ALMA MATER STUDIORUM - UNIVERSITÀ DI BOLOGNA. p. 142.
137. Christen, A. and R. Vogt, *Energy and radiation balance of a central European city.* International Journal of Climatology, 2004. **24**(11): p. 1395-1421.
138. Voogt, J.A., *Urban Heat Island.* Encyclopedia of Global Environmental Change, 2002. **3**.
139. Santamouris, M., et al., *Using cool paving materials to improve microclimate of urban areas –*

Design realization and results of the flisvos project. Building and Environment, 2012. **53**(0): p. 128-136.

140. Doulos, L., M. Santamouris, and I. Livada, *Passive cooling of outdoor urban spaces. The role of materials.* Solar Energy, 2004. **77**(2): p. 231-249.
141. Kolokotsa, D., M. Santamouris, and S.C. Zerefos, *Green and cool roofs' urban heat island mitigation potential in European climates for office buildings under free floating conditions.* Solar Energy, 2013. **95**(0): p. 118-130.
142. Rajagopalan, P., K.C. Lim, and E. Jamei, *Urban heat island and wind flow characteristics of a tropical city.* Solar Energy, 2014. **107**(0): p. 159-170.
143. Hassid, S., et al., *The effect of the Athens heat island on air conditioning load.* Energy and Buildings, 2000. **32**(2): p. 131-141.
144. Chan, A.L.S., *Developing a modified typical meteorological year weather file for Hong Kong taking into account the urban heat island effect.* Building and Environment, 2011. **46**(12): p. 2434-2441.
145. Radhi, H. and S. Sharples, *Quantifying the domestic electricity consumption for air-conditioning due to urban heat islands in hot arid regions.* Applied Energy, 2013. **112**(0): p. 371-380.
146. Hirano, Y. and T. Fujita, *Evaluation of the impact of the urban heat island on residential and commercial energy consumption in Tokyo.* Energy, 2012. **37**(1): p. 371-383.
147. Bueno, B., et al., *The urban weather generator.* Journal of Building Performance Simulation, 2012. **6**(4): p. 269-281.
148. Ren, Z., et al., *Constructing weather data for building simulation considering urban heat island.* Building Services Engineering Research & Technology, 2014. **35**(1).
149. Peng, Z., et al., *Generation of ambient temperature bin data of 26 cities in China.* Energy Conversion and Management, 2009. **50**(3): p. 543-553.
150. Kolokotroni, M., I. Giannitsaris, and R. Watkins, *The effect of the London urban heat island on building summer cooling demand and night ventilation strategies.* Solar Energy, 2006. **80**(4): p. 383-392.
151. Radhi, H., *A comparison of the accuracy of building energy analysis in Bahrain using data from different weather periods.* Renewable Energy, 2009. **34**(3): p. 869-875.
152. Belcher, S.E., J.N. Hacker, and D.S. Powell, *Constructing design weather data for future climates.* Building Services Engineering Research And Technology, 2005. **26**(4): p. 49-62.
153. Hu, J., et al., *Design standard for energy efficiency of public buildings*. 2007, China Planning Press: Beijing. p. 155.
154. Team, E.D., *Input output reference: the encyclopedic reference to EnergyPlus input and output*. 2013.
155. Ashtiani, A., P.A. Mirzaei, and F. Haghighat, *Indoor thermal condition in urban heat island: Comparison of the artificial neural network and regression methods prediction.* Energy and Buildings, 2014. **76**(0): p. 597-604.
156. Szymanowski, M. and M. Kryza, *Application of geographically weighted regression for modelling the spatial structure of urban heat island in the city of Wroclaw (SW Poland).* Procedia Environmental Sciences, 2011. **3**(0): p. 87-92.
157. Maitha H. Al Shamisi, Ali H. Assi, and h.A.N. Hejase, *Using MATLAB to Develop Artificial*

Neural Network Models for Predicting Global Solar Radiation in Al Ain City - UAE in *Engineering Education and Research Using MATLAB*, A.H. Assi, Editor. 2011, InTech: United Arab Emirates. p. 219-238.

158. Robyn Ball and P. Tissot, *Demonstration of Artificial Neural Network in Matlab* 2006.
159. Yi, J. and V.R. Prybutok, *A neural network model forecasting for prediction of daily maximum ozone concentration in an industrialized urban area.* Environmental Pollution, 1996. **92**(3): p. 349-357.
160. Jiang, D., et al., *Progress in developing an ANN model for air pollution index forecast.* Atmospheric Environment, 2004. **38**(40): p. 7055-7064.
161. Altan Dombaycı, Ö. and M. Gölcü, *Daily means ambient temperature prediction using artificial neural network method: A case study of Turkey.* Renewable Energy, 2009. **34**(4): p. 1158-1161.
162. Mahboubeh Afzali, Afsaneh Afzali, and G. Zahedi, *Ambient Air Temperature Forecasting Using Artificial Neural Network Approach.* ICECS2011, 2011. **19**: p. 176-180.
163. Gobakis, K., et al., *Development of a model for urban heat island prediction using neural network techniques.* Sustainable Cities and Society, 2011. **1**(2): p. 104-115.
164. MATLAB. 2010, THe MathWorks, Inc.
165. MathWorks. *R2013a Documentation*. 2013; Available from: http://www.mathworks.cn/cn/help/documentation-center.html.
166. Koza, J.R. and R. Poli, *A Genetic Programming Tutorial.* 2003.
167. Banzhaf, W., et al., *Genetic programming.* Intelligent Systems and their Applications, IEEE, 2000. **15**(3): p. 74-84.
168. Poli, R., B. Langdon, and N. McPhee, *A Field Guide to Gentic Programming*. 2008: Lulu Enterprises, UK Ltd 252.
169. Banzhaf, W., et al., *Genetic programming: an introduction: on the automaticevolution of computer programs and its applications*. 1997, San Francisco, CA, USA: Morgan Kaufmann Publishers Inc.
170. Makkeasorn, A., N.B. Chang, and X. Zhou, *Short-term streamflow forecasting with global climate change implications – A comparative study between genetic programming and neural network models.* Journal of Hydrology, 2008. **352**(3–4): p. 336-354.
171. Zhang, Y. and S. Bhattacharyya, *Genetic programming in classifying large-scale data: an ensemble method.* Information Sciences, 2004. **163**(1–3): p. 85-101.
172. Angeline, P.J., *Genetic programming: On the programming of computers by means of natural selection,: John R. Koza, A Bradford Book, MIT Press, Cambridge MA, 1992, ISBN 0-262-11170-5, xiv + 819pp., US$55.00.* Biosystems, 1994. **33**(1): p. 69-73.

APPENDIX 1

Characteristics of the selected measurement sites in Hangzhou city

Station NO.	Station name	District	Land-use	Distance from city centre	Surrounding Albedo	Sky View Factor
1	Hangzhou Tower Shopping Centre	Shangcheng	Commercial	0km	0.13	0.85
2	Lizi Urban Apartment Building	Xiacheng	Residential	1.5km	0.13	0.51
3	Lakeside of West Lake	West Lake	Water space	1.8 km	0.22	0.2
4	Zhejiang University of Technology	Xiacheng	Educational	2 km	0.17	0.75
5	Hangzhou Centre Railway Station	Shangcheng	Commercial	2.2 km	0.11	0.70
6	Wushan Plaza	Shangcheng	Commercial	3.6 km	0.19	0.51
7	Daguan Residential Community	Xiacheng	Residential	3.6 km	0.13	0.23
8	Qingyunju Residential Community	West Lake	Residential	4.3 km	0.2	0.54
9	Mantou Mountain	West Lake	Mountain	5.2 km	0.26	0.49
10	Canal Plaza	Gongshu	Commercial	5.6 km	0.19	0.43
11	Xingzhou Garden Residential Community	West Lake	Residential	5.6 km	0.13	0.29
12	Jianqiao Airport	Jianggan	Airport	7.2 km	0.12	0.49
13	Liuxia Industry Area	West Lake	Industry	7.5 km	0.18	0.88
14	Hangzhou Iron & Steel Hospital	Gongshu	Mountain	9.3 km	0.2	0.27
15	Zhejiang Business College	Binjiang	Educational	9.6 km	0.17	0.20
16	Xixi Wetland	West Lake	Green space	10.8 km	0.18	0.92
17	Hangzhou International Jewellery City	Xiaoshan	Commercial	11.1 km	0.13	0.68
18	Hangzhou Foreign Language School	West Lake	Educational	12.1 km	0.19	0.34
19	New Century Hotel	Xiaoshan	Commercial	13.3 km	0.13	0.54
20	Xiang Lake	Xiaoshan	Water space	13.5 km	0.22	0.83
21	Chonghua Residential Community	Xiaoshan	Residential	14.3 km	0.14	0.57
22	Hangzhou Institute of Technology	Jianggan	Educational	14.4 km	0.15	0.69

23	Qiantang River	Jianggan	Water Space	15.6 km	0.2	0.92
24	Hangzhou Xiaoshan International Airport	Xiaoshan	Airport	18.3 km	0.21	0.34
25	Yaqian Industrial Area	Xiaoshan	Industrial	21.6 km	0.17	0.66
26	Reclaimed Land area	Xiaoshan	Farmland	25.7 km	0.25	0.29

Characteristics of the selected measurement sites in Ningbo city

Station NO.	Station name	District	Land-use	Distance from city centre	Surrounding Albedo	Sky View Factor
1	Tianyi Square	Haishu	Commercial	0 km	0.12	0.61
2	Fu Mao Mansion	Haishu	Commercial	0.4 km	0.13	0.34
3	Construction Mansion	Haishu	Commercial	0.5 km	0.1	0.46
4	The Old Bund	Jiangbei	Commercial	0.6 km	0.18	0.81
5	Gu Lou	Haishu	Commercial	0.9 km	0.17	0.69
6	Liu Yi Garden Residential Community	Haishu	Residential	1 km	0.13	0.51
7	Moon Lake Park	Haishu	Green space	1.1 km	0.24	0.82
8	Tian Yi Ge	Haishu	Commercial	1.4 km	0.12	0.26
9	Ningbo South Station	Haishu	Commercial	1.9 km	0.11	0.57
10	Jiangdong South Road	Jiangdong	Residential	2.1 km	0.13	
11	Ningbo Engineering University	Yinzhou	Educational	2.4 km	0.17	0.58
12	Cui Bai Er Li Residential Community	Haishu	Residential	2.6 km	0.14	0.21
13	Sun Lake Park	Jiangbei	Green space	2.9 km	0.24	0.94
14	Yageer Indoor Stadium	Jiangdong	Commercial	2.9 km	0.11	0.91
15	Bai Yun Park	Haishu	Green space	3.1 km	0.21	0.31
16	Dong Hu Garden Residential Community	Yinzhou	Residential	3.8 km	0.18	0.55
17	Dong Fang Rui Shi Residential Community	Jiangdong	Residential	3.9 km	0.13	0.55
18	Lianfeng Industrial Area	Haishu	Industrial	4.5 km	0.12	0.85
19	Sangjia Industrial Area	Jiangdong	Industrial	4.5 km	0.09	0.76
20	Sheng Shi Hua Cheng Residential Community	Yinzhou	Residential	5.1 km	0.2	0.62
21	Liansheng Square	Yinzhou	Commercial	5.2 km	0.19	
22	Zhuangqiao Town	Jiangbei	Residential	6 km	0.18	0.74
23	Yageer Industrial Area	Yinzhou	Industrial	7.4 km	0.18	0.79
24	High Tech Plaza	Jiangdong	Commercial	7.9 km	0.2	0.88
25	University of	Yinzhou	Educational	7.9 km	0.2	0.54

	Nottingham Ningbo					
26	Hui Jia Xin Yuan Residential Community	Jiangbei	Residential	9.1 km	0.2	0.43
27	Ningbo Lishe International Airport	Yinzhou	Airport	10.5 km	0.21	0.98
28	Jiangshan Town Farmland	Yinzhou	Farmland	13.2 km	0.25	0.99
29	Dongqian Lake	Yinzhou	Water space	14 km	0.22	0.82

APPENDIX 2

Sensor accuracy test: Temperature (unit: ℃)

Time	11:00	12:00	13:00	14:00	15:00	16:00	17:00	18:00	19:00
NO.1	3.835	10.802	1.071	-8.556	-9.186	32.695	25.139	17.695	16.254
NO.2	3.983	10.704	1.09	-8.549	-9.243	31.789	25.545	17.975	16.347
NO.3	4.181	10.701	1.169	-8.38	-9.197	30.843	24.596	17.465	16.276
NO.4	4.242	10.772	1.224	-8.347	-9.167	30.358	24.986	17.479	16.351
NO.5	4.181	10.764	1.169	-8.443	-9.134	30.968	25.846	18.091	16.401
NO.6	4.189	10.713	1.112	-8.444	-9.199	31.044	25.234	17.603	16.289
NO.7	4.131	10.714	1.057	-8.554	-9.183	31.604	25.483	17.54	16.288
NO.8	4.115	10.832	1.098	-8.533	-9.163	32.289	25.17	17.099	16.222
NO.9	4.063	10.713	1.05	-8.57	-9.199	32.479	25.234	16.977	16.226
NO.10	4.145	10.738	1.127	-8.509	-9.203	31.947	23.828	17.383	16.193
NO.11	4.242	10.772	1.161	-8.41	-9.104	31.544	24.236	16.602	16.163
NO.12	4.171	10.703	1.09	-8.549	-9.243	31.228	24.295	17.411	16.221
NO.13	4.172	10.747	1.164	-8.43	-9.121	31.695	24.635	17.569	16.192
NO.14	4.146	10.802	1.19	-8.447	-9.141	31.886	25.143	17.51	16.32
NO.15	4.089	10.666	1.08	-8.455	-9.208	31.302	24.805	17.176	16.175
NO.16	3.938	10.713	1.05	-8.632	-9.262	32.292	23.547	17.29	17.228
NO.17	3.943	10.651	1.057	-8.554	-9.183	31.854	23.482	16.225	16.1
NO.18	4.006	10.714	1.12	-8.491	-9.182	31.604	23.732	16.789	16.413
NO.19	3.905	10.753	1.075	-8.566	-9.197	32.277	23.345	16.522	16.647
NO.20	3.935	10.787	1.102	-8.55	-9.182	32.44	24.697	17.562	16.309
NO.21	4.181	10.764	1.232	-8.38	-9.134	31.967	24.721	17.465	16.338
NO.22	4.423	10.829	1.278	-8.234	-9.054	30.853	25.67	17.975	16.409
NO.23	4.46	10.74	1.253	-8.258	-9.141	30.202	24.83	17.447	16.257
NO.24	4.514	10.717	1.317	-8.223	-9.102	30.106	25.045	17.791	16.289
NO.25	4.423	10.703	1.215	-8.36	-9.18	30.229	25.295	17.286	16.284
NO.26	4.548	10.703	1.278	-8.297	-9.18	30.167	24.545	16.91	16.221
NO.27	4.682	10.701	1.294	-8.192	-9.135	29.844	24.721	16.964	16.213
NO.28	4.589	10.676	1.259	-8.304	-9.186	30.073	25.389	17.444	16.317
NO.29	4.503	10.713	1.238	-8.318	-9.136	30.482	25.359	17.541	16.289
NO.30	4.514	10.717	1.254	-8.286	-9.102	30.481	24.732	17.541	16.289
NO.31	4.62	10.701	1.294	-8.254	-9.134	30.281	24.846	17.215	16.276
NO.32	4.481	10.625	1.219	-8.328	-9.145	30.453	24.518	17.012	16.198
NO.33	4.597	10.753	1.326	-8.314	-9.134	30.342	25.408	17.649	16.396
NO.34	4.597	10.753	1.264	-8.313	-9.197	30.53	25.221	17.587	16.334
NO.35	4.586	10.677	1.253	-8.321	-9.204	30.514	24.83	17.948	16.257
NO.36	4.587	10.736	1.258	-8.302	-9.12	30.507	23.697	16.438	16.939

NO.37	4.606	10.748	1.281	-8.327	-9.081	31.075	24.891	17.26	16.509
NO.38	4.702	10.717	1.316	-8.286	-9.102	30.418	24.232	16.978	16.852
NO.39	4.577	10.717	1.316	-8.223	-9.102	30.293	23.482	17.103	16.414
NO.40	4.543	10.702	1.271	-8.313	-9.197	30.418	23.296	16.034	16.347
NO.41	4.492	10.769	1.224	-8.343	-9.099	31.915	24.608	17.225	16.724
NO.42	4.486	10.703	1.278	-8.36	-9.117	31.103	24.858	17.725	16.785
NO.43	4.069	10.714	1.119	-8.428	-9.183	31.791	24.67	17.477	16.601
NO.44	4.327	10.782	1.254	-8.29	-9.106	31.109	24.736	16.981	16.605
NO.45	4.306	10.764	1.232	-8.317	-9.134	30.906	25.346	17.653	16.714
NO.46	4.377	10.713	1.238	-8.255	-9.136	30.17	24.859	17.165	16.602
NO.47	4.369	10.701	1.232	-8.254	-9.134	30.094	23.595	17.152	16.151
NO.48	4.462	10.736	1.258	-8.239	-9.12	30.07	24.135	17.378	16.501
NO.49	4.492	10.707	1.287	-8.28	-9.162	30.105	24.357	16.724	16.598
NO.50	4.506	10.718	1.302	-8.26	-9.142	30.302	23.93	16.859	16.985
NO.51	4.555	10.707	1.287	-8.217	-9.162	29.98	24.42	17.726	16.724
NO.52	4.548	10.703	1.278	-8.297	-9.117	30.229	23.857	17.036	16.785
NO.53	4.451	10.717	1.254	-8.286	-9.102	30.543	24.732	17.478	16.727
NO.54	4.367	10.707	1.161	-8.406	-9.162	31.79	24.795	17.6	16.786
NO.55	4.46	10.74	1.253	-8.321	-9.141	30.701	24.268	16.884	16.132
NO.56	4.508	10.652	1.183	-8.302	-9.182	30.48	25.045	17.602	16.851
NO.57	4.653	10.666	1.269	-8.266	-9.145	30.116	24.117	17.176	16.425
NO.58	4.668	10.748	1.344	-8.201	-9.081	30.638	24.703	17.511	16.822
NO.59	4.548	10.703	1.215	-8.36	-9.18	30.604	24.232	17.474	16.597
NO.60	4.465	10.666	1.206	-8.392	-9.208	31.24	24.742	17.363	16.8
NO.61	4.493	10.709	1.224	-8.347	-9.167	30.92	24.486	17.729	16.602
NO.62	4.556	10.709	1.287	-8.284	-9.167	30.67	24.799	17.854	16.79
NO.63	4.584	11.114	1.566	-8.006	-9.015	31.635	24.641	17.633	17.132

Sensor accuracy test: Specific humidity (unit: %)

Time	11:00	12:00	13:00	14:00	15:00	16:00	17:00	18:00	19:00
NO.1	25.721	20.104	25.097	28.215	29.617	87.545	75.882	84.48	84.633
NO.2	25.319	19.585	24.63	28.056	28.906	92.441	80.319	89.22	77.102
NO.3	24.693	18.218	24.346	27.447	28.473	85.496	86.275	83.398	76.668
NO.4	24.381	18.633	24.725	26.785	28.49	90.574	80.757	86.325	78.041
NO.5	26.503	19.18	26.342	28.276	29.401	86.736	80.285	88.261	84.366
NO.6	24.282	19.255	25.938	28.238	28.892	90.726	73.861	83.523	80.748
NO.7	26.59	20.534	26.089	27.589	29.246	89.301	82.093	84.657	84.119
NO.8	24.488	19.409	25.659	27.82	28.976	89.75	79.363	89.152	80.002
NO.9	25.114	19.995	25.959	27.975	29.811	92.36	78.604	80.998	81.13
NO.10	25.006	19.199	25.68	27.693	30.186	89.977	74.552	77.029	80.478
NO.11	25.47	21.066	26.309	27.978	29.472	88.923	66.002	81.301	80.916
NO.12	24.62	19.77	24.951	27.587	29.222	90.804	81.982	82.486	83.488

NO.13	25.385	19.95	25.558	27.631	29.175	90.176	74.513	81.897	80.58
NO.14	24.298	19.25	24.987	27.385	29.085	92.403	80.027	83.964	82.007
NO.15	25.083	20.577	25.083	28.051	29.035	93.332	71.567	81.489	80.958
NO.16	25.395	19.13	25.721	27.994	29.284	92.25	75.861	83.49	81.964
NO.17	25.656	19.557	25.828	28.396	29.754	93.625	75.286	83.253	81.463
NO.18	25.477	19.606	25.989	28.364	29.712	88.821	74.063	80.973	81.233
NO.19	24.798	19.717	25.301	28.295	29.615	89.914	77.564	82.22	83.084
NO.20	24.287	19.395	26.123	27.948	29.433	94.484	76.865	79.173	82.122
NO.21	25.09	19.843	26.095	27.597	29.753	90.055	84.255	84.124	85.17
NO.22	25.094	20.392	25.428	27.419	29.398	90.594	77.64	85.206	84.293
NO.23	24.894	19.274	25.223	28.173	29.315	90.617	74.684	80.405	82.295
NO.24	24.386	18.627	25.531	27.653	28.629	90.825	76.892	83.395	83.689
NO.25	24.297	19.364	25.342	27.591	29.65	92.076	77.94	82.518	82.518
NO.26	24.989	19.198	25.683	28.438	29.634	87.721	73.672	80.533	81.19
NO.27	25.468	20.757	25.967	27.956	29.602	93.562	86.368	81.308	82.807
NO.28	25.003	18.683	26.215	28.792	29.133	85.798	80.636	90.286	83.498
NO.29	25.091	20.033	26.092	28.411	30.056	93.44	76.153	81.969	82.981
NO.30	24.693	18.499	26.049	27.399	29.41	85.78	84.288	83.787	83.284
NO.31	24.11	20.017	25.022	27.303	28.217	95.115	73.806	83.147	83.147
NO.32	26.144	19.577	25.478	28.135	28.96	85.666	76.421	84.521	82.854
NO.33	24.272	19.217	25.306	28.043	29.401	93.725	72.62	81.173	82.982
NO.34	24.781	20.267	25.278	28.406	29.55	94.417	77.089	84.974	83.578
NO.35	25.419	19.413	25.928	28.461	29.468	86.758	82.171	87.146	84.545
NO.36	24.647	20.188	25.327	27.358	29.374	90.06	78.086	86.592	84.24
NO.37	25.159	20.506	25.5	28.048	29.398	92.216	80.359	85.955	84.542
NO.38	24.247	19.896	25.245	27.891	29.207	91.24	82.099	90.838	84.45
NO.39	24.816	19.198	24.642	28.095	29.122	90.569	84.94	88.967	84.94
NO.40	25.529	19.895	26.035	28.382	29.879	89.617	83.425	87.155	84.277
NO.41	24.636	19.416	26.466	27.955	29.929	86.07	76.227	87.343	85.174
NO.42	24.547	19.519	25.839	26.968	29.221	94.303	80.998	83.384	83.532
NO.43	24.338	19.655	24.807	27.466	28.249	99.027	79.813	85.607	85.285
NO.44	25.652	19.74	25.485	27.98	29.301	88.11	83.942	88.953	83.443
NO.45	25.147	19.622	25.147	27.361	29.389	89.028	82.362	87.134	84.96
NO.46	25.142	20.241	25.477	28.636	29.954	86.812	75.79	86.568	85.217
NO.47	24.665	18.89	25.356	27.932	29.295	86.966	81.513	86.717	84.836
NO.48	24.315	19.255	25.177	27.408	28.94	89.971	80.437	87.491	85.981
NO.49	26.19	19.976	25.336	28.061	29.076	86.827	82.744	93.583	84.544
NO.50	24.733	18.358	24.563	27.611	28.787	88.083	82.337	86.483	85.614
NO.51	25.592	19.724	25.933	28.138	29.484	89.084	80.487	85.471	87.049
NO.52	25.204	19.493	25.529	26.99	28.609	96.654	81.628	85.198	85.494
NO.53	24.971	19.458	24.971	28.36	29.201	91.295	88.08	95.271	85.431
NO.54	24.257	19.74	24.601	27.341	29.039	92.897	85.82	87.214	84.67

NO.55	25.84	19.682	26.683	27.858	30.026	93.186	84.026	83.537	85.602
NO.56	24.198	19.914	24.515	27.368	28.477	93.624	82.717	92.068	89.421
NO.57	24.243	18.856	25.615	27.319	29.349	94.186	85.993	88.906	86.971
NO.58	25.328	19.717	25.169	27.716	28.826	91.566	88.36	91.705	86.818
NO.59	24.675	19.755	25.371	27.446	29.335	93.633	90.706	93.15	87.714
NO.60	25.311	19.806	26.162	27.855	29.537	90.313	83.639	90.805	87.704
NO.61	23.856	19.514	25.256	26.97	28.843	93.19	82.763	90.532	88.874
NO.62	24.015	19.288	24.801	26.688	28.258	100.549	84.962	90.123	88.91
NO.63	24.672	19.852	24.89	27.023	28.672	98.67	83.233	89.331	88.213

APPENDIX 3

Radiation shield and Accessories Specification

Radiation Shield

Saucers:

10 colormatt saucers with the diameter of 16cm were required for each radiation shield. There were 4 sets of holes need to be drilled on saucers. They could be standardised as follow (also refer to manufacturing drawing):

1. Three numbers of Ø6 mm holes 47mm from centre of saucers spaced at 81mm from each other
2. Two numbers of Ø4 mm holes 47mm from centre of saucers opposite to each other. These holes should not be too close to any of the three holes in set 1, 10mm or more is recommended
3. One Ø60mm hole at centre of saucers.
4. Several vents of Ø5 mm regularly spaced on surfaces of saucers

Numbers of saucers with different holes arrangement for making a radiation shield could be found in the table below. Please also refer to manufacturing drawings

Hole set arrangement required	Number of Saucers
1	1
1,2,3	1
1,3	7
1,4	1

Top circular metal:

A circular metal of 2mm thick aluminum alloy should be created with the diameter of 120mm. Set 1 holes should be drilled in the correct position as indicated in the drawing. Four Ø5mm holes should also be drilled for attaching the “arm” in the later stage.

Arm:

The “arm” of the radiation shield was made of 2.5mm thick aluminum alloy with the size of 500mm × 40mm. It should be cut to size as indicated in the drawing and rolled to the indicated radius. Four extra Ø5mm holes should be drilled at one end for attaching the “arm” to the “Top circular metal” by M5 stainless steel bolts and nuts

Studding:

M4 zinc studding

M4 zinc studding should be bended to the distance described on the drawing. This M4 bended studding should then be mounted on saucers with set 2 holes by double polystyrene nuts and washers on both sides. It will be used for hanging the sensors

M6 studding

M6 Studding with screw thread should be cut into 165mm long as indicated in drawing.

Assembly procedure:

Three M6 studs were threaded through the saucers and a circular metal plate on top. This circular metal plate should be attached to the “arm” by M4 stainless steel bolts and nuts. Polystyrene dome nuts were then placed on the studs above the bracket. The ten saucers were stacked onto the studding with two M6 nuts as spacers between each pair of saucers. All three studs were secured at the bottom by M6 dome nuts and "Lock tight".

APPENDIX 4

MANUFACTURING DRAWINGS FOR RADIATION SHIELD (Part A)		SCALE: 1:7 @A4 UNIT: mm	DATE: 02/02/2012 BY: TIANFENG SHEN
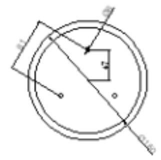 NO. OF PIECES: 1 Ø160mm Colormatt Plastic Saucer with three holes of Ø6mm equally spaced	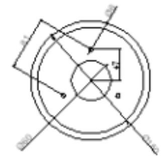 NO. OF PIECES: 7 Ø160mm Colormatt Plastic Saucer with three holes of Ø6mm equally spaced and single center hole of Ø60mm	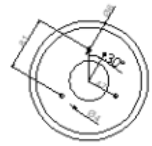 NO. OF PIECES: 1 Ø160mm Colormatt Plastic Saucer with three holes of Ø6mm equally spaced and two holes of Ø4mm opposite to each other	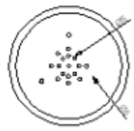 NO. OF PIECES: 1 Ø160mm Colormatt Plastic Saucer with three holes of Ø6mm equally spaced and several vents of Ø5mm regularly spaced
 NO. OF PIECES: 3 Ø6mm stainless steel studding with screw thread, Length 165mm	 NO. OF PIECES: 1 Ø4mm zinc studding bended with screw thread, Length 132mm	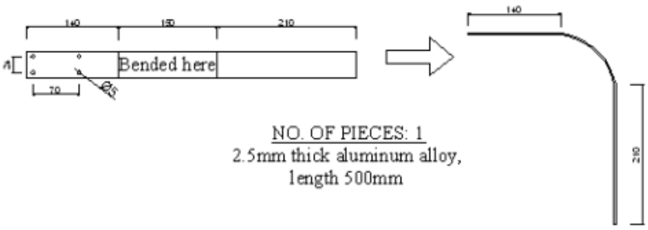 NO. OF PIECES: 1 2.5mm thick aluminum alloy, length 500mm	

MANUFACTURING DRAWINGS FOR RADIATION SHIELD (Part B)	SCALE: 1:7 @A4 DATE: 02/02/2012 UNIT: mm BY: TIANFENG SHEN
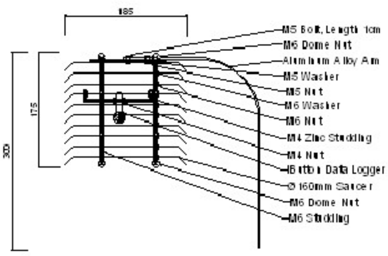 Sectional View	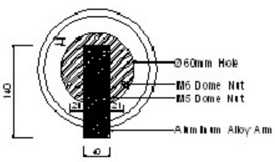 Top View
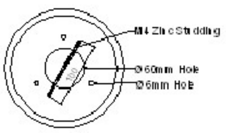 Cross Sectional View	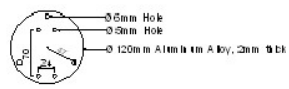 NO. OF PIECES: 1 Ø120mm Aluminum Alloy with three holes of Ø6mm equally spaced and four holes of Ø5mm regularly spaced